Effect of Ethylene glycol and Polyols on Thermal Stability of Globular Proteins

A Thesis Submitted for the Degree of

Doctor of Philosophy

by K. Tejaswi Naidu



Department of Biotechnology and Bioinformatics
School of Life Sciences
University of Hyderabad
Hyderabad – 500046, India
January 2021



UNIVERSITY OF HYDERABAD

(A central university established in 1974 by an act of Parliament)

Department of Biotechnology and Bioinformatics

School of Life Sciences

University of Hyderabad, Hyderabad 500 046, India

STATEMENT

I, K. Tejaswi Naidu, hereby declare that the work presented in this thesis, entitled as "**Effect of Ethylene glycol and Polyols on Thermal Stability of Globular Proteins**" has been carried out by me under the supervision of *Dr. N. Prakash Prabhu* at Department of Biotechnology and Bioinformatics. To the best of my knowledge, this work has not been submitted for the award of any degree or diploma to this or any other university or institute. A report on plagiarism statistics from the University Librarian is enclosed.

K. Tejaswi naidu

K. Tejaswi Naidu

(13LTPH03)

Place: Hyderabad

Date: 07-01-2021

Supervisor

Dr. N. Prakash Prabhu

N. Prakash Prabhu, Ph.D.
Assistant Professor
Dept. Biotechnology & Bioinformatics
School of Life Sciences
University of Hyderabad
Hyderabad-500 046



UNIVERSITY OF HYDERABAD

(A central university established in 1974 by an act of Parliament)

Department of Biotechnology and Bioinformatics

School of Life Sciences

University of Hyderabad, Hyderabad 500 046, India

CERTIFICATE

This is to certify that the thesis entitled "Effect of Ethylene glycol and Polyols on Thermal Stability of Globular Proteins" submitted by *Mr. K. Tejaswi Naidu* bearing registration number 13LTPH03 in partial fulfilment of the requirements for the award of Doctor of Philosophy in the Department of Biotechnology and Bioinformatics, School of Life Sciences is a bonafide work carried out by him under my supervision and guidance.

This thesis is free from plagiarism and has not been submitted previously in part or in full to this or any other university or institution for award of any degree or diploma

Further, the student has the following publication(s) before submission of the thesis/monograph for the adjudication and has produced evidence for the same in the form of acceptance letter or the reprint in the relevant area of his research:

- K.T. Naidu, D.K. Rao, N.P. Prabhu, Cryo vs Thermo: Duality of Ethylene Glycol on the Stability of Proteins, J. Phys. Chem. B. 124, (2020), 10077-10088. https://doi.org/10.1021/acs.jpcb.0c06247. (ISSN Number: 1520-5207), Chapters of dissertation where this publication appears 2 and 3
- 2. K. Tejaswi Naidu, N. Prakash Prabhu, An able-cryoprotectant and a moderate denaturant: distinctive character of ethylene glycol on protein stability, J. Biomol. Struct. Dyn. (2020) 1–13. https://doi.org/10.1080/07391102.2020.1819422. (ISSN Number: 1538-0254), chapter of dissertation where this publication appears 4

has made presentations in the following conferences

- 1. As a poster in "Bio-Quest 2015" Symposium held at School of Life Sciences, University of Hyderabad on 23-24th Sept 2015. (National)
- 2. As a poster in "43rd Indian Biophysical Society Meeting (Molecules to Systems)" held at Indian Institute of Science Education and Research, Kolkata on 15-17th March 2019. (International)

Further, the student has passed the following courses towards the fulfilment of the course work requirement of the Ph.D. degree.

S.No.	Course code	Name	Credits	Pass/Fail
1	BT 801	Seminar I	1	PASS
2	BT 802	Research Ethics & Management	2	PASS
3	BT 803	Biostatistics	2	PASS
4	BT 804	Analytical Techniques	3	PASS
5	BT 805	Lab Work	4	PASS

Supervisor

Head of Department of Biotechnology and Bioinformatics

N. Prakash Prabhu, Ph.D. Assistant Professor Dept Biotechnology & Bioinformatics

School of Life Sciences University of Hyderabad Hyderabad-500 046 HEAD *
Dept. of Biotechnology & Bioinformatics
University of Hyderabad

Hyderabad.

DEAN School of Life Sciences University of Hyderabad Hyderabad - 500 046.

ఈ గ్రంథం

నా ప్రియమైన తల్లిదండ్రులకి,

పూజ్యులైన నా గురుదేవులు (చారిజి మరియు దాజి)

మరియు

 ∞

క్రి

అంకితం

ACKNOWLEDGMENTS

The path towards this thesis has been a lot of ebbs-and-flow. Its completion is thanks in large to all the special people who struck with me supported me along this entire journey.

I am tremendously fortunate to have **Dr. N. Prakash Prabhu**, my mentor, who provided continuous support, motivation during the course of my Ph.D. I sincerely thank him for his guidance, thoughtful feedback and always aimed at moving me forward.

Besides my guide, I am also grateful to my thesis committee: Prof. Jogadhenu Syama Sundar Prakash and Dr. Sunanda Bhattacharyya for their encouragement and for insightful inputs. I would like to thank the Prof. K.P.M.S.V. Padmasree (Head of the Department of Biotechnology and Bioinformatics) and Prof. Niyaz Ahmed, Prof. Anand K. Kondapi (former Heads) for providing necessary facilities during these years. I would like to express my gratitude to Prof. Dayananda Siddavattam (Dean of the School of Life Sciences) and Prof. A.S. Raghavendra, Prof. P. Reddanna, Prof. KVA Ramaiah (former Deans) for providing necessary facilitates in the school. I sincerely thank the office staff of the Department Mr. Rajshekhar, Mr. Rahul, Mr. Shekhar, Mr. Murali and Mr. Krishna for their invaluable support. I thank BIF and CMSD for providing me with the computational facility which was indispensable for my work.

It will be indispensable to acknowledge the financial support provided by UGC (JRF/SRF), without which it would be impossible to complete my Ph.D. with tranquillity. I would also like to thank DST and CSIR for funding support to the lab.

I thank all my present (Archi Saurabh, Subhasree Ghosh, Pratibha Kushwaha and Sanjay Kumar) and former lab (Dr. Neshatul Haque, Dr. Kiran Kumar, Dr. Bramhini Anumalla) Ph.D. students for their valuable discussions and for providing a pleasant working environment in our lab. I also would like to thank all the former project students of the lab Deepak Prasad, Audrey, Gangasagar (Ganges ocean), Krishna kanth (KK), Sushree Rekha, Haider, Sai Abhilash Reddy, Sharath Mohan, Manikyaprabhu, Swathi, Dhanyasree, Sreevidya, Dipasree Hajra, Sowmya, Soumyaranjan Pujahari, Mouly Chatterjee, Harshita joshi, Shashikant patel, Vani Gangwar and Sanjana.

I am deeply indebted to Neshat bhai for his valuable and insightful discussions regarding my work and his personal support as a brother. His has a great scientific vigour which always inspires me even today.

My heartful thanks to my room mates and friends Satyajit Mukhopadhyay and Suraj Chauhan for their seamless support and patience they showed from that past two years. Along with that I would like to thank friends Neha Tomar, Sai Kiran Madireddi, Santosh, Sayan Are, Tanvi Suhane Gupta, Farhan, Moin bhai for their moral support. My Special thanks to Tanu for bearing with all my inadequacies and for her immense patience. It would be unvirtuous of me if I do not acknowledge my seniors and batchmates of the Department of Biotechnology and Bioinformatics and the School of Life Sciences

I would like to express my eternal appreciation towards "My Parents" for their unconditional love and for the moral, emotional and financial support during this entire journey. I am too indebted them and can never pay them back for all the troubles they took during all these years of my life. I sincerely thank my Akka (Siri) and Bava (Satish) and both my nephews Sriyansh and Srivatsal.

The most important of all I would like to thank the almighty "*My Master*" for bestowing upon me his benevolence, kindness and beneficence without which this long journey was absolutely impossible.

... K. Tejaswi Naidu

ABBREVIATIONS

BLG - Bovine β-lactoglobulin Cyt - Horse heart cytochrome *c*

Mb - Horse myoglobin

ACT - Bovine pancreatic α-lactalbumin

 $\alpha ext{-LA}$ - Bovine $\alpha ext{-lactalbumin}$

EG - Ethylene glycol

Gly - Glycerol

Gdm - Guanidinium hydrochloride

NaCl - Sodium chloride T - Temperature

T_m - Heat transition midpoint temperature
 Tc - Cold transition midpoint temperature

 ΔH_m - Change in enthalpy at the heat transition midpoint temperature ΔH_c - Change in enthalpy at the cold transition midpoint temperature ΔS_m - Change in entropy at the heat transition midpoint temperature ΔS_c - Change in entropy at the cold transition midpoint temperature

 T_{max} - Temperature of maximum stability

 ΔC_P - Change in heat capacity CD - Circular dichroism

 ΔG_{unf} - Free energy of Unfolding

m_g Slope of the chemical denaturation transition
 C_m Chemical denaturation transition midpoint

MD - Molecular Dynamics PDB - Protein Data Bank

RMSD - Root mean square deviation
SASA - Solvent accessible surface area
RDF - Radial distribution function

RDF_{surf} - Radial distribution function considering all surface residues

H-bond - Hydrogen bonds

 K_p - local-bulk partition coefficient Γ_{EG} - preferential interaction coefficient

 n_W - Number of water molecules within a cut-off distance from protein n_{EG} - Number of EG molecules within a cut-off distance from protein

 N_W - Total number of water molecules in the system

 N_{EG} - Total number of EG molecules

 n_{W-hyd} - number of water molecules nearer to hydrophobic residues

 n_{W-pol} - number of water molecules nearer to polar residues

 n_{EG-hyd} - number of EG molecules nearer to hydrophobic residues

 n_{EG-pol} - number of EG molecules nearer to polar residues

REMD - Replica exchange molecular dynamics

CA - Contact area

RMSIP - Root mean square inner produce

FEL - Free energy landscape G_{23} - Kirkwood-Buff Integral g(r) - Radial distribution function

r - Distance

CONTENTS

CHAPTER 1	0
Introduction	0
1.1. HISTORICAL PERSPECTIVE OF PROTEIN STRUCTURE AND FOLDING	1
1.2. THEORIES AND MODELS OF PROTEIN FOLDING	4
1.2.1. Diffusion-collision theory	4
1.2.2. Framework theory	4
1.2.3. Energy landscape theory	6
1.3. PROTEIN STABILITY AND THE EFFECTS OF ADDITIVES	7
1.4. METHODS TO STUDY PROTEIN STABILITY	9
1.4.1. Thermal denaturation	9
1.4.2. Chemical denaturation	10
1.4.3. Molecular dynamics simulations	11
1.5. ABOUT THE PRESENT STUDY	13
1.6. REFERENCES	15
CHAPTER 2	24
Cryo vs Thermo: Duality of Ethylene Glycol on the Stability of Proteins	24
2.1. ABSTRACT	25
2.2. INTRODUCTION	26
2.3. MATERIALS AND METHODS	29
2.3.1. Materials	29
2.3.2. Thermal denaturation	30
2.3.3. Chemical denaturation	31
2.4. RESULTS	32
2.4.1. Thermal denaturation of Proteins	32
2.4.2. Chemical denaturation of proteins	35
2.5. DISCUSSION	37
2.5.1. Effect of EG on thermal denaturation	37

2.5.2. Enthalpy-entropy compensation	38
2.5.3. Effect of EG on Gdm-induced unfolding	39
2.6. CONCLUSION	40
2.7. REFERENCES	40
CHAPTER 3	45
Molecular Mechanism of Temperature-Dependent Stabilizing Nature of Ethylene Glycol	45
3.1. ABSTRACT	46
3.2. INTRODUCTION	47
3.3. METHODS	48
3.4. ANALYSIS	50
3.5. RESULTS	52
3.5.1. Validation of parameters of EG	52
3.5.2. Structural changes of proteins in different solvent conditions with temperature	53
3.5.3. Distribution of solvent and cosolvent around proteins	56
3.5.4. H-bond between protein-solvent and protein-EG	60
3.5.5. Preferential interaction of EG with proteins	60
3.5.6. Hydrophobic hydration	62
3.6. DISCUSSION	63
3.6.1. Effect of EG on the conformation of proteins	63
3.6.2. Interaction of EG with the proteins	63
3.7. CONCLUSION	65
3.8. REFERENCES	65
CHAPTER 4	72
Analysing the Distinctive Character of Ethylene Glycol on Protein Stability by Replica Exchange Molecular Dynamics Simulation	72
4.1. ABSTRACT	73
4.2. INTRODUCTION	74
4.2.1 Theory of REMD	74
4.3. METHODS	79
4.3.1. Materials	79
4.3.2 Thermal denaturation experiments	79

4.3.3. Molecular dynamic simulations	79
4.4. ANALYSIS	81
4.4.1. Thermal denaturation	81
4.4.2. Contact area	81
4.4.3. Free-energy landscape	81
4.4.4. Radial distribution function, H-bonds and hydrophobic hydration	82
4.4.5. Partition coefficient and preferential interaction	83
4.5. RESULTS	84
4.5.2 Efficiency of REMD simulation	85
4.5.3 Structural Changes During Molecular Dynamic Simulation of α-LA	87
4.5.4 Solvent verses cosolvent interactions with α -LA	92
4.6. DISCUSSION	100
4.6.1 Effect of EG on the thermal denaturation and structure of α-LA	100
4.6.2 Interaction of EG with α-LA	101
4.7 CONCLUSION	104
4.8 REFERENCES	104
CHAPTER 5	113
Effect of Polyols on Thermal Unfolding Intermediate of Cytochrome c	113
5.1. ABSTRACT	114
5.2. INTRODUCTION	115
5.3. MATERIALS AND METHODS	117
5.3.1 Materials	117
5.3.2. Spectroscopic measurements	118
5.3.3. Data analysis	118
5.3.4. Global analysis	119
5.4. RESULTS	120
5.4.1 Thermal unfolding of cytochrome <i>c</i>	120
5.4.2 Effect of denaturants and ionic salt on the intermediate	123
5.4.3. Effect of polyols on the intermediate	125

5.5. DISCUSSION	129
5.5.1 Characteristics of thermal denaturation intermediate of Cyt	130
5.5.2 Interactions that stabilizing the intermediate state	132
5.5.3 Polyols alter the energy landscape of folding intermediates	132
5.6. CONCLUSION	134
5.7. REFERENCES	135
List of Publications	145
Plagiarism Certificate	146

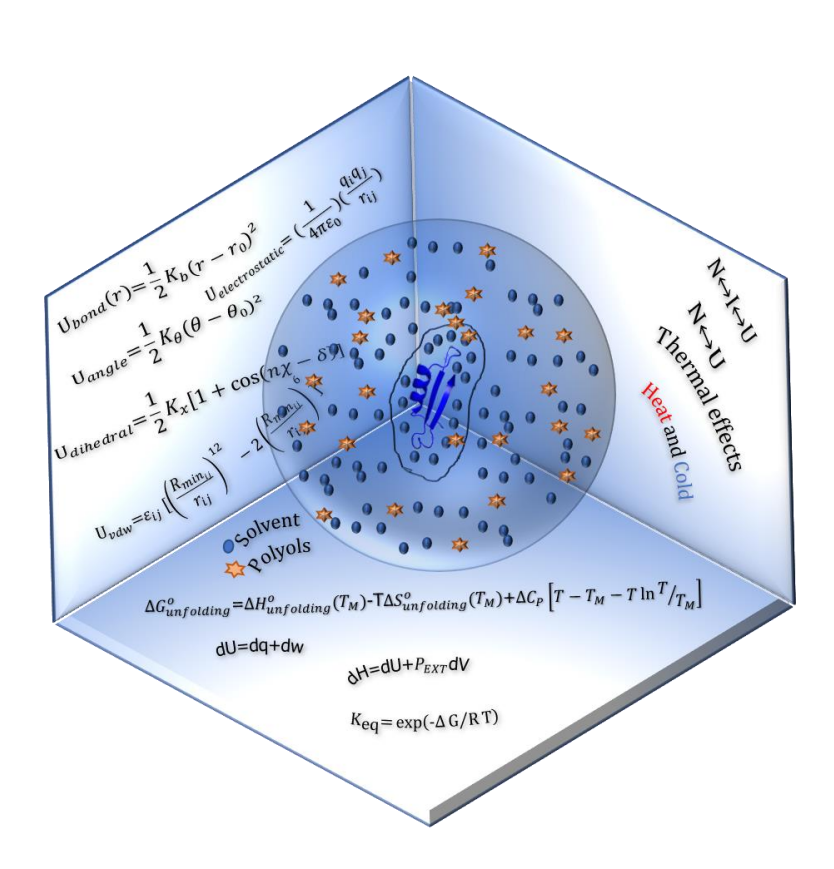
PREFACE

"A poet once said, "The whole universe is in a glass of wine." We will probably never know in what sense he said that, for poets do not write to be understood. But it is true that if we look in glass of wine closely enough, we see the entire universe. There are the things of physics: the twisting liquid which evaporates depending on the wind and weather, the reflections in the glass, and our imagination adds the atoms. The glass is a distillation of the earth's rocks, and in its composition, we see the secrets of the universe's age, and the evolution of the stars. What strange array of chemicals are in the wine? How did they come to be? There are the ferments, the enzymes, the substrates, and the products. There in wine is found the great generalization: all life is fermentation. Nobody can discover the chemistry of wine without discovering the cause of much disease. How vivid is the claret, pressing its existence into the consciousness that watches it! If our small minds, for some convenience, divide this glass of wine, this universe, into parts — physics, biology, geology, astronomy, psychology, and so on — remember that nature does not know it! So, let us put it all back together, not forgetting ultimately what it is for. Let us give one more final pleasure: drink it and forget it all!"

Richard Feynman

CHAPTER 1

Introduction



"Function follows structure" is an often well-accepted paradigm in biology. Nature always favors the attainment of the functional forms in biological macromolecules spontaneously, rooted within the molecules themselves. Among these macromolecules, proteins (addressed as nanomachines) perform a plethora of functions in all the three kingdoms of life, and are known to be most heterogeneous in structure. The building blocks of proteins are amino acids, and the linear chain of amino acids constitute the "primary structure" of the protein. For a protein to function, the linear chain must fold and attain a unique three-dimensional structure [1].

1.1. HISTORICAL PERSPECTIVE OF PROTEIN STRUCTURE AND FOLDING

In the early 1900's Hofmeister and Fischer independently proposed that proteins are polymers constituted by amino acids linked with peptide bonds [2]. The earliest work on the structure of proteins was reported by Astbury & Street in 1931, who used X-ray diffraction to show that human hair exhibits a characteristic diffraction pattern, which changes upon stretching. They named the extended forms as β -keratin while contracted form as α -keratin [3]. Two years later in 1933, Astbury & Woods proposed that β -keratin is the one with extended sheets, held by interaction between carbonyl groups and imino groups [4]. These interactions were recognized as a hydrogen bond [5]. Pauling proposed the existence of two helical conformations, α - helix (with 3.7 residues per turn) and γ -helix (with 5.1 residues per turn), as shown in Fig. 1.1, based on the crystal structures of amino acids, peptides and other simple substances related to proteins [6,7].

The first hierarchical organization of protein structure was introduced by LinderstrØme-Lang in 1952 as: primary, secondary, tertiary and quaternary structures [8]. The first concrete evidence for the existence of such a structural organization in proteins was confirmed from the work of Kendrew & Perutz, who solved the crystal structures of myoglobin [9] and hemoglobin [10] and were awarded the Nobel Prize in 1962. These data also provided the first evidence for the existence of a definite 3D-structure for proteins held by various non-covalent interactions and might possess a hydrophobic core.

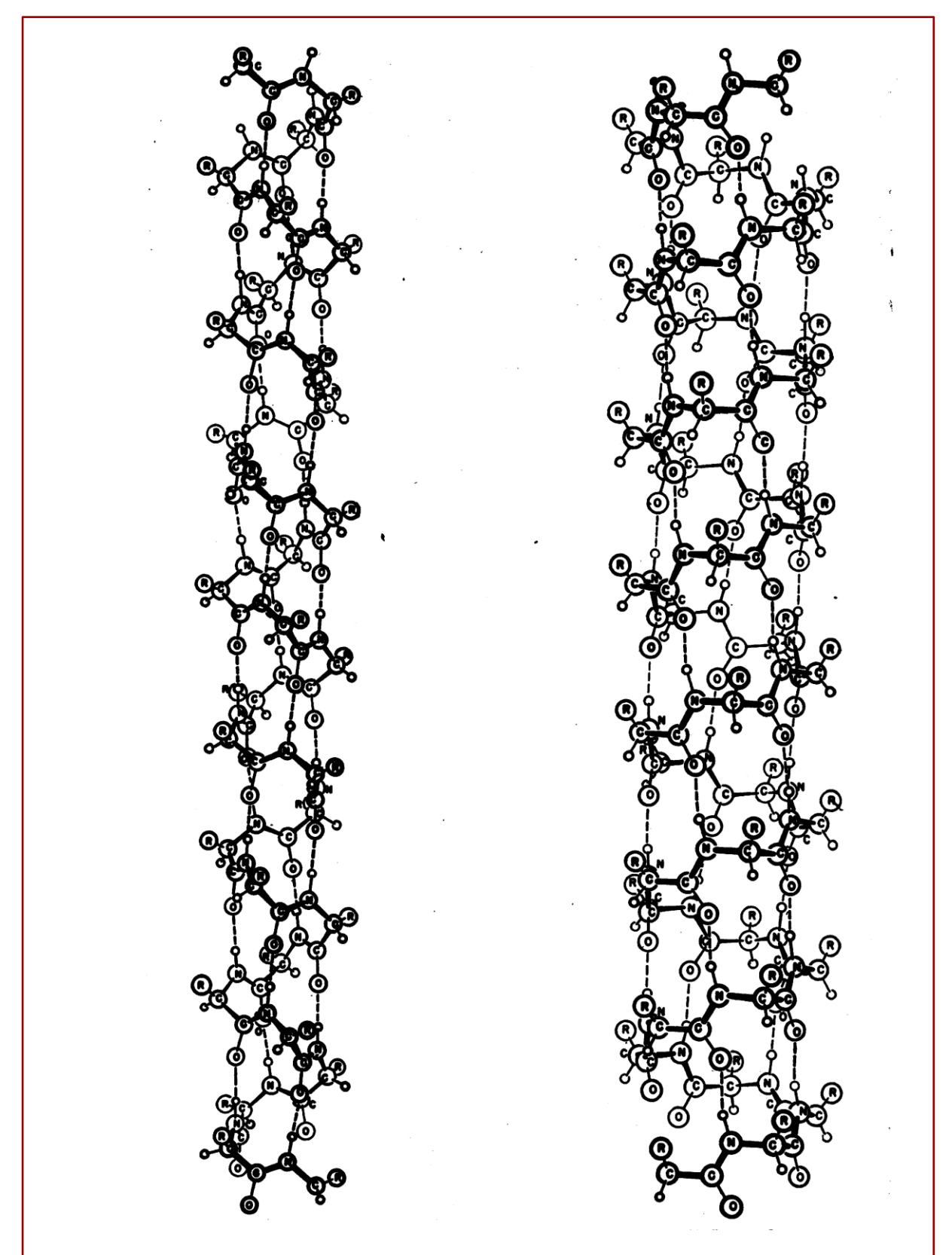


Fig. 1.1. Drawings of (A) α -helix and (B) γ - helix. The structure of proteins: two hydrogen-bonded helical configurations of the polypeptide chain. Adopted from Pauling et.al., 1951

In the mid-20th century, many groups around the world were studying the process of protein folding, as stated by Anfinsen in his Nobel lecture "The work that my colleagues and I have carried out on the nature of the process that controls the folding of polypeptide chain into unique three-dimensional structures of proteins was, indeed, strongly influenced by observations on the ribonuclease molecule. Many others including Anson and Mirsky in the 1930s and Lumry and Eyring in the 1950s had observed and discussed the reversibility of denaturation of proteins. However, the true elegance of this consequence of natural selection was dramatized by the ribonuclease work, since the refolding of this molecule, after full denaturation by reductive cleavage of its four disulfide bonds, required that only 1 of the 105 possible pairings of eight sulfhydryl groups form four disulfide linkages take place." Further, Anfinsen's proposal of the "thermodynamic hypothesis", which states "the three-dimensional structure of a native protein in its normal physiological milieu (solvent, pH, ionic strength, presence of other components such as metal ions or prosthetic groups, temperature and others) is the one in which the Gibbs free energy of the whole system is the lowest; that is, that the native conformation is determined by the totality of the interatomic interactions and hence by the amino acid sequence, in a given environment" [11]. The thermodynamic hypothesis, although the most accepted theory primarily focuses on the spontaneity of the protein to attain the native state, but does not provide any insights into the pathway(s) of the protein folding.

The theory undermining the pathways of protein folding was first hypothesized by Levinthal [12], who reported a *gedanken* experiment stating that, of all the enormous number of possible configurations in a protein of 100 amino acids (assuming 2n number of backbone torsional angles of an n residue protein, with a minimum of 3 stable conformations, totally yield $3^{2n} \approx 10^n$ conformations if the side-chain conformations are ignored), if the molecule explores 10^{13} conformations per second, still the total time taken for the protein to fold would be 10^{87} seconds. This would be equal to ~ 13 billion years, but apparently proteins fold in the time scale of millisecond regime. This discrepancy is classically called Levinthal's paradox. Levinthal further argues that the folded conformation need not be the lowest energy state, but could be a metastable state sufficiently deep in the energy well so as to survive the perturbations in the biological system. These arguments of Levinthal led to the proposal of protein folding pathways, in which, the intermediate states would act as milestones in the enormous conformational space of the protein to reach the minima (the native state).

Anfinsen's thermodynamic view and Levinthal's pivotal argument on folding pathways raised two basic questions in the field of protein folding, (i) if the pathways are thermodynamically driven, how does a protein fold within milliseconds after the synthesis of polypeptide chain? and (ii) if the process is kinetically driven, how are the misfolded states minimized or completely avoided? These questions although mutually exclusive led to the proposal of new theories and models of protein folding.

1.2. THEORIES AND MODELS OF PROTEIN FOLDING

1.2.1. Diffusion-collision theory

According to this model, a protein molecule consists of multiple elementary microdomains, such that each domain can search for their own conformational space and form a stable structural domain. These microdomains then diffuse under the influence of internal and external forces resulting in their collision. Collision leads to the formation of higher-order subdomains. This overall process can lead to the formation of a stable molten globule like state, which finally undergoes diffusion to generate a stable tertiary structure, with proper side-chain packaging [13]. The theory was proposed by Karplus & Weaver in 1976 [14]. The process of folding might follow a unique single pathway or might have multiple initial pathways. However, the microdomains containing structures formed might lead to off-pathway intermediate structures [15]. Further the model does not provide information about the atomistic details of the motions in the folding process, nor deals with the energetic barriers and the population of various conformations during the folding, thus is a semi-quantitative model [16].

1.2.2. Framework theory

After six years of the proposal of the diffusion-collision model, Kim & Baldwin (1982) proposed the framework model, which is an extension of the diffusion-collision model. The model suggests that folding begins with the formation of secondary structures which then interact and pack against each other to form a final stable tertiary structure [17,18]. The fundamental drawback of the framework theory is, in many cases the secondary structures are formed even in the denatured state, which fluctuates with the random coiled structure [19]. Notwithstanding, in many fast-folding proteins like helical coiled GCN4 [20],

protein L [21] it was demonstrated that secondary interactions play only minor role in the determination of protein folding kinetics [22].

Apart from these above-mentioned models, some of the other early protein folding theories are nucleation-condensation model and hydrophobic collapse model. In the nucleation-condensation model, some of the key residues in the protein form a nucleus, on which the entire protein tertiary structure develops [23,24]. In the hydrophobic collapse model, the process of folding begins with the collapse of some hydrophobic residues, non-specifically, followed by the formation of secondary and tertiary structures [25]. All these models are called classical models that deal with the existence of different intermediate states of proteins apart from the native (N) and the unfolded (U) states during the folding process. The most commonly observed pathways are: off-pathway scheme [26]

$$\begin{array}{c}
N \rightleftharpoons U \\
\uparrow\downarrow \\
X
\end{array} \tag{1.2.1}$$

on-pathway model [27]

$$N \rightleftarrows X \rightleftarrows U$$
 (1.2.2)

and sequential model [28]

$$N \rightleftarrows X_1 \rightleftarrows X_2 \rightleftarrows \cdots \rightleftarrows U$$
 (1.2.3)

Where U represents the fully unfolded state, X_i represents the intermediate state and N represents the native state.

1.2.3. Energy landscape theory

This theory comes from the statistical mechanical perspective of protein folding, also called as "folding funnel" model. According to this theory, a statistical ensemble of unfolded states sieves through the funnel via a myriad of pathways to the minima, corresponding to the lowest energy and entropy [29].

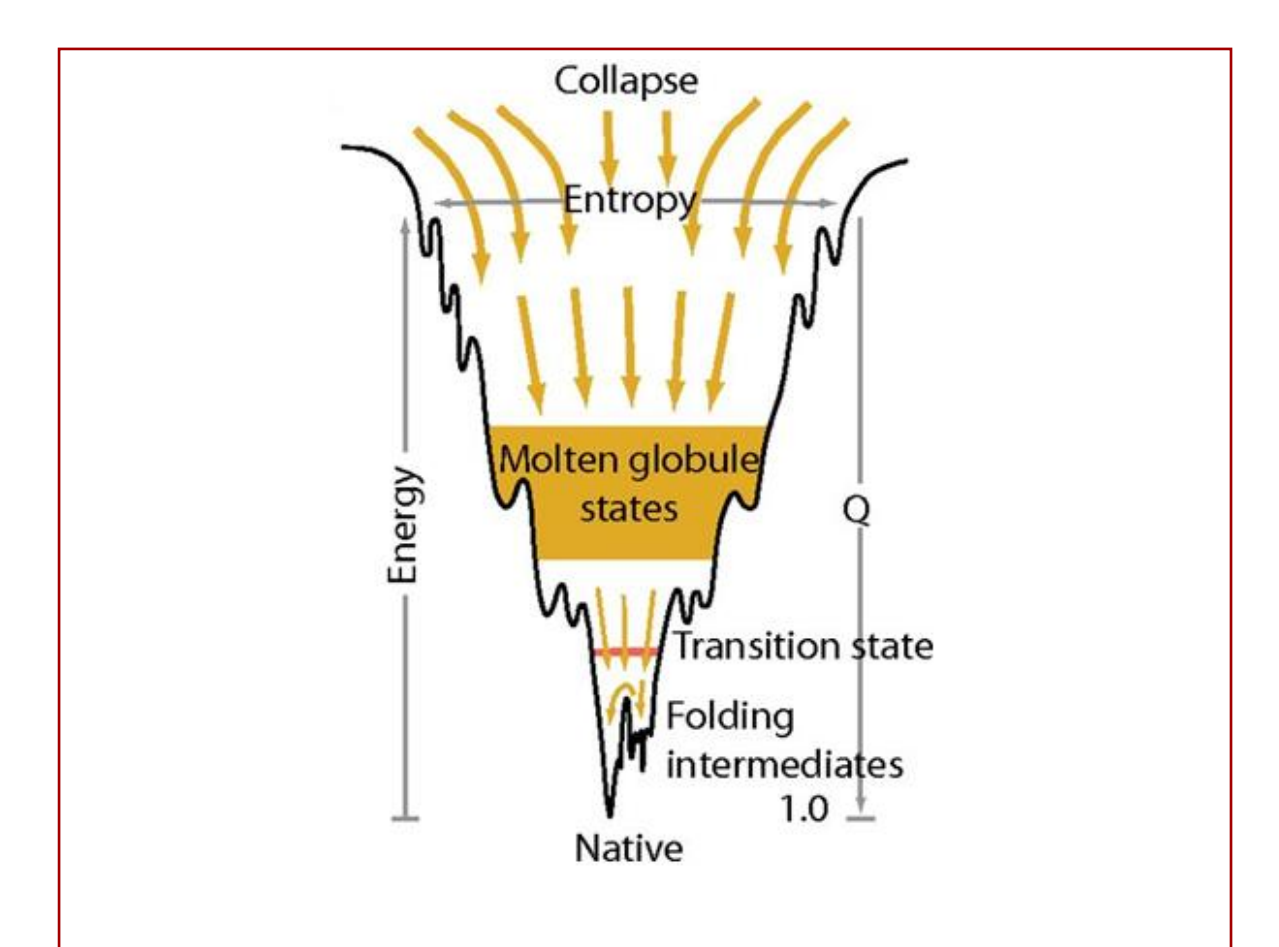


Fig. 1.2. Illustration of a free energy landscape of a fast folding 60 amino acid protein. The picture depicts the new view of protein folding pathway inferring that the protein must folds energetically downhill through intermediate states like the molten globule before attaining the Native conformation. The width and the depth of the funnel corresponds to the entropy and energy of the protein, respectively. Adopted from Wolynes et.al., 1997

A folding energy landscape is usually a plot of energy against conformational entropy. An example of the funnel energy landscape of a 60 amino acid protein is illustrated in Fig. 1.2 [30,31]. Understanding and modulating the free energy landscapes of proteins help us to learn how organisms have evolved through eons of ages to live under hostile

environmental conditions. Further, these principles are essential in the fields of biotechnology to develop better methods for engineering proteins with desired properties.

1.3. PROTEIN STABILITY AND THE EFFECTS OF ADDITIVES

A common practice among the biochemists is to use cosolvents in the medium during the isolation of organs, organelles and biomolecules in order to retain their function and activity. These cosolvents are commonly referred as osmolytes [32]. These are small organic molecules that are strategically accumulated intracellularly by various organisms across the living kingdoms to counter different environmental stress [33,34]. They are classified into three categories: polyols and sugars (glycerol, sorbitol, sucrose etc.) [35], amino acids and derivatives (glutamate, betaine etc.) [36] and amine oxides (TMAO) [37]. It is believed that most of these osmolytes stabilize via a common mechanism of "preferential interaction" [38].

Preferential interaction can be expressed as preferential binding or as preferential exclusion (or preferential hydration) of the cosolvent on the protein loci. The term "preferential" is a measure of relative affinity. If the affinity of cosolvent is greater than water, it results in preferential binding, while less affinity results in preferential hydration. In thermodynamic viewpoint at constant temperature and pressure preferential binding can be expressed as [39],

$$\left(\frac{\partial m_C}{\partial m_P}\right)_{\mu_C} = -\frac{\left(\frac{\partial \mu_C}{\partial m_P}\right)_{m_C}}{\left(\frac{\partial \mu_C}{\partial m_C}\right)_{m_P}}$$
(1.3.1)

$$= -\left(\frac{\partial \mu_P}{\partial \mu_C}\right)_{m_p} \equiv \Gamma_{PC} \tag{1.3.2}$$

where m_P and m_C are the molal concentrations of the protein and cosolvent respectively, while μ_P and μ_C are the corresponding chemical potentials. Equation 1.3.2 suggests that preferential binding (Γ_{PC}) is the mutual adjustment of the number of solvent and cosolvent composition within the vicinity of the protein (mutual perturbation of chemical potentials) [40]. If Γ_{PC} is negative, the interaction between the cosolvent and protein is unfavorable (preferential exclusion of cosolvent) and the surface hydration is favorable which is usually observed for stabilizing or compatible osmolytes. If Γ_{PC} is positive, the interaction of cosolvent is

favorable (preferential binding) over surface hydration of the proteins which is usually observed for denaturants (non-compatible osmolytes) as depicted in Fig. 1.3.

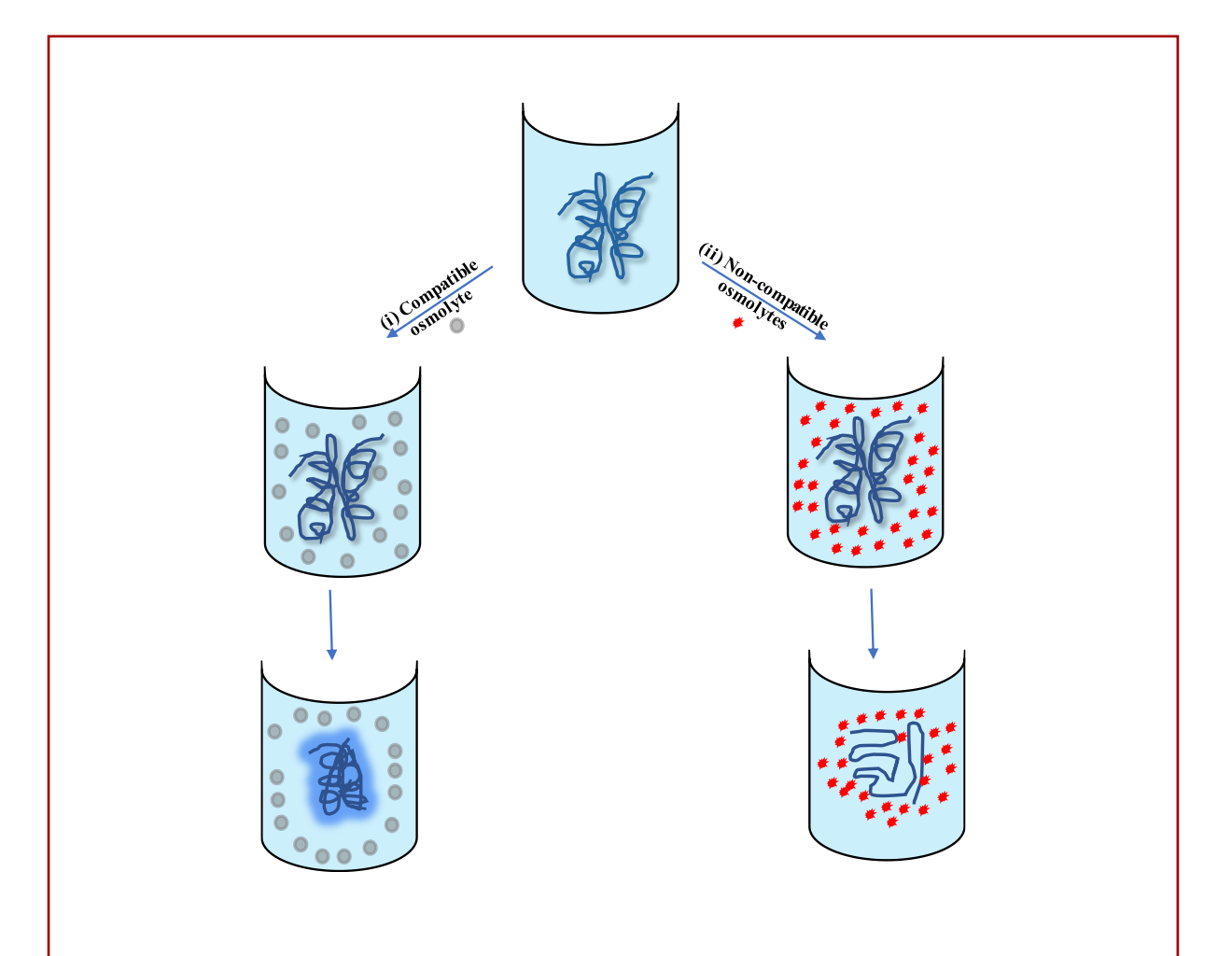


Fig. 1.3. A Schematic depiction of mode of action of a stabilizing osmolyte and a denaturant. Scheme (i) Addition of a compatible osmolyte (stabilizing osmolyte (●)) to the protein solution results in preferential exclusion and protein compaction. Scheme (ii) while addition of a non-compatible osmolyte (a denaturant (►)) results in preferential binding of the cosolvent and protein denaturation.

1.4. METHODS TO STUDY PROTEIN STABILITY

Experimentally, protein stability is studied by perturbing the structure of the protein by thermal denaturation, chemical denaturation, pressure denaturation or altering the pH [41–44]. Among these methods, the most widely used procedures are heat and chemical denaturation.

1.4.1. Thermal denaturation

The experimental approach employed to study protein thermal stability is to track the change in some property of the protein with temperature. The most common techniques include absorbance, CD, NMR [45]. The variation of the chosen property measures as a function of temperature is called a thermogram, which upon fitting to an appropriate equation can yield equilibrium thermodynamic parameters like the transition temperature (T_m or T_c described below) and the change in enthalpy at the transition temperature (ΔH) [46]. These parameters can be used to construct a protein stability curve, as first defined by Schellman [41], is a plot of free energy of unfolding (ΔG) as a function of temperature, which is a valuable tool for studying protein stability. A typical protein stability curve is shown in Fig. 1.4. The curve

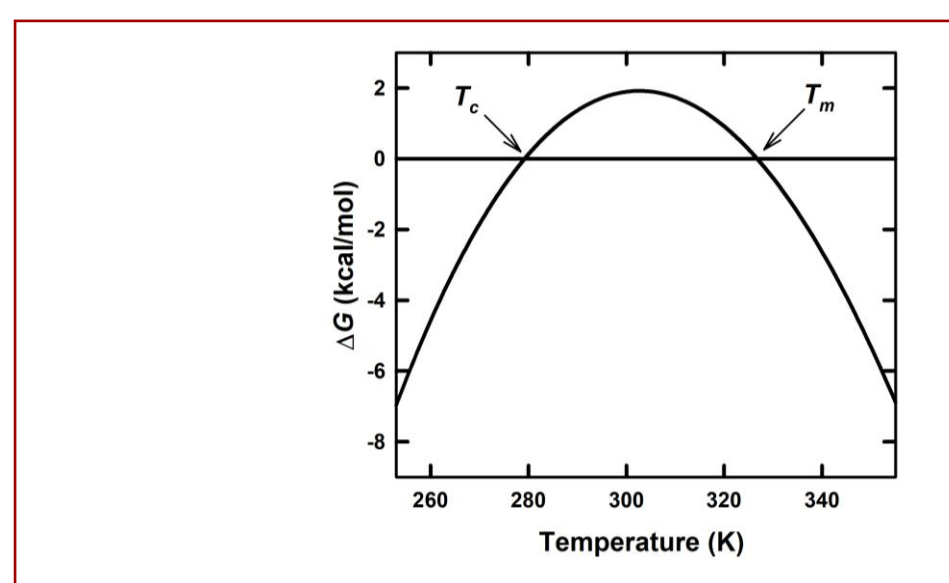


Fig. 1.4. A typical stability curve of a protein. It is derived from the temperature variation of the enthalpy and entropy of protein unfolding.

suggests that a protein can undergo denaturation both upon increase and decrease in temperature. The stability curve intersects the zero point at two temperatures corresponding to heat transition temperature (T_m) and cold transition temperature (T_c). These parameters along with enthalpy of unfolding measured at transition midpoint for both heat (ΔH_m) and cold (ΔH_c) denaturation are important thermodynamic parameters to define protein stability [41]. An increase of T_m and ΔH_m in presence of a cosolvent implies that the protein is stabilized by the cosolvent, while a decrease indicates a denaturant. On the other hand, a decrease in T_c and ΔH_c (more negative) in presence of a cosolvent implies stabilization against cold stress, while an increase of these parameters implies destabilization.

1.4.2. Chemical denaturation

Chemical denaturation is another routinely used method to study protein stability. In this process, protein in titrated against an increasing concentration of denaturant like guanidine hydrochloride or urea. The cause of denaturation is due to the negative transfer free energy,

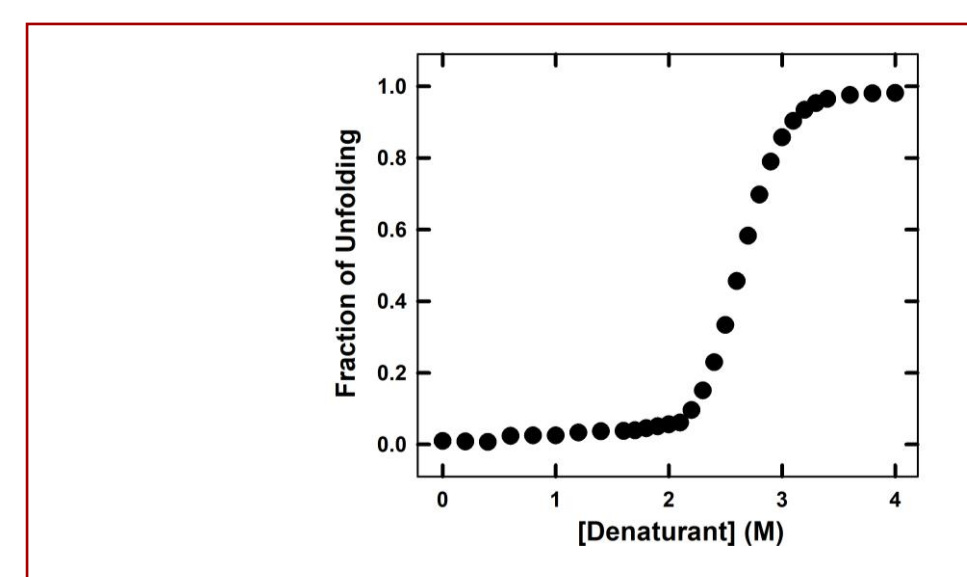


Fig 1.5. A typical protein chemical denaturation curve. It is a plot of concentration of the denaturant against the fraction of unfolding which can be calculated from any spectroscopic data recorded during protein chemical denaturation.

upon transfer of a protein from aqueous medium into the denaturant solution [47]. A typical protein denaturation curve is shown in Fig. 1.5. The data when fit to an appropriate equation by a non-linear least square method stability parameters such as free energy of unfolding (ΔG),

measure of dependence of ΔG on denaturant concentration (m_g) and transition mid-point of unfolding (C_m) can be calculated. An increase in ΔG and C_m in presence of a cosolvent implies that the cosolvent is a protein stabilizer, while a decrease in the values implies destabiliser. The above techniques, although very handy cannot provide a thorough insight into the molecular mechanism of the stabilization of proteins by cosolvents. The most convenient methods which evolved in the recent times to deal with mechanistic aspects of biological, biochemical processes and to understand protein denaturation are "Molecular dynamics simulations".

1.4.3. Molecular dynamics simulations

Molecular dynamic (MD) simulations are used to study the time evolution of interaction of molecules in a system. In this technique, configurations are generated successively by the integrating the "Newton's laws of motion". This results in a trajectory which provides information about the momentum and position of particles with time.

Force field methods are employed to perform MD simulation studies, in which electronic motions are ignored and the energy calculations are performed according to the position of the nucleus. Of the various MD force field employed, the "hard sphere potential" [48] and the "square well potential" [49] are of historic importance for the study of interacting classical particles. The first successful simulation involving the use of molecules was performed by Rahman in 1964. He simulated 864 particles of liquid argon interacting via Lennard-Jones potential and found that the calculated values of self-diffusion coefficient and pair correlation function were in concordance with that of the experimental values [50]. The first molecular mechanics force field and a computer program for macromolecules (like proteins and nucleic acids), was "AMBER" (Assisted Model Building with Energy Refinement) developed by Kollman & co-workers in 1981 [51]. Following this Karplus group developed another computer program in 1983 and a force field, "CHARMM" (Chemistry at HARvard Macromolecular Mechanics) [52], van Gunsteren group built GROMOS (Groningen molecular simulation) in 1987 [53] and Jorgensen group developed OPLS force field in 1988 [54]. Most of the molecular mechanics force fields typically consists of functions describing inter- and intra-molecular forces [55]. An example of the functional form of the potential energy function (equation 1.4.1) used to model a molecular system is [56]:

$$U(r) = \sum_{bonds} k_b (b - b_0)^2 + \sum_{angles} k_\theta (\theta - \theta_0)^2 + \sum_{dihedrals} k_\chi [\cos(n\chi - \delta) + 1]$$

$$+ \sum_{vdW,i\neq j} \varepsilon_{ij} \left[\left(\frac{R_{min,\ ij}}{r_{ij}} \right)^{12} - 2 \left(\frac{R_{min,\ ij}}{r_{ij}} \right)^6 \right] + \sum_{elec,i\neq j} \frac{q_i q_j}{4\pi \varepsilon_0 \, r_{ij}}$$

$$(1.4.1)$$

Where U(r) denotes the potential energy as a function of position of atoms. The first summation in the function accounts for the bond stretching, where k_b is the bond force constant and $(b-b_0)$ is the deviation from the equilibrium bond length. The second term accounts for the bond angles, where k_{θ} is the force constant for bond angle and $(\theta - \theta_0)$ represents the deviation from the equilibrium bond angle. The third term represents the dihedral or torsional angle, where k_{χ} is the force constant for the torsional angle, n is the multiplicity, χ is the torsional angle and δ is the phase shift. The non-bonded interactions are represented by the last two terms, where van Der Waals energy (Lennard-Jones 6-12 potential) is calculated by the fourth term and the electrostatic energy is calculated by the fifth term (Coulombic potential). All the molecular mechanics force fields contain the above terms, with some additional terms which are force field specific. Given the great importance of water in biology, a number of interaction potentials were developed for water molecules to be used in simulations. Among these, the most prominent ones are the rigid non-polarizable water models with (i) three interaction sites (SPC/E and TIP3P), (ii) four interaction sites (TIP4P and TIP4P/2005) and (iii) five interaction sites (TIP5P) [57]. The simplest water model of TIPn (N-point model) is the TIP3P water, which is based on gas phase geometry of water ($\angle HOH = 104.5^{\circ}$ and the 3point charges placed on the nuclei). To reproduce the quadrupole moment of water, the negative point charges on the oxygen of TIP3P was displaced onto the bisect of HOH towards the H-atoms leading to TIP4P water model [58]. Later, the point charge was replaced by two negative charges to replicate the lone pair of electrons on the oxygen atom leading to the TIP5P model [59]. Additional water models built on TIP4P of significance is the TIP4P/2005 model (used in this study), developed based on the fit to the temperature of maximum density estimated from the hexagonal ice melting point [60].

In the past twenty years, because of a considerable advancement in the computation power, MD simulations were successfully used to understand the molecular mechanism behind

many biological reactions such as ligand binding [61–63], protein-protein interactions [64,65], enzyme conformational changes [66,67], protein-cosolvent interactions [68–71]. Further most of the above-mentioned force fields are regularly updating new parameters for additional chemical entities and are also developing algorithms and servers to automatically identify and generate new parameters for small molecules. Some examples for such servers are CGenFF for CHARMM (used in this study) [72,73], PRODRG [74] and ATB [75] for GROMOS, AnteChamber for GAFF and AMBER [76]. For the study of all the above-mentioned biochemical processes classical MD simulations can provide valuable insights into the atomistic details and the energetics of the processes. However, to study processes like protein folding and protein fibrillation classical MD simulations cannot provide deeper insights as sample conformations that are separated by a high energy barrier (rugged energy landscape) cannot be attained via classical simulations. To overcome such drawbacks enhanced sampling methods like REMD (Replica Exchange Molecular Dynamics) [77,78], umbrella sampling [79] etc are employed. In REMD simulation, several copies of the simulation system are run in parallel at different temperatures and exchange between the adjacent replicas is attempted with the probability provided by Metropolis criterion. The exchange process often allows the conformation to escape an energy minimum, thus enhancing the sample space. In umbrella sampling, conformational dynamics along a reaction coordinates are performed and the relative free energy difference between the states is analyzed [80]. System coordinates are assembled into sets of collective variables, with each set corresponding to an umbrella window. A restraint bias potential (usually a harmonic or a quadratic function) determines the weighting function of each window, thus forces the collective variable to remain within the centre of mass of the window. However, a slight overlap between the windows allows correct reconstruction of the transition [81]. After the simulation, WHAM (Weighted Histogram Analysis Method) [82] is employed to recover the unbiased free energy.

1.5. ABOUT THE PRESENT STUDY

A major part of the thesis deals with the effect of ethylene glycol on the thermal stability (heat and cold denaturation) of proteins. Chapter 2 deals with the effect of ethylene glycol on the stability of proteins against heat and cold. Four model proteins were used in the study (β -lactoglobulin, cytochrome c, myoglobin and α - chymotrypsin). All the four model proteins showed a clear destabilization upon heat denaturation, while showed a significant stabilizing

effect against cold denaturation. Further, upon performing guanidine hydrochloride induced unfolding in presence of ethylene glycol, the proteins were destabilized at room temperature (293 K), while they were stabilized under sub-zero condition (263 K). The thermal and chemical denaturation results were compared with the well-known protein stabilizer glycerol, where the proteins were found to stabilized both against heat and cold denaturation. In order to obtain an atomistic insight into the molecular mechanism of the contrasting nature of ethylene glycol (EG) on the stability of proteins with temperature (chapter 3), MD simulations were performed for all the above proteins at three different temperatures (240K, 300K and 340K) under two different cosolvent concentrations, 20% and 40% (v/v) of EG. The MD simulations suggested that the mode of stabilization of EG under sub-zero temperatures is due to preferential binding of the cosolvent to the protein, thus decreasing the hydrophobic hydration of the proteins, therefore stabilizing the proteins under sub-zero temperatures.

As there was no prominent unfolding of the model proteins in the MD simulations, to confirm the temperature dependant effect, REMD simulation (chapter 4) of α -lactalbumin were performed in two temperature ranges (240- 300K) and (290-340K). Two solvent conditions were employed (i) protein in water and (ii) protein in 30% (v/v) of EG. To confirm that EG imparts a similar temperature dependant effect, heat and cold denaturation of α -lactalbumin was also performed with increasing concentration of EG. The data from both experiments and the simulation reaffirms that EG stabilizes the protein under sub-zero conditions while destabilizes the protein at higher temperatures. Further, dynamics of the solvent and cosolvent around α -lactalbumin also suggested that preferential binding of EG to protein at lower temperature stabilized the protein, while at higher temperature preferential binding resulted in destabilization of the protein as observed in case of other denaturants [70,83,84].

In the last chapter (chapter 5), effect of polyols (ethylene glycol, glycerol. erythritol, xylitol and sorbitol) on the equilibrium intermediate identified during the thermal denaturation of cytochrome c at pH 5 was investigated. The results suggested that all the polyols could destabilize the intermediate. However, the extent of destabilization varied based on the number of -OH groups. EG clearly destabilized the intermediate while glycerol only slightly destabilized the intermediate. In case of ethylene glycol and glycerol, the temperature at which the intermediate is maximally populated also decreased with the increase in the concentration of cosolvent. Higher order polyols such as erythritol, xylitol and sorbitol also slightly

destabilized the intermediate, but the temperature at which maximum population of intermediate exists increased to a higher temperature.

1.6. REFERENCES

- [1] J.S. Richardson, The Anatomy and Taxonomy of Protein Structure, in: C.B. Anfinsen, J.T. Edsall, F.M.B.T.-A. in P.C. Richards (Eds.), Academic Press, 1981: pp. 167–339. https://doi.org/10.1016/S0065-3233(08)60520-3.
- [2] D. Voet, J.G. Voet, Biochemistry, Wiley, 2004. https://books.google.co.in/books?id=EopFAQAAIAAJ.
- [3] W.T. Astbury, A. Street, W.H. Bragg, X-ray studies of the structure of hair, wool, and related fibres.- I. General, Philos. Trans. R. Soc. London. Ser. A, Contain. Pap. a Math. or Phys. Character. 230 (1931) 75–101. https://doi.org/10.1098/rsta.1932.0003.
- [4] W.T. Astbury, H.J. Woods, W.L. Bragg, X-Ray studies of the structure of hair, wool, and related fibres. II.- the molecular structure and elastic properties of hair keratin, Philos. Trans. R. Soc. London. Ser. A, Contain. Pap. a Math. or Phys. Character. 232 (1933) 333–394. https://doi.org/10.1098/rsta.1934.0010.
- [5] A.E. Mirsky, L. Pauling, On the Structure of Native, Denatured, and Coagulated Proteins, Proc. Natl. Acad. Sci. 22 (1936) 439 447. https://doi.org/10.1073/pnas.22.7.439.
- [6] L. Pauling, R.B. Corey, H.R. Branson, The structure of proteins: Two hydrogen-bonded helical configurations of the polypeptide chain, Proc. Natl. Acad. Sci. 37 (1951) 205 211. https://doi.org/10.1073/pnas.37.4.205.
- [7] L.C. Pauling, R.B. Corey, W.T. Astbury, Stable configurations of polypeptide chains, Proc. R. Soc. London. Ser. B Biol. Sci. 141 (1953) 21–33. https://doi.org/10.1098/rspb.1953.0012.
- [8] J.A. Schellman, C.G. Schellman, Kaj Ulrik Linderstrøm-Lang (1896–1959), Protein
 Sci. 6 (1997) 1092–1100. https://doi.org/10.1002/pro.5560060516.

- [9] J.C. Kendrew, G. Bodo, H.M. Dintzis, R.G. Parrish, et al., A Three-Dimensional Model of the Myoglobin Molecule Obtained by X-Ray Analysis, Nature. 181 (1958) 662–666. https://doi.org/10.1038/181662a0.
- [10] M.F. Perutz, M.G. Rossmann, A.N.N.F. Cullis, H. Muirhead, et al., Structure of Hemoglobin: A Three-Dimensional Fourier Synthesis at 5.5-Å. Resolution, Obtained by X-Ray Analysis, Nature. 185 (1960) 416–422. https://doi.org/10.1038/185416a0.
- [11] C.B. Anfinsen, Principles that Govern the Folding of Protein Chains, Science (80-.). 181 (1973) 223 230. https://doi.org/10.1126/science.181.4096.223.
- [12] C. Levinthal, How to fold graciously, Mössbauer Spectrosc. Biol. Syst. Proc. (1969). https://doi.org/citeulike-article-id:380320.
- [13] M. Karplus, D.L. Weaver, Protein folding dynamics: The diffusion-collision model and experimental data, Protein Sci. 3 (1994) 650–668. https://doi.org/10.1002/pro.5560030413.
- [14] M. Karplus, D.L. Weaver, Protein-folding dynamics, Nature. 260 (1976) 404–406. https://doi.org/10.1038/260404a0.
- [15] A.R. Fersht, V. Daggett, Protein Folding and Unfolding at Atomic Resolution, Cell. 108 (2002) 573–582. https://doi.org/10.1016/S0092-8674(02)00620-7.
- [16] S.-Q. Liu, Protein Folding, Binding and Energy Landscape: A Synthesis, in: X.-L. Ji (Ed.), IntechOpen, Rijeka, 2012: p. Ch. 10. https://doi.org/10.5772/30440.
- [17] P.S. Kim, R.L. Baldwin, Specific Intermediates in the Folding Reactions of Small Proteins and the Mechanism of Protein Folding, Annu. Rev. Biochem. 51 (1982) 459–489. https://doi.org/10.1146/annurev.bi.51.070182.002331.
- [18] J.B. Udgaonkar, R.L. Baldwin, NMR evidence for an early framework intermediate on the folding pathway of ribonuclease A, Nature. 335 (1988) 694–699. https://doi.org/10.1038/335694a0.
- [19] J.K. Myers, T.G. Oas, Mechanisms of Fast Protein Folding, Annu. Rev. Biochem. 71 (2002) 783–815. https://doi.org/10.1146/annurev.biochem.71.110601.135346.

- [20] T.R. Sosnick, S. Jackson, R.R. Wilk, S.W. Englander, et al., The role of helix formation in the folding of a fully α-helical coiled coil, Proteins Struct. Funct. Bioinforma. 24 (1996) 427–432. https://doi.org/10.1002/(SICI)1097-0134(199604)24:4<427::AID-PROT2>3.0.CO;2-B.
- [21] D.L. Luisi, B. Kuhlman, K. Sideras, P.A. Evans, et al., Effects of varying the local propensity to form secondary structure on the stability and folding kinetics of a rapid folding mixed α/β protein: characterization of a truncation mutant of the N-terminal domain of the ribosomal protein L911Edited by P. E. W, J. Mol. Biol. 289 (1999) 167–174. https://doi.org/10.1006/jmbi.1999.2742.
- [22] L. Mirny, E. Shakhnovich, Protein Folding Theory: From Lattice to All-Atom Models, Annu. Rev. Biophys. Biomol. Struct. 30 (2001) 361–396. https://doi.org/10.1146/annurev.biophys.30.1.361.
- [23] A.R. Fersht, Nucleation mechanisms in protein folding, Curr. Opin. Struct. Biol. 7 (1997) 3–9. https://doi.org/10.1016/S0959-440X(97)80002-4.
- [24] D.B. Wetlaufer, Nucleation, rapid folding, and globular intrachain regions in proteins, Proc. Natl. Acad. Sci. U. S. A. 70 (1973) 697–701. https://doi.org/10.1073/pnas.70.3.697.
- [25] V.R. Agashe, M.C.R. Shastry, J.B. Udgaonkar, Initial hydrophobic collapse in the folding of barstar, Nature. 377 (1995) 754–757. https://doi.org/10.1038/377754a0.
- [26] A. Bachmann, T. Kiefhaber, Kinetic Mechanisms in Protein Folding, Protein Fold. Handb. (2005) 377–410. https://doi.org/doi:10.1002/9783527619498.ch12a.
- [27] G.R. Spence, A.P. Capaldi, S.E. Radford, Trapping the On-pathway Folding Intermediate of Im7 at Equilibrium, J. Mol. Biol. 341 (2004) 215–226. https://doi.org/10.1016/j.jmb.2004.05.049.
- [28] K. Tejaswi Naidu, N. Prakash Prabhu, Protein–Surfactant Interaction: Sodium Dodecyl Sulfate-Induced Unfolding of Ribonuclease A, J. Phys. Chem. B. 115 (2011) 14760–14767. https://doi.org/10.1021/jp2062496.

- [29] J.N. Onuchic, Z. Luthey-Schulten, P.G. Wolynes, THEORY OF PROTEIN FOLDING: The Energy Landscape Perspective, Annu. Rev. Phys. Chem. 48 (1997) 545–600. https://doi.org/10.1146/annurev.physchem.48.1.545.
- [30] P.G. Wolynes, J.N. Onuchic, D. Thirumalai, Navigating the folding routes, Science (80-.). 267 (1995) 1619 1620. https://doi.org/10.1126/science.7886447.
- [31] J.N. Onuchic, P.G. Wolynes, Z. Luthey-Schulten, N.D. Socci, Toward an outline of the topography of a realistic protein-folding funnel., Proc. Natl. Acad. Sci. 92 (1995) 3626–3630. https://doi.org/10.1073/pnas.92.8.3626.
- [32] S.N. Timasheff, Control of Protein Stability and Reactions by Weakly Interacting Cosolvents: The Simplicity of the Complicated, in: E.B.T.-A. in P.C. Di Cera (Ed.), Link. Thermodyn. Macromol. Interact., Academic Press, 1998: pp. 355–432. https://doi.org/10.1016/S0065-3233(08)60656-7.
- [33] M.B. Burg, J.D. Ferraris, Intracellular Organic Osmolytes: Function and Regulation, J. Biol. Chem. . 283 (2008) 7309–7313. https://doi.org/10.1074/jbc.R700042200.
- [34] P.H. Yancey, Organic osmolytes as compatible, metabolic and counteracting cytoprotectants in high osmolarity and other stresses, J. Exp. Biol. 208 (2005) 2819–2830. https://doi.org/10.1242/jeb.01730.
- [35] J.K. Kaushik, R. Bhat, Thermal Stability of Proteins in Aqueous Polyol Solutions: Role of the Surface Tension of Water in the Stabilizing Effect of Polyols, J. Phys. Chem. B. 102 (1998) 7058–7066. https://doi.org/10.1021/jp9811191.
- [36] S. Taneja, F. Ahmad, Increased thermal stability of proteins in the presence of amino acids, Biochem. J. 303 (1994) 147 153. https://doi.org/10.1042/bj3030147.
- [37] I. Baskakov, A. Wang, D.W. Bolen, Trimethylamine-N-Oxide Counteracts Urea Effects on Rabbit Muscle Lactate Dehydrogenase Function: A Test of the Counteraction Hypothesis, Biophys. J. 74 (1998) 2666–2673. https://doi.org/10.1016/S0006-3495(98)77972-X.

- [38] S.N. Timasheff, The Control of Protein Stability and Association by Weak Interactions with Water: How Do Solvents Affect These Processes?, Annu. Rev. Biophys. Biomol. Struct. 22 (1993) 67–97. https://doi.org/10.1146/annurev.bb.22.060193.000435.
- [39] S.N. Timasheff, Protein-solvent preferential interactions, protein hydration, and the modulation of biochemical reactions by solvent components, Proc. Natl. Acad. Sci. 99 (2002) 9721–9726. https://doi.org/10.1073/pnas.122225399.
- [40] J.A. Schellman, The relation between the free energy of interaction and binding, Biophys. Chem. 45 (1993) 273–279. https://doi.org/10.1016/0301-4622(93)80008-7.
- [41] W.J. Becktel, J.A. Schellman, Protein stability curves, Biopolymers. 26 (1987) 1859–1877. https://doi.org/10.1002/bip.360261104.
- [42] M.M. Santoro, D.W. Bolen, Unfolding free energy changes determined by the linear extrapolation method. 1. Unfolding of phenylmethanesulfonyl .alpha.-chymotrypsin using different denaturants, Biochemistry. 27 (1988) 8063–8068. https://doi.org/10.1021/bi00421a014.
- [43] A.-S. Yang, B. Honig, On the pH Dependence of Protein Stability, J. Mol. Biol. 231 (1993) 459–474. https://doi.org/10.1006/jmbi.1993.1294.
- [44] J. Roche, C.A. Royer, Lessons from pressure denaturation of proteins, J. R. Soc. Interface. 15 (2018) 20180244. https://doi.org/10.1098/rsif.2018.0244.
- [45] F. Schmid, Spectroscopic Techniques to Study Protein Folding and Stability, Protein Fold. Handb. (2005) 22–44. https://doi.org/doi:10.1002/9783527619498.ch2.
- [46] D. Sanfelice, P.A. Temussi, Cold denaturation as a tool to measure protein stability, Biophys. Chem. 208 (2016) 4–8. https://doi.org/10.1016/j.bpc.2015.05.007.
- [47] C.N. Pace, G.R. Grimsley, J.M. Scholtz, Denaturation of Proteins by Urea and Guanidine Hydrochloride, Protein Fold. Handb. (2005) 45–69. https://doi.org/doi:10.1002/9783527619498.ch3.
- [48] B.J. Alder, T.E. Wainwright, Phase Transition for a Hard Sphere System, J. Chem. Phys. 27 (1957) 1208–1209. https://doi.org/10.1063/1.1743957.

- [49] B.J. Alder, T.E. Wainwright, Studies in Molecular Dynamics. I. General Method, J. Chem. Phys. 31 (1959) 459–466. https://doi.org/10.1063/1.1730376.
- [50] A. Rahman, Correlations in the Motion of Atoms in Liquid Argon, Phys. Rev. 136 (1964) A405–A411. https://doi.org/10.1103/PhysRev.136.A405.
- [51] P.K. Weiner, P.A. Kollman, AMBER: Assisted model building with energy refinement. A general program for modeling molecules and their interactions, J. Comput. Chem. 2 (1981) 287–303. https://doi.org/10.1002/jcc.540020311.
- [52] B.R. Brooks, R.E. Bruccoleri, B.D. Olafson, D.J. States, et al., CHARMM: A program for macromolecular energy, minimization, and dynamics calculations, J. Comput. Chem. 4 (1983) 187–217. https://doi.org/10.1002/jcc.540040211.
- [53] W.F. van Gunsteren, Groningen Molecular Simulation (GROMOS) Library Manual, Biomos, Groningen, The Netherlands. (1987) 1–221.
- [54] W.L. Jorgensen, J. Tirado-Rives, The OPLS [optimized potentials for liquid simulations] potential functions for proteins, energy minimizations for crystals of cyclic peptides and crambin, J. Am. Chem. Soc. 110 (1988) 1657–1666. https://doi.org/10.1021/ja00214a001.
- [55] J.W. Ponder, D.A.B.T.-A. in P.C. Case, Force Fields for Protein Simulations, in: Protein Simulations, Academic Press, 2003: pp. 27–85. https://doi.org/10.1016/S0065-3233(03)66002-X.
- [56] F.-Y. Lin, A.D. MacKerell, Force Fields for Small Molecules BT Biomolecular Simulations: Methods and Protocols, in: M. Bonomi, C. Camilloni (Eds.), Springer New York, New York, NY, 2019: pp. 21–54. https://doi.org/10.1007/978-1-4939-9608-7_2.
- [57] A. V Onufriev, S. Izadi, Water models for biomolecular simulations, WIREs Comput. Mol. Sci. 8 (2018) e1347. https://doi.org/10.1002/wcms.1347.
- [58] W.L. Jorgensen, J. Chandrasekhar, J.D. Madura, R.W. Impey, et al., Comparison of simple potential functions for simulating liquid water, J. Chem. Phys. 79 (1983) 926– 935. https://doi.org/10.1063/1.445869.

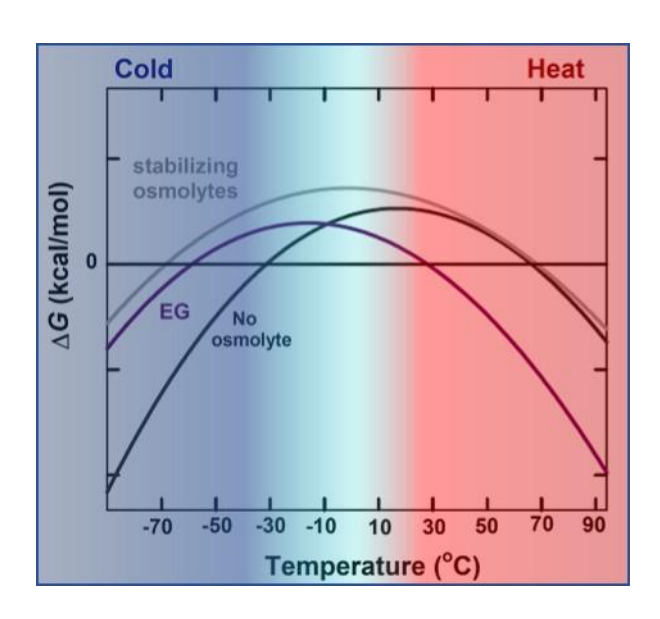
- [59] M.W. Mahoney, W.L. Jorgensen, A five-site model for liquid water and the reproduction of the density anomaly by rigid, nonpolarizable potential functions, J. Chem. Phys. 112 (2000) 8910–8922. https://doi.org/10.1063/1.481505.
- [60] J.L.F. Abascal, C. Vega, A general purpose model for the condensed phases of water: TIP4P/2005, J. Chem. Phys. 123 (2005) 234505. https://doi.org/10.1063/1.2121687.
- [61] J. Åqvist, V.B. Luzhkov, B.O. Brandsdal, Ligand Binding Affinities from MD Simulations, Acc. Chem. Res. 35 (2002) 358–365. https://doi.org/10.1021/ar010014p.
- [62] S. Decherchi, A. Berteotti, G. Bottegoni, W. Rocchia, et al., The ligand binding mechanism to purine nucleoside phosphorylase elucidated via molecular dynamics and machine learning, Nat. Commun. 6 (2015) 6155. https://doi.org/10.1038/ncomms7155.
- [63] N. Haque, K. Baratam, N.P. Prabhu, Analysing the microenvironment of 2-p-toluidinylnaphthalene-6-sulfonate (TNS) in solvents and in different conformational states of proteins in relation to its fluorescence properties: a computational study, Phys. Chem. Chem. Phys. 19 (2017) 24656–24666. https://doi.org/10.1039/C7CP03951D.
- [64] C. Rakers, M. Bermudez, B.G. Keller, J. Mortier, et al., Computational close up on protein–protein interactions: how to unravel the invisible using molecular dynamics simulations?, WIREs Comput. Mol. Sci. 5 (2015) 345–359. https://doi.org/10.1002/wcms.1222.
- [65] A.C. Pan, D. Jacobson, K. Yatsenko, D. Sritharan, et al., Atomic-level characterization of protein–protein association, Proc. Natl. Acad. Sci. 116 (2019) 4244 – 4249. https://doi.org/10.1073/pnas.1815431116.
- [66] N. Haque, N.P. Prabhu, Lid dynamics of porcine pancreatic lipase in non-aqueous solvents, Biochim. Biophys. Acta Gen. Subj. 1860 (2016) 2326–2334. https://doi.org/10.1016/j.bbagen.2016.05.006.
- [67] N. Haque, N.P. Prabhu, Lid closure dynamics of porcine pancreatic lipase in aqueous solution, Biochim. Biophys. Acta Gen. Subj. 1860 (2016) 2313–2325. https://doi.org/10.1016/j.bbagen.2016.05.004.

- [68] D.R. Canchi, D. Paschek, A.E. García, Equilibrium Study of Protein Denaturation by Urea, J. Am. Chem. Soc. 132 (2010) 2338–2344. https://doi.org/10.1021/ja909348c.
- [69] P. Ganguly, P. Boserman, N.F.A. van der Vegt, J.-E. Shea, Trimethylamine N-oxide Counteracts Urea Denaturation by Inhibiting Protein–Urea Preferential Interaction, J. Am. Chem. Soc. 140 (2018) 483–492. https://doi.org/10.1021/jacs.7b11695.
- [70] D.R. Canchi, A.E. García, Cosolvent Effects on Protein Stability, Annu. Rev. Phys. Chem. 64 (2013) 273–293. https://doi.org/10.1146/annurev-physchem-040412-110156.
- [71] B. Anumalla, N.P. Prabhu, Surface hydration and preferential interaction directs the charged amino acids-induced changes in protein stability, J. Mol. Graph. Model. 98 (2020) 107602. https://doi.org/10.1016/j.jmgm.2020.107602.
- [72] K. Vanommeslaeghe, A.D. MacKerell, Automation of the CHARMM General Force Field (CGenFF) I: Bond Perception and Atom Typing, J. Chem. Inf. Model. 52 (2012) 3144–3154. https://doi.org/10.1021/ci300363c.
- [73] K. Vanommeslaeghe, E.P. Raman, A.D. MacKerell, Automation of the CHARMM General Force Field (CGenFF) II: Assignment of Bonded Parameters and Partial Atomic Charges, J. Chem. Inf. Model. 52 (2012) 3155–3168. https://doi.org/10.1021/ci3003649.
- [74] D.M.F. van Aalten, R. Bywater, J.B.C. Findlay, M. Hendlich, et al., PRODRG, a program for generating molecular topologies and unique molecular descriptors from coordinates of small molecules, J. Comput. Aided. Mol. Des. 10 (1996) 255–262. https://doi.org/10.1007/BF00355047.
- [75] A.K. Malde, L. Zuo, M. Breeze, M. Stroet, et al., An Automated Force Field Topology Builder (ATB) and Repository: Version 1.0, J. Chem. Theory Comput. 7 (2011) 4026–4037. https://doi.org/10.1021/ct200196m.
- [76] J. Wang, W. Wang, P.A. Kollman, D.A. Case, Automatic atom type and bond type perception in molecular mechanical calculations, J. Mol. Graph. Model. 25 (2006) 247–260. https://doi.org/10.1016/j.jmgm.2005.12.005.

- [77] C. Yang, S. Jang, Y. Pak, A fully atomistic computer simulation study of cold denaturation of a β-hairpin, Nat. Commun. 5 (2014) 5773. https://doi.org/10.1038/ncomms6773.
- [78] S.B. Kim, J.C. Palmer, P.G. Debenedetti, Computational investigation of cold denaturation in the Trp-cage miniprotein, Proc. Natl. Acad. Sci. 113 (2016) 8991 – 8996. https://doi.org/10.1073/pnas.1607500113.
- [79] J.A. Lemkul, D.R. Bevan, Assessing the Stability of Alzheimer's Amyloid Protofibrils Using Molecular Dynamics, J. Phys. Chem. B. 114 (2010) 1652–1660. https://doi.org/10.1021/jp9110794.
- [80] G.M. Torrie, J.P. Valleau, Nonphysical sampling distributions in Monte Carlo free-energy estimation: Umbrella sampling, J. Comput. Phys. 23 (1977) 187–199. https://doi.org/10.1016/0021-9991(77)90121-8.
- [81] L. Zheng, A.A. Alhossary, C.-K. Kwoh, Y. Mu, Molecular Dynamics and Simulation, in: S. Ranganathan, M. Gribskov, K. Nakai, C.B.T.-E. of B. and C.B. Schönbach (Eds.), Academic Press, Oxford, 2019: pp. 550–566. https://doi.org/10.1016/B978-0-12-809633-8.20284-7.
- [82] S. Kumar, J.M. Rosenberg, D. Bouzida, R.H. Swendsen, et al., THE weighted histogram analysis method for free-energy calculations on biomolecules. I. The method, J. Comput. Chem. 13 (1992) 1011–1021. https://doi.org/10.1002/jcc.540130812.
- [83] B. Adamczak, M. Wieczór, M. Kogut, J. Stangret, et al., Molecular basis of the osmolyte effect on protein stability: a lesson from the mechanical unfolding of lysozyme, Biochem. J. 473 (2016) 3705–3724. https://doi.org/10.1042/BCJ20160604.
- [84] B. Anumalla, N.P. Prabhu, Chain Compaction and Synergistic Destabilization of Globular Proteins by Mixture of Denaturants, ChemistrySelect. 4 (2019) 13797– 13801. https://doi.org/10.1002/slct.201903122.

CHAPTER 2

Cryo vs Thermo: Duality of Ethylene Glycol on the Stability of Proteins



2.1. ABSTRACT

Osmolytes are known to stabilize proteins under stress conditions. In this chapter, we analyse the effect of ethylene glycol (EG), a polyol class of osmolyte, on the stability of four model proteins, β -lactoglobulin, cytochrome c, myoglobin, α -chymotrypsin. In order to obtain a complete stability curve, both heat and cold denaturation of the proteins was carried out in the presence of varying concentrations of EG. The free energy change over the entire temperature range was analysed in the presence and the absence of EG for all the four proteins. The results suggest that the addition of EG stabilizes the proteins against cold-denaturation whereas destabilizes during heat-induced denaturation. Further, chemical denaturation experiments were performed at room temperature and at sub-zero temperature (-10 °C) with increasing concentrations of EG. It was observed that EG imparts stability to the proteins at lower temperature against chemical denaturation, while at room temperature it destabilizes. The results were compared with a well-known stabilising osmolyte, glycerol which stabilized the proteins under all the temperature conditions. To the best of our knowledge, a temperature-dependent differential stabilization effect has not been reported for any other osmolyte and might be specific to EG.

2.2. INTRODUCTION

Temperature governs most of the biochemical processes such as enzyme kinetics, ligand binding, and protein folding ↔ unfolding equilibrium, to name a few. Though most of the proteins effectively function at physiological temperature, food, pharmaceutical and other biotechnology-related industries require the use of sub-zero temperatures for storage of proteins and peptides [1,2]. Nevertheless, freezing can have detrimental effects on proteins including denaturation, aggregation and loss of their activity. The substances used to prevent and protect proteins from these detrimental effects are called cryo-protectants. Many osmolytes can act as cryo-protectants particularly polyol class of osmolytes. Osmolytes are naturally occurring organic molecules used by both plant and animal kingdoms to protect themselves against the natural environmental extremum [3,4]. Accumulation of osmolytes is one of the key survival strategies of the organisms living under extreme conditions such as heat, cold, pressure and high salt [3]. Osmolyte molecules increase or decrease the free energy of unfolding, thus stabilize or destabilize the proteins, respectively [5].

Proteins undergo denaturation under both the extrema of temperatures, termed as heat denaturation (by increase in temperature) and cold denaturation (by decrease in temperature),. There are remarkable differences in the conformations of proteins resulting from heat and cold denaturation. Heat denaturation is an entropically driven process, where the unfolding happens as a result of gain in conformational entropy. The process of cold denaturation is an enthalpically driven caused by the negation in the solvophobic interactions [6–8]. Thermodynamically, the process of protein thermal denaturation is a consequence of an increase in the heat capacity (C_p) and the extent of increase is protein specific [9]. This concludes that the difference in the thermodynamic parameters of the two macroscopic states (native and denatured) are certainly temperature dependent functions. For a thermodynamic process occurring at constant pressure [10],

$$\frac{\partial \Delta H}{\partial T} = \Delta C_p \text{ and } \frac{\partial \Delta S}{\partial T} = \frac{\Delta C_p}{T}$$
 (2.2.1)

Since enthalpy is a state function, the change in enthalpy for the process can be written as

$$\Delta H(T) = H^{D}(T) - H^{N}(T)$$

$$= \Delta H(T^{o}) + \int_{T^{o}}^{T} \Delta C_{p} dT$$

$$= \Delta H(T^{o}) + \Delta C_{p}(T - T^{o}) \qquad (2.2.2)$$

Similarly, entropy can be written as

$$\Delta S(T) = S^{D}(T) - S^{N}(T)$$

$$= \Delta S(T^{o}) + \int_{T^{o}}^{T} \frac{T\Delta C_{p}}{T} dT$$

$$= \Delta S(T^{o}) + \Delta C_{p} \ln \left(\frac{T}{T^{o}}\right)$$
(2.2.3)

Where, ΔC_p is the difference in heat capacity between the denatured and the native state. T^o is a reference temperature and in this case $T^o = T_m$, the transition midpoint temperature.

For the phase transitions like protein unfolding, the change in Gibbs free energy at the transition temperature is equal to zero. Hence,

$$\Delta G = \Delta H(T_m) - T_m \Delta S(T_m) = 0$$
 (2.2.4)

and thus,

$$\Delta S(T_{\rm m}) = \frac{\Delta H(T_{\rm m})}{T_{\rm m}}$$

where, $\Delta H(T^{o})$ is the enthalpy at the transition temperature.

From equation 2.2.2, it is evident that the change in the enthalpy is a linear function of temperature which decrease with decrease in temperature and at a certain temperature it is expected to change its sign to a negative value. This temperature, is called inversion temperature [11], which can be written as

$$T_{\rm inv} = T^{\rm o} - \frac{\Delta H}{\Delta C_{\rm p}}$$
 (2.2.5)

Similarly, the change in entropy is should also decrease with decrease in temperature (equation 2.2.3) but in a nonlinear fashion.

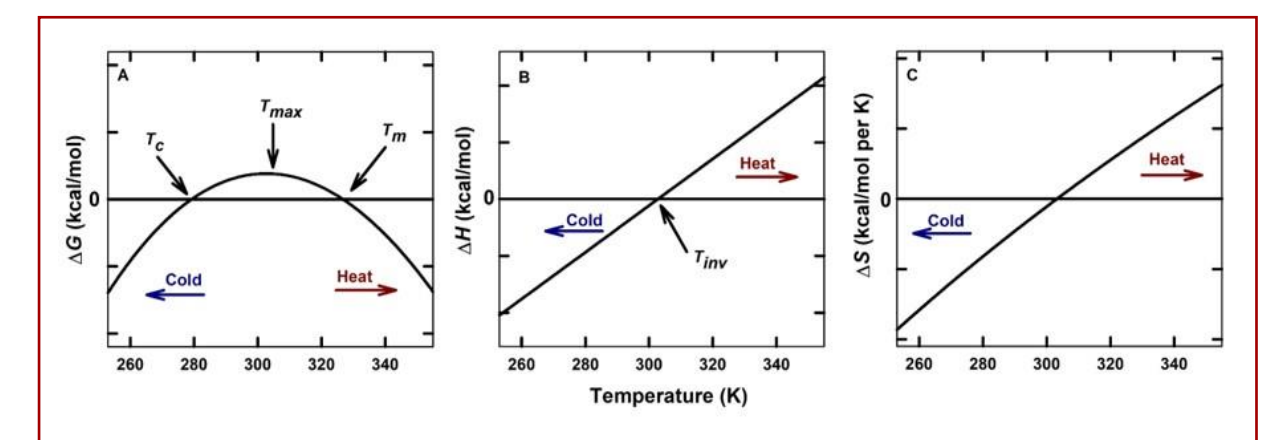


Fig 2.1 Representative plots of temperature dependent change in (A) free energy, (B) enthalpy and (C) entropy during protein unfolding by cold and heat induced denaturation processes. Here in (A) Tm and Tc represents the transition midpoint temperatures of heat and cold transitions, respectively. Tmax is the temperature at which Gibbs free energy of denaturation is at its maximum value. In (B) Tinv is the inversion temperature where change in enthalpy is equal to zero.

The Gibbs free energy difference as a function of temperature for the transition can then be written as following,

$$\Delta G = \Delta H(T_m) \left(1 - \frac{T}{T_m} \right) + \Delta C_p \left(T - T_m - \ln \frac{T}{T_m} \right)$$
 (2.2.6)

A plot of free energy (ΔG), enthalpy (ΔH) and entropy (ΔS) as a function of temperature for a small globular protein that follows a two-state transition is shown in Fig. 2.1. The plot of free energy (ΔG) against temperature is generally referred as a stability curve of a protein (Fig. 2.1A) and has the following salient features. The slope of the plot is given by $\frac{\partial \Delta G}{\partial T} = -\Delta S$. The temperature at which the slope becomes equal to zero ($\Delta S = 0$) is defined as the temperature of maximum stability of the protein (T_{max}). The stability curve intersects the abscissa ($\Delta G = 0$) at two temperature values represented by T_m and T_c . These points constitute the heat and the cold transition midpoint temperatures, respectively. A comparison of the stability curves of different

proteins or a same protein under different conditions is one of the most valuable tools to assess the protein stability.

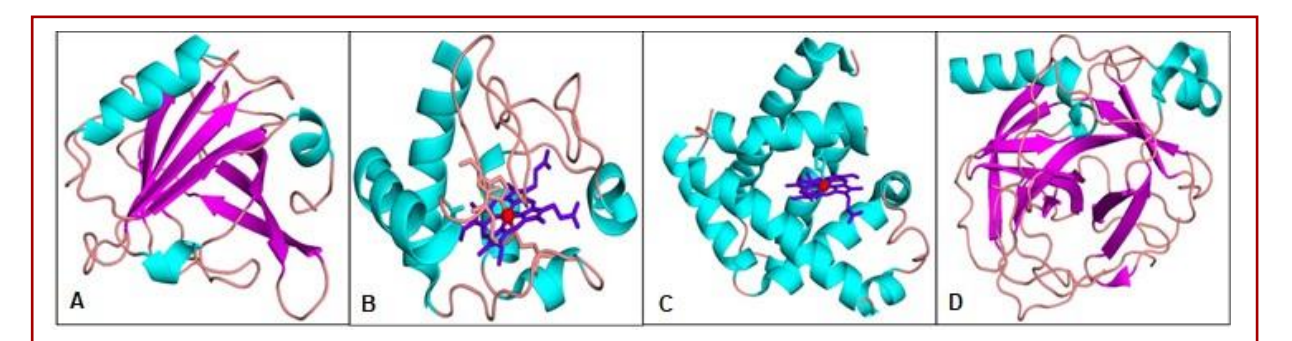


Fig 2.2 Cartoon diagrams of the model proteins used in the study. (A) β -lactoglobulin (3BLG), (B) cytochrome c (1HRC) (C) myoglobin (1YMb) and (D) α -chymotrypsin (1YPH). The three-dimensional structures are from the protein data bank and their PDB ids are given in parentheses. Light blue, pink and brown ribbons represent α -helix, β -sheet and loops, respectively. Purple sticks are heme and red spheres are iron atoms.

Osmolytes hitherto reported are known to either protect proteins against both heat and cold denaturation (for instance, glycerol and sucrose) or promote both heat and cold induced denaturation (for instance, urea) [12–14]. Here, we report the effect of ethylene glycol (EG), a diol, on four model proteins, β -lactoglobulin (BLG), myoglobin (Mb), cytochrome c (Cyt), and α -chymotrypsin (ACT). All the model proteins are different in their sequence, structure (Fig. 2.2) and biological functions. The effect of EG on the proteins were measured by cold- and heat-induced denaturation of the proteins. Also, Gdm- induced unfolding of the proteins in the presence of EG was also measured at room temperature and at a sub-zero temperature as well. The results suggest that EG exhibits a temperature dependent stabilizing effect on the proteins. It destabilizes the proteins at room temperature while stabilizes under sub-zero temperature conditions. The results were compared with that of a well-known protein stabilizer, glycerol (Gly) which stabilizes the proteins against all the denaturing conditions.

2.3. MATERIALS AND METHODS

2.3.1. Materials

All the proteins, bovine β -lactoglobulin, horse myoglobin, horse cytochrome c and bovine α -chymotrypsin were purchased from Sigma-Aldrich. Both the cosolvents ethylene

glycol and glycerol were also from Sigma-Aldrich. Guanidinium chloride (Gdm), urea and all the buffer salts were purchased from SRL Pvt. Ltd.

2.3.2. Thermal denaturation

All the thermal denaturation measurements were recorded using JASCO J1500 circular dichroism spectrophotometer attached to a circulating water bath, Julabo F32. In case of BLG (in 4M urea and pH 2) [15], change in the ellipticity was followed in the near-UV region, while in case of Mb (pH 4) [11], Cyt (in 2 M Gdm at pH 5) and ACT (in 1.5 M Gdm at pH 4) ellipticity changes in the far-UV region were followed to measure the unfolding. All the experiments were performed at a scan rate of 0.5 °C/min. In case of BLG, Cyt and ACT, a low concentration of denaturant was added to induce an early cold denaturation that is within the experimentally accessible range and to reduce the freezing point of the buffer. The concentrations of the denaturants were chosen such that it was within the pre-transition baseline of their corresponding chemical denaturation curves [16–19].

All the denaturation transitions were analysed using a two-state model (Native \leftrightarrow Unfolded). The unfolding transitions were followed by change in ellipticity at 293 nm for BLG, 222 nm for Mb and Cyt, and 230 nm for ACT. The ellipticity values were normalized to calculate the fraction of unfolding at each temperature. From the fraction of unfolding equilibrium constant ($K_{eq} = [\text{Unfolded}]/[\text{folded}]$) was evaluated, and the thermodynamic parameters for the transitions were obtained by fitting the equilibrium constant data to the following equation [20].

$$\ln K_{eq} = A + B\left(\frac{T^{o}}{T}\right) + C\ln\left(\frac{T^{o}}{T}\right)$$
 (2.3.1)

With

$$A = \left[\frac{-\Delta C_{p} + \Delta S_{m}(T^{o})}{R} \right]$$

$$B = \left[\frac{\Delta C_{p} - \Delta S_{m}(T^{o})}{R} \right] - \frac{\Delta G'(T^{o})}{RT_{m}}$$

$$C = -\frac{\Delta C_p}{R}$$

Where, T^o is the transition temperature, $\Delta G'$ is the change in the Gibbs free energy of the transition, ΔS_m is the change in entropy at the transition temperature and ΔC_p is the change in the heat capacity of the transition. The $\ln K_{eq}$ values at different temperatures were used to calculate the protein stability curve i.e. change in free energy vs temperature. The stability curves were extrapolated to lower temperatures, if necessary, to evaluate the thermodynamic parameters for the cold denaturation process. The ΔC_p is assumed to be constant for entire temperature range [20–22].

2.3.3. Chemical denaturation

Chemical denaturation of the proteins was performed at 293 and 263 K using Gdm as a denaturant. The protein samples were prepared in varying concentration of the denaturant and were pre-incubated in a water bath at 293 or 263 K for 45 minutes before recording their spectra. In case of BLG and ACT, intrinsic fluorescence of the protein at 332 nm was used to follow the unfolding of the protein after exciting the samples at 280 nm. The measurements were performed in JASCO FP8500 spectrofluorometer connected with a circulating water bath. In case of Mb and Cyt, unfolding transitions were followed using the changes in ellipticity at 222 nm. All the chemical denaturation transitions were also analysed using the two-state model [23] with the following equation.

$$Y = \frac{\frac{(y_f + m_f[Gdm]) + (y_u + m_u[Gdm])e}{RT}}{\frac{\left((-\Delta G_{unf} + m_g[Gdm])\right)}{RT}}$$

$$1 + e^{\frac{\left((-\Delta G_{unf} + m_g[Gdm])\right)}{RT}}$$
(2.3.2)

Where Y is the normalized spectroscopic signal for the unfolding fraction, y_f and y_u are the intercepts of the native and the unfolded baselines, m_f and m_u are the corresponding slopes of the native and the unfolded baselines, respectively. ΔG_{unf} is the Gibbs free energy of unfolding and m_g is the slope of the transition region. R is the gas constant and T is the experimental temperature.

2.4. RESULTS

2.4.1. Thermal denaturation of Proteins

The structural stability of all four model proteins upon changing the solution temperature, from 300 to 350 K and also from 300 to 255 K, was monitored by the change in ellipticity of the proteins in the presence of varying concentrations of EG. As a control experiment, stability of the proteins was also measured in presence of 20% of glycerol. Gly is known to stabilize proteins against various temperature and pH stress conditions [12,24]. The unfolding thermograms of all the four proteins (Fig. 2.3 A1-D1), suggested that upon addition of EG,

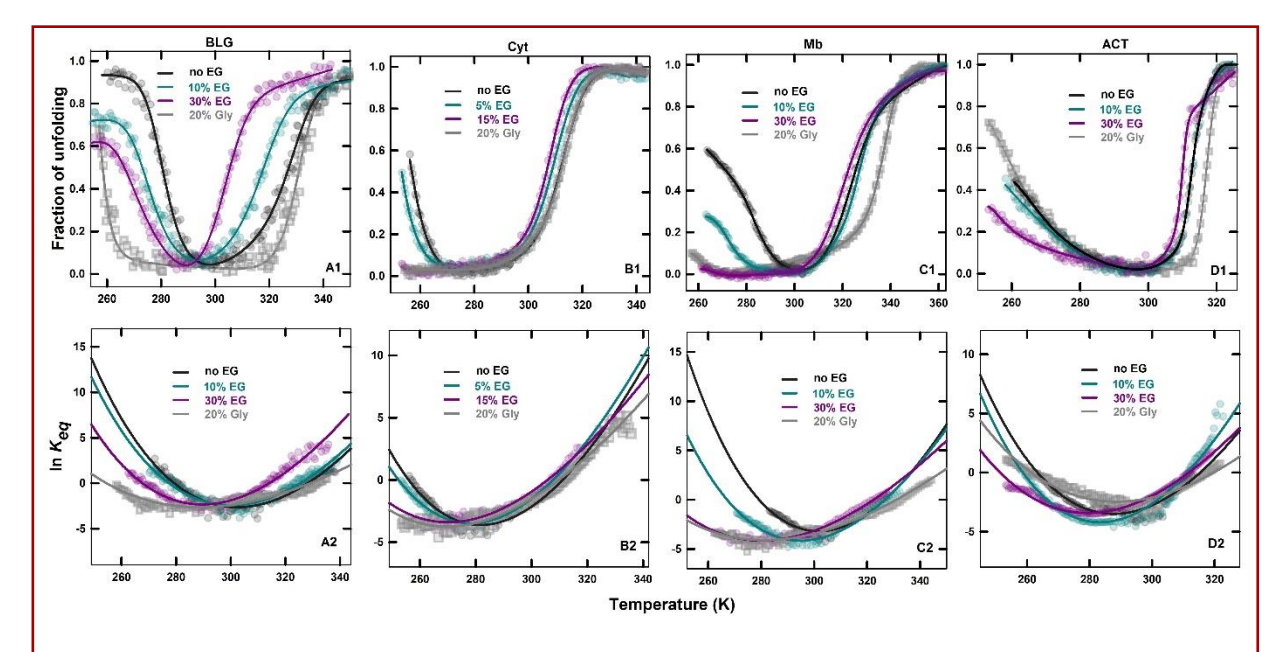


Fig 2.3. (A1-D1) Representative plots of fraction of unfolding measured against temperature for BLG, Cyt, Mb and ACT in the absence (black) and the presence of EG (cyan and pink), and in the presence of Gly (grey). The solid lines are for visual clarity to follow the changes. (A2-D2) Representative plots of $\ln K_{eq}$ calculated from the fraction of unfolding of the proteins in the absence (black circles) and in the presence (pink circles) of EG. The solid lines are data fit using equation. 2.3.1.

the heat denaturation was induced earlier whereas cold denaturation occurred later than in absence of EG. Using the two-state assumption, the fractions of unfolded and folded forms were calculated, and the equilibrium constants as a function of temperature were determined. The resultant plots are presented in Fig. 2.3 (A2-D2) and were fit to constant ΔC_p model using equation 2.3.1. Change in the free energy of the proteins against temperature (Fig. 2.4 A1-D1) was calculated from the transitions and the transition midpoint temperatures of the heat

 (T_m) and cold denaturation (T_c) were estimated by locating the points on the free energy curve, where $\Delta G = 0$.

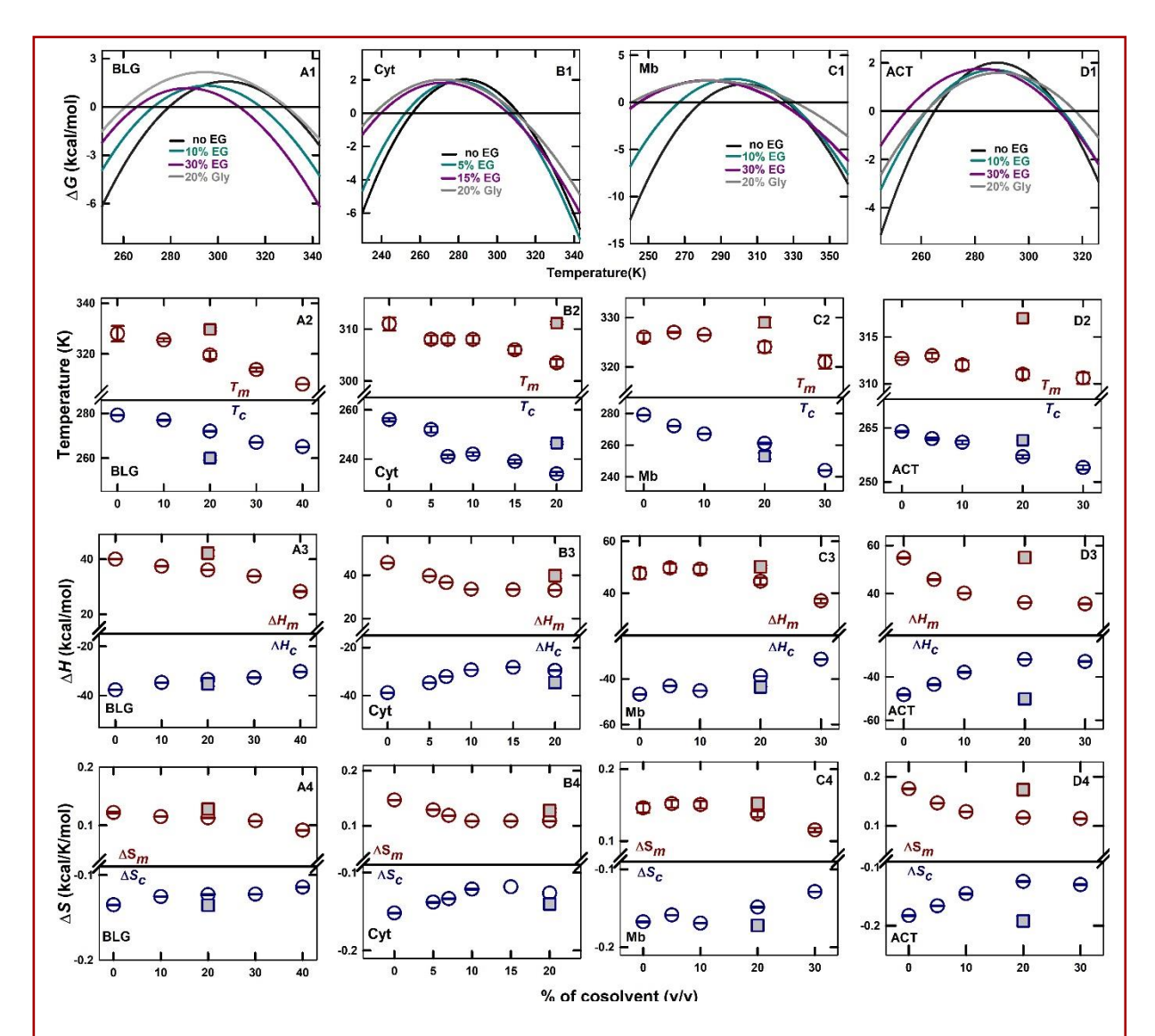


Fig 2.4. Free energy of unfolding of BLG (A1), Cyt (B1), Mb (C1) and ACT (D1) calculated from the transition curves in Fig. 2.3 in the absence (black) and in presence of EG (cyan and pink) or Gly (grey). Transition midpoints of heat-induced denaturation, Tm (red), and cold-induced denaturation, Tc (blue), for (A2) BLG, (B2) Cyt, (C2) Mb and (D2) in the absence and presence of varying concentrations of EG (circles) and in the presence of 20% Gly (squares). Enthalpy of unfolding measured at transition midpoint temperatures of heat- and cold-induced denaturation, Δ Hm (red) and Δ Hc (blue), respectively, for (A3) BLG (B3) Cyt (C3) Mb and (D3) ACT. Entropy of unfolding measured at transitions midpoint temperatures of heat- and cold-induced denaturation, Δ Sm (red) and Δ Sc (blue), respectively represented as T Δ S values for (A4) BLG, (B4) Cyt, (C4) Mb and (D4) ACT in the absence and the presence of varying concentrations of EG (T-transition midpoint temperature).

The values of the transition midpoints suggested that the proteins were destabilized in presence of EG during heat denaturation, thus lowering the T_m value whereas they were stabilized during cold denaturation as T_c values were further lowered to sub-zero temperatures (Fig. 2.4 A2-D2). In the presence of Gly, T_m value was slightly increased and T_c value decreased suggesting that Gly stabilized the protein against both heat and cold induced denaturation. The enthalpy of unfolding of heat-induced denaturation (ΔH_m) decreased upon the addition of EG whereas it was slightly increased in presence of Gly. The enthalpy changes upon cold denaturation (ΔH_c) is negative as observed in the case of other globular proteins [20,25], and it increased upon the addition of both EG and Gly (Fig. 2.4 A3-D3). The entropy of unfolding calculated at midpoint temperature, ΔS_m and ΔS_c also showed the similar trend for all the four proteins (Fig. 2.4 A4-D4).

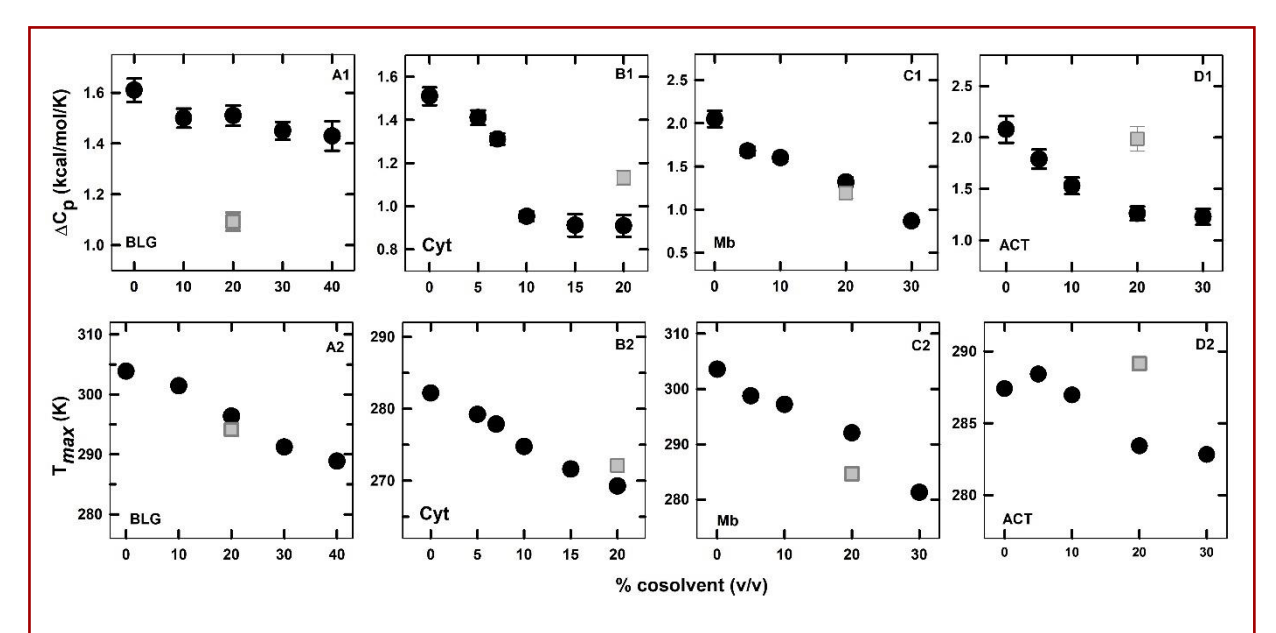


Fig 2.5. The change in heat capacity (Δ Cp) during thermal denaturation of the proteins (A1-D1), and the temperature of maximum stability (Tmax) of the proteins (A2-D2) in presence of varying concentrations of EG (black circles) and Gly (grey squares) evaluated from their respective free energy curves in Fig. 2.4 A1-D1 and using equation 2.3.1.

The change in heat capacity (ΔC_p) of the overall thermal transitions were evaluated from their respective free energy curves (Fig. 2.5 A1-D1). ΔC_p values of all of the four proteins decreased upon addition of EG, though the extent of decrease was marginal in case of BLG. Further, the temperature of maximum stability (T_{max} , the temperature at which $\Delta S = 0$), was also evaluated for all the proteins (Fig. 2.5 A2-D2). The addition of EG and Gly, shifted the

 T_{max} towards lower temperature. It may be noted that the addition of cosolvents such as Gdm and ficoll [14,26] do not change the T_{max} values of proteins during thermal denaturation, but alcohols shift the T_{max} value towards lower temperature [13]. These observations suggest that the change in T_{max} might be specific to the interaction of osmolytes with the proteins.

2.4.2. Chemical denaturation of proteins

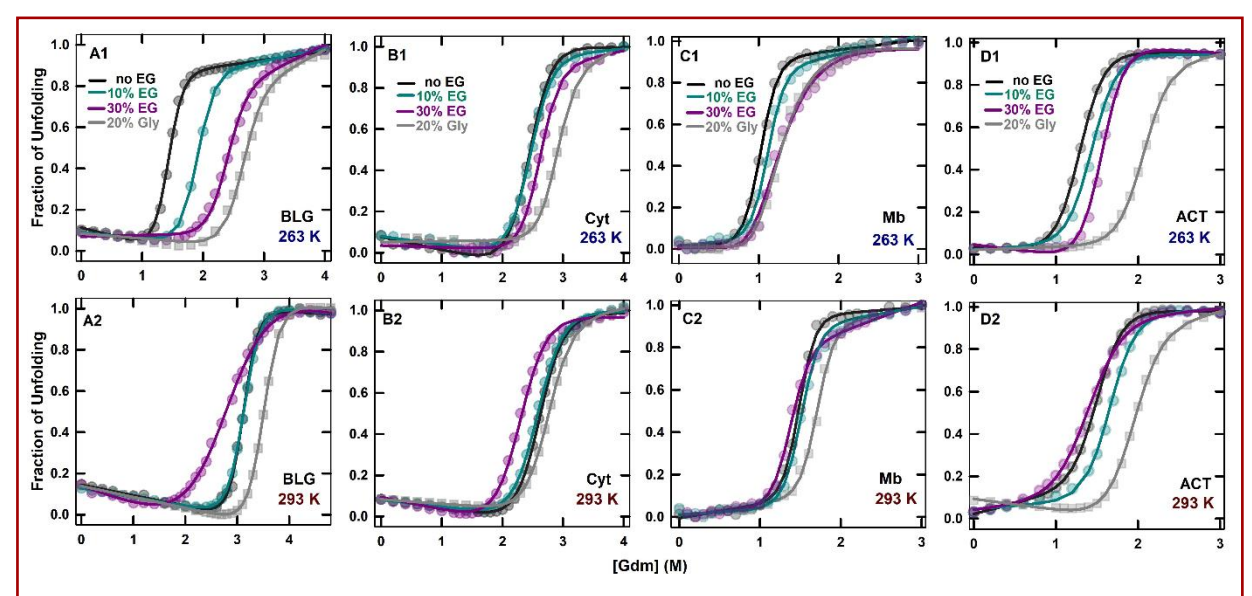


Fig 2.6. Representative Gdm-induced denaturation transitions of the proteins BLG, Cyt, Mb and ACT carried out at 263 K (A1-D1) and at 293 K (A2-D2) in the absence (black) and the presence of (cyan and pink) of EG and in the presence of Gly (grey). The solid lines represent data-fit with an assumption of two-state transition using equation 2.3.2.

To further ascertain the temperature dependent changes on the effect of EG, Gdm-induced unfolding of all the four model proteins was performed in presence of varying concentrations of EG at 263 K and at 293 K. The chemical denaturation curves of all the model proteins measured at 263 K showed that the transitions were moved towards higher denaturant concentration upon addition of both EG and Gly (Fig. 2.6 A1-D1). When the experiments were performed at 293 K, the transitions shifted to a lower denaturant concentration with the addition of EG, whereas they moved toward the higher side in the presence of Gly in all proteins (Fig. 2.6 A2-D2).

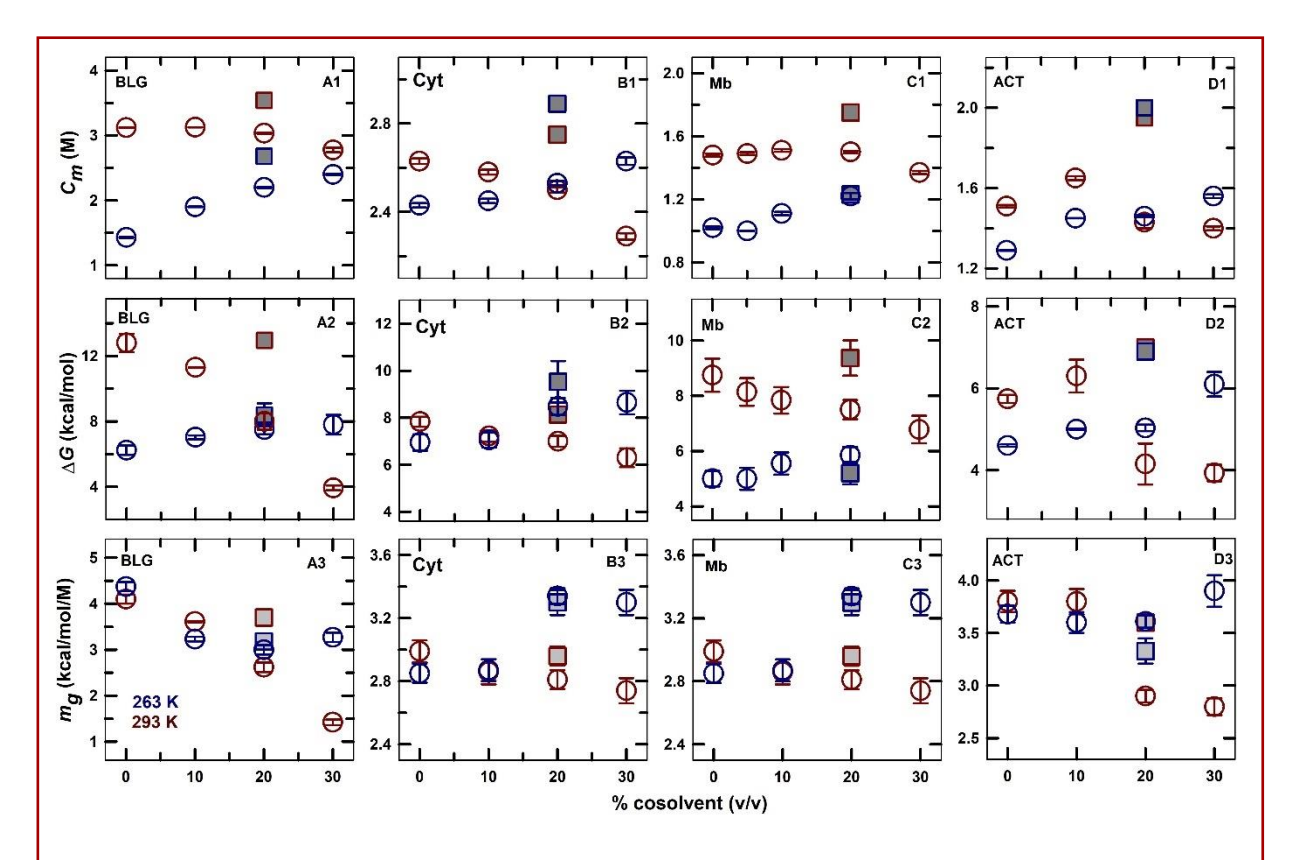


Fig 2.7. Upper panels: the unfolding transition midpoint concentrations (C_ms) from Gdm-induced denaturation of (A1) BLG, (B1) Cyt, (C1) Mb, and (D1) ACT measured at 263 K (blue) and 293 K (red) in the absence and presence of varying concentrations of EG (circles) and in the presence of 20% Gly (squares). Middle panels: free energy of unfolding (ΔGunf) calculated from the Gdm-induced denaturation transitions at 263 K (blue) and at 293 K (blue) in the presence of EG (circles) or Gly (squares) for (A2) BLG, (B2) Cyt, (C2) Mb, and (D2) ACT. Lower panels: The mg-values of chemical denaturation transitions of the proteins, (A3) BLG, (B3) Cyt, (C3) Mb, and (D3) ACT measured at 263 K (blue) and at 293 K (red) in the absence and presence of varying concentrations of EG (circles) and in presence of 20% Gly. The values were calculated from their respective chemical denaturation transition curves (Fig. 2.6) using equation 2.3.2.

From the transition curves, the midpoint concentration (C_m), the free energies of unfolding (ΔG_{unf}) and the slopes of the unfolding transitions (m_g) were evaluated by a nonlinear least square fit of the denaturation curves to equation 2.3.2 (Fig. 2.7). The C_m (Fig. 2.7 A1-D1) values and ΔG_{unf} (Fig. 2.7 A2-D2) at 263 K increased upon addition of EG and Gly suggesting stabilization of the proteins by both the osmolytes. At 293 K there was a decrease in both the values of C_m (Fig. 2.7 A1-D1) and ΔG_{unf} (Fig. 2.7 A2-D2) upon increase in the concentration of EG whereas the values slightly increased in presence of Gly. The only exception found was the case of ACT, where at lower concentration of EG, there was a slight

increase in both the parameters suggesting a slight stabilization, but at higher concentrations there was a clear destabilizing effect. Further, the m_g values, the slope of the unfolding transitions, were also analyzed for all the denaturation transitions (Fig. 2.7 A3-D3). The m_g values increased upon the addition of EG at 263 K, except in the case of BLG. However, it is decreased with the increase in the concentration of EG at 293 K.

2.5. DISCUSSION

2.5.1. Effect of EG on thermal denaturation

Characterization of thermodynamic stability of proteins against temperature would not be fully complete without analysing the cold-induced denaturation process of the proteins [27]. For evaluating the effect of osmolyte molecules, the energy profiles of the proteins covering both heat and cold denaturation processes are to be investigated.

Experimental investigation on the effect of EG on the thermal stability of four globular proteins indicate that the proteins are destabilized during heat denaturation while there is a stabilizing effect against cold denaturation. The overall change in the free energy profiles of the proteins upon addition of EG (Fig. 2.4 A1-D1) is a combined effect of decrease in ΔC_p (Fig. 2.5 A1-D1) and shift in T_{max} value towards lower temperatures (Fig. 2.5 A2-D2). The curvature of a free energy curve can be defined as $\approx \Delta C_p/T$ and the decrease in ΔC_p broadens the curvature [13,28]. This accompanied with the change in T_{max} provides pronounced shift in both T_m and T_c values towards lower temperature. This demonstrates that the addition of EG can broaden the stability range of the proteins around T_{max} . Further, the low-temperature stabilization is associated with decrease in both negative enthalpy and entropy. Since the negative enthalpy could be attributed to the hydrophobic hydration of the proteins at low temperature, the decreasing value might indicate the reduction of hydration of hydrophobic residues upon the addition of EG. At the same time, the increase in entropy (less negative) might arise due to increasing configurational entropy of water molecules. Destabilization of the proteins by EG during heat-induced unfolding transitions, on the other hand, is due to decrease in both enthalpy and entropy. This is similar to the changes observed with the addition of denaturants such as urea and Gdm during the thermal denaturation of proteins [14] rather than stabilizing osmolytes such as Gly [24].

2.5.2. Enthalpy-entropy compensation

The enthalpy-entropy compensation of EG-induced changes on the proteins can be analysed by plotting $\Delta\Delta H_m$ (ΔH_m in water - ΔH_m in EG) against $T\Delta\Delta S_m$ ($T\Delta S_m$ in water - $T\Delta S_m$ in EG, where T represents the transition midpoint temperature). The combined analysis of enthalpy-entropy contributions [29,30] of the thermal transitions of all the four proteins (Fig. 2.8) suggest that the stabilization effect imparted by EG during cold denaturation is mainly enthalpy-driven. For small cosolutes, it has been proposed that enthalpic contribution would be significant in the stabilization of macromolecules [31]. The destabilization by EG during heat denaturation might arise due to a decrease in the enthalpy of unfolding similar to the effect of denaturant molecules such as urea, which induces enthalpy-driven destabilization [14]. These thermodynamic parameters suggest that the soft interactions between the protein and EG could be the major factor in altering the stability, which could be mainly governed by preferential interaction of the cosolutes [31].

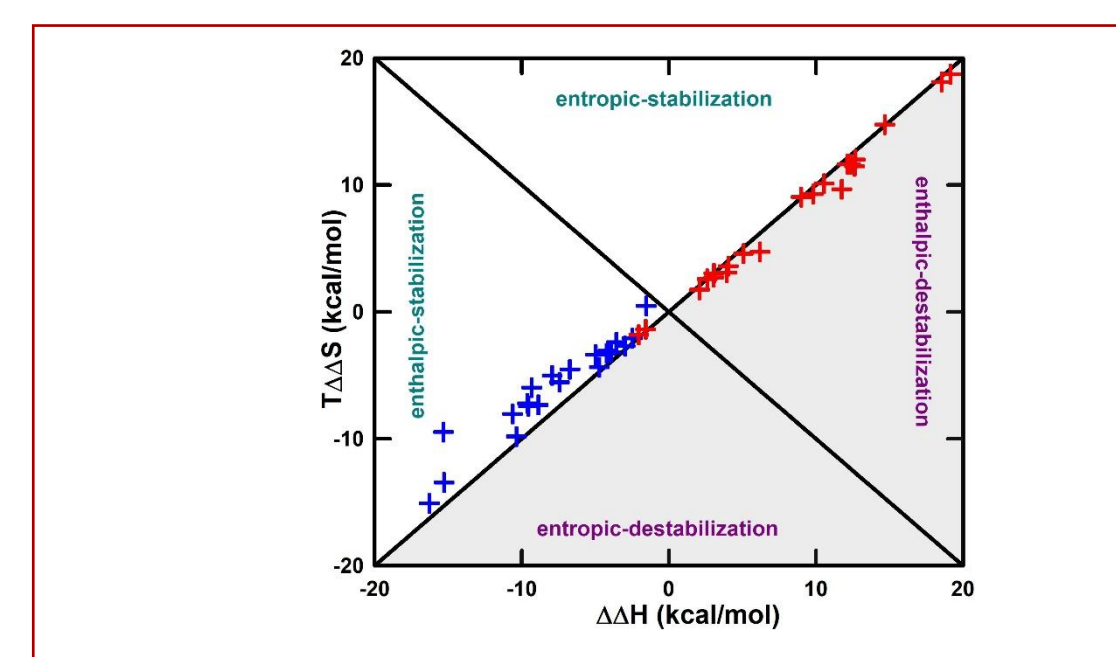


Fig 2.8. Enthalpy-entropy plot for EG-induced changes on the stability of the proteins. The blue crosses represent the changes observed during cold denaturation and red crosses represent the changes during heat denaturation in the presence of varying concentrations of EG calculated for all the four model proteins.

Polyols and alcohols are reported to alter protein stability similarly during heat- and cold-denaturation condition [12,13]; however, only EG shows difference in its effect. There are

certain ionic liquids such as 1-butyl-3-methylimidazolium that shows a differential effect on protein stability [32], but this is the first report on a polyol class of osmolyte.

The extent of stabilization is not found to be equal to the extent of destabilization exerted by EG (in terms of either temperature midpoint or enthalpy of unfolding) on the same protein. It is observed that the stabilization provided by EG during cold denaturation is slightly larger than its destabilizing effect at higher temperature. Most of the osmolytes and denaturants as well show such inequality [14,33]. For instance, guanidinium hydrochloride (Gdm) destabilizes T4 lysozyme and its effect is more pronounced at sub-zero temperature compared to the ambient temperature [20]. Yeast frataxin is stabilized by lower concentrations of alcohols against cold and heat denaturation, but the extent of stability is more against cold denaturation [13]. However, in the case of barstar, the effect of Gdm is almost same against both heat- and cold- induced unfolding transitions [14]. These variations are generally attributed to the difference in the structure of heat- and cold-induced unfolded states and the difference in their unfolding pathways [34,35].

2.5.3. Effect of EG on Gdm-induced unfolding

The free energy of unfolding (ΔG_{unf}) (Fig. 2.7 A2-D2) and concentration midpoint (C_m) (Fig. 2.7 A1-D1) values obtained from Gdm-induced denaturation of the proteins (Fig. 2.6 and 2.7) also suggest that EG stabilizes the proteins at sub-zero temperature similar to Gly and destabilizes them at room temperature. Interestingly, the stability of all the proteins is less at 263 K (-10 °C) compared to those at 293 K (20 °C) in the absence of EG. The m_g -value of chemical denaturation represents the exposure of buried residues during unfolding [36]. An increase in mg values, at lower temperatures, in the presence of EG (except for BLG) suggests that EG might preferentially interact with the hydrophobic residues of the proteins. The decrease in mg values at higher temperatures upon addition of EG could be due to its mild denaturing effects [37]. This further emphasizes that the change in hydration of the proteins could be the major factor for the dual behaviour of EG.

2.6. CONCLUSION

The experimental results evidently show that EG imparts different effects on the stability of the proteins during heat- and cold-induced denaturation. The chemical denaturation studies carried out at room temperature and at sub-zero temperature further confirm the fact that EG acts as a stabilizing osmolyte at sub-zero temperature whereas it is a destabilizing osmolyte at room temperature. Such an effect has not been observed so far for any other osmolyte molecule against proteins. The cold denaturation is found to be enthalpy-driven and the enthalpy of denaturation reduces upon addition of EG suggesting the probable reduction of hydrophobic hydration of the proteins. Further, the addition of either EG or Gly, broadens the stability range of the proteins and shifts the temperature of maximum stability to lower temperature.

2.7. REFERENCES

- [1] J.-R. Authelin, M.A. Rodrigues, S. Tchessalov, S.K. Singh, et al., Freezing of Biologicals Revisited: Scale, Stability, Excipients, and Degradation Stresses, J. Pharm. Sci. 109 (2020) 44–61. https://doi.org/https://doi.org/10.1016/j.xphs.2019.10.062.
- [2] N. Rathore, R.S. Rajan, Current Perspectives on Stability of Protein Drug Products during Formulation, Fill and Finish Operations, Biotechnol. Prog. 24 (2008) 504–514. https://doi.org/10.1021/bp070462h.
- [3] M.B. Burg, J.D. Ferraris, Intracellular Organic Osmolytes: Function and Regulation, J. Biol. Chem. . 283 (2008) 7309–7313. https://doi.org/10.1074/jbc.R700042200.
- [4] P.H. Yancey, Organic osmolytes as compatible, metabolic and counteracting cytoprotectants in high osmolarity and other stresses, J. Exp. Biol. 208 (2005) 2819 2830. https://doi.org/10.1242/jeb.01730.
- [5] M. Auton, J. Rösgen, M. Sinev, L.M.F. Holthauzen, et al., Osmolyte effects on protein stability and solubility: A balancing act between backbone and side-chains, Biophys. Chem. 159 (2011) 90–99. https://doi.org/https://doi.org/10.1016/j.bpc.2011.05.012.

- [6] K.A. Dill, D.O. V Alonso, K. Hutchinson, Thermal stabilities of globular proteins, Biochemistry. 28 (1989) 5439–5449. https://doi.org/10.1021/bi00439a019.
- [7] P.L. Privalov, Cold Denaturation of Protein, Crit. Rev. Biochem. Mol. Biol. 25 (1990) 281–306. https://doi.org/10.3109/10409239009090613.
- [8] G. Graziano, On the molecular origin of cold denaturation of globular proteins, Phys. Chem. Chem. Phys. 12 (2010) 14245–14252. https://doi.org/10.1039/C0CP00945H.
- [9] P.L. Privalov, Stability of Proteins Small Globular Proteins, in: C.B. Anfinsen, J.T. Edsall, F.M.B.T.-A. in P.C. Richards (Eds.), Academic Press, 1979: pp. 167–241. https://doi.org/https://doi.org/10.1016/S0065-3233(08)60460-X.
- [10] P.L. Privalov, S.A.B.T.-M. in E. Potekhin, [2]Scanning microcalorimetry in studying temperature-induced changes in proteins, in: Enzym. Struct. Part L, Academic Press, 1986: pp. 4–51. https://doi.org/https://doi.org/10.1016/0076-6879(86)31033-4.
- [11] P.L. Privalov, Y.V. Griko, S.Y. Venyaminov, V.P. Kutyshenko, Cold denaturation of myoglobin, J. Mol. Biol. 190 (1986) 487–498. https://doi.org/https://doi.org/10.1016/0022-2836(86)90017-3.
- [12] X. Tang, M.J. Pikal, The Effect of Stabilizers and Denaturants on the Cold Denaturation Temperatures of Proteins and Implications for Freeze-Drying, Pharm. Res. 22 (2005) 1167–1175. https://doi.org/10.1007/s11095-005-6035-4.
- [13] S.R. Martin, V. Esposito, P. De Los Rios, A. Pastore, et al., Cold Denaturation of Yeast Frataxin Offers the Clue to Understand the Effect of Alcohols on Protein Stability, J. Am. Chem. Soc. 130 (2008) 9963–9970. https://doi.org/10.1021/ja803280e.
- [14] V.R. Agashe, J.B. Udgaonkar, Thermodynamics of Denaturation of Barstar: Evidence for Cold Denaturation and Evaluation of the Interaction with Guanidine Hydrochloride, Biochemistry. 34 (1995) 3286–3299. https://doi.org/10.1021/bi00010a019.

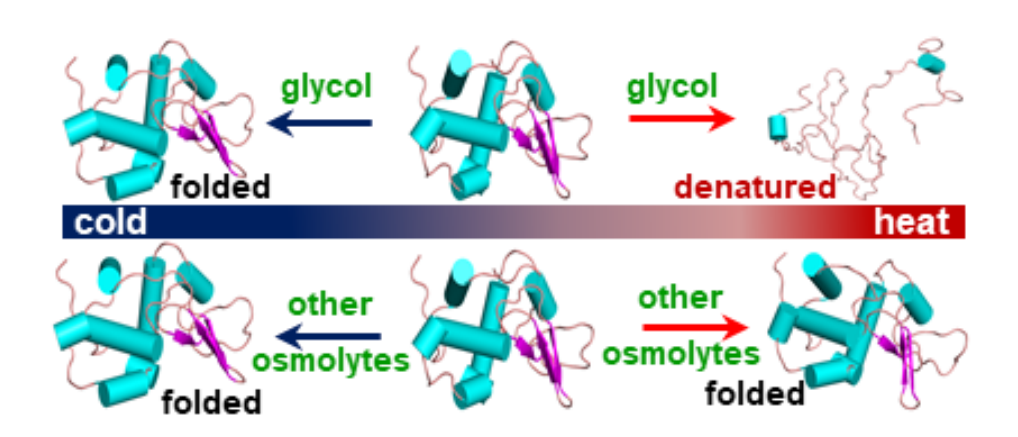
- [15] Y. V Griko, P.L. Privalov, Calorimetric study of the heat and cold denaturation of .beta.-lactoglobulin, Biochemistry. 31 (1992) 8810–8815. https://doi.org/10.1021/bi00152a017.
- [16] C.N. Pace, C. Tanford, Thermodynamics of the unfolding of β-lactoglobulin A in aqueous urea solutions between 5 and 55°, Biochemistry. 7 (1968) 198–208. https://doi.org/10.1021/bi00841a025.
- [17] M. Davidovic, C. Mattea, J. Qvist, B. Halle, Protein Cold Denaturation as Seen From the Solvent, J. Am. Chem. Soc. 131 (2009) 1025–1036. https://doi.org/10.1021/ja8056419.
- [18] R.F. Latypov, H. Cheng, N.A. Roder, J. Zhang, et al., Structural Characterization of an Equilibrium Unfolding Intermediate in Cytochrome c, J. Mol. Biol. 357 (2006) 1009–1025. https://doi.org/https://doi.org/10.1016/j.jmb.2006.01.055.
- [19] R.F. Greene, C.N. Pace, Urea and Guanidine Hydrochloride Denaturation of Ribonuclease, Lysozyme, α-Chymotrypsin, and β-Lactoglobulin, J. Biol. Chem. . 249 (1974) 5388–5393. http://www.jbc.org/content/249/17/5388.abstract.
- [20] B.L. Chen, J.A. Schellman, Low-temperature unfolding of a mutant of phage T4 lysozyme. 1. Equilibrium studies, Biochemistry. 28 (1989) 685–691. https://doi.org/10.1021/bi00428a041.
- [21] W.J. Becktel, J.A. Schellman, Protein stability curves, Biopolymers. 26 (1987) 1859–1877. https://doi.org/10.1002/bip.360261104.
- [22] N. V Prabhu, K.A. Sharp, HEAT CAPACITY IN PROTEINS, Annu. Rev. Phys. Chem. 56 (2004) 521–548. https://doi.org/10.1146/annurev.physchem.56.092503.141202.
- [23] M.M. Santoro, D.W. Bolen, Unfolding free energy changes determined by the linear extrapolation method. 1. Unfolding of phenylmethanesulfonyl .alpha.-chymotrypsin using different denaturants, Biochemistry. 27 (1988) 8063–8068. https://doi.org/10.1021/bi00421a014.

- [24] S. Jain, J.C. Ahluwalia, Synergetic effect of polyols with tetrabutylammonium bromide and urea on the thermal stability of lysozyme, Thermochim. Acta. 302 (1997) 17–24. https://doi.org/https://doi.org/10.1016/S0040-6031(97)00149-4.
- [25] A. Pastore, S.R. Martin, A. Politou, K.C. Kondapalli, et al., Unbiased Cold Denaturation: Low- and High-Temperature Unfolding of Yeast Frataxin under Physiological Conditions, J. Am. Chem. Soc. 129 (2007) 5374–5375. https://doi.org/10.1021/ja0714538.
- [26] A.P. D. Sanfelice, A. Politou, S. R. Martin, P. De Los Rios, P. Temussi, The effect of crowding and confinement: a comparison of Yfh1 stability in different environments, Phys. Biol. 10 (2013) 5002. http://dx.doi.org/10.1016/0022-2836(77)90078-X.
- [27] D. Sanfelice, P.A. Temussi, Cold denaturation as a tool to measure protein stability, Biophys. Chem. 208 (2016) 4–8. https://doi.org/https://doi.org/10.1016/j.bpc.2015.05.007.
- [28] B.W.J. and S.J. A, Protein stability curves, Biopolymers. 26 (1987) 1859.http://dx.doi.org/10.1002/bip.360261104.
- [29] R. Politi, D. Harries, Enthalpically driven peptide stabilization by protective osmolytes, Chem. Commun. 46 (2010) 6449–6451. https://doi.org/10.1039/C0CC01763A.
- [30] S. Sukenik, L. Sapir, D. Harries, Balance of enthalpy and entropy in depletion forces, Curr. Opin. Colloid Interface Sci. 18 (2013) 495–501. https://doi.org/https://doi.org/10.1016/j.cocis.2013.10.002.
- [31] L. Sapir, D. Harries, Macromolecular Stabilization by Excluded Cosolutes: Mean Field Theory of Crowded Solutions, J. Chem. Theory Comput. 11 (2015) 3478–3490. https://doi.org/10.1021/acs.jctc.5b00258.
- [32] M. Senske, D. Constantinescu-Aruxandei, M. Havenith, C. Herrmann, et al., The temperature dependence of the Hofmeister series: thermodynamic fingerprints of cosolute–protein interactions, Phys. Chem. Chem. Phys. 18 (2016) 29698–29708. https://doi.org/10.1039/C6CP05080H.

- [33] C. Alfano, D. Sanfelice, S.R. Martin, A. Pastore, et al., An optimized strategy to measure protein stability highlights differences between cold and hot unfolded states, Nat. Commun. 8 (2017) 15428. https://doi.org/10.1038/ncomms15428.
- [34] S.B. Kim, J.C. Palmer, P.G. Debenedetti, Computational investigation of cold denaturation in the Trp-cage miniprotein, Proc. Natl. Acad. Sci. 113 (2016) 8991 – 8996. https://doi.org/10.1073/pnas.1607500113.
- [35] Y. Yamada, T. Yajima, K. Fujiwara, M. Arai, et al., Helical and Expanded Conformation of Equine β-Lactoglobulin in the Cold-denatured State, J. Mol. Biol. 350 (2005) 338–348. https://doi.org/https://doi.org/10.1016/j.jmb.2005.05.003.
- [36] J.K. Myers, C. Nick Pace, J. Martin Scholtz, Denaturant m values and heat capacity changes: Relation to changes in accessible surface areas of protein unfolding, Protein Sci. 4 (1995) 2138–2148. https://doi.org/10.1002/pro.5560041020.
- [37] A.K. Bhuyan, R. Kumar, Kinetic Barriers to the Folding of Horse Cytochrome c in the Reduced State, Biochemistry. 41 (2002) 12821–12834. https://doi.org/10.1021/bi0204443.

CHAPTER 3

Molecular Mechanism of Temperature-Dependent Stabilizing Nature of Ethylene Glycol



3.1. ABSTRACT

Protein stability in a mixed solvent system is determined by relative abundance of cosolvent and solvent molecules in the bulk and solvation domains. To understand the differential effect of ethylene glycol on protein stability (reported in chapter 2), preferential interaction of ethylene glycol with all the four-model proteins (β -lactoglobulin, cytochrome c, myoglobin, α -chymotrypsin) was studied at 240, 300 and 340 K using molecular dynamics simulation. The simulation studies suggested that ethylene glycol preferentially binds to the proteins at all the three temperatures. It was also observed that ethylene glycol preferably accumulates around the hydrophobic residues of the proteins and reduces the hydrophobic hydration of the proteins at lower temperature leading to stabilization of the proteins at 240 K. This is in contrast to the preferential interaction hypothesis on protein stability which proposes that an osmolyte is completely excluded from the protein surface to impart stability to the protein. At 340 K, however, reduction of preferential hydration of the protein, and the preferential binding of EG destabilizes the protein like common denaturants.

3.2. INTRODUCTION

Addition of cosolvents will have a significant influence on the structural stability [1,2] and biological activity [3] of proteins. Cosolvents such as glycerol, TMAO, and glutamate (termed as compatible osmolytes or protein stabilizers) are known to stabilize proteins [4–6], while urea and arginine are known (termed as non-compatible osmolytes or denaturants) to denature proteins to a varying degree [7,8]. Cosolvent molecules alter the chemical potential of a protein in the system by either strong or weak association, a phenomenon referred to as "preferential interaction" [9]. The change in chemical potential of a protein upon addition of cosolvent (X) is depicted as [10]

$$\Delta \mu_{\rm P}^{\rm tr} = \int_0^{m_{\rm X}} (\frac{\partial \mu_{\rm P}}{\partial m_{\rm X}})_{\rm m_{\rm P}} \, \mathrm{d}m_{\rm X} \tag{3.2.1}$$

$$= -\int_0^{m_X} \left(\frac{\partial \mu_X}{\partial m_X}\right)_{m_P} \left(\frac{\partial m_X}{\partial m_P}\right)_{\mu_X} dm_X$$
 (3.2.2)

Where $\Delta \mu_P^{tr}$ is the free energy of transfer of protein from water to a mixed solvent system, m is the molality. The subscripts P and X corresponds to protein and cosolvent, respectively. In equation 3.2.2 the first partial derivative corresponds to the dependence of cosolvent's chemical potential on its molality and the second term is called the "preferential binding coefficient" (Γ_{XP}):

$$\Gamma_{\rm XP} = \left(\frac{\partial m_{\rm X}}{\partial m_{\rm P}}\right)_{\mu_{\rm X}} \tag{3.2.3}$$

The preferential binding coefficient (particularly useful when the binding is weak and non-specific) is the measure of excess or deficit of cosolvent molecules in the protein hydration domain as compared to the bulk [11]. A broad range of priori experimental and simulation studies suggests that a denaturant would exhibit a positive Γ_{XP} value, thus reduces the protein's chemical potential resulting in denaturation (preferential binding), while a protein stabilizer exhibits a negative Γ_{XP} value and increases the chemical potential of the protein (preferential hydration) [12–17].

In order to elucidate the molecular mechanism behind the differential effect of ethylene glycol (EG) with temperature on protein stability (as discussed in Chapter 2), molecular dynamics (MD) simulations of the protein were performed in the presence of EG. MD simulations are proven to be an invariable tool to obtain a comprehensive understanding of processes that occur in the time scale of femtoseconds to milliseconds [18,19]. This includes the processes such as protein dynamics, protein ligand interactions, protein stability and solvent dynamics to name a few [20-23]. The term MD simulations underlines the use of a potential energy function interpreted in terms of inter- and intra-molecular forces to model a molecular system [24]. MD simulations of four model proteins, β-lactoglobulin (BLG), myoglobin (Mb), cytochrome c (Cyt), and α-chymotrypsin (ACT) were performed at three different temperatures (240 K, 300 K and 340 K) in absence and in presence of 20% and 40% (v/v) of EG. The results were analysed according to the theory of preferential interaction. The data suggests that the preferential binding of EG at sub-zero temperatures resulted in stabilizing the protein, while at higher temperatures it resulted in destabilization. The stabilizing effect at lower temperature might be a result of EG's interaction with the hydrophobic residues of the protein and protecting them from hydrophobic hydration.

3.3. METHODS

All the MD simulations were performed in GROMACS [25] molecular dynamics package (Version 5.1.4). Three dimensional structures of the model proteins were obtained from protein data bank having the PDB ids 3blg (BLG), 1hrc (Cyt), 1ymb (Mb) and 1yph (ACT) [26]. After the removal of any ligands in the PDB structure, the protein was placed in a virtual box and filled with water molecules. This system was energy minimized using CHARMM 36 force field [27]. The system was then equilibrated for NVT (N: number of particles in the system, V: system Volume and T: absolute Temperature) and NPT (N: number of particles in the system, P: system Pressure and T: absolute Temperature) ensemble conditions for 1 ns each using V- rescale thermostat [28] and Parrinello- Rahman barostat [29] for 300 K temperature and 1 atm pressure, respectively. Following this, production simulation was carried out for 100 ns. To study the effect of EG, water molecules in the system were replaced with EG to obtain the concentration of either 20% of EG or 40% of EG. These systems were also simulated with the above conditions. All the four protein simulations with and without EG were carried out for the temperature conditions 240 K and 340 K as well. Since the

simulations are of wide range of temperature, TIP4P-2005 water model was used for all the simulations. This water model has been optimized and tested for the temperature ranging from 123 K to 573 K [30]. The list of the simulations performed are given in Table 3.1.

Table 3.1. List of MD Simulations

Protein	PDB id	Solvent system (% in v/v)	Temperature (K)	Simulation Time (ns) [†]
		Water (TIP4P-2005)	240 K	
β-lactoglobulin (BLG)	3BLG	20 % EG	300 K	900
		40 % EG	340 K	
Cytochrome c (Cyt)	1HRC	- do -	- do -	900
Myoglobin (Mb)	1YMB	- do -	- do -	900
α-chymotrypsin (ACT)	1YPH	- do -	- do -	900
		Tota	al simulation time	3600

^{† -} simulation run for 100 ns in each solvent condition at each temperature

The parameters of EG (Fig. 3.1) were obtained from CGenFF [31,32] and are tabulated in Table 3.2.

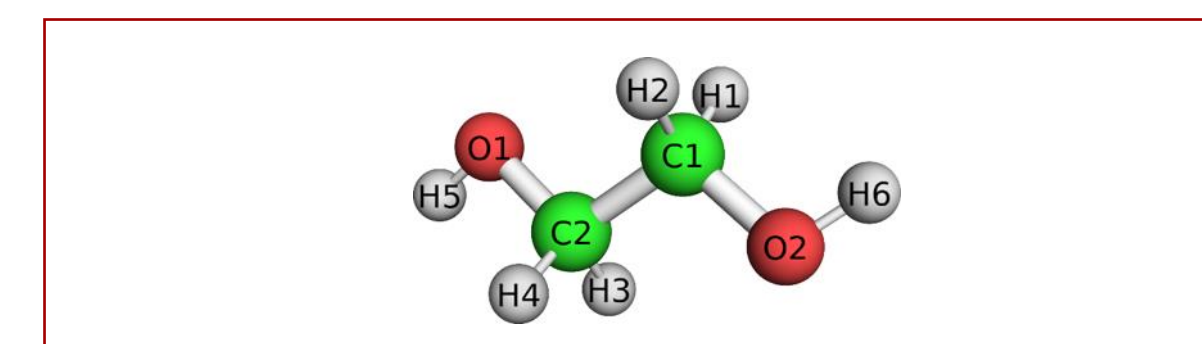


Fig 3.1 Ball and stick model of ethylene glycol with the atom labels as used in the simulation parameter file shown in Table 3.2.

Atom label	Mass	Charge	Atom type [†]
C1 and C2	12.011	0.050	CG321
H1, H2, H3, H4	1.008	0.090	HGA2
O1 and O2	15.999	-0.650	OG311
H5 and H6	1.008	0.420	HGP1

Table 3.2. Parameters of EG used in MD simulation

3.4. ANALYSIS

The parameters of EG were validated by calculating heat of vaporization (ΔH_{vap}) [33] and density of EG. ΔH_{vap} was calculated from the following relation.

$$\Delta H_{\text{vap}} = H_{\text{gas}} - H_{\text{liquid}}$$

$$= U_{\text{gas}} - U_{\text{liquid}} + P(V_{\text{gas}} - V_{\text{liquid}}) \qquad (3.4.1)$$

 $V_{gas} >> V_{liquid}$ as the assumption is that of ideal gas

$$= U_{gas} - U_{liquid} + P(V_{gas})$$

$$= U_{gas} - \frac{U_{liquid}}{n_{mol}} + RT$$
(3.4.2)

Where U_{gas} and U_{liquid} are the potential energies in liquid and gas phases, R is the universal gas constant and T is the temperature. To calculate U_{gas} , EG molecule was simulated in vacuo. Density of EG was calculated directly using the gmx density tool.

Root mean square deviation (RMSD) and the solvent accessible surface area (SASA) were calculated using gromacs tools gmx rms and gmx sasa. Radial distribution function (RDF) was calculated using gmx rdf tool of gromacs. RDF of water around protein was evaluated by indexing the oxygen of water molecules and the heavy-atoms of proteins. RDF of EG around protein was derived by indexing oxygens of EG and the heavy atoms of protein. The number of hydrogen bonds between protein and solvent from each simulation trajectory was obtained

[†] As obtained from CGenFF.

using Gromacs tool gmx hound with the default distance and angle cut-off of 0.35 nm and 30°, respectively [34].

To analyse the preferential interaction of EG from the simulation trajectories, two different parameters were employed. First is the local-bulk partition coefficient (K_p) that is evaluated using the following relation [35].

$$K_p = \frac{\langle n_{EG} \rangle N_W^{tot}}{\langle n_W \rangle N_{EG}^{tot}}$$
 (3.4.3)

Where $\langle n_{EG} \rangle$ and $\langle n_W \rangle$ are the average number of EG and water molecules within 0.5 nm distance from the protein surface, while N_W^{tot} and N_{EG}^{tot} are the total number of EG and water molecules in the system. $K_p > 1$ would suggest that the accumulation of the cosolvent around the protein is higher than its bulk concentration. The average value of last 40 ns of the respective simulations were considered for analysis.

The other parameter is preferential interaction coefficient [2,36,37] of EG (Γ_{EG}) that was calculated from the surface of the protein to 0.8 nm for every 0.1 Å interval using the following relation with an in-house python code,

$$\Gamma_{EG} = \langle n_{EG} - \frac{N_{EG} - n_{EG}}{N_W - n_W} n_W \rangle$$
 (3.4.4)

where n_{EG} and n_W represents the number of EG and water molecules within the distance cutoff from the surface of the protein. N_{EG} and N_W represents the total number of EG and water molecules in the system. For calculating Γ_{EG} values, the average values of the last 40 ns of the respective simulation trajectories were considered. The preferential interaction coefficients calculated in the 20% EG and 40% EG are labelled as (Γ_{20-EG}) and (Γ_{40-EG}), respectively.

The interaction of water molecules with the hydrophobic residues were calculated as hydrophobic hydration such that

hydrophobic hydration =
$$\frac{\langle n_{W-hyd} \rangle / hydrophobic - SASA}{\langle n_{W-pol} \rangle / polar - SASA}$$
 (3.4.5)

where, n_{W-hyd} and n_{W-pol} is the number of water molecules nearer to hydrophobic residues and polar residues, respectively, within the cut-off of 0.4 nm from the surface of the proteins representing the second hydration shell. The hydrophobic and polar solvent accessible surface area (SASA) values were calculated from the MD simulation using Gromacs tool gmx sasa and the average value of the last 40 ns was used to calculate the hydrophobic hydration. Similarly, the interaction of EG with the hydrophobic residues of the proteins were calculated as hydrophobic cosolvation,

hydrophobic hydration =
$$\frac{\langle n_{EG-hyd} \rangle / hydrophobic - SASA}{\langle n_{EG-pol} \rangle / polar - SASA}$$
 (3.4.6)

where n_{EG-hyd} and n_{EG-pol} is the number of EG nearer to hydrophobic residues and polar residues, respectively.

3.5. RESULTS

3.5.1. Validation of parameters of EG

The simulation parameters of EG derived from CGenFF were validated by calculating the heat of vaporization (ΔH_{vap}) of pure EG and comparing it with the experimental data from literature [38]. The ΔH_{vap} value obtained from the MD simulation of EG, calculated using equation 3.4.2, was 68 kJ/mol which is found to be within the error range of experimentally derived value of 65 \pm 3 kJ/mol. Further, the densities of different concentration of EG calculated from MD simulation (Table 3.3) were also within 5% of deviation from the experimental values [39].

Table 3.3. Densities of EG calculated from simulation

S. No.	% of EG (v/v)	Density (kg m ⁻³)	Density (kg m ⁻³)
		(Experimental data)	(Calculated from simulation)
1	20	1025	1024
2	40	1052	1034
3	60	1076	1045
4	80	1095	1055
5	100	1110	1065

3.5.2. Structural changes of proteins in different solvent conditions with temperature

In order to analyse the molecular mechanism of EG induced changes on the proteins at different temperatures, MD simulations of the proteins were performed at 240, 300 and 340 K in absence and in the presence of 20% (v/v) and 40% (v/v) of EG (Table 3.1).

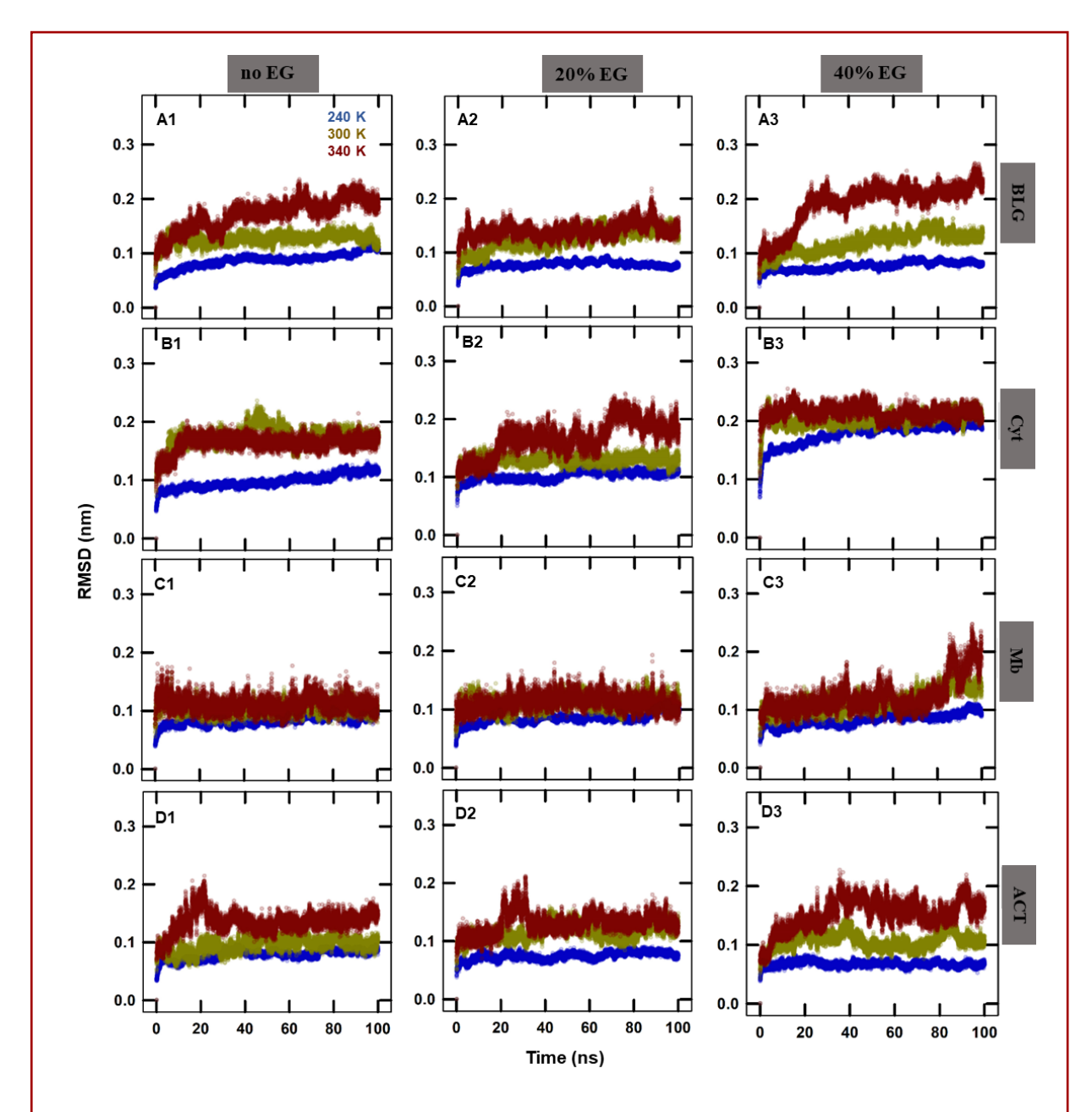


Fig. 3.2. Root mean square deviation (RMSD) of $C\alpha$ atoms of (A1-A3) BLG, (B1-B3) Cyt, (C1-C3) Mb and (D1-D3) ACT calculated from their respective MD simulations performed at 240 K (blue), 300 K (yellow) and 340 K (red) in the absence (A1-D1) and in presence of 20% EG (A2-D2) and 40% EG (A3-D3).

The structural distortion in the proteins during the course of the simulation were initially analysed by calculating the root mean square deviation (RMSD) of the $C\alpha$ atoms. The data suggests that the mean fluctuations of the proteins were higher at 340 K (Fig. 3.2). In presence of EG, the RMSD was slightly reduced at 240 K, whereas it was slightly increased at 340 K as compared in the absence of EG (Fig. 3.2 A2-A3, B2-B3, C2-C3 and D2-D3).

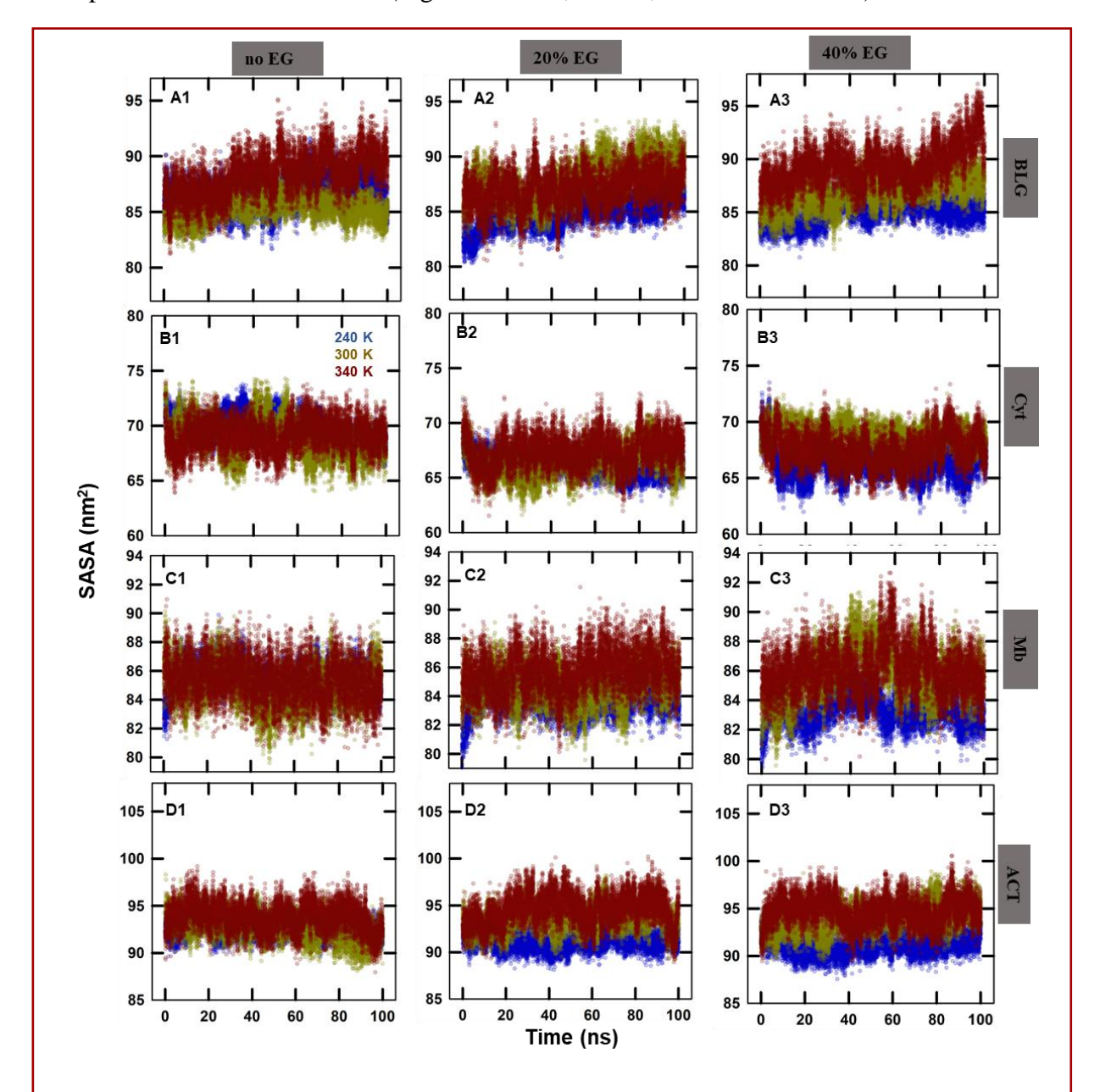


Fig. 3.3. Solvent accessible surface area (SASA) of (A1-A3) BLG, (B1-B3) Cyt, (C1-C3) Mb and (D1-D3) ACT, calculated from their respective MD simulations performed at 240 K (blue), 300 K (yellow) and 340 K (red) in the absence (A1-D1) and in presence of 20% EG (A2-D2) and 40% EG (A3-D3).

Further the structural integrity of the proteins was also assessed using the SASA (Fig. 3.3). In presence of EG, SASA values decreased at 240 K, while there was a slight increase at 340 K. The representative structures obtained from each simulation is presented in Fig. 3.4.

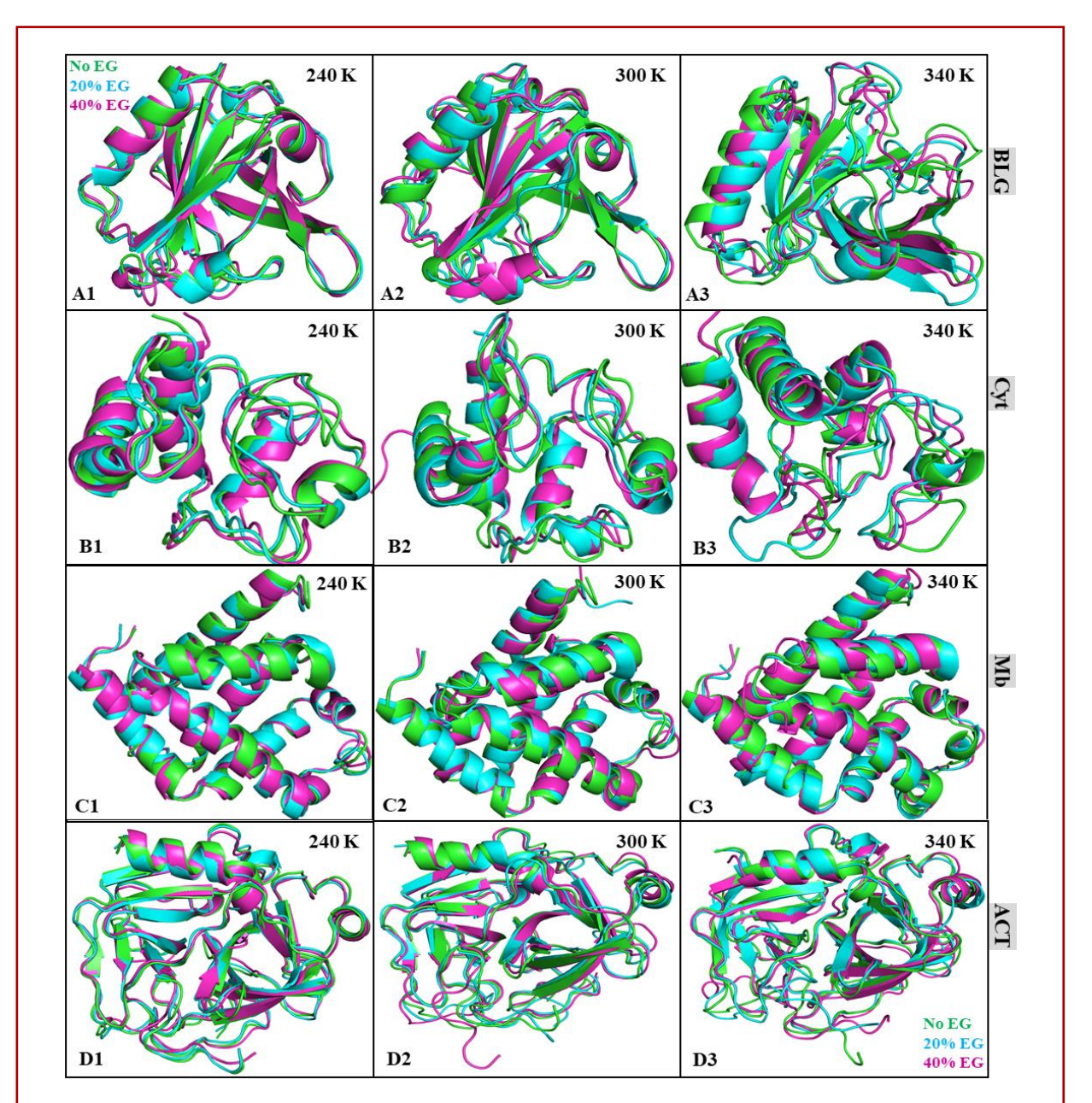


Fig. 3.4. Representative structure of the proteins, (A1-A3) BLG, (B1-B3) Cyt, (C1-C3) Mb, and (D1-D3) ACT obtained from the MD simulations carried out in the absence (green) and in the presence of 20% EG (blue) and 40% EG (pink) at 240 K (left panels), 300 K (middle panels) and 340 K (right panels). For better visualisation, heme groups are not shown in Cyt and Mb.

3.5.3. Distribution of solvent and cosolvent around proteins

The distribution of water and EG around the proteins were initially analysed using radial distribution function (RDF) calculated using heavy-atoms of the proteins as reference sites. RDF plot of water around the protein showed a maxima at 0.26 and 0.37 nm distance from the surface of the protein that are consistent with the earlier studies on protein-water interactions[17,41,42] (Fig. 3.5 A1-D3). As the simulation temperature increased from 240 K

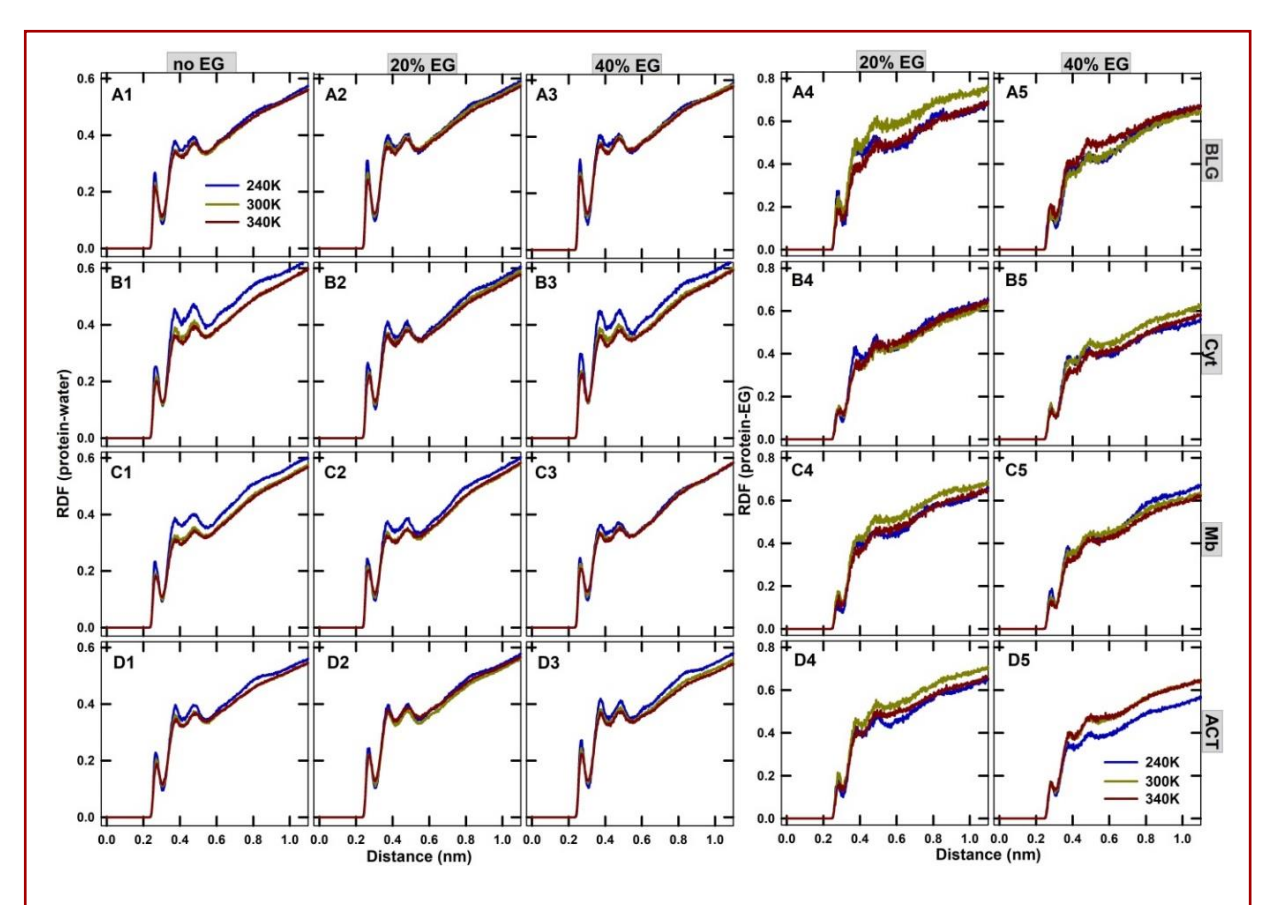


Fig. 3.5. Radial distribution functions calculated with reference to the heavy atoms of the proteins to evaluate water around the proteins for (A1-A3) BLG, (B2-B3) Cyt, (C1-C3) Mb, and (D1-D3) ACT in the absence (A1-D1), and in the presence of 20% EG (A2-D2), and 40% EG (A3-D3) at 240 K (blue), 300 K (green) and 340 K (red). Radial distribution functions of EG around the proteins calculated for (A4-A5) BLG, (B4-B5) Cyt, (C4-C5) Mb, and (D4-D5) ACT in the presence of 20% EG (A4-D4), and 40% EG (A5-D5).

to 300 K, there was a notable decrease in the water density in the first and second hydration shells in all the four proteins (Fig. 3.6 A1-B4). Such a temperature dependent change in water density around the protein has been observed earlier as well [43,44]. Similarly, the RDF

values were calculated for the distribution of EG around the proteins as well (Fig. 3.5 A4-D5). The first and the second minima were observed at 0.28 nm and 0.40 nm which again corresponds to the first and the second hydration shells of the proteins (Fig. 3.6 C1-C4 and D1-D4). The RDFs of protein-EG interactions for both first and second solvation shells did not show any common behaviour in their temperature-dependent changes.

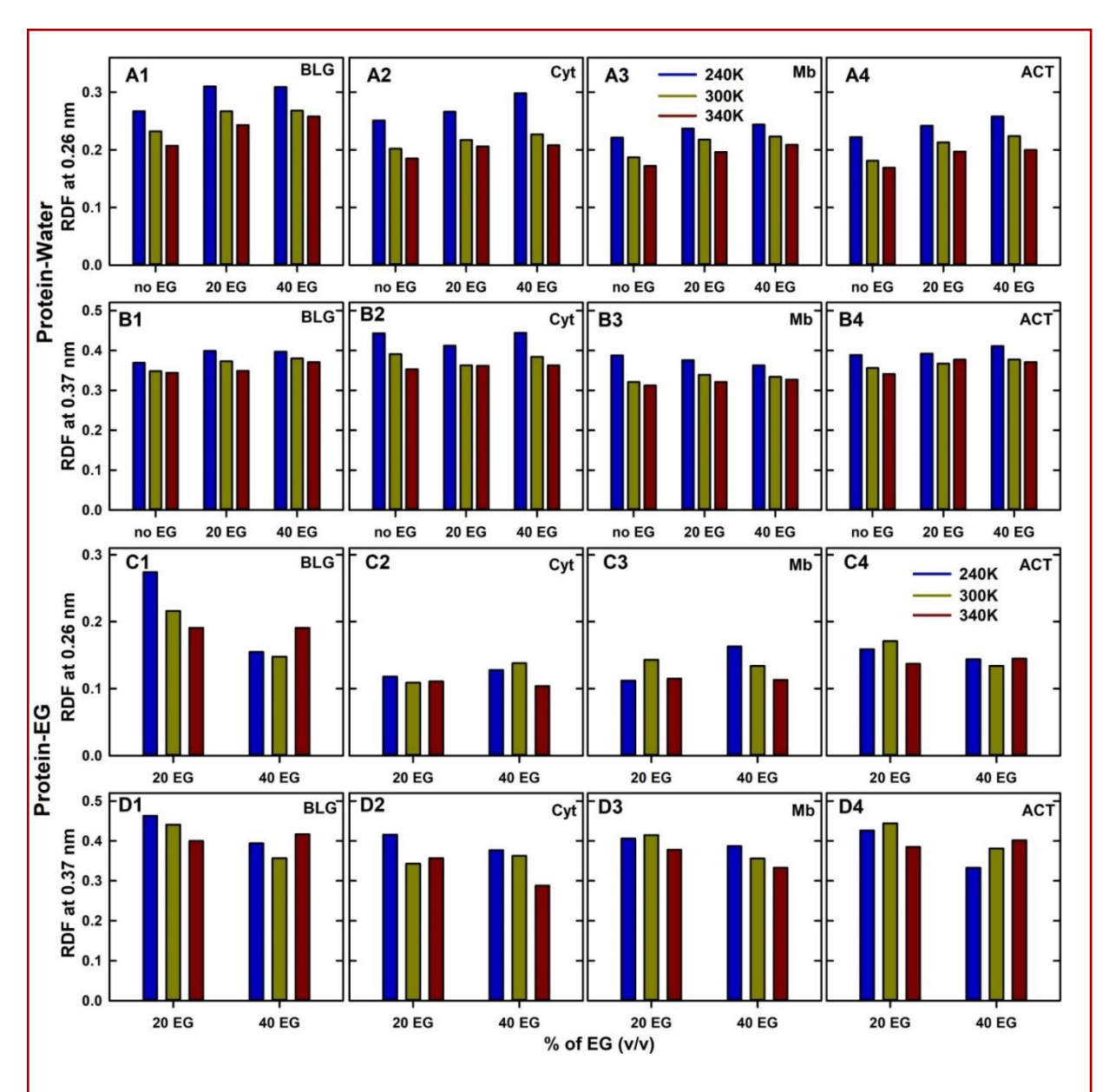


Fig. 3.6. The radial distribution values at first (0.26 nm) and second (0.37 nm) maxima for the distribution of water around the proteins (A1-A4 and B1-B4, respectively) and for the distribution of EG around the proteins (C1-C4 and D1-D4, respectively) at 240 K (blue), 300 K (green) and 340 K (red) extracted from their RDF curves presented in Fig. 3.5.

The first and the second minima were observed at 0.28 nm and 0.40 nm which again corresponds to the first and the second hydration shells of the proteins (Fig. 3.6 C1-C4 and D1-D4). The RDFs of protein-EG interactions for both first and second solvation shells did not show any common behaviour in their temperature-dependent changes.

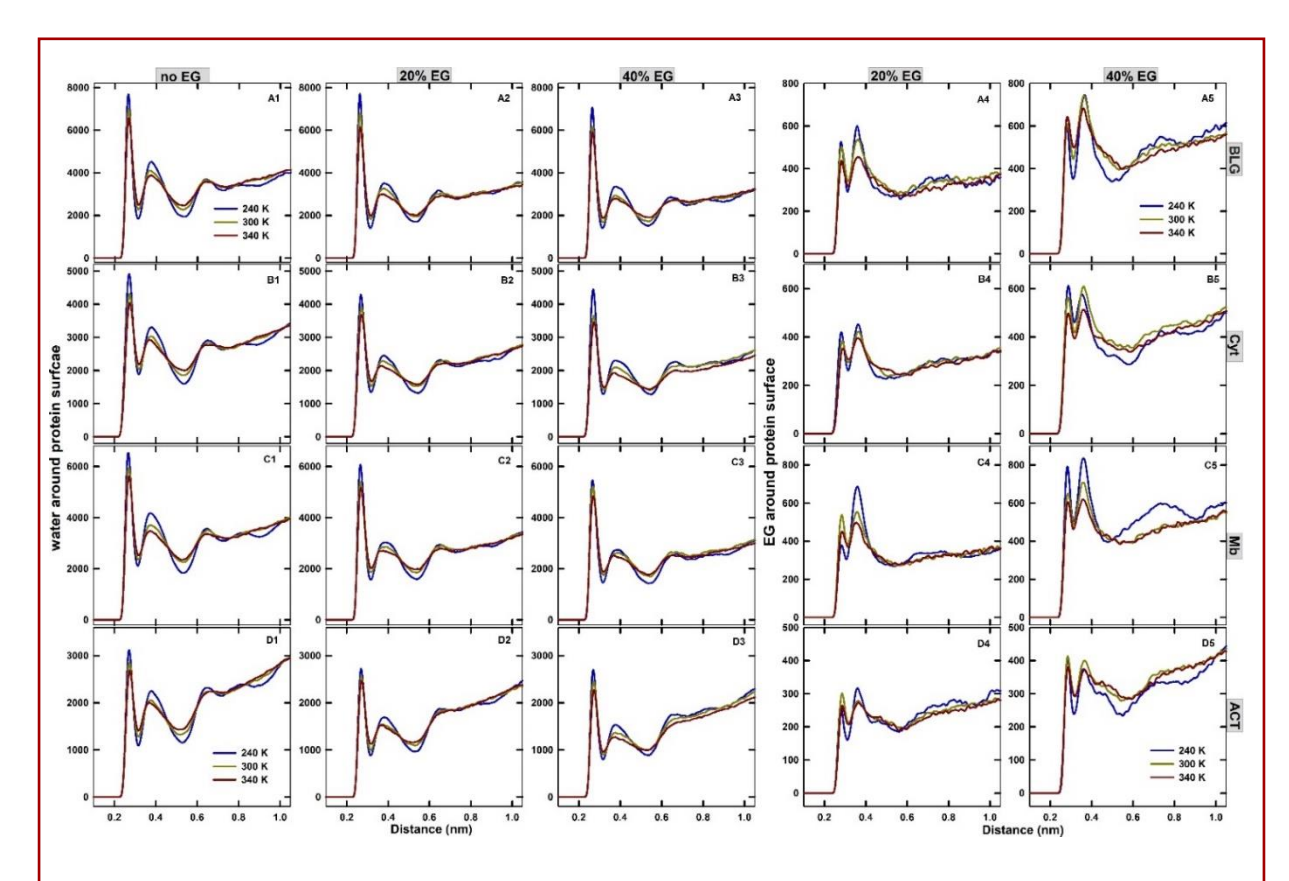


Fig. 3.7. Radial distribution function of water around the surface of the proteins (RDFsurf) calculated for (A1-A3) BLG, (B2-B3) Cyt, (C1-C3) Mb, and (D1-D3) ACT in the absence (A1-D1), and in the presence of 20% EG (A2-D2), and 40% EG (A3-D3) at 240 K (blue), 300 K (green) and 340 K (red). Radial distribution function of EG around the proteins calculated for (A4-A5) BLG, (B4-B5) Cyt, (C4-C5) Mb, and (D4-D5) ACT in the presence of 20% EG (A4-D4), and 40% EG (A5-D5).

Further, the number of solvent molecules around the surface of the protein were evaluated using the radial distribution function considering all the surface residues, RDF_{surf} (Fig. 3.7). The first and the second maxima of the RDF_{surf} plot was analysed for all the four proteins (Fig. 3.8). This showed a similar change that as the temperature increased the number of water molecules around the protein was decreased. Similarly, the distribution of EG was also calculated which again did not show any common behaviour.

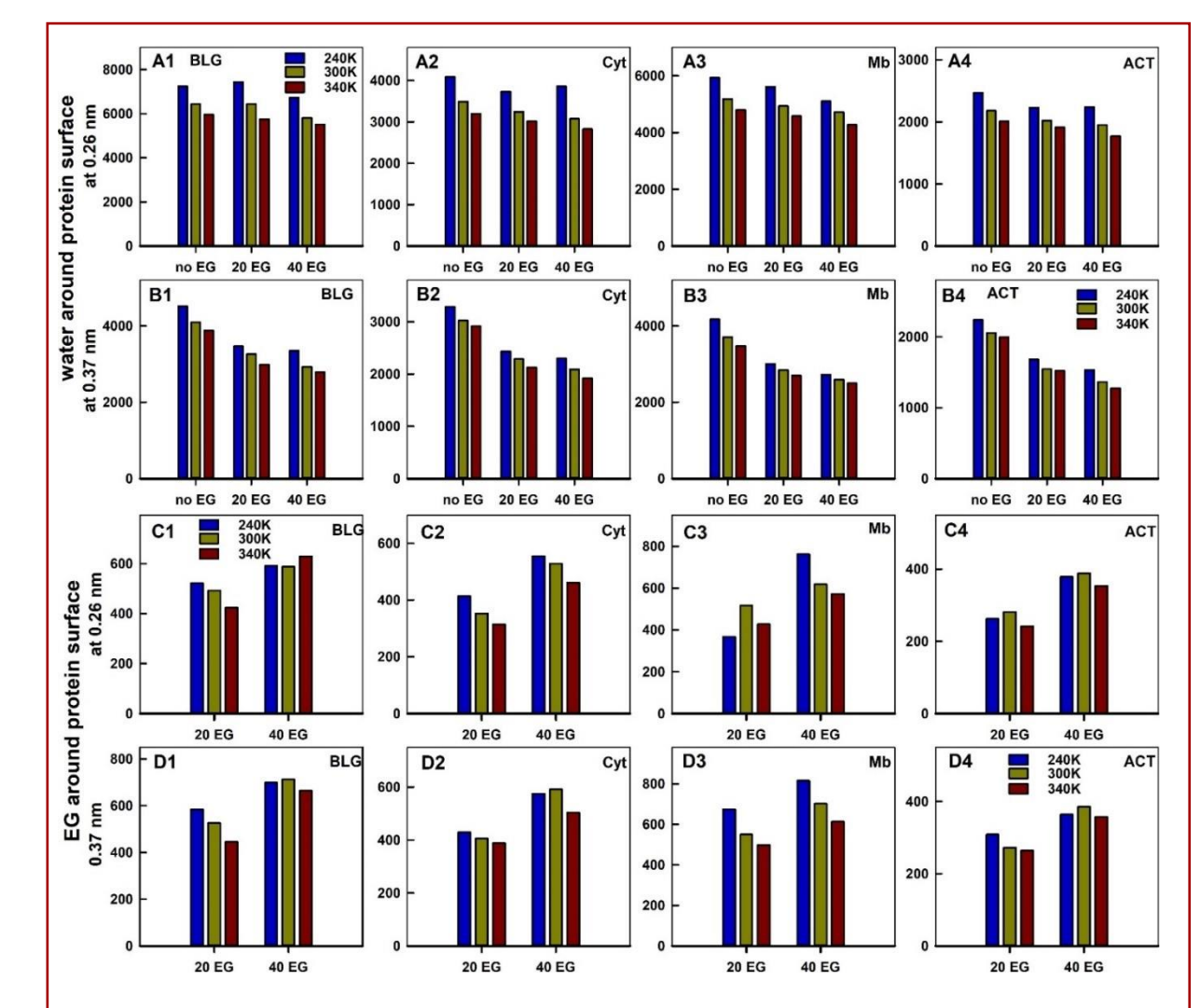


Fig. 3.8. The radial distribution values calculated for surface atoms of the proteins (RDFsurf) at first (0.26 nm) and second (0.37 nm) maxima for the distribution of water around the proteins (A1-A4 and B1-B4, respectively) and for the distribution of EG around the proteins (C1-C4 and D1-D4, respectively) at 240 K (blue), 300 K (green) and 340 K (red) extracted from their RDF curves presented in Fig. 3.7.

3.5.4. H-bond between protein-solvent and protein-EG

For further analysis, the number of hydrogen bonds formed between protein and water, and between protein and EG were calculated from all the MD simulations (Fig. 3.9). The increase in temperature decreased the number of H-bonds between the proteins and water. Also, the addition of EG slightly reduced the number of H-bonds between protein and water. This could be due to replacement of some of the protein-water H-bonds by EG molecules. The analysis of H-bonds between protein and EG showed that the number of H-bonds ranged from 15 to 60 that varied with the protein and temperature.

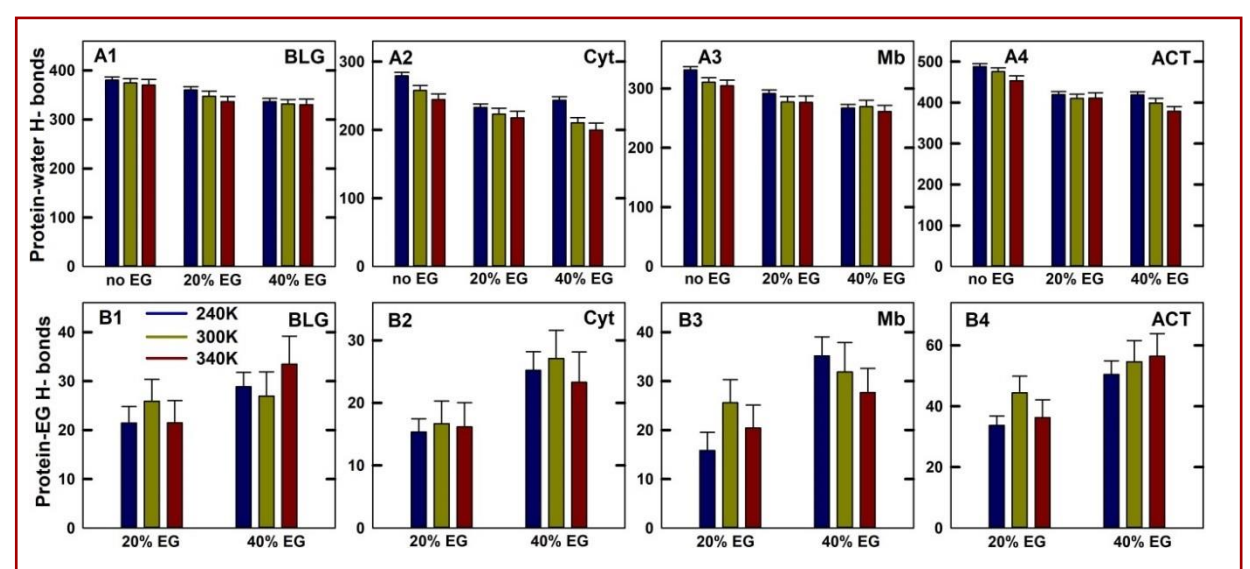


Fig. 3.9. Number of hydrogen bonding interactions between protein-water (A1-A4) and protein-EG (B1-B4) calculated from the MD simulations of all the four model proteins at 240 K (blue), 300 K (green) and 340 K (red) in the absence and in the presence of 20% EG and 40% EG.

3.5.5. Preferential interaction of EG with proteins

The fraction of EG between the surface of the proteins and the bulk was compared with the fraction of water as partition coefficient (K_p) using equation 3.4.3. The K_p value greater than one (Fig. 3.10) suggested that the fractional occupation of EG was more around the protein surface as compared to the bulk. To further decipher the effects of EG, the extent of hydration changes was analysed in terms of preferential interaction coefficient of EG (Γ_{EG}) with the protein using equation 3.4.4. As discussed above, preferential interaction coefficient represents the change in the chemical potential of the protein upon cosolvent addition.

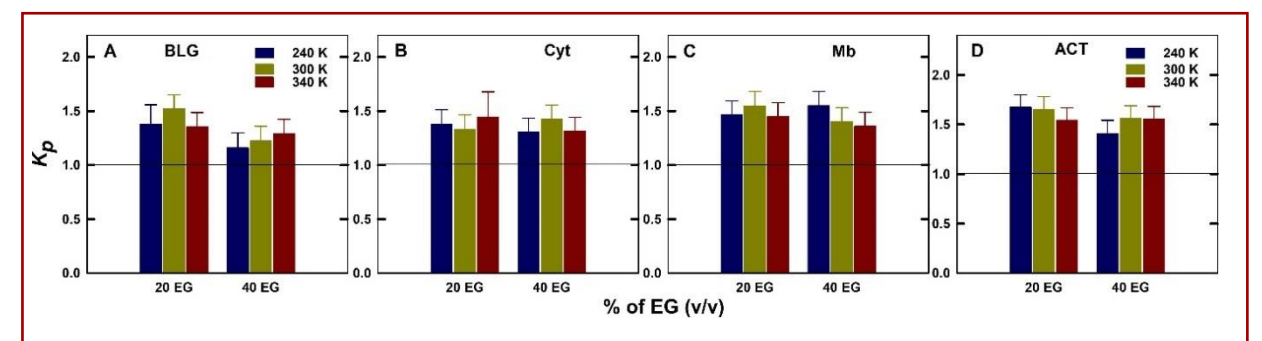


Fig. 3.10. The partition coefficient of EG molecules between the protein surface and bulk solvent calculated using equation 3.4.3 from the MD simulations performed at 240 (blue), 300 (green) and 340 K (red) for the proteins (A) BLG, (B) Cyt, (C) Mb, and (D) ACT.

A negative value of Γ till the bulk domain of the protein is a suggestive of preferential hydration, which is characteristic of stabilizing osmolytes whereas a positive value within the hydration shell of the protein would represent preferential interaction of the osmolyte, which might destabilize the protein.

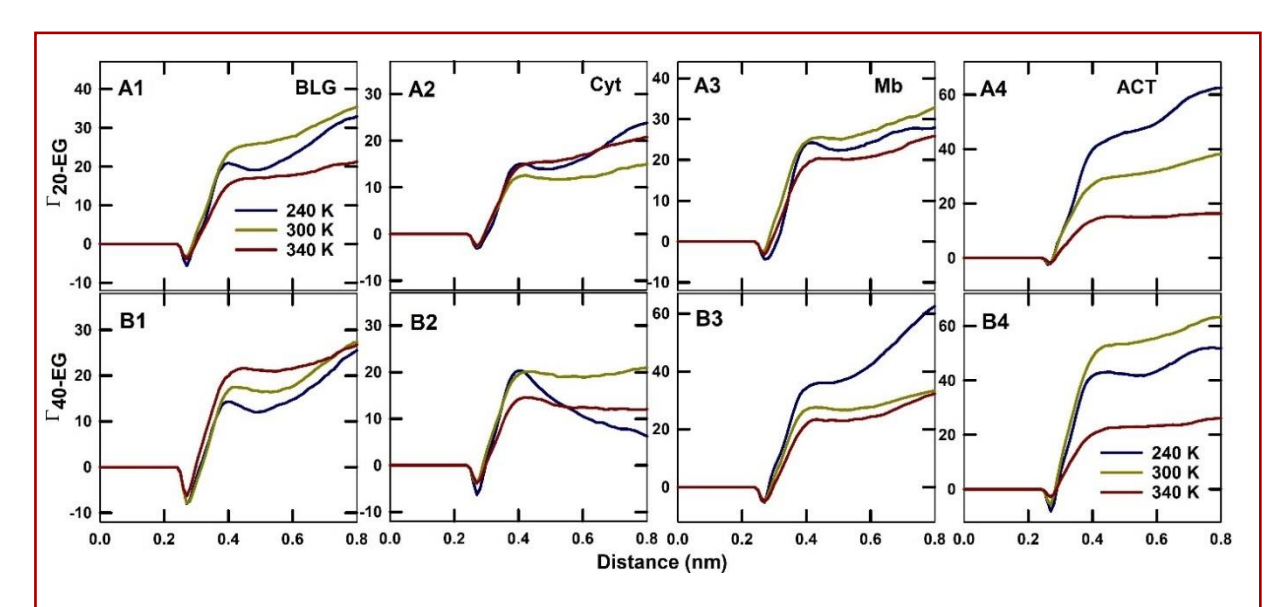


Fig. 3.11. Distance-dependent preferential interaction coefficient of 20% EG (A1-A4) and 40% EG (B1-B4) calculated from the surface of the protein to 0.8 nm distance at the regular interval of 0.1 Å from the MD simulations performed at 240 K (blue), 300 K (green), and 340 K (red) for all the four model proteins (BLG, Cyt, Mb and ACT) using equation 3.4.4.

The Γ_{EG} values at varying distances from the surface of the protein calculated for all the proteins in presence of both 20% EG ($\Gamma_{20\text{-EG}}$) and 40% EG ($\Gamma_{40\text{-EG}}$) is presented in Fig. 3.11.

All the proteins showed a minimum (negative value) at the distance of \sim 0.24 nm; however, the Γ_{EG} values become positive at above 0.3 nm. These changes suggested that EG preferentially interacts with the proteins at both the concentrations and at all three temperature conditions.

3.5.6. Hydrophobic hydration

The earlier studies have proposed that the cold denaturation is induced by hydrophobic hydration of the proteins at low temperature [45,46]. The RDF and Γ_{EG} values in the present study also evidences that the hydration around the protein was significantly altered with temperature. Therefore, we calculated the distribution of water and EG around the hydrophobic residues of the proteins using equation 3.4.5 and 3.4.6, respectively. These parameters are named as hydrophobic hydration and hydrophobic cosolvation, respectively. The addition of EG decreased the hydration around the hydrophobic residues at all three temperatures for BLG,

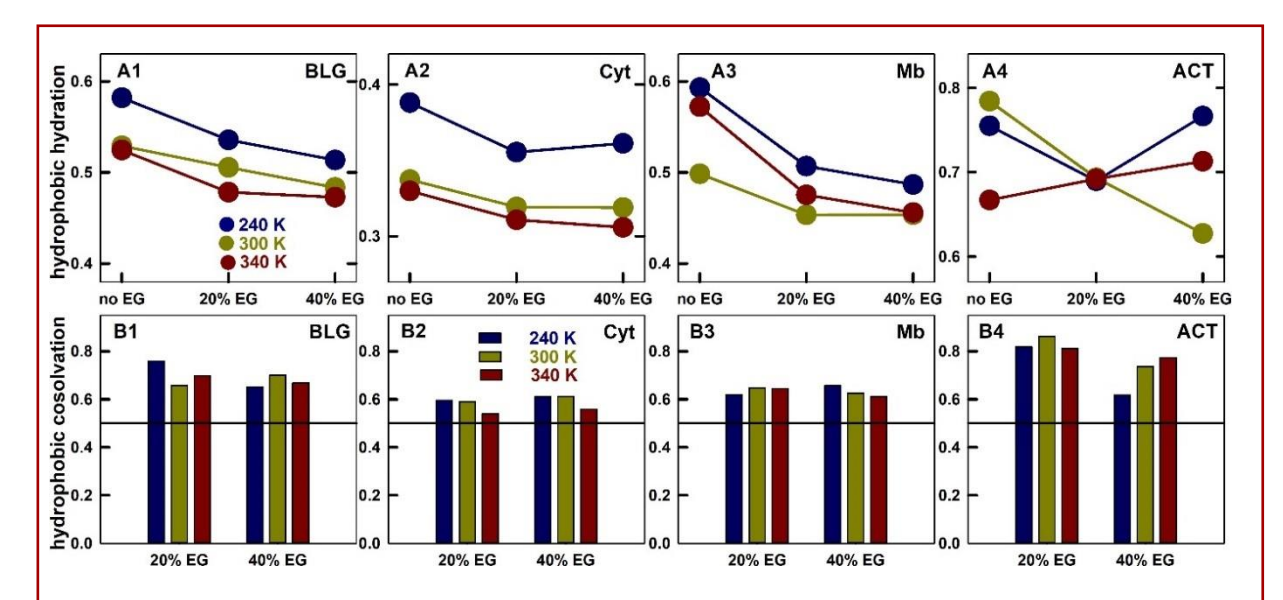


Fig. 3.12. (A1-A4) Fraction of water molecules around the hydrophobic residues (hydrophobic hydration), and (B1-B4) fraction of EG molecules around the hydrophobic residues (hydrophobic cosolvation) of the proteins calculated at 240 K (blue), 300 K (green), and 340 K (red) using equation 3.4.5 and 3.4.6. The horizontal line in the panels B1 to B4 represent the fractional value of 0.5.

Cyt and Mb (Figure 3.12, A1-A3). The extent of reduction was found to be more for 240 and 340 K compared to 300 K. In case of ACT (Figure 3.12, A4), the change in hydrophobic hydration was marginal at low and high temperatures whereas it was significantly reduced at

300 K. The hydrophobic cosolvation by EG molecules was high (the fractional values are above 0.5) in all the cases (Figure 3.11, B1-B4) suggesting that the number of water molecules replaced by EG around the hydrophobic residues were more than that around the polar residues.

3.6. DISCUSSION

3.6.1. Effect of EG on the conformation of proteins

The experimental data presented in Chapter 2, provided vital clues on the thermodynamic nature of the stabilization changes induced by EG; however, it lacked the information on molecular-level interactions. MD simulations has been established as a reliable computational tool to analyse protein-cosolvent interactions in different conditions [5,6,15]. A preliminary analysis was performed on the simulation trajectories of the proteins in EG using RMSD and SASA values. RMSD values show a slight increase at higher temperatures, but a decrease at lower temperature (Fig. 3.2). The SASA also shows a slight increase at higher temperature and a decrease at lower temperature (Fig. 3.3).

3.6.2. Interaction of EG with the proteins

The analysis of both RDF between heavy atoms of protein and water (Fig. 3.5), and RDF_{surf} (Fig. 3.7) calculated between surface residues and water reveals that the hydration of proteins is more at lower temperatures than at higher temperatures. The number of H-bonds (Fig. 3.9, A1- A4) between protein and water also complements the same observations. However, the analysis of protein-EG interactions by RDF, RDF_{surf} and the number of H-bonds could not show any particular feature for stability changes. The partition coefficient of EG (K_p) between the protein surface and the bulk clearly indicates that EG preferentially interacts with proteins at all the three temperature conditions for all the proteins (Fig. 3.10). An earlier study [47] on the measurement of K_p values suggest that diols and low molecular weight PEGs show preferential interaction with proteins whereas glycerol shows preferential exclusion from protein surface.

Preferential interaction or exclusion of an osmolyte molecule from protein surface is an important factor that determining osmolyte-induced stability changes in proteins. Higher preferential binding of an osmolyte to the denatured state of a protein destabilizes the protein

by decreasing the free energy of unfolding. On the other hand, unfavourable binding of an osmolyte to the denatured state preferentially excludes the osmolytes from the protein surface and increases surface hydration of the protein, thus stabilizing it [2,39,48,49]. Though the interaction of osmolytes with denatured-state is an influential factor for the stability, obtaining denatured conformations for both heat and cold induced states for these model proteins are computationally a limiting factor. Therefore, we have constrained our discussions on preferential interaction within near-native conformational states.

The distance based preferential interaction coefficient (Γ) calculated (Fig. 3.11) for the proteins suggests that the EG preferentially interacts with the protein (positive Γ_{EG} value above 0.3 nm). A positive Γ value has been observed for chemical denaturants whereas for stabilizing osmolytes a negative value of Γ has been reported in various simulation studies carried out at room temperature and at higher temperatures [2,50]. However, cold-denaturation phenomenon is different from heat-induced denaturation process. The preferential hydration of hydrophobic residues at sub-zero temperatures is attributed to the cold-denaturation of proteins, since hydrophobic effect is largely negated at sub-zero temperatures and the denaturation is said to be enthalpically-driven [51,52]. However, addition of EG reduces the hydrophobic hydration, the fraction of water around the hydrophobic surface over the water molecules around polar surface, which might stabilize the proteins against cold denaturation (Fig. 3.12, A1- A4). This is complemented by the hydrophobic cosolvation of non-polar residues by EG (Fig. 3.12 B1-B4), that the presence of EG is more around hydrophobic residues than the polar residues. Therefore, we propose that the EG molecules around the hydrophobic residues reduce the hydrophobic hydration of the proteins, thus, stabilizing the proteins at lower temperature. However, at higher temperatures, the preferential binding of EG might destabilize the proteins as it is commonly observed in the case of chemical denaturants such as urea and arginine [2,50,53]. The preferential binding of EG around the hydrophobic residues could decrease the cost of hydrophobic exposure of the residues at higher temperature, thus destabilizing the native conformation. These observations indicate that the effect of preferential binding of the cosolvent on protein stability might change with temperature particularly at sub-zero temperature conditions, and the nature of the interactions they exert with the proteins.

Only ACT shows an exceptional trend in the values of hydrophobic hydration. In fact, ACT during the chemical denaturation at 293 K shows a marginal increase in stability at lower EG concentrations (Chapter 2, Section 2.4.2). Therefore, it can be assumed that the interaction of ACT with EG might vary from other proteins. In addition, ACT consists of three polypeptide chains of different lengths connected with disulphide bonds [54,55]. The solvation of interfacial chains might be different from the solvation properties of single-chain globular proteins. Within the limitations of the present MD simulation studies, we could not quantitatively analyse those solvation effects and their plausible effect on the hydration changes in the protein.

3.7. CONCLUSION

The experimental data reported (in chapter 2), suggested that EG destabilizes the proteins during heat denaturation while stabilizes the proteins against cold denaturation. Further, cold stabilization induced by EG is enthalpy driven. This thermodynamic observation is corroborated by the MD simulation data, which suggests that EG induced cold stabilization might be due to preferential binding of EG with the protein, which results in reduction in hydrophobic hydration. At room temperature and higher temperatures these EG protein interactions might destabilize the proteins similar to most of chemical denaturants.

3.8. REFERENCES

- [1] S.N. Timasheff, Protein-solvent preferential interactions, protein hydration, and the modulation of biochemical reactions by solvent components, Proc. Natl. Acad. Sci. 99 (2002) 9721 9726. https://doi.org/10.1073/pnas.122225399.
- [2] D.R. Canchi, A.E. García, Cosolvent Effects on Protein Stability, Annu. Rev. Phys. Chem. 64 (2013) 273–293. https://doi.org/10.1146/annurev-physchem-040412-110156.
- [3] E.J. Loveridge, L.-H. Tey, R.K. Allemann, Solvent Effects on Catalysis by Escherichia coli Dihydrofolate Reductase, J. Am. Chem. Soc. 132 (2010) 1137–1143. https://doi.org/10.1021/ja909353c.

- [4] N. Chéron, M. Naepels, E. Pluhařová, D. Laage, Protein Preferential Solvation in Water:Glycerol Mixtures, J. Phys. Chem. B. 124 (2020) 1424–1437. https://doi.org/10.1021/acs.jpcb.9b11190.
- [5] P. Ganguly, P. Boserman, N.F.A. van der Vegt, J.-E. Shea, Trimethylamine N-oxide Counteracts Urea Denaturation by Inhibiting Protein—Urea Preferential Interaction, J. Am. Chem. Soc. 140 (2018) 483–492. https://doi.org/10.1021/jacs.7b11695.
- [6] B. Anumalla, N.P. Prabhu, Glutamate Induced Thermal Equilibrium Intermediate and Counteracting Effect on Chemical Denaturation of Proteins, J. Phys. Chem. B. 122 (2018) 1132–1144. https://doi.org/10.1021/acs.jpcb.7b10561.
- [7] D.R. Canchi, D. Paschek, A.E. García, Equilibrium Study of Protein Denaturation by Urea, J. Am. Chem. Soc. 132 (2010) 2338–2344. https://doi.org/10.1021/ja909348c.
- [8] B. Anumalla, N.P. Prabhu, Counteracting Effect of Charged Amino Acids Against the Destabilization of Proteins by Arginine, Appl. Biochem. Biotechnol. 189 (2019) 541– 555. https://doi.org/10.1007/s12010-019-03026-w.
- [9] S.N. Timasheff, The Control of Protein Stability and Association by Weak Interactions with Water: How Do Solvents Affect These Processes?, Annu. Rev. Biophys. Biomol. Struct. 22 (1993) 67–97. https://doi.org/10.1146/annurev.bb.22.060193.000435.
- [10] J.C. Lee, S.N. Timasheff, The stabilization of proteins by sucrose., J. Biol. Chem. . 256 (1981) 7193–7201. http://www.jbc.org/content/256/14/7193.abstract.
- [11] B.M. Baynes, B.L. Trout, Proteins in Mixed Solvents: A Molecular-Level Perspective,J. Phys. Chem. B. 107 (2003) 14058–14067. https://doi.org/10.1021/jp0363996.
- [12] J.C. Lee, S.N. Timasheff, Partial specific volumes and interactions with solvent components of proteins in guanidine hydrochloride, Biochemistry. 13 (1974) 257–265. https://doi.org/10.1021/bi00699a005.
- [13] M.S. Lehmann, G. Zacca, Neutron small-angle scattering studies of ribonuclease in mixed aqueous solutions and determination of the preferentially bound water, Biochemistry. 23 (1984) 1939–1942. https://doi.org/10.1021/bi00304a008.

- [14] R. Sinibaldi, M.G. Ortore, F. Spinozzi, F. Carsughi, et al., Preferential hydration of lysozyme in water/glycerol mixtures: A small-angle neutron scattering study, J. Chem. Phys. 126 (2007) 235101. https://doi.org/10.1063/1.2735620.
- [15] V. Vagenende, M.G.S. Yap, B.L. Trout, Mechanisms of Protein Stabilization and Prevention of Protein Aggregation by Glycerol, Biochemistry. 48 (2009) 11084–11096. https://doi.org/10.1021/bi900649t.
- [16] D.R. Canchi, P. Jayasimha, D.C. Rau, G.I. Makhatadze, et al., Molecular Mechanism for the Preferential Exclusion of TMAO from Protein Surfaces, J. Phys. Chem. B. 116 (2012) 12095–12104. https://doi.org/10.1021/jp304298c.
- [17] B. Anumalla, N.P. Prabhu, Surface hydration and preferential interaction directs the charged amino acids-induced changes in protein stability, J. Mol. Graph. Model. 98 (2020) 107602. https://doi.org/10.1016/j.jmgm.2020.107602.
- [18] J.K. Kaushik, R. Bhat, Thermal Stability of Proteins in Aqueous Polyol Solutions: Role of the Surface Tension of Water in the Stabilizing Effect of Polyols, J. Phys. Chem. B. 102 (1998) 7058–7066. https://doi.org/10.1021/jp9811191.
- [19] I. Haque, A. Islam, R. Singh, A.A. Moosavi-Movahedi, et al., Stability of proteins in the presence of polyols estimated from their guanidinium chloride-induced transition curves at different pH values and 25 °C, Biophys. Chem. 119 (2006) 224–233. https://doi.org/10.1016/j.bpc.2005.09.016.
- [20] M. Karplus, J. Kuriyan, Molecular dynamics and protein function, Proc. Natl. Acad. Sci. U. S. A. 102 (2005) 6679 6685. https://doi.org/10.1073/pnas.0408930102.
- [21] R.O. Dror, R.M. Dirks, J.P. Grossman, H. Xu, et al., Biomolecular Simulation: A Computational Microscope for Molecular Biology, Annu. Rev. Biophys. 41 (2012) 429–452. https://doi.org/10.1146/annurev-biophys-042910-155245.
- [22] N. Haque, N.P. Prabhu, Lid closure dynamics of porcine pancreatic lipase in aqueous solution, Biochim. Biophys. Acta Gen. Subj. 1860 (2016) 2313–2325. https://doi.org/10.1016/j.bbagen.2016.05.004.

- [23] N. Haque, K. Baratam, N.P. Prabhu, Analysing the microenvironment of 2-p-toluidinylnaphthalene-6-sulfonate (TNS) in solvents and in different conformational states of proteins in relation to its fluorescence properties: a computational study, Phys. Chem. Chem. Phys. 19 (2017) 24656–24666. https://doi.org/10.1039/C7CP03951D.
- [24] J. Åqvist, V.B. Luzhkov, B.O. Brandsdal, Ligand Binding Affinities from MD Simulations, Acc. Chem. Res. 35 (2002) 358–365. https://doi.org/10.1021/ar010014p.
- [25] G.S. Jas, E.C. Rentchler, A.M. Słowicka, J.R. Hermansen, et al., Reorientation Motion and Preferential Interactions of a Peptide in Denaturants and Osmolyte, J. Phys. Chem. B. 120 (2016) 3089–3099. https://doi.org/10.1021/acs.jpcb.6b00028.
- [26] S.A. Adcock, J.A. McCammon, Molecular Dynamics: Survey of Methods for Simulating the Activity of Proteins, Chem. Rev. 106 (2006) 1589–1615. https://doi.org/10.1021/cr040426m.
- [27] M.J. Abraham, T. Murtola, R. Schulz, S. Páll, et al., GROMACS: High performance molecular simulations through multi-level parallelism from laptops to supercomputers, SoftwareX. 1–2 (2015) 19–25. https://doi.org/10.1016/j.softx.2015.06.001.
- [28] S.K. Burley, H.M. Berman, C. Bhikadiya, C. Bi, et al., RCSB Protein Data Bank: biological macromolecular structures enabling research and education in fundamental biology, biomedicine, biotechnology and energy, Nucleic Acids Res. 47 (2018) D464–D474. https://doi.org/10.1093/nar/gky1004.
- [29] J. Huang, A.D. MacKerell Jr, CHARMM36 all-atom additive protein force field: Validation based on comparison to NMR data, J. Comput. Chem. 34 (2013) 2135–2145. https://doi.org/10.1002/jcc.23354.
- [30] G. Bussi, D. Donadio, M. Parrinello, Canonical sampling through velocity rescaling, J. Chem. Phys. 126 (2007) 14101. https://doi.org/10.1063/1.2408420.
- [31] M. Parrinello, A. Rahman, Polymorphic transitions in single crystals: A new molecular dynamics method, J. Appl. Phys. 52 (1981) 7182–7190. https://doi.org/10.1063/1.328693.

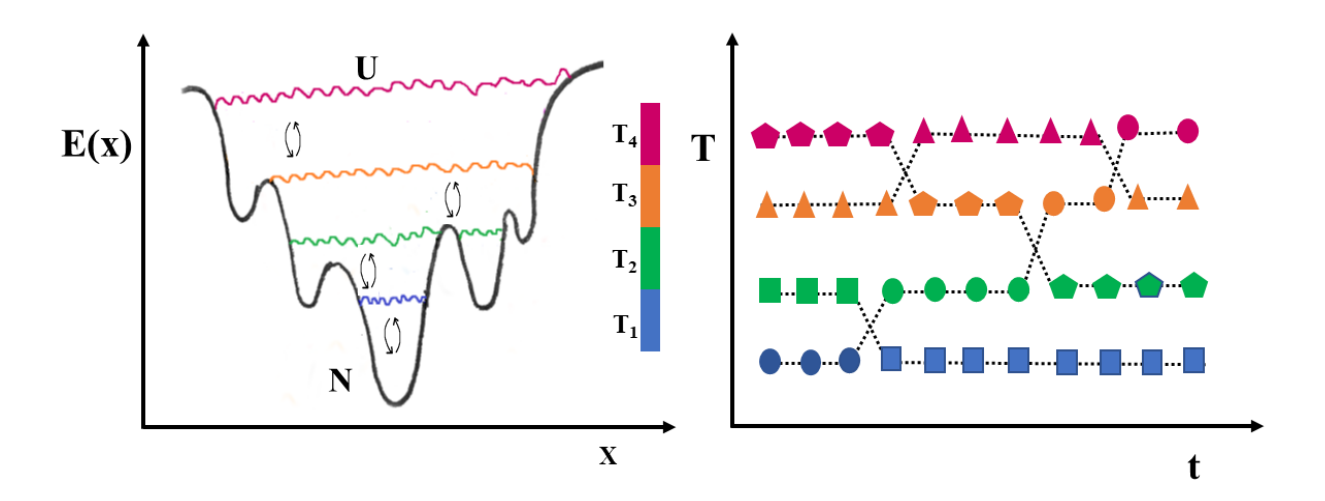
- [32] J.L.F. Abascal, C. Vega, A general purpose model for the condensed phases of water: TIP4P/2005, J. Chem. Phys. 123 (2005) 234505. https://doi.org/10.1063/1.2121687.
- [33] K. Vanommeslaeghe, A.D. MacKerell, Automation of the CHARMM General Force Field (CGenFF) I: Bond Perception and Atom Typing, J. Chem. Inf. Model. 52 (2012) 3144–3154. https://doi.org/10.1021/ci300363c.
- [34] K. Vanommeslaeghe, E.P. Raman, A.D. MacKerell, Automation of the CHARMM General Force Field (CGenFF) II: Assignment of Bonded Parameters and Partial Atomic Charges, J. Chem. Inf. Model. 52 (2012) 3155–3168. https://doi.org/10.1021/ci3003649.
- [35] J. Wang, T. Hou, Application of Molecular Dynamics Simulations in Molecular Property Prediction. 1. Density and Heat of Vaporization, J. Chem. Theory Comput. 7 (2011) 2151–2165. https://doi.org/10.1021/ct200142z.
- [36] W. Kabsch, C. Sander, Dictionary of protein secondary structure: Pattern recognition of hydrogen-bonded and geometrical features, Biopolymers. 22 (1983) 2577–2637. https://doi.org/10.1002/bip.360221211.
- [37] E.S. Courtenay, M.W. Capp, C.F. Anderson, M.T. Record, Vapor Pressure Osmometry Studies of Osmolyte–Protein Interactions: Implications for the Action of Osmoprotectants in Vivo and for the Interpretation of "Osmotic Stress" Experiments in Vitro, Biochemistry. 39 (2000) 4455–4471. https://doi.org/10.1021/bi9928871.
- [38] D. Shukla, C. Shinde, B.L. Trout, Molecular Computations of Preferential Interaction Coefficients of Proteins, J. Phys. Chem. B. 113 (2009) 12546–12554. https://doi.org/10.1021/jp810949t.
- [39] J. Mondal, G. Stirnemann, B.J. Berne, When Does Trimethylamine N-Oxide Fold a Polymer Chain and Urea Unfold It?, J. Phys. Chem. B. 117 (2013) 8723–8732. https://doi.org/10.1021/jp405609j.
- [40] S.N. Timasheff, H. Inoue, Preferential binding of solvent components to proteins in mixed water-organic solvent systems, Biochemistry. 7 (1968) 2501–2513. https://doi.org/10.1021/bi00847a009.

- [41] S.S. Cho, G. Reddy, J.E. Straub, D. Thirumalai, Entropic Stabilization of Proteins by TMAO, J. Phys. Chem. B. 115 (2011) 13401–13407. https://doi.org/10.1021/jp207289b.
- [42] M. Mukherjee, J. Mondal, Osmolyte-Induced Macromolecular Aggregation Is Length-Scale Dependent, J. Phys. Chem. B. 123 (2019) 8697–8703. https://doi.org/10.1021/acs.jpcb.9b07746.
- [43] M. Adrover, G. Martorell, S.R. Martin, D. Urosev, et al., The Role of Hydration in Protein Stability: Comparison of the Cold and Heat Unfolded States of Yfh1, J. Mol. Biol. 417 (2012) 413–424. https://doi.org/10.1016/j.jmb.2012.02.002.
- [44] P. Chatterjee, S. Bagchi, N. Sengupta, The non-uniform early structural response of globular proteins to cold denaturing conditions: A case study with Yfh1, J. Chem. Phys. 141 (2014) 205103. https://doi.org/10.1063/1.4901897.
- [45] P.L. Privalov, Y.V. Griko, S.Y. Venyaminov, V.P. Kutyshenko, Cold denaturation of myoglobin, J. Mol. Biol. 190 (1986) 487–498. https://doi.org/10.1016/0022-2836(86)90017-3.
- [46] P.L. Privalov, Cold Denaturation of Protein, Crit. Rev. Biochem. Mol. Biol. 25 (1990) 281–306. https://doi.org/10.3109/10409239009090613.
- [47] D.B. Knowles, I.A. Shkel, N.M. Phan, M. Sternke, et al., Chemical Interactions of Polyethylene Glycols (PEGs) and Glycerol with Protein Functional Groups: Applications to Effects of PEG and Glycerol on Protein Processes, Biochemistry. 54 (2015) 3528–3542. https://doi.org/10.1021/acs.biochem.5b00246.
- [48] G. Xie, S.N. Timasheff, Mechanism of the stabilization of ribonuclease a by sorbitol: Preferential hydration is greater for the denatured than for the native protein, Protein Sci. 6 (1997) 211–221. https://doi.org/10.1002/pro.5560060123.
- [49] M. Mukherjee, J. Mondal, Unifying the Contrasting Mechanisms of Protein-Stabilizing Osmolytes, J. Phys. Chem. B. 124 (2020) 6565–6574. https://doi.org/10.1021/acs.jpcb.0c04757.

- [50] B. Adamczak, M. Wieczór, M. Kogut, J. Stangret, et al., Molecular basis of the osmolyte effect on protein stability: a lesson from the mechanical unfolding of lysozyme, Biochem. J. 473 (2016) 3705–3724. https://doi.org/10.1042/BCJ20160604.
- [51] C.F. Lopez, R.K. Darst, P.J. Rossky, Mechanistic Elements of Protein Cold Denaturation, J. Phys. Chem. B. 112 (2008) 5961–5967. https://doi.org/10.1021/jp075928t.
- [52] S.B. Kim, J.C. Palmer, P.G. Debenedetti, Computational investigation of cold denaturation in the Trp-cage miniprotein, Proc. Natl. Acad. Sci. 113 (2016) 8991 – 8996. https://doi.org/10.1073/pnas.1607500113.
- [53] B. Anumalla, N.P. Prabhu, Chain Compaction and Synergistic Destabilization of Globular Proteins by Mixture of Denaturants, ChemistrySelect. 4 (2019) 13797– 13801. https://doi.org/10.1002/slct.201903122.
- [54] C. Niemann, Alpha-Chymotrypsin and the Nature of Enzyme Catalysis, Science (80-.). 143 (1964) 1287 1296. https://doi.org/10.1126/science.143.3612.1287.
- [55] A. Marshall, B. Keiller, J. Pederick, A. Abell, et al., Crystal Structure of Bovine Alpha-Chymotrypsin in Space Group P65, Crystals. 8 (2018) 460. https://doi.org/10.3390/cryst8120460.

CHAPTER 4

Analysing the Distinctive Character of Ethylene Glycol on Protein Stability by Replica Exchange Molecular Dynamics Simulation



4.1. ABSTRACT

Osmolytes are known to stabilize proteins against denaturing conditions. Ethylene glycol (EG), however, shows a distinctive effect on α -lactalbumin (α -LA) that it stabilizes the protein against cold-induced denaturation, whereas it destabilizes during heat denaturation. The replica exchange molecular dynamics (REMD) simulation of α-LA in the presence of EG shows that EG denatures the protein at higher temperatures whereas it retards the denaturation at sub-zero temperature. Representative structures of α -LA were selected from REMD trajectories at three different temperature conditions (240, 300 and 340 K) with and without EG, and classical molecular dynamics (MD) simulations were performed. The results suggest that the presence of water around α -LA is more at lower temperatures; however, water around the hydrophobic residues is reduced with the addition of EG at sub-zero temperature. The partition coefficient of EG showed that the binding of EG with hydrophobic residues was higher at lower temperatures. Preferential interaction parameters at different temperatures were calculated based on the mean distribution (Γ_{23}) and Kirkwood–Buff integral (G_{23}) methods. Γ_{23} shows a larger positive value at 240 K compared to higher temperatures. G₂₃ shows positive values at lower temperatures, whereas it becomes negative at above 280 K. These results indicate that the preferential binding of EG with α-LA is more at sub-zero temperature compared to higher temperature conditions. Thus, the study suggests that the preferential binding of EG reduces the hydrophobic hydration of α-LA at lower temperatures, and stabilizes the protein against cold denaturation. However, the preferential binding of EG at higher temperature drives the folding equilibrium towards the denatured state.

4.2. INTRODUCTION

Computer simulations although have emerged as an important tool in various fields of chemistry [1,2], physics [3], soft matter [4,5] and biology [6–10] over decades, still a large gap exists between the time scale that can be achieved in simulations and that observed experimentally [11,12]. One of the most common cause for the problem is insufficient sampling, which is to a greater extent attributed to the ruggedness in the energy landscape (containing many local minima often separated by high-energy barriers) of the system being studied. [13,14]. In order to overcome the issues related to sampling, many enhanced sampling methods such as replica-exchange molecular dynamics (REMD) [15], simulated annealing [16], and metadynamics [17] were developed. Among these REMD represents a versatile approach to study and understand a wide range of biological processes such as, protein folding kinetics [18], protein cold denaturation [19], peptide binding to membrane [20], and constant pH processes [21].

REMD is a hybrid approach combining molecular mechanics with Monte Carlo algorithm [15]. The method involves performing a finite number of MD simulations or replicas of an original system (a canonical ensemble) at different temperatures. The systems at higher temperature are responsible for sampling over a large phase space, while the ones at lower temperature helps in precisely sampling those regions of phase space involving local energy minima. A good sampling is achieved as the system is allowed to exchange the complete configuration at different temperatures.

4.2.1 Theory of REMD

A system consisting of N particles of mass m_k (k = 1, 2, 3, ..., N) with the position vectors $q \equiv (q_1, q_2, q_3, ..., q_N)$ and corresponding momenta being $p \equiv (p_1, p_2, p_3, ..., p_N)$, the Hamiltonian of the system [22] can be written as a sum of the potential energy E(q) and the kinetic energy K(p):

$$H(p,q) = E(q) + K(p)$$
 (4.2.1)

Where

$$K(p) = \sum_{k=1}^{N} \frac{P_k^2}{2m_k}$$
 (4.2.2)

For a canonical ensemble at temperature T, each state $x \equiv (q,p)$ with the Hamiltonian H(q,p) is weighted by Boltzmann factor [23]:

$$W_R(x;T) = e^{-\beta H(q,p)}$$
 (4.2.3)

Where β is the inversion temperature defined as $\beta = 1/k_BT$ (k_B is the Boltzmann constant). The average kinetic energy for a specific temperature T [24] is given by

$$\langle K_{(p)} \rangle_T = \langle \sum_{k=1}^N \frac{p_k^2}{2m_k} \rangle_T = \frac{3}{2} N k_B T$$
 (4.2.4)

In general, for M non-interacting replicas [15] at M different temperatures (T_m , where m = 1, 2, 3, ..., M)), such that there is always one replica at each temperature. The labels i (i = 1, 2, 3, ..., M) for replicas is a permutation of m labels (m = 1, 2, 3, ..., M) for temperatures, and vice versa:

$$\begin{cases} i = i(m) \equiv f(m) \\ m = m(i) \equiv f^{-1}(i) \end{cases}$$
(4.2.5)

Where f(m) and f'(i) correspond to the permutation` function of m and its inverse respectively.

Let $X = \left(x_i^{[i(1)]}, \dots, x_i^{[i(M)]}\right) = \left(x_{m(1)}^{[i]}, \dots, x_{m(M)}^{[M]}\right)$ be a state in this generalized ensemble. The subscripts and superscripts represent the temperature and the replica, respectively. The state X is specified for J sets of coordinates and momenta of N atoms in the replica k at temperature T_j :

$$x_m^{[i]} = (q^{[i]}, p^{[i]})_j (4.2.6)$$

The weighting factor for each state *X* can be written as

$$W_{REM}(X) = exp^{\left\{-\sum_{k=1}^{M} \beta_{m(i)} H(q^{[i]}, p^{[i]})\right\}} = exp^{\left\{-\sum_{m=1}^{M} \beta_{m} H(q^{[i(m)]}, p^{[i(m)]})\right\}}$$
(4.2.7)

Upon considering exchange between a pair of replicas (suppose k and l replicas between temperature T_i and T_n , respectively):

$$X = \left(\dots, x_m^{[i]}, \dots, x_n^{[j]}, \dots \right) \to X' = \left(\dots, x_m^{[j]'}, \dots, x_n^{[i]'}, \dots \right)$$
 (4.2.8)

The resulting permutation function f upon exchange is given as:

$$\begin{cases} i = f(m) \to j = f'(m), \\ j = f(n) \to i = f'(n). \end{cases}$$
 (4.2.9)

The detailed form for the exchange is thus,

$$\begin{cases} x_m^{[i]} \equiv (q^{[i]}, p^{[i]})_m \to x_m^{[j]'} \equiv (q^{[j]}, p^{[j]'})_m, \\ x_n^{[j]} \equiv (q^{[j]}, p^{[j]})_n \to x_n^{[i]'} \equiv (q^{[i]}, p^{[i]'})_n \end{cases}$$
(4.2.10)

Where *p* represents the momentum and is given as:

$$\begin{cases} p^{[i]'} \equiv \sqrt{\frac{T_n}{T_m}} \ p^{[i]} \\ p^{[j]'} \equiv \sqrt{\frac{T_m}{T_n}} \ p^{[j]} \end{cases}$$
(4.2.11)

This assignment represents the uniform rescaling of velocities of all the atoms by the square root of the two temperatures such that conditions in equation 4.2.4 are satisfied.

In order to converge to an equilibrium distribution, it is necessary to impose the detailed balance condition on the transition probability $w(X \rightarrow X')$:

$$W_{REM}(X) w(X \to X') = W_{REM}(X') w(X' \to X)$$
 (4.2.12)

From equations 4.2.1, 4.2.2, 4.2.7, 4.2.11 and 4.2.12, we have

$$\frac{w(X \to X')}{w(X' \to X)} = exp^{\left\{-\beta_m \left[K\left(p^{[j]'}\right) + E(q^{[j]})\right] - \beta_n \left[K\left(p^{[i]'}\right) + E(q^{[i]})\right]\right\}} + \beta_m \left[K\left(p^{[i]}\right) + E(q^{[i]})\right] + \beta_n \left[K\left(p^{[i]}\right) + E(q^{[i]})\right]} \\
= exp^{\left\{-\beta_m \frac{T_m}{T_n} K\left(p^{[j]}\right) - \beta_n \frac{T_n}{T_m} K\left(p^{[i]}\right) + \beta_m K\left(p^{[i]}\right) + \beta_n K\left(p^{[j]}\right)\right\}} \\
= exp^{\left\{-\beta_m \left[E\left(q^{[j]}\right) - E\left(q^{[i]}\right)\right] - \beta_n \left[E\left(q^{[i]}\right) - E\left(q^{[j]}\right)\right]\right\}} \\
= exp^{\left\{-\Delta\right\}} \tag{4.2.13}$$

where

$$\Delta \equiv [\beta_n - \beta_m](E(q^{[i]}) - E(q^{[j]})) \tag{4.2.14}$$

here i, j, m and n are related to equation 4.2.5, before exchange:

$$i = f(m), j = f(n)$$
 (4.2.15)

which can be satisfied by Metropolis criterion:

$$w(X \to X') \equiv w\left(x_m^i \middle| x_n^j\right) = \begin{cases} 1, & \text{for } \Delta \le 0, \\ exp^{(-\Delta)}, & \text{for } \Delta > 0. \end{cases}$$
 (4.2.16)

It is assumed that $\beta_1 < \beta_2 < \beta_3 < ... < \beta_M$. An REMD simulation can then be written as a two-step process, where

- (i) Each replica of the canonical ensemble at a fixed temperature is simulated simultaneously and independently for MD step.
- (ii) A pair of replicas, say $x_m^{[i]}$ and $x_{m+1}^{[j]}$, at neighboring temperatures undergo exchange according to metropolis algorithm.

The Hamiltonian expressed in equation 4.2.1 was described for an NVT simulation. The above discussed scheme can be adapted for an NPT ensemble with the Hamiltonian of the system expressed as [25]

$$H(q, p) = E(q) + K(p) + PV$$
 (4.2.17)

where V and P are the volume and pressure of the system, respectively. The contribution of fluctuations in volume to the total energy was found to be negligible [26].

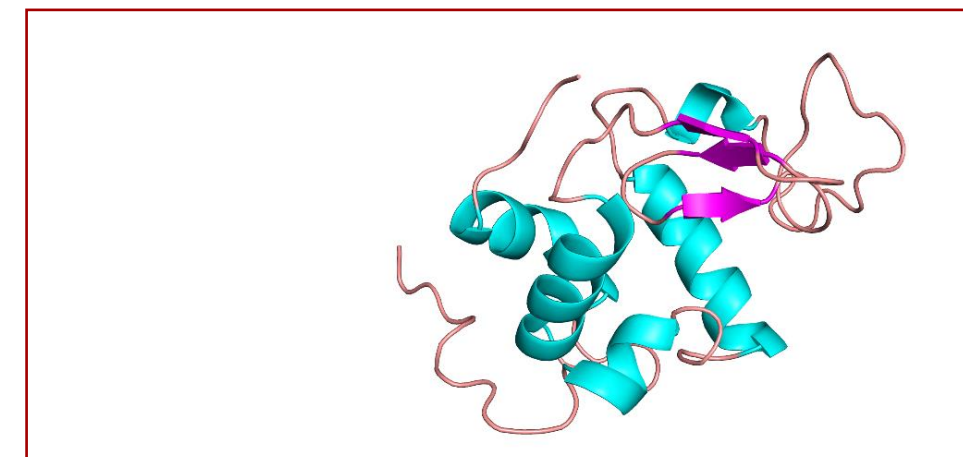


Fig. 4. 1. Cartoon diagram of α -LA. The three-dimensional structure was taken from the protein data bank (PDB id: 1HFZ). Light blue, pink and brown ribbons represent α -helix, β -sheet and loops, respectively.

Although, classical simulations performed at fixed temperatures (Chapter 3) could provide valuable information about dual nature of EG on protein stability, the major drawback was the lack of sufficient sampling of unfolded states. Further, specific affinity of EG to different types of amino acids in the denatured states also could not be evaluated from the classical simulations performed at fixed temperatures. In order to overcome these drawbacks REMD simulations of a model protein was performed in the temperature range of 300 to 240

K and 290 to 340 K both in absence and the presence of EG (30% (v/v)). The model protein employed for this study was α -lactalbumin (α -LA). α -LA is a 124 amino acid protein, mainly an α + β protein (Fig. 4.1.). Initially, the dual nature of EG, as observed for other model proteins, was tested on α -LA using circular dichroism spectroscopy. The data clearly suggested that α -LA was stabilized against cold denaturation by EG, while it was destabilized during heat denaturation. The trajectories obtained from REMD and classical simulations were analyzed according to the theory of preferential interaction. The results suggested that the distinctive effect shown by EG could be attributed to the temperature-dependent changes in the preferential interaction (PI) of EG with the protein.

4.3. METHODS

4.3.1. Materials

 α -LA was purchased from Sigma-Aldrich and was used without any further processing. Ethylene glycol and glycerol were also purchased from Sigma-Aldrich. Guanidine hydrochloride (Gdm) and phosphate buffer components were purchased from SRL Pvt. Ltd.

4.3.2. Thermal denaturation experiments

Thermal denaturation of α -LA was performed at pH 7 in presence of 2M Gdm [27]. Gdm was added in order to induce early cold denaturation, and the concentration was chosen such that it was within the pre-transition baseline of the Gdm induced denaturation curve of the protein [27]. The heat and cold unfolding was followed at 270 nm with a scan rate of 0.5° C/min in Jasco-J1500 circular dichroism (CD) spectrophotometer attached to Julabo-F32 circulating water bath.

4.3.3. Molecular dynamic simulations

REMD simulations of α -LA were performed in two different temperature ranges. (i) 300-240 K and (ii) 290-340 K. The protein structure was obtained from protein data bank (PDB id: 1hfz) [28]. All the water and the ligand molecules in the structure were removed and the protein was enclosed in a cubic box. In both the temperature ranges, α -LA was simulated in presence of water and in presence of 30% EG (four simulations in total). The temperature intervals for all the four simulations were determined using REMD temperature generator [29] and the temperatures are listed in Table 4.1.

Table 4.1. List of temperatures employed in REMD simulation

Simulation condition	Temperatures in K		
	300, 298.60, 297.12, 295.65, 294.19, 292.73, 291.28, 289.83, 299.39, 286.96,		
without EG, cold	285.53, 284.10, 282.68, 281.27, 279.86, 278.45, 277.06, 275.67, 274.28,		
	272.90, 271.52, 270.15, 268.78, 267.42, 266.07, 264.72, 263.37, 262.03,		
	260.69, 259.36, 258.04, 256.72, 255.41, 254.10, 252.79, 251.49, 250.20,		
	248.91, 247.62, 246.34, 245.06, 243.79, 242.52, 241.26, 240		
Without EG, heat	290, 291.45, 292.90, 294.36, 295.83, 297.30, 298.77, 300.25, 301.74, 303.23,		
	304.73, 306.24, 307.75, 309.27, 310.79, 312.32, 313.85, 315.39, 316.94,		
	318.49, 320.05, 321.61, 323.19, 324.76, 326.35, 327.94, 329.53, 331.13,		
	332.74, 334.35, 335.97, 337.60, 339.23, 340		
30% of EG, cold	300, 297.46, 295.52, 293.59, 291.67, 289.76, 287.85, 285.96, 284.68, 282.21,		
	280.35, 278.49, 276.63, 274.80, 272.97, 271.16, 269.35, 267.55, 265.77,		
	263.99, 262.22, 260.46, 258.70, 256.96, 255.22, 253.49, 251.79, 250.08,		
	248.38, 246.69, 245, 243.33, 241.66, 240		
30% of EG, heat	290, 291.91, 293.83, 295.76, 297.70, 299.65, 301.61, 303.58, 305.56, 307.55,		
	309.56, 311.57, 313.59, 315.62, 317.66, 319.71, 321.78, 323.85, 325.93,		
	328.03, 330.13, 332.25, 334.38, 336.51, 338.67, 340		

All the simulations were performed in GROMACS 5.1.4 [30] using CHARMM 36 force field [31]. Charges were assigned to the protein termini to emulate zwitterionic nature and the overall system was neutralized using seven Na⁺ ions. The system was energy minimized using steepest descent method and then equilibrated at the respective temperatures and 1 atm pressure for 1 ns using V- rescale thermostat [32] and Parrinello-Rahman barostat [33]. The production run was performed for 100 ns with an average exchange attempted for every 2 ps to attain an acceptance ratio of exchange up to 25%. This acceptance ratio was used in earlier studies on cold denaturation of small proteins as well [19,34]. The water model used was TIP4P-2005 [35] which is efficient for low-temperature simulations.

4.4. ANALYSIS

4.4.1. Thermal denaturation

The denaturation curves were analyzed and the thermodynamic parameters were derived using equation 2.3.1 as discussed in Chapter 2 of the thesis.

4.4.2. Contact area

The extent of protein's structural loss was analyzed using contact area (CA) calculated by the following relation [36].

$$CA = \sum_{i=1}^{n} SASA_{hydrophobic} - SASA_{core}$$
 (4.4.1)

Here, *SASA*_{hydrophobic} is sum of the solvent accessible surface area of hydrophobic residues (Ala, Gly, Val, Leu, Ile, Phe, Tyr, Trp, Met and Pro) in the protein calculated in presence of all the surrounding residues and *n* is the number of hydrophobic residues. *SASA*_{core} represents the total-SASA of the hydrophobic residues by considering the steric interference of the neighboring residues, but excluding the residues that are in tertiary contacts. The difference in SASA values would provide the contact area of the hydrophobic core of the protein. A decrease in contact area would indicate stabilization (intact hydrophobic core), while an increase in contact area would imply destabilization (more exposed hydrophobic core) of the protein. The SASA calculations for CA were performed in VMD using the in-built package [37]. The SASA values for the classical simulations (described below) were calculated using gmx SASA tool of Gromacs using probe radius of 0.14 nm [38,39].

4.4.3. Free-energy landscape

The trajectories from the three extreme temperatures that is 240, 300 and 340 K were separated from the REMD simulation of α -LA in both the presence and the absence of EG (six trajectories in total). The covariance matrix for each trajectory was created from the cartesian coordinates of the $C\alpha$ atoms of the protein and the principle component analysis (PCA) was performed by diagonalization of the covariance matrix using gmx covar in Gromacs [40]. The eigenvector and eigenvalues were obtained for all the six trajectories separately. The

convergence of the trajectories was then analyzed by root mean square inner products (RMSIP) for each trajectory. RMSIP is the measurement of similarities between subspaces (two subparts of the same trajectory) with an assumption that the essential subspace of the system is defined by first 10 eigenvectors with higher eigenvalues [9,41,42].

$$RMSIP = \frac{1}{10} \sqrt[2]{(\sum_{i=1}^{10} \sum_{j=1}^{10} n_i \cdot v_j)}$$
 (4.4.2)

where n_i and v_j are the eigenvectors of the subspaces. The trajectories were split into 10 ns subspaces and their covariance values were calculated.

The free energy landscape (FEL) was constructed using the first and the second eigenvectors as reaction coordinates for all the six conditions. The structures from the minima of each energy landscape were extracted from all the three temperature conditions (240, 300 and 340 K) in the absence and presence of EG. For those selected six conformations, classical simulations (C-MD) were performed using the same force field, water model and EG parameters. The simulations were performed with NPT ensemble conditions at their respective temperatures that is 240, 300 and 340 K for 200 ns each.

4.4.4. Radial distribution function, H-bonds and hydrophobic hydration

Radial distribution functions and number of hydrogen bonds for protein-water and protein-EG were calculated using gromacs tools gmx rdf and gmx hbond, respectively as described in section 3.2 of Chapter 3. The last 40 ns of the simulation trajectories were used for the purpose of analysis of the C-MD trajectories and trajectories obtained for selected temperatures from REMD simulation.

The extent of hydrophobic hydration was calculated using the equation 3.4.5 as described in Chapter 3. The function was calculated at a distance cut-off of 0.28 and 0.40 nm of the hydrophobic and polar residues of the protein. The cut-off values correspond to the first and the second hydration shells of the protein as identified from the first and second dips in the RDF plots of the protein, respectively. The last 40 ns of the simulation trajectories were used for calculation of hydrophobic hydration.

4.4.5. Partition coefficient and preferential interaction

The partition coefficient (K_p) was calculated according to equation 3.4.3 as discussed in Chapter 3. Residue specific K_p was also calculated using the same function, but the number of water and EG molecules were calculated from individual amino acid residues. For the purpose of analysis, amino acids were divided into hydrophobic (Ala, Gly, Ile, Val, Leu, Phe, Trp and Tyr), less polar (Thr, Ser, Pro, Cys and Met) and highly polar (His, Glu, Gln, Asp, Asn, Lys and Arg). Domain-based (local vs. bulk) preferential binding coefficient was calculated using equation 3.4.4.

Preferential binding of EG was also evaluated using Kirkwood-Buff integral from the RDF [43–45] of protein-water and protein-EG as,

$$G_{23} = \rho_3 \left(G_3(r) - G_2(r) \right) \tag{4.4.3}$$

while

$$G(r) = \int_{0}^{r} 4\pi r^{2} (g(r) - 1) dr$$
 (4.4.4)

where ρ_3 is the density of cosolvent and $G_2(r)$ and $G_3(r)$ is the Kirkwood-Buff integral of the solvent and the cosolvent, respectively. The G_{23} values were calculated with the distance cutoff (r) of 0.5 nm. The value of ρ_3 was calculated as a number density of the bulk domain at each temperature. Based on the definition of Trout and co-workers [46], the region above 6 Å from the surface of the protein was considered as bulk domain for calculations.

4.5. RESULTS

4.5.1 Thermal unfolding of α-LA

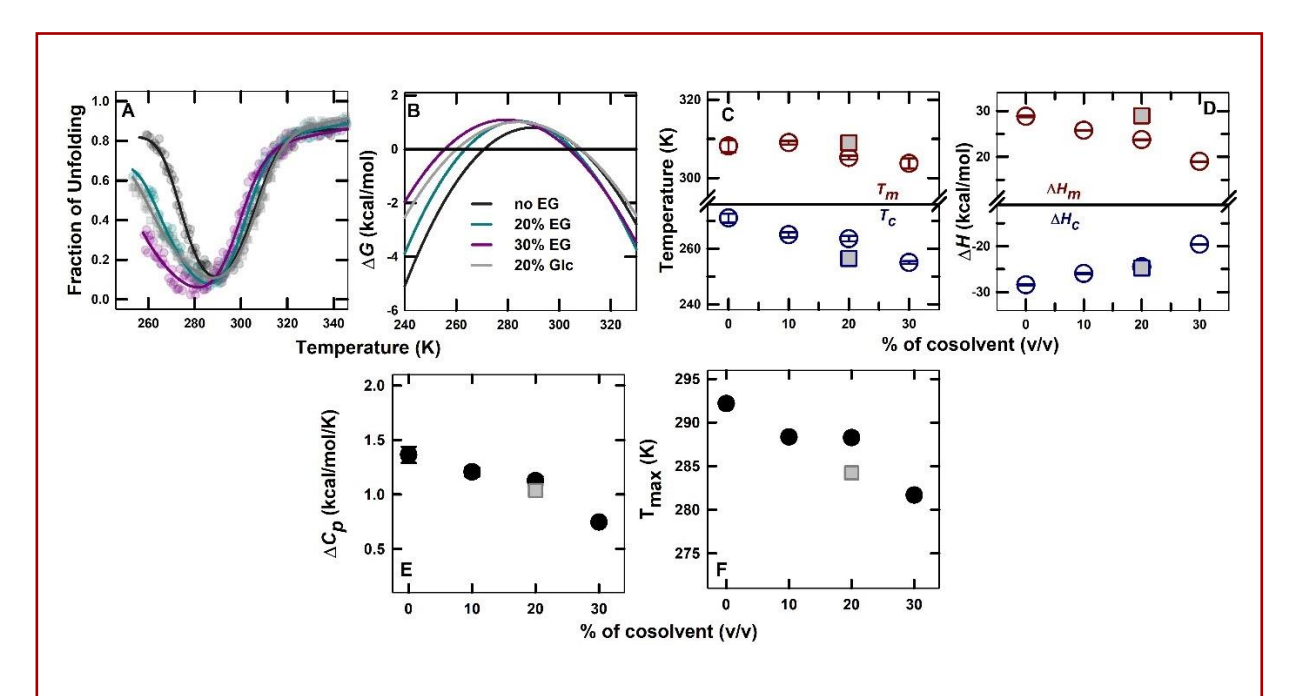


Fig. 4.2. Thermal denaturation of α -LA. Representative plot of fraction of unfolding (A) in absence (black) and in presence of EG (cyan and pink), and in presence of 20% Gly (grey). The solid lines are for visual clarity to follow the trend. Temperature-dependent free-energy curves of α -LA derived from the transition curves (B). Transition midpoint temperature of heat (T_m) and cold (T_c) denaturation (C) and the corresponding change in enthalpy at transition midpoint temperature (D). Change in heat capacity during thermal denaturation (E) and temperature of maximum stability (F) in varying concentration of EG. Circles and squares represent the parameters obtained in the presence of EG and Gly, respectively. Red and blue symbols represent the parameters calculated from heat- and cold-induced transitions, respectively.

The change in stability of α -LA during heat and cold denaturation was monitored using near UV-CD in presence of varying concentrations of EG ranging from 0 to 30% (v/v). The change in the ellipticity at 270 nm was used to follow the unfolding transitions of α -LA (Fig. 4.2A). The addition of EG shifted both cold- and heat-induced transition towards lower temperatures. Temperature-dependent free-energy changes were derived from the transition curves (Fig. 4.2B) and the temperature midpoint of both heat and cold transitions were evaluated (Fig. 4.2C). The temperature midpoint of heat denaturation (T_m) decreased upon addition of EG, suggesting destabilization. However, the decrease in the temperature midpoint of unfolding of cold denaturation (T_c) upon addition of EG indicated the stabilization of α -LA

upon addition of EG. The enthalpy of unfolding at the T_m value (ΔH_m) decreased with increasing EG. However, the enthalpy of unfolding at T_c (ΔH_c) showed a negative value as observed in case of other globular proteins [47–49] and increased with increasing EG concentration (Fig. 4.2D). As a control experiment, thermal denaturation experiments were performed in presence of 20% Gly. From the free-energy profile, the transition temperatures (T_m and T_c) and the enthalpy of unfolding (ΔH_m and ΔH_c), it was evident that Gly could protect α -LA both against heat and cold denaturation. Further, the change in heat capacity (ΔC_p) decreased (Fig. 4.2E) and the temperature of maximum stability (T_{max}) of α -LA shifted towards a lower value (Fig. 4.2F) upon addition of both EG and Gly as observed for other proteins (Chapter 2). These results suggested that EG destabilizes α -LA during the heat denaturation process, whereas stabilized the protein against cold denaturation.

4.5.2 Efficiency of REMD simulation

REMD simulations of α -LA were performed in absence and in the presence of 30% (v/v) of EG in two different temperature ranges; 240 - 303 K representing cold denaturation and 290 - 340 K representing heat induced denaturation. In order to attain a high acceptance probability as suggested by equation 4.1.15, the potential energy difference or the difference in the temperature between the replicas must be small [15,25]. A plot of the potential energy distributions of the replicas (Fig. 4.3) suggested that the necessary criteria for sampling [50,51] were attained in all the four REMD simulations performed. The curves of the neighbouring replicas exhibit a considerable overlap ensuring sufficient overlap between the replicas [52].

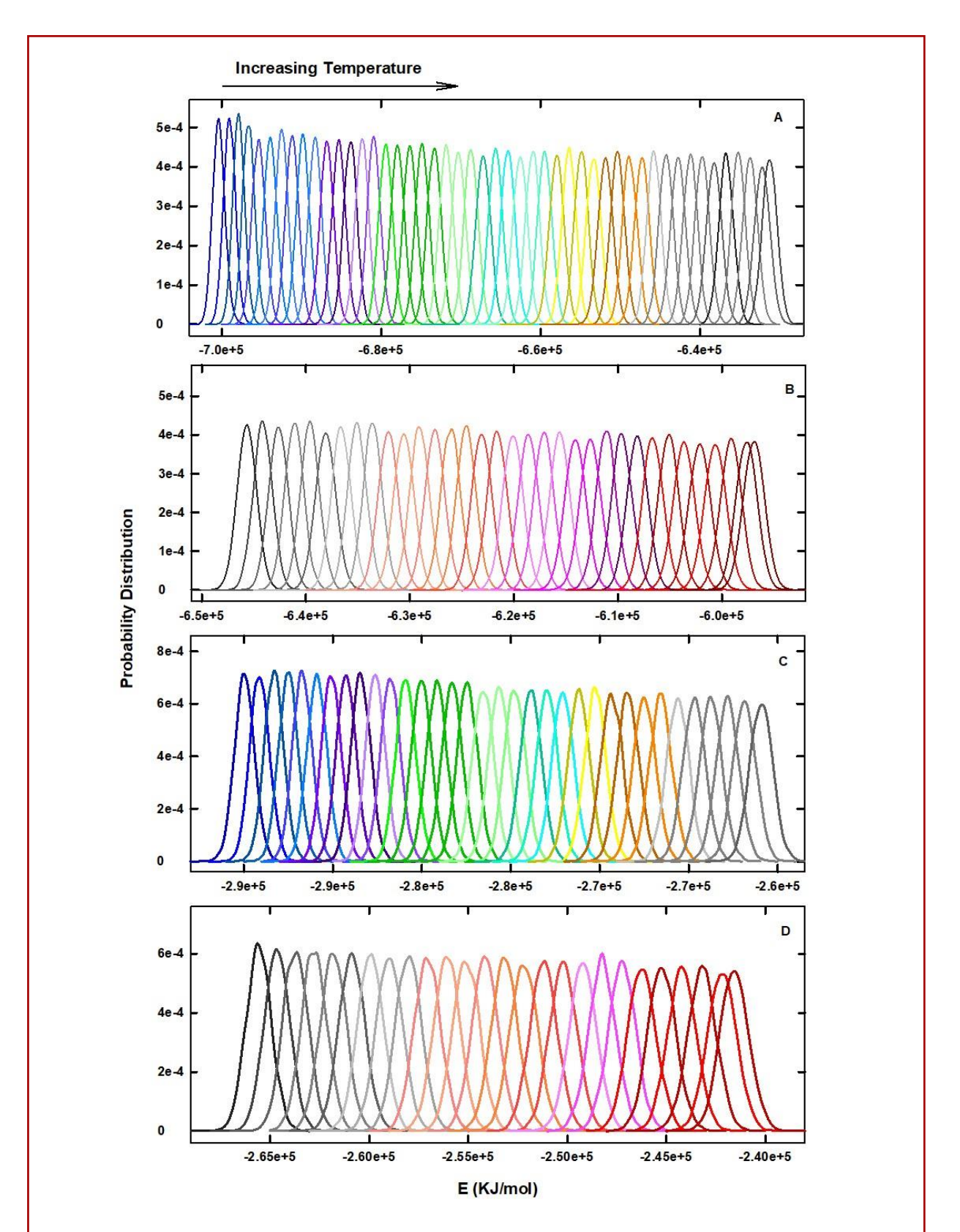


Fig. 4.3. Distribution of potential energy in the four REMD simulations performed (A) between 240-303 K without EG, (B) between 290-340 K without EG, (C) between 240-303 K with 30% of EG, and (D) between 290-340 K with 30% of EG.

4.5.3 Structural Changes During Molecular Dynamic Simulation of α-LA

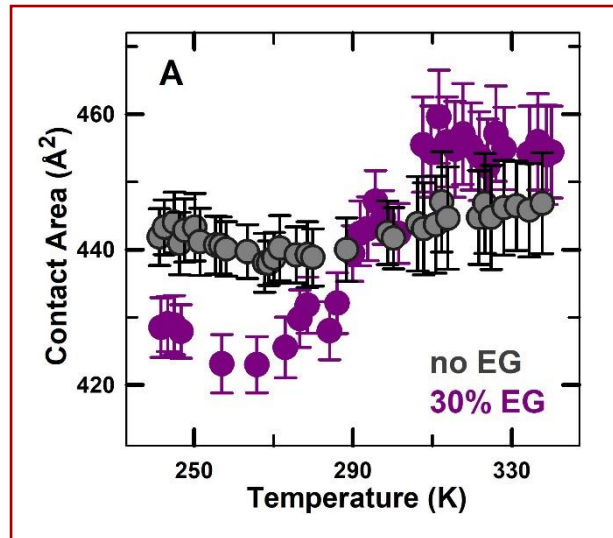


Fig. 4.4. Contact area of hydrophobic core as a function of temperature calculated from the REMD simulations of α -LA in the absence (grey) and in the presence (pink) of 30% EG. Contact area was calculated using equation 4.4.1

The extent of unfolding of the protein from all the four REMD simulations were quantified using a parameter referred as contact area (CA) of the hydrophobic core [36] of the protein (equation 4.4.1). A decrease in CA would indicate stabilization (an intact hydrophobic core), whereas an increase imply destabilization exposed hydrophobic core) of a protein. The average CA of α -LA at each temperature replica was calculated and plotted against temperature (Fig. 4.4). It is evident from the plot that the CA is

reduced at lower temperatures in presence of EG as compared to control (in absence of EG). However, at higher temperatures, the presence of EG increases the CA. This suggested that REMD simulation trajectories reflect the experimental observations and could be used to analyse the conformational changes of α -LA. To analyse the temperature-dependant changes

Table 4.2. RMSIP values calculated for the trajectories chosen from REMD simulations

Simulation condition	RMSIP [†]	
α-LA in water at 240 K	0.637	
α-LA in water at 300 K	0.730	
α-LA in water at 340 K	0.728	
α-LA in 30% EG at 240 K	0.673	
α-LA in 30% EG at 300 K	0.742	
α-LA in 30% EG at 340 K	0.719	

[†]RMSIP - root mean square inner product

induced by EG on the protein, the conformational states at three different temperatures 240, 300 and 340 K were extracted from the REMD simulations in the absence and in the presence of EG (six different conditions in total). The convergence of the conformational states of all the six trajectories were analysed by RMSIP using equation 4.4.2. The RSMIP values of >0.6 for all the six trajectories (Table 4.2) suggested that the simulation trajectories were sufficiently converged. Covariance matrix of the fluctuations in the positions of $C\alpha$ -atoms were generated at each condition and the PCA was performed. Free-energy landscapes were then constructed by projecting the first and the second eigenvectors obtained from their respective PCA (Fig. 4.5).

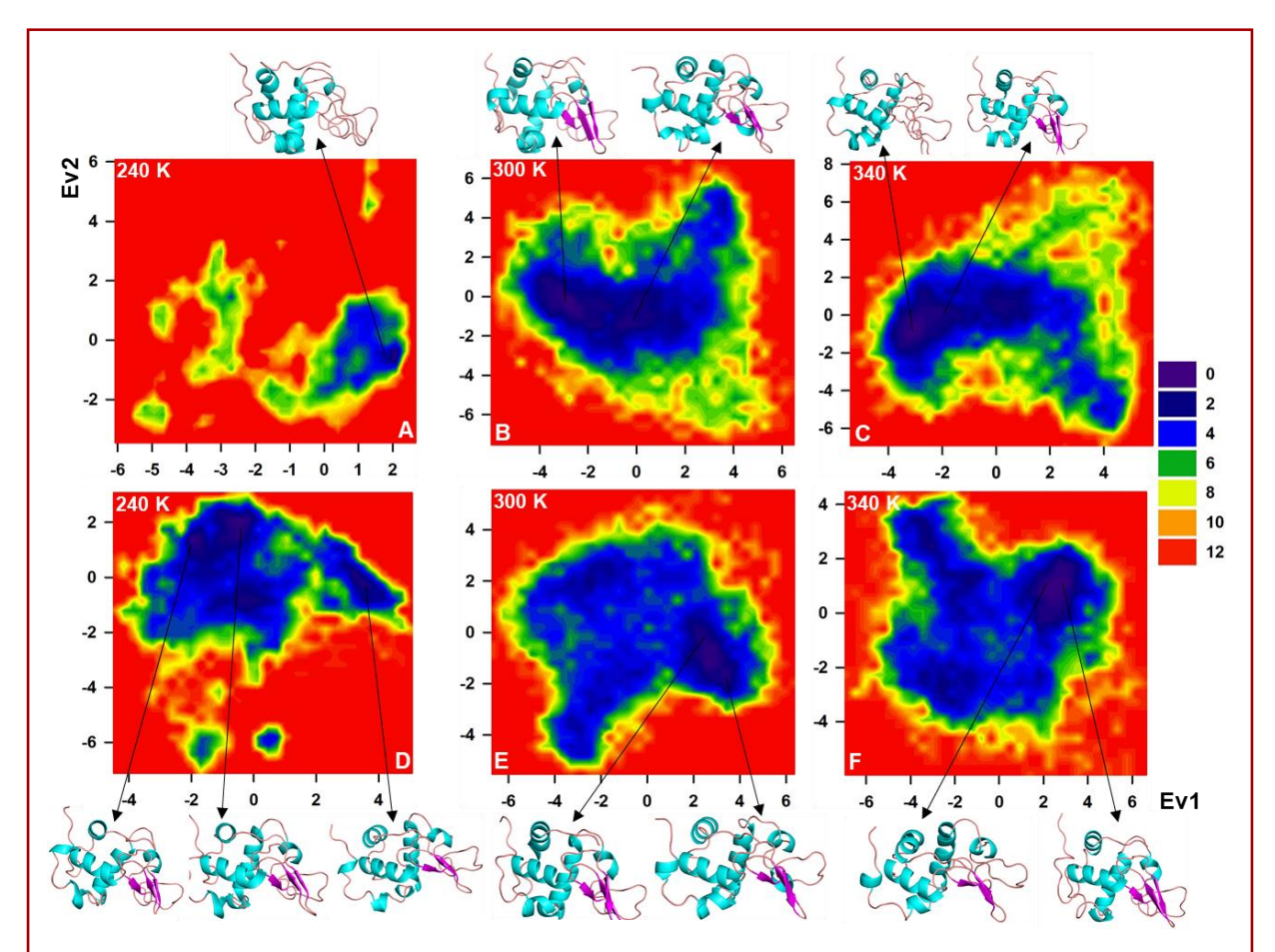
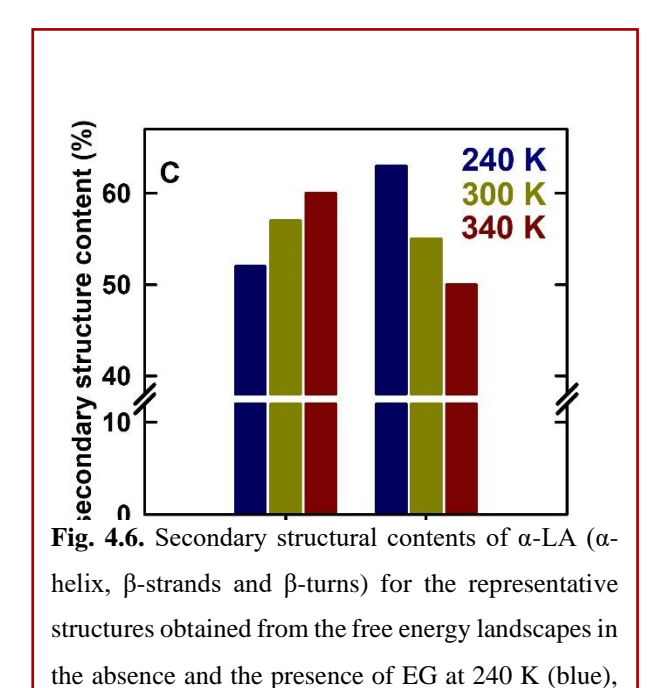


Fig. 4.5. Free energy landscape of α -LA constructed by projecting the first and second eigen vectors of PCA derived from the covariance matrix of fluctuations in Cα atoms of the protein. The REMD trajectories at 240, 300 and 340 K in the absence of EG (A-C) and in presence of 30% EG (D-F) were used for the construction of FEL. Representative conformations of minimum energy states are shown as cartoon diagram where cyan, pink and brown indicate helices, sheets and loops, respectively. The energy levels are depicted by colours ranging from purple (0 kJ/mol) to red (12 kJ/mol) as given in the legend.



300 K (green) and 340 K (red).

In order to examine the interactions between the protein and EG at different temperature conditions, a representative low-energy conformational states were obtained from each FEL and the key differences in the secondary structures were analysed (Fig. 4.6) using DSSP [53]. The calculated values suggested that the structural content of α -LA was less at 240 K compared to its native state at 300 K. In the presence of EG, the overall structure was increased at 240 K, whereas marginally reduced at 340 K.

For further elucidation of their conformational changes, classical MD simulations (C-MD) of the selected-representative conformations were performed for 200 ns each at their respective temperatures. Initial analysis of RMSD of $C\alpha$ atoms suggested that the mean fluctuation of the protein was higher at 340 K (Fig. 4.7). In presence of EG, RMSD was reduced at 240 K, whereas it increased at 340 K compared to its value in absence of EG.

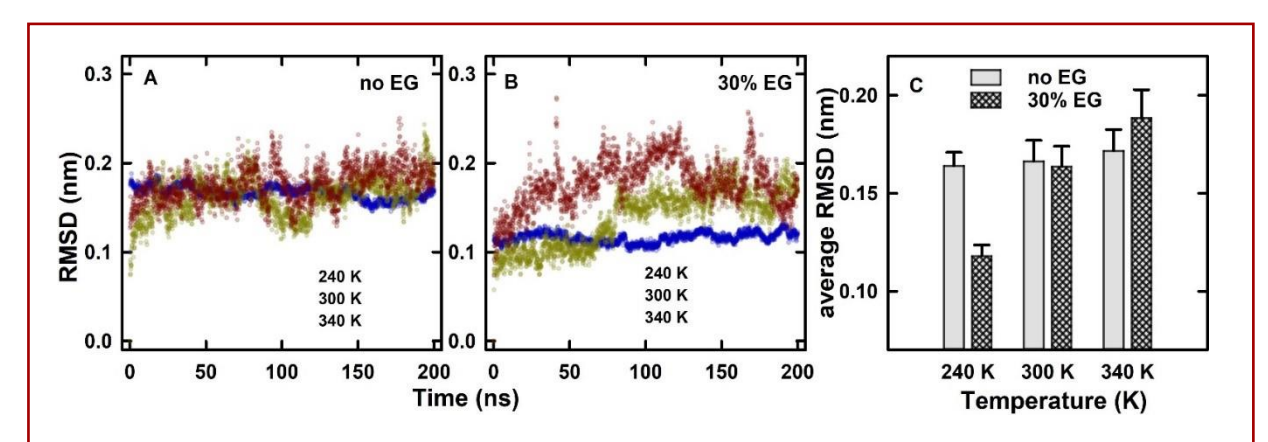


Fig. 4.7. Root mean square deviation (REMD) of $C\alpha$ atoms of α -LA for the representative structures obtained from REMD simulations at different temperatures, 240 K (blue), 300 K (green), and 340 K (red) in the absence (A) and the presence (B) of EG. (C) The average of RMSD values calculated for the last 100 ns in the absence (grey-filled bars) and the presence of EG (grid-filled bars) at different temperatures.

The structural integrity of the protein was assessed using the change in SASA during the C-MD simulations. The probability distribution function of SASA of α -LA was evaluated at three different temperatures (Fig. 4.8A). The plot shows a unimodal distribution at 240 and 300 K, and the distribution was wider at 300 K compared to 240 K. The addition of EG at 240 K, shifted the SASA distribution to a lower value and at 300 K the SASA was not significantly altered. This suggests that EG stabilizes the native conformation of the protein at 240 K, whereas it did not show significant effect at room temperature. At 340 K, α -LA showed a bimodal distribution with significant amount of conformational states with higher SASA. With the addition of EG, the conformations with higher SASA values increased and

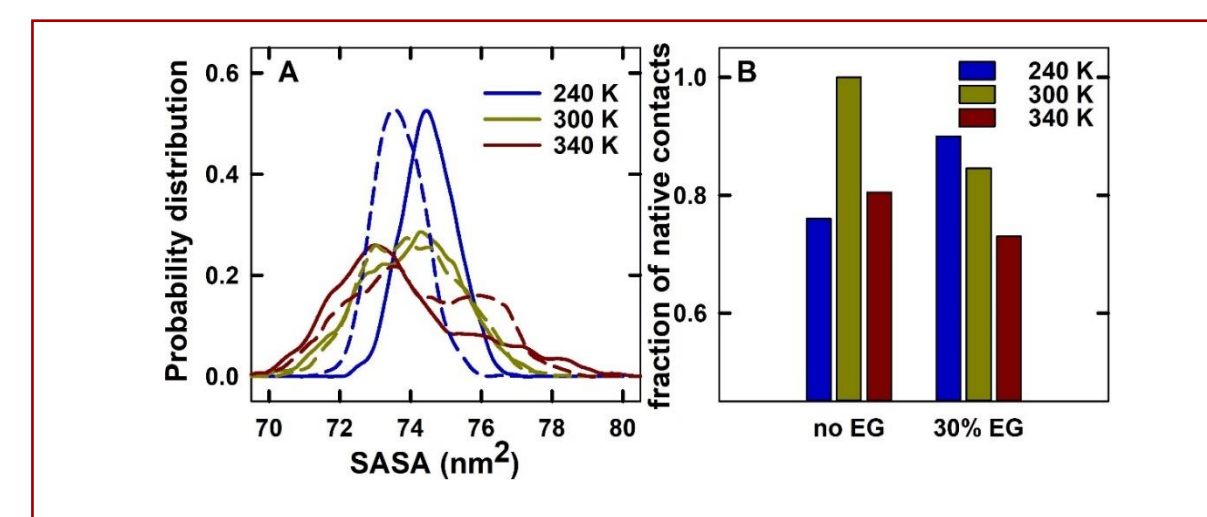


Fig. 4.8. (A) Normalized probability distribution of solvent accessible surface area (SASA) and (B) the fraction of native contacts in α -LA (with reference to the number of contacts in the absence of EG at 300 K) calculated from the C-MD simulations of \square -LA carried out at 240 (blue), 300 (green) and 340 K (red) in the absence (solid lines) and in the presence of (broken lines) 30 % of EG.

the peak at lower SASA values also shifted towards higher values. The conformational changes were also evaluated with the fraction of native contacts retained at various conditions by considering the conformational state of α -LA at 300 K in the absence of EG as fully native (Fig. 4.8B). The calculations showed that either increase or decrease in simulation temperature reduced the number of native contacts in α -LA. However, in presence of EG, the number of native contacts were more at 240 K, whereas it was less at 340 K. The results were complementing with the experimental observations that EG stabilizes the protein at lower temperatures, whereas destabilizes at higher temperatures, whereas destabilizes at higher temperature.

To identify the specific structural changes, a representative conformational state from each C-MD simulation was obtained and analysed (Fig. 4.9 and Table 4.3). The conformation of α -LA obtained at 300 K in the absence of EG was considered as fully native conformation. The secondary structures are labelled as per the convention of PDBsum [54] which uses Promotif [55] to assign secondary structures. At 240 K, all the β -strands were unfolded along with distortion in β -turns 9 and 10, and the helix was partially unfolded. The addition of EG prevented the unfolding of strand-1 and strand-2, and the distortion of β -turns. At 340 K, only strand-3 was fully unfolded along with the partial unfolding of helix-1 and helix-8. With the

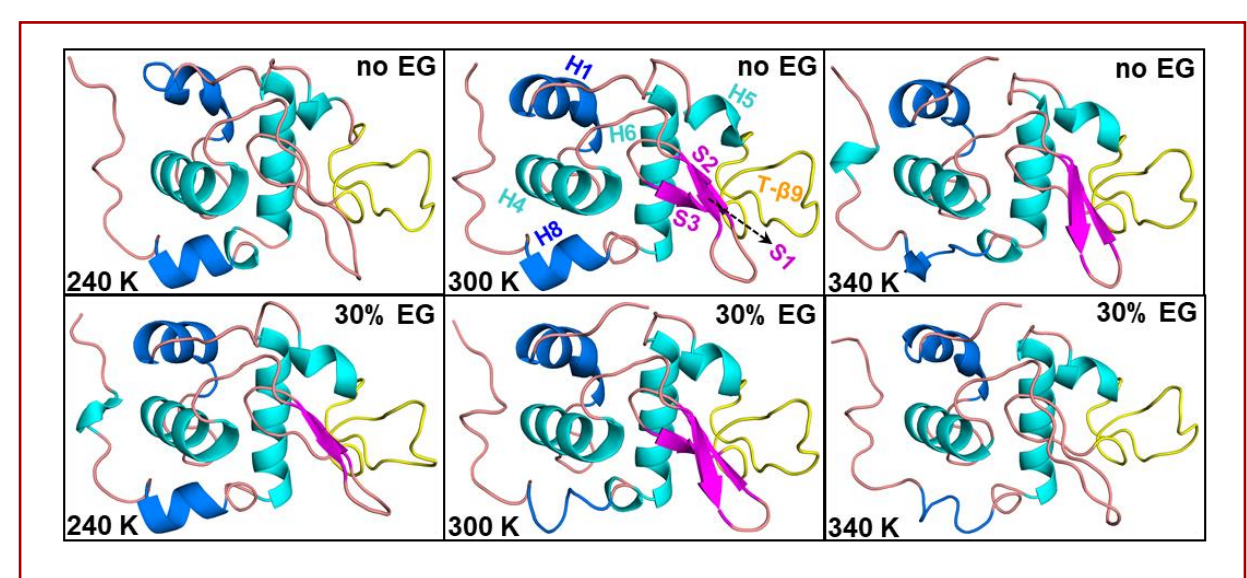


Fig. 4.9. The minimum energy conformational states obtained from the free energy landscapes of α -LA constructed at different temperature conditions in the absence (upper panels) and the presence (lower panels) of 30 % EG (Fig. 4.5. free energy surface plots). The structure of α -LA at 300 K in the absence of EG is considered as a fully-native conformation and the loss of structures at different conditions are listed in Table 4.3. The symbols represent, H: helix. S: strand and T-β: β-turn.

addition of EG, all three strands and helix-8 were fully unfolded along with distortions in β -turns 9 and 10. The conformations of α -LA at 300 K showed that the addition of EG only partial unfolding of helix-8 at ambient conditions. These structural changes indicate that the simulations carried out at different conditions reflect experimentally observed results that α -LA is stabilized against cold denaturation at 240 K, whereas it is more destabilized at 340 K with the addition of EG. Earlier experimental studies [27,56] also show that denaturation

of α -LA is initiated by the disruption of β -strands followed by unfolding of termini helices, helix-1 and helix-8. Therefore, these simulation trajectories were used for further analysis to illustrate the mechanism of interactions between α -LA and EG.

Table 4.3. Secondary structures unfolded during simulation calculated from snapshots in Fig. 4.9.

Cosolvent	Temperature			
	240 K	300 K	340 K	
No EG	Helix 1 (p)	All native	Helix 1 (p)	
	Strands 1 to 3 (f)		Strand 3 (f)	
	β-turns 9 &10 (d)		Helix 7 (c)	
	Helix 7 (c)		Helix 8 (p)	
30% EG	Helix1 (p) Strand 3 (f) Helix 9 (c)		Helix 1(p)	
		Helix 7 (c)	Strands 1 to 3 (f)	
		Helix 8 (p)	β-turns 9 &10 (d)	
			Helix 8 (f)	
†n-nartially	v unfolded. f - fully u	ınfolded d -di		

4.5.4 Solvent verses cosolvent interactions with α -LA

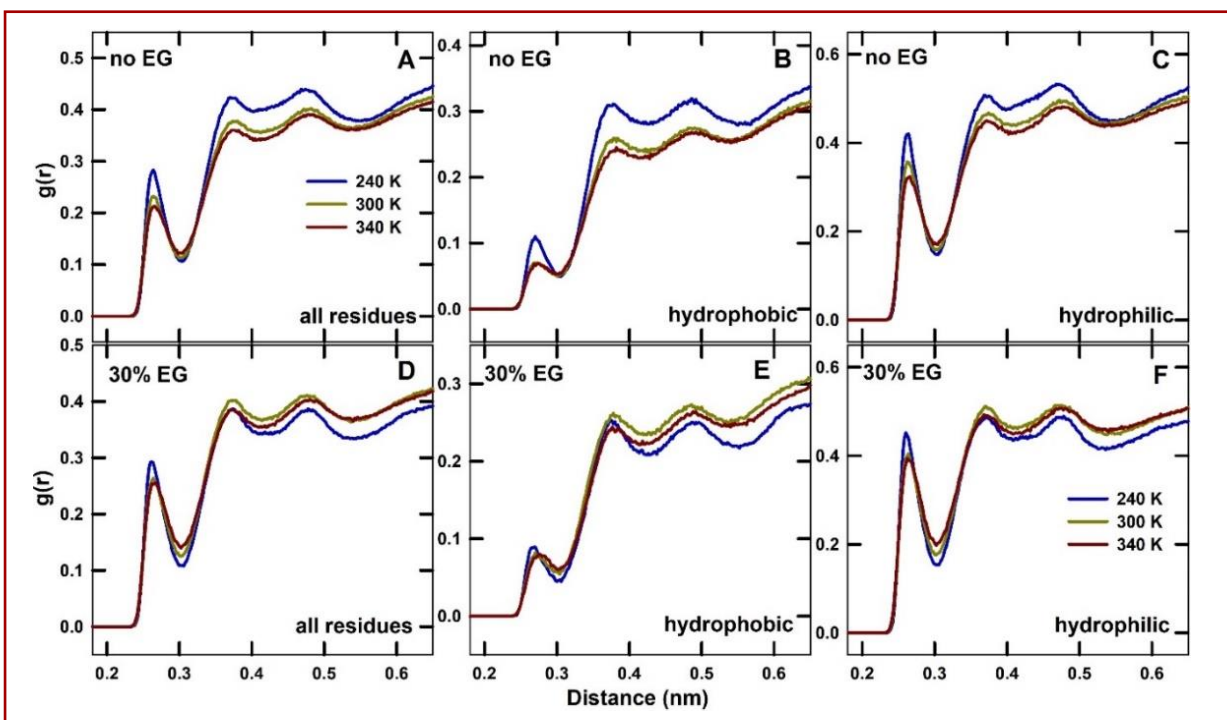


Fig. 4.10. Radial distribution function of water around all the residues of α-LA (A & D), only around hydrophobic residues (B & E) and only around hydrophilic residues (C & F) calculated in the absence (upper panels) and in the presence of (lower panels) EG from the C-MD simulations carried out at 240 (blue), 300 (green) and 340 K (red).

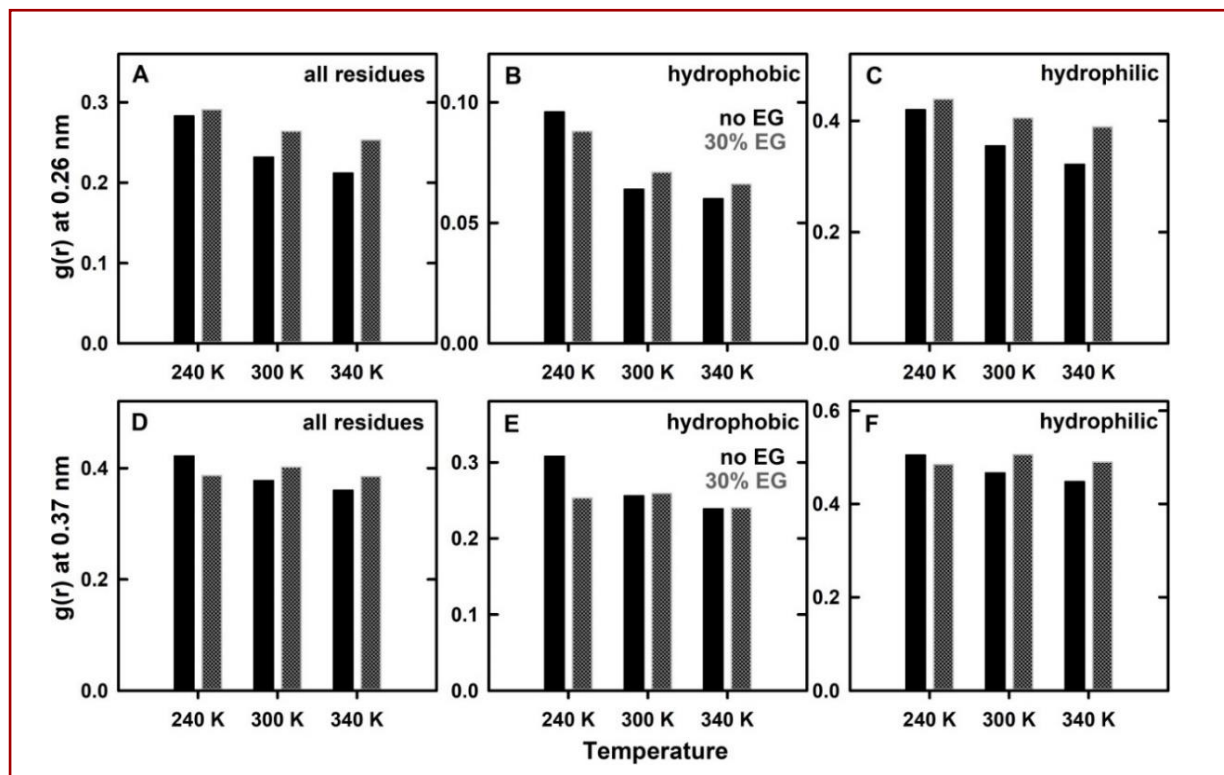


Fig. 4.11. The values of first (top panels) and second (bottom panels) peaks of RDF plots for the distribution of water molecules around α -LA (Fig. 10) obtained from C-MD simulations of the protein at different temperatures in the absence (black bars) and the presence (grey textured bars) of EG. The peak values were obtained from the RDFs plotted by taking into account of all the residues of the protein (A & D), only the hydrophobic residues (B & E) and only the hydrophilic residues (C & F).

To evaluate the solvent and cosolvent occupancy around the protein, RDF for water and EG around α -LA were analysed from C-MD simulations. The RDF of water (Fig. 4.10) decreased with increasing temperature around both the hydrophobic and the hydrophilic residues of α -LA in the absence of EG. In the presence of EG as well, the distribution of water was reduced at higher temperatures. However, the distribution of water around hydrophobic residues was reduced at lower temperature (240 K) upon addition of EG and at higher temperatures the changes were minimal (Fig. 4.11). The water molecules around polar residues were notably increased at higher temperatures (300 and 340 K) in the presence of EG.

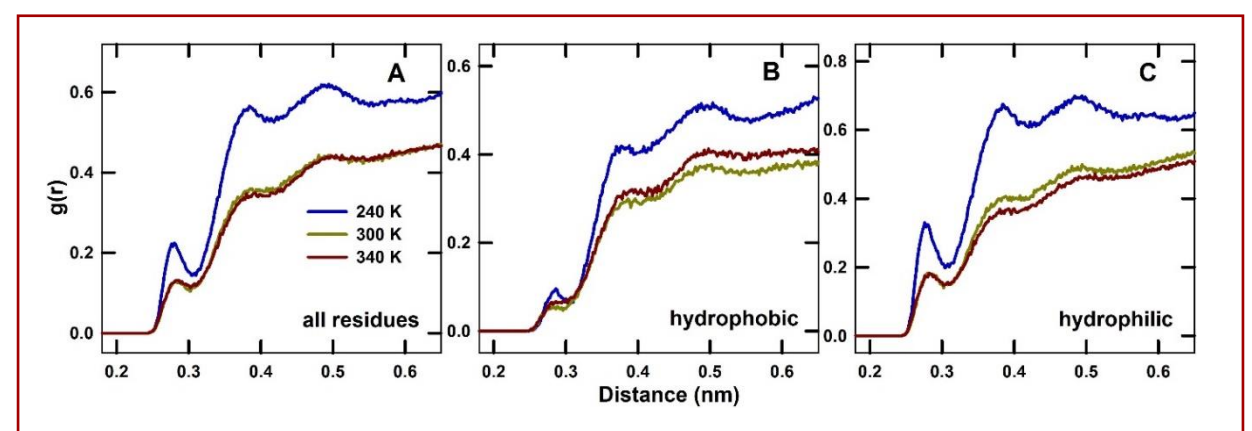


Fig. 4.12. Radial distribution function of EG around all the surface residues of α -LA, only around hydrophobic residues and only around hydrophilic residues calculated from the C-MD simulations carried out at 240 (blue), 300 (green) and 340 K (red).

In addition, RDF of EG around the protein (Fig. 4.12) suggested that the distribution of EG reduced at higher temperatures. The EG around hydrophobic residues was slightly more at 240 K (Fig. 4.13) and it showed significantly higher values around hydrophilic residues at lower temperatures.

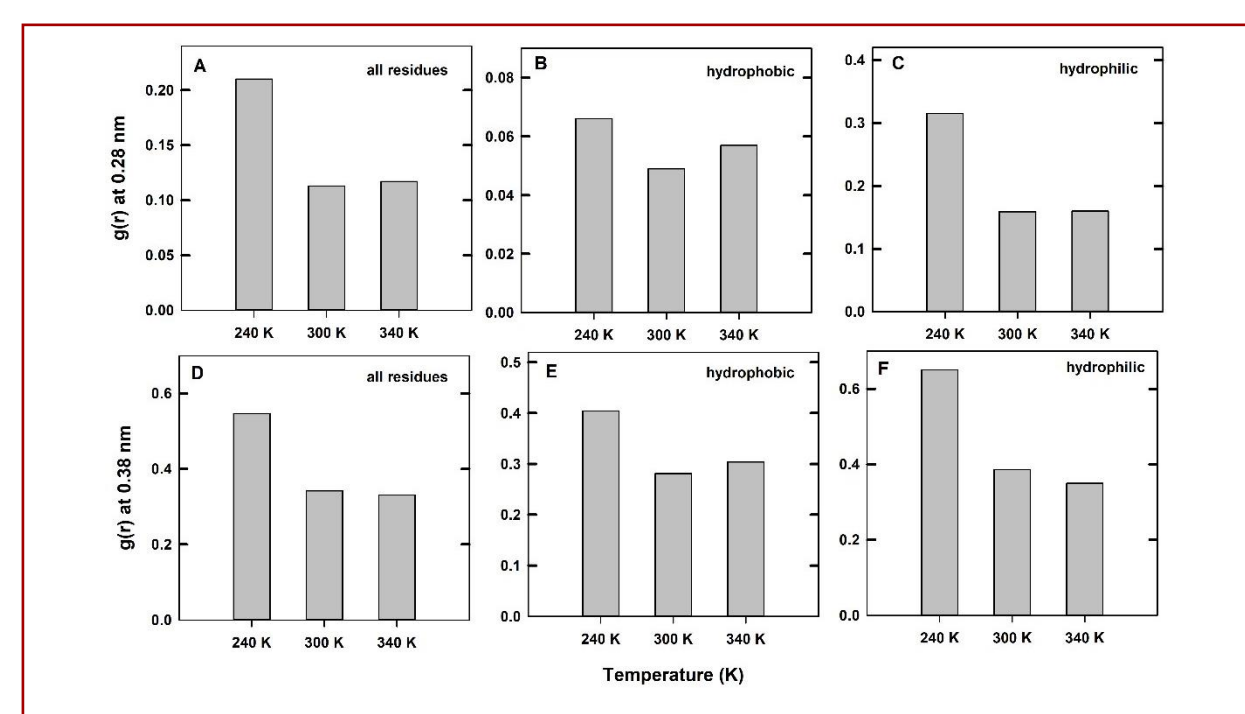


Fig. 4.13. The values of first (top panels) and second (bottom panels) peaks of RDF plots for the distribution of EG molecules around α -LA (Fig. 4.12). The peak values were obtained from the RDFs plotted by taking into account of all the residues of the protein (A & D), only the hydrophobic residues (B & E) and only the hydrophilic residues (C & F).

The RDFs were also plotted for the trajectories obtained from REMD simulations at four different temperatures. They also showed similar changes (Fig. 4.14 and 4.15) in RDF plots. These results indicated that the distribution of water and EG around hydrophilic and hydrophobic residues was significantly altered with temperature.

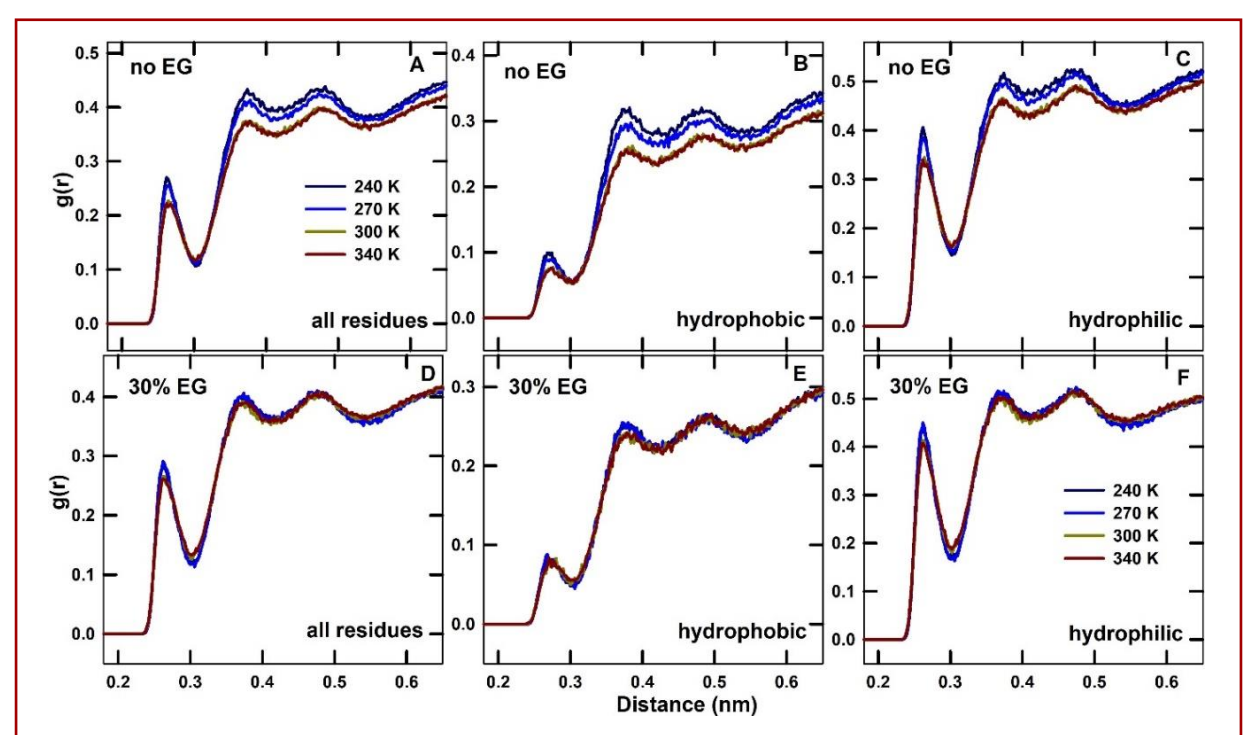


Fig. 4.14. Radial distribution function of water around α -LA calculated from the conformations extracted from REMD simulation at varying temperatures, 240 K (dark blue), 270 K (light blue), 300 K (green), and 340 K (red), in the absence (upper panels) and the presence (lower panel) of EG. The distribution of water around all the residues (A and D), only hydrophobic residues (B and E), and only hydrophilic residues (C and F) of α -LA

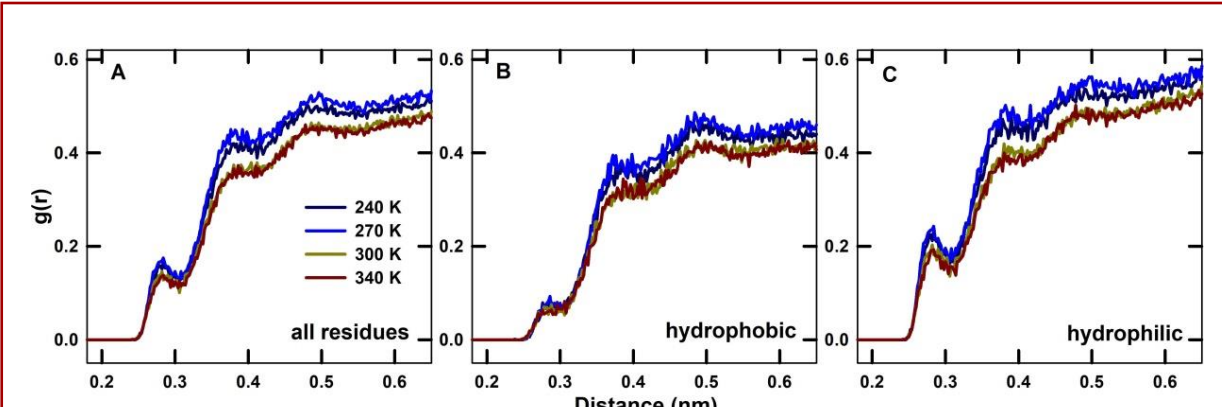


Fig. 4.15 Radial distribution function of EG around α -LA calculated from the conformations extracted from REMD simulation at varying temperatures, 240 K (dark blue), 270 K (light blue), 300 K (green), and 340 K (red). The distribution of cosolvent around all the residues (A and D), only hydrophobic residues (B and E), and only hydrophilic residues (C and F) of α -LA.

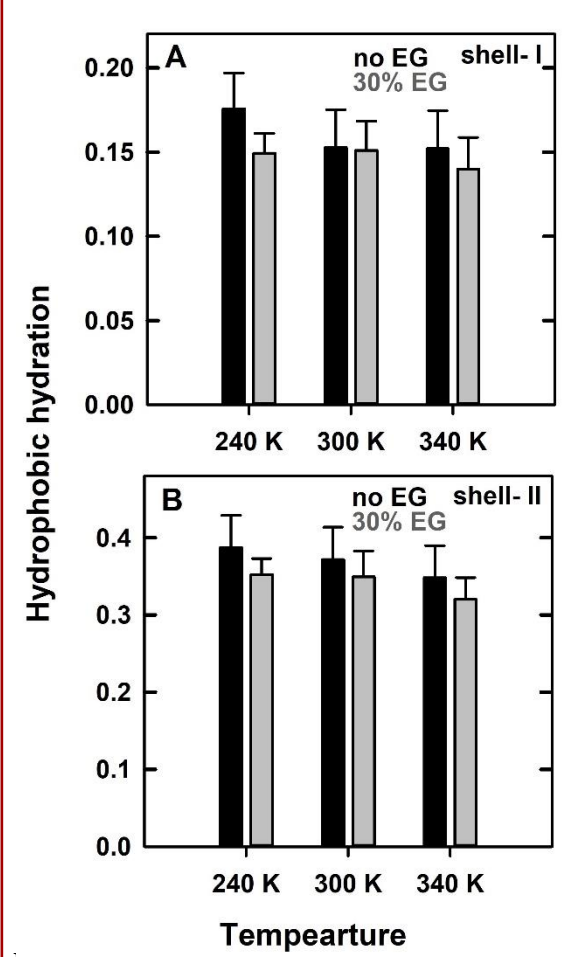


Fig. 4.16. Hydrophobic hydration of α -LA calculated using equation 3.4.5 at different temperatures in the absence (black) and the presence (grey) of EG with a cut-off of 0.28 nm (A) and 0.40 nm (B) representing first and second hydration shells on the protein surface, respectively.

For further insight into these changes, the hydration ratio between hydrophobic and the hydrophilic surfaces was calculated using equation 3.4.5 with the distance cutoffs 0.28 and 0.40 nm (Fig. 4.16). These cut-off values corresponded to the first and the second dips of the RDF plots, representing the first and the secondhydration shells from the protein surface, respectively. Hydrophobic hydration decreased as the temperature increased and notably the addition of EG decreased the value at all the temperatures in both the first- and second- hydration shells. The distribution of EG between the surface of the protein and the bulk solvent is one of the crucial determinants on its effect on the stability of proteins. This was measured as local-bulk partition coefficient (K_p) for each and every amino acid residue as given by equation 3.4.3 [57].

 K_p values were calculated from the trajectories obtained from C-MD and from four-selected temperatures (240, 270, 300 and 340 K) of REMD simulation (Fig. 4.17). K_p values were higher at 240 K compared to 300 K for all the amino acid residues except for Pro and Met. Though the K_p values for some of the hydrophobic residues are slightly higher at 340 K compared to 300 K, they were still significantly lesser than the K_p values at 240 K. It was also observed that the K_p values were higher for the hydrophobic residues Trp, Tyr, Ala, Gly, Ile, and Leu, and for charged residues Gln, Asp and His. The values were lowest for Glu and Asp residues.

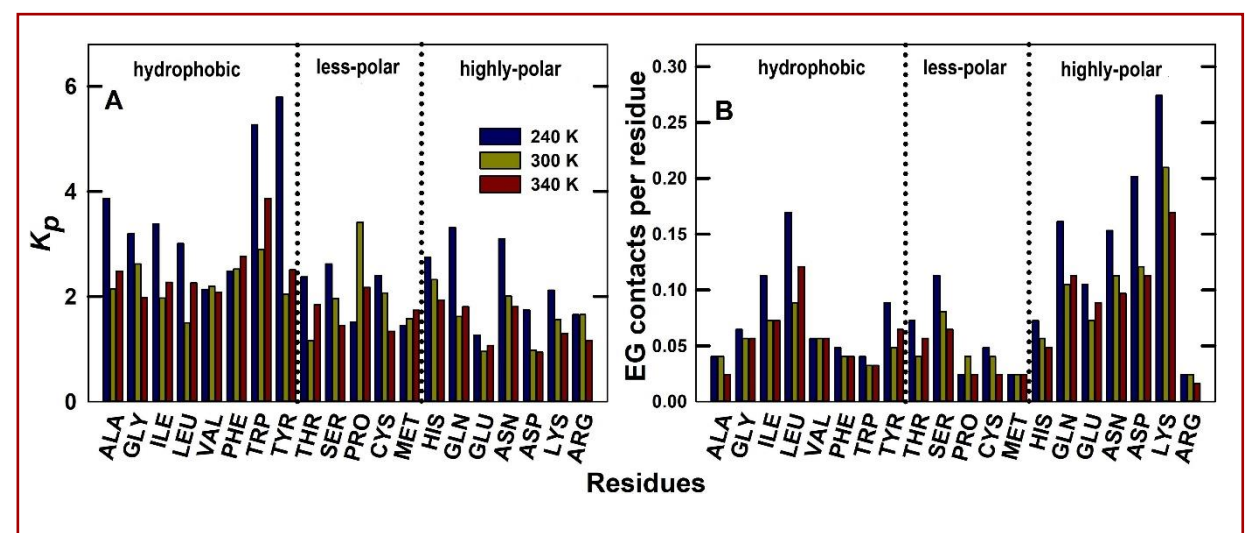


Fig. 4.17. The partition coefficient of EG around the protein (K_p) calculated using equation 3.4.3 for each residue (A) from C-MD simulations performed at 240 K (blue), 300 K (green) and 340 K (red), and (B) from REMD trajectories at selected temperatures, 240 K (dark blue), 270 K (blue), 300 K (green), and 340 K (red).

For better interpretation, K_p values were calculated for different residue types (hydrophobic, less-polar and highly-polar) and compared with the values obtained for the whole protein (Fig. 4.18). The higher K_p values for the overall protein at lower temperatures suggested that the extent of binding of EG with α -LA was significantly high at sub-zero temperature.

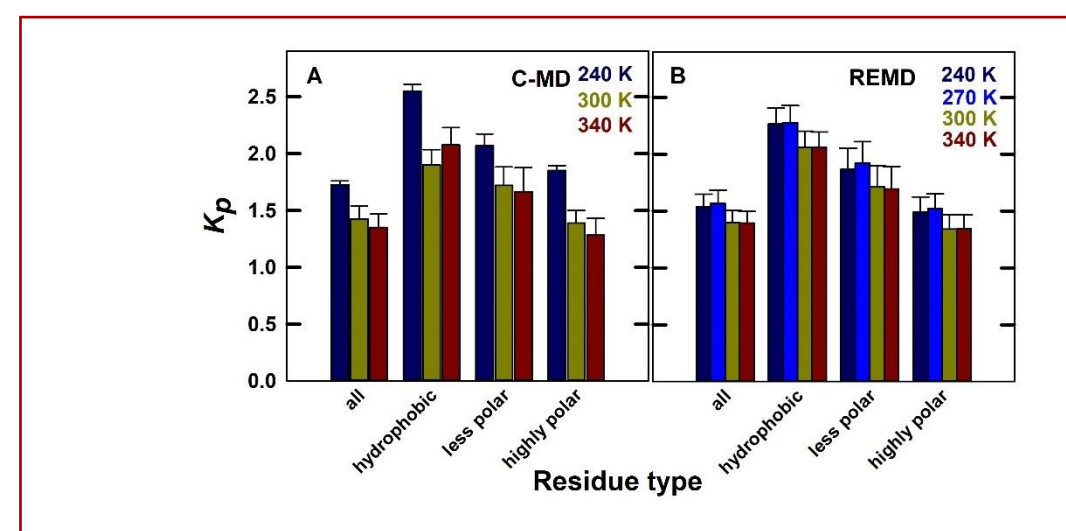


Fig. 4.18. The partition coefficient of EG around the protein (K_p) calculated using equation 3.4.3 for all the residues and different residue types (hydrophobic, less polar and highly polar) from C-MD simulation (A) and at selected temperatures from REMD trajectories (B).

The K_p values calculated for individual residue types suggested that the binding of EG around the hydrophobic residues were more compared to the other residues and highly polar residues have less binding with EG. In addition, K_p values calculated from the trajectories obtained from REMD simulations at varying temperatures (Fig. 4.18B) also showed similar trend, reiterating the fact that the binding of EG with hydrophobic residues was higher at lower temperatures.

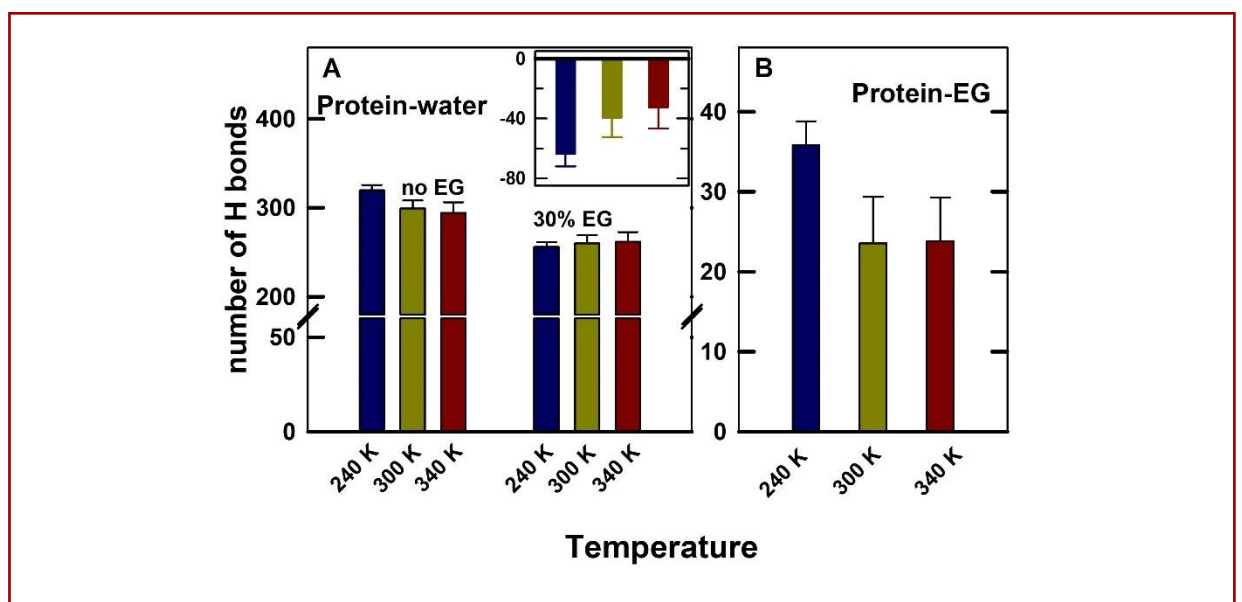


Fig. 4.19. (A) The number of hydrogen bonds between α -LA and water in the absence and the presence of EG calculated at different temperatures from C-MD simulations. The inset shows the number of H-bonds lost between α -LA and water upon addition of EG. (B) The number of H-bonds between α -LA and EG.

To ascertain this, the number of H-bonding interactions formed by water and EG with α -LA was evaluated, as H-bonding could be the primary interaction of these molecules with the protein. It was observed that the number of H-bonds formed by water was reduced at higher temperatures in absence of any cosolvent, whereas it was marginally increased in presence of EG (Fig. 4.19). The number of H-bonds lost upon the addition of EG was more at 240 K (inset Fig. 4.19). At the same time, the number of H-bonds between EG and protein was significantly higher at lower temperature (Fig. 4.19B). These observations complement the K_p values that EG has more interactions with the protein at sub-zero temperature by replacing a significant number of water molecules around the protein.

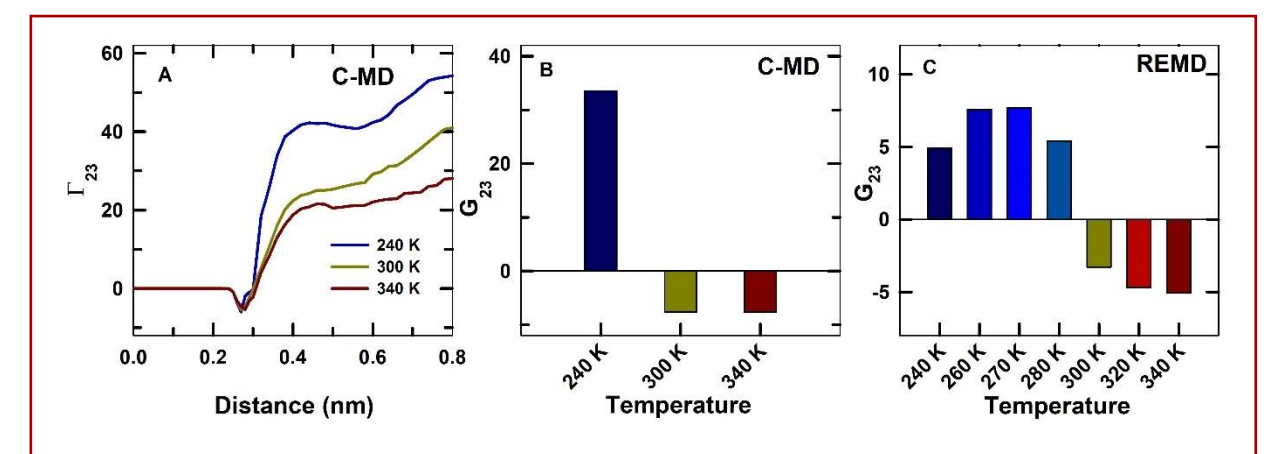


Fig. 4.20. (A) Distance-wise preferential binding coefficient (Γ 23) for EG with α-LA calculated using equation 3.4.4 at different temperatures from C-MD simulations. (B) The preferential binding calculated by Kirkwood-Buff integral (G₂₃) using equation 4.4.3 from C-MD simulations. (C) The preferential binding calculated by Kirkwood-Buff integral (G₂₃) from REMD trajectories.

Preferential interaction (PI) of the cosolvent, EG was evaluated by two different parameters. Domain-based mean distribution of solvent and cosolvent (Γ_{23}) [58] was calculated at regular intervals of the distance from the protein surface (Fig. 4.20A) using equation 3.4.4. Also, PI was calculated from Kirkwood-Buff integral approach (G_{23}) using equation 4.4.3. based on RDF with the cut-off of 0.5 nm from C-MD simulation trajectories (Fig. 4.20B).

Distance-based Γ_{23} showed a small negative value at 0.27 nm corresponding to the first solvation-shell; however, it became positive above the distance of 0.3 nm. At 240 K, the Γ_{23} values of EG were significantly higher than the values at 300 K which were slightly negative at higher temperatures. The G_{23} values was found to be positive at 240 K and was slightly negative at higher temperatures. Also, the temperature-dependent G_{23} values calculated from REMD (Fig. 4.20C) simulations showed that PI of EG with protein was positive up to 280 K and became negative above 280 K. These observations clearly indicated that the preferential binding of EG at lower temperature is significantly larger compared to its values at above 300 K.

4.6. DISCUSSION

4.6.1 Effect of EG on the thermal denaturation and structure of α-LA

The experimental observations (Fig. 4.2) show that α -LA is stabilized by EG during cold denaturation, whereas EG destabilizes the protein during heat-induced denaturation. The resultant shift in the free-energy profile (Fig. 4.2B) is found to be due to reduction in overall heat capacity (ΔC_p) (Fig. 4.2E) and shift in the temperature of maximum stability to a lower value (Fig. 4.2F). The positive heat capacity change during the thermal denaturation is mainly attributed to the strong temperature dependence of enthalpy and entropy of exposure of buried hydrophobic residues to the water [59,60]. Reduction in ΔC_p values suggests that the hydrophobic exposure is reduced upon the addition of EG. The accompanying shift in the T_{max} towards lower temperature indicates that this effect would be significant at lower temperatures.

The structural changes in α -LA analysed by MD simulation trajectories indicate that there are significant changes in the secondary structural content of the protein during thermal denaturation (Fig. 4.6). This is also associated with an increase in SASA and significant loss of native contacts in the protein (Fig. 4.7). Earlier experimental studies show that the initial unfolding of α -LA occurs around β -subdomains along with the turns in the region which forms molten globule-like structural intermediate [27,56]. The hydrogen exchange experiments have also shown that β -subdomain is less protected in the MG-like state and helix-8 is the least protected among all α -helices in the protein [56]. The present MD simulation studies show that either an increase or decrease in simulation temperature led to the loss of all the β -strands in the protein (Fig. 4.9 and Table 4.3). At lower temperature, α -LA shows a partial unfolding of helix-1 and during higher temperature simulation helix-8 is also partially unfolded. The initial loss of β -strands has been noted during the cold denaturation of protein L9 [61] and yeast frataxin [62] as well. Kim *et al* (2016) relate the high stability of α -helices against cold-induced denaturation to the prevalent presence of helices in the anti-freeze peptides of cold organisms and hypothesized that this might be an evolutionary constraint.

EG does not significantly alter the secondary structure of α -LA at room temperature. However, at lower temperatures, the presence of EG retarded the denaturation of strand 1 and 3 and the β -turns during cold denaturation. In contrast, the presence of EG at higher temperature

denatures the strands and helix-8 as well. The overall structural changes assessed from MD simulations using SASA, native contacts and secondary structural contents suggests that the cold-induced unfolding of α -LA is reduced by the addition of EG, whereas the protein is destabilized in the presence of EG at higher temperatures.

4.6.2 Interaction of EG with α-LA

The density of water and cosolvent around the surface of a protein is mainly attributed to the stability changes of the protein during cold denaturation [63,64]. The initial analysis of RDF values shows that the distribution of water around the protein decreases with increasing temperature, whereas the water around the hydrophobic residues is notably reduced at low temperature in the presence of EG which is evident from the first two peaks of RDFs of the protein (Fig. 4.11B and 4.11C). The hydrophobic hydration values calculated for the first and second solvation (Fig. 4.16) shells also suggest a decrease in the number of water molecules around the protein with an increase in temperature and with addition of EG as well. Cold denaturation study with a simple protein monomer-water model [63] predicts that at lower temperature water molecules destabilize the hydrophobic contacts through 'solvent-separated configurations' by forming clusters around hydrophobic residues. This configuration is proposed to be similar to the pressure-induced unfolded states of proteins. The solvent layers around hydrophobic residues might decrease the entropy of the system during cold denaturation as observed in experiments [49,65–68]. Thus, the decrease in water molecules in the presence of EG at lower temperature might indicate the reduction in cold-induced unfolding of the protein.

Furthermore, the partition coefficient of EG (K_p) around the protein is higher at lower temperatures. The residue-wise analysis (Fig. 4.17 and 4.18) clearly demonstrates that the K_p values are significantly larger for hydrophobic residues at lower temperatures, complementing the observations that EG preferably binds to hydrophobic residues at lower temperatures. Also, the number of H-bonds between the protein and water is reduced with the addition of EG and protein-EG interactions are higher at sub-zero temperature (Fig. 4.19). These results suggest that the binding of EG with α -LA at lower temperature reduces the hydration of hydrophobic residues. Earlier experimental results show that hydrophobic hydration is the major driving force in the enthalpy driven cold denaturation process [59,69]. Computational studies also suggest that solvent penetration into the hydrophobic regions promotes cold-induced

denaturation of proteins [19,62]. Therefore, we propose that the addition of EG might stabilize the protein by reducing the hydration of hydrophobic residues of α -LA. This also corroborates with the experimental observation that the negative enthalpy of cold-induced denaturation reduces with addition of EG. (Fig. 4.2D)

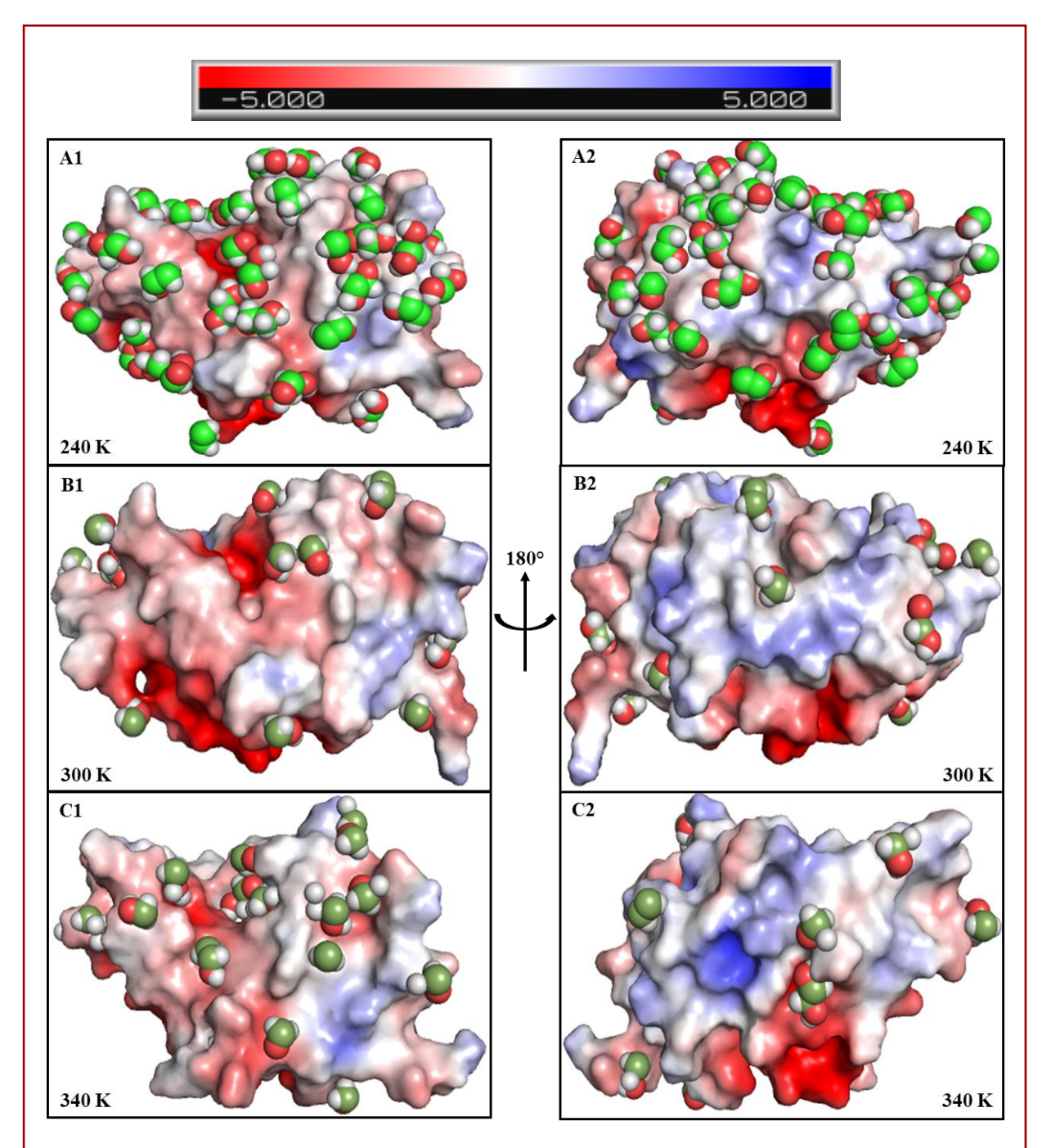


Fig. 4.21. Representative cartoons of binding of EG (spheres) on α -LA (surface) obtained from CMD simulations performed at 240 K (A1-A2), 300 K (B1-B2) and 340 K (C1 and C2). The right panels are 180° rotation of left panels. Red, blue and white colours on the protein surface represent negative, positive and non-polar charge distribution.

At higher temperatures, the binding of EG is reduced; however, the preferential binding of EG with the protein shifts its equilibrium towards more unfolded state as seen in the case of the denaturants [70,71]. In contrast, the other polyols such as glycerol [72] and trehalose [73] increase the preferential hydration of solvent molecules and stabilize the hydration shells around proteins. However, larger polyols such as chitosan and PEG are found to interact with proteins through hydrophobic interactions and hydrogen bonding and stabilizes the proteins by increasing the compactness [74,75]. Furthermore, the PI parameters (Fig. 4.19) calculated by mean distribution (Γ_{23}) and by Kirkwood-Buff integral (G_{23}) suggest that the preferential binding of EG is significantly higher at sub-zero temperature, whereas it is reduced at higher temperatures, even it shows a marginal amount of preferential hydration character (Fig. 4.20B). Representative surface cartoon diagrams were created from C-MD simulation trajectories to explain the overall interaction between α -LA and EG at different temperature conditions (Fig.4. 21). The structural representations clearly indicate the preferential binding of EG to the hydrophobic residues at lower temperature and the decrease in interaction of EG with the protein at higher temperature.

The commonly accepted hypothesis on osmolyte-induced stability changes on protein proposes that a destabilizing osmolyte would preferentially interact with the protein, thus shifts the equilibrium towards unfolded state. A stabilizing osmolyte would be exclude from the surface of the protein to confer stability by increasing it surface hydration. This might be valid at ambient conditions; however, this phenomenon could not be simply extended to sub-zero temperature conditions. The thermal denaturation studies of α -LA suggest that EG stabilizes the protein by preferentially binding to the protein, particularly around the hydrophobic residues, during cold-induced denaturation. However, the preferential binding of EG destabilizes the protein against heat denaturation denaturation processes. Furthermore, this study is limited to the polyol class of osmolyte alone. The effect of other classes of osmolytes on cold-induced denaturation of proteins also need to be examined which might establish the complete role of hydrophobic hydration on the stability of proteins at sub-zero temperatures.

4.7 CONCLUSION

The thermal denaturation experiment indicates that EG acts as a stabilizing agent or a denaturant depending on the temperature, whereas the other osmolytes so far reported show stabilizing effects at all the temperature ranges. Computational studies suggest that a decrease in the hydration of hydrophobic residues along with increased binding of EG around the hydrophobic residues stabilizes α -LA during cold-induced denaturation. This could be associated with the experimentally observed decrease in the negative enthalpy of cold denaturation upon addition of EG. The presence of EG destabilizes the protein at higher temperature via preferential binding similar to chemical denaturants.

4.8 REFERENCES

- [1] F.J.A.L. Cruz, J.N. Canongia Lopes, J.C.G. Calado, M.E. Minas da Piedade, A Molecular Dynamics Study of the Thermodynamic Properties of Calcium Apatites. 1. Hexagonal Phases, J. Phys. Chem. B. 109 (2005) 24473–24479. https://doi.org/10.1021/jp054304p.
- [2] D.W. Brenner, Empirical potential for hydrocarbons for use in simulating the chemical vapor deposition of diamond films, Phys. Rev. B. 42 (1990) 9458–9471. https://doi.org/10.1103/PhysRevB.42.9458.
- [3] P.-W. Ma, W.C. Liu, C.H. Woo, S.L. Dudarev, Large-scale molecular dynamics simulation of magnetic properties of amorphous iron under pressure, J. Appl. Phys. 101 (2007) 73908. https://doi.org/10.1063/1.2715753.
- [4] J.-L. Barrat, J. Baschnagel, A. Lyulin, Molecular dynamics simulations of glassy polymers, Soft Matter. 6 (2010) 3430–3446. https://doi.org/10.1039/B927044B.
- [5] G. Ciccotti, L. Delle Site, The physics of open systems for the simulation of complex molecular environments in soft matter, Soft Matter. 15 (2019) 2114–2124. https://doi.org/10.1039/C8SM02523A.

- [6] R.M. Venable, A. Krämer, R.W. Pastor, Molecular Dynamics Simulations of Membrane Permeability, Chem. Rev. 119 (2019) 5954–5997. https://doi.org/10.1021/acs.chemrev.8b00486.
- [7] D.E. Shaw, P. Maragakis, K. Lindorff-Larsen, S. Piana, et al., Atomic-Level Characterization of the Structural Dynamics of Proteins, Science (80-.). 330 (2010) 341 346. https://doi.org/10.1126/science.1187409.
- [8] T. Heydari, M. Heidari, O. Mashinchian, M. Wojcik, et al., Development of a Virtual Cell Model to Predict Cell Response to Substrate Topography, ACS Nano. 11 (2017) 9084–9092. https://doi.org/10.1021/acsnano.7b03732.
- [9] N. Haque, N.P. Prabhu, Lid dynamics of porcine pancreatic lipase in non-aqueous solvents, Biochim. Biophys. Acta Gen. Subj. 1860 (2016) 2326–2334. https://doi.org/10.1016/j.bbagen.2016.05.006.
- [10] N. Haque, N.P. Prabhu, Lid closure dynamics of porcine pancreatic lipase in aqueous solution, Biochim. Biophys. Acta Gen. Subj. 1860 (2016) 2313–2325. https://doi.org/10.1016/j.bbagen.2016.05.004.
- [11] M. Feig, G. Nawrocki, I. Yu, P. Wang, et al., Challenges and opportunities in connecting simulations with experiments via molecular dynamics of cellular environments, J. Phys. Conf. Ser. 1036 (2018) 12010. https://doi.org/10.1088/1742-6596/1036/1/012010.
- [12] S. Bottaro, K. Lindorff-Larsen, Biophysical experiments and biomolecular simulations: A perfect match?, Science (80-.). 361 (2018) 355 360. https://doi.org/10.1126/science.aat4010.
- [13] A. Hospital, J.R. Goñi, M. Orozco, J.L. Gelpí, Molecular dynamics simulations: advances and applications, Adv. Appl. Bioinform. Chem. 8 (2015) 37–47. https://doi.org/10.2147/AABC.S70333.
- [14] T.J. Lane, D. Shukla, K.A. Beauchamp, V.S. Pande, To milliseconds and beyond: challenges in the simulation of protein folding, Curr. Opin. Struct. Biol. 23 (2013) 58– 65. https://doi.org/10.1016/j.sbi.2012.11.002.

- [15] Y. Sugita, Y. Okamoto, Replica-exchange molecular dynamics method for protein folding, Chem. Phys. Lett. 314 (1999) 141–151. https://doi.org/10.1016/S0009-2614(99)01123-9.
- [16] A. Friedman, Simulated annealing in protein folding BT Mathematics in Industrial Problems: Part 5, in: A. Friedman (Ed.), Springer New York, New York, NY, 1992: pp. 78–87. https://doi.org/10.1007/978-1-4615-7405-7_8.
- [17] A. Barducci, M. Bonomi, M. Parrinello, Metadynamics, WIREs Comput. Mol. Sci. 1 (2011) 826–843. https://doi.org/10.1002/wcms.31.
- [18] N.-V. Buchete, G. Hummer, Peptide folding kinetics from replica exchange molecular dynamics, Phys. Rev. E. 77 (2008) 30902. https://doi.org/10.1103/PhysRevE.77.030902.
- [19] S.B. Kim, J.C. Palmer, P.G. Debenedetti, Computational investigation of cold denaturation in the Trp-cage miniprotein, Proc. Natl. Acad. Sci. 113 (2016) 8991 – 8996. https://doi.org/10.1073/pnas.1607500113.
- [20] S.T. Ngo, H.M. Hung, K.N. Tran, M.T. Nguyen, Replica exchange molecular dynamics study of the amyloid beta (11–40) trimer penetrating a membrane, RSC Adv. 7 (2017) 7346–7357. https://doi.org/10.1039/C6RA26461A.
- [21] A. V Yeager, J.M. Swails, B.R. Miller, Improved Accuracy for Constant pH-REMD Simulations through Modification of Carboxylate Effective Radii, J. Chem. Theory Comput. 13 (2017) 4624–4635. https://doi.org/10.1021/acs.jctc.7b00638.
- [22] R. Piziak, J.J. Mitchell, Hamiltonian formalism and the state of a physical system, Comput. Math. with Appl. 42 (2001) 793–805. https://doi.org/10.1016/S0898-1221(01)00199-7.
- [23] D.A. McQuarrie, M.Q.D. A, Statistical Mechanics, Harper & Row, 1975. https://books.google.co.in/books?id=PANRAAAAMAAJ.
- [24] D.A. McQuarrie, Molecular Thermodynamics, Viva Books Private Limited, 2010. https://books.google.co.in/books?id=zN7mTgEACAAJ.

- [25] R. Qi, G. Wei, B. Ma, R. Nussinov, Replica Exchange Molecular Dynamics: A Practical Application Protocol with Solutions to Common Problems and a Peptide Aggregation and Self-Assembly Example BT Peptide Self-Assembly: Methods and Protocols, in: B.L. Nilsson, T.M. Doran (Eds.), Springer New York, New York, NY, 2018: pp. 101–119. https://doi.org/10.1007/978-1-4939-7811-3_5.
- [26] M.M. Seibert, A. Patriksson, B. Hess, D. van der Spoel, Reproducible Polypeptide Folding and Structure Prediction using Molecular Dynamics Simulations, J. Mol. Biol. 354 (2005) 173–183. https://doi.org/10.1016/j.jmb.2005.09.030.
- [27] M. Mizuguchi, D. Hashimoto, M. Sakurai, K. Nitta, Cold denaturation of α-lactalbumin, Proteins Struct. Funct. Bioinforma. 38 (2000) 407–413. https://doi.org/10.1002/(SICI)1097-0134(20000301)38.
- [28] A.C.W. Pike, K. Brew, K.R. Acharya, Crystal structures of guinea-pig, goat and bovine α-lactalbumin highlight the enhanced conformational flexibility of regions that are significant for its action in lactose synthase, Structure. 4 (1996) 691–703. https://doi.org/10.1016/S0969-2126(96)00075-5.
- [29] A. Patriksson, D. van der Spoel, A temperature predictor for parallel tempering simulations, Phys. Chem. Chem. Phys. 10 (2008) 2073–2077. https://doi.org/10.1039/B716554D.
- [30] M.J. Abraham, T. Murtola, R. Schulz, S. Páll, et al., GROMACS: High performance molecular simulations through multi-level parallelism from laptops to supercomputers, SoftwareX. 1–2 (2015) 19–25. https://doi.org/10.1016/j.softx.2015.06.001.
- [31] J. Huang, A.D. MacKerell Jr, CHARMM36 all-atom additive protein force field: Validation based on comparison to NMR data, J. Comput. Chem. 34 (2013) 2135–2145. https://doi.org/10.1002/jcc.23354.
- [32] G. Bussi, D. Donadio, M. Parrinello, Canonical sampling through velocity rescaling, J. Chem. Phys. 126 (2007) 14101. https://doi.org/10.1063/1.2408420.
- [33] M. Parrinello, A. Rahman, Polymorphic transitions in single crystals: A new molecular dynamics method, J. Appl. Phys. 52 (1981) 7182–7190. https://doi.org/10.1063/1.328693.

- [34] C. Yang, S. Jang, Y. Pak, A fully atomistic computer simulation study of cold denaturation of a β-hairpin, Nat. Commun. 5 (2014) 5773. https://doi.org/10.1038/ncomms6773.
- [35] J.L.F. Abascal, C. Vega, A general purpose model for the condensed phases of water: TIP4P/2005, J. Chem. Phys. 123 (2005) 234505. https://doi.org/10.1063/1.2121687.
- [36] S. Menon, N. Sengupta, The Cold Thermal Response of an Amyloid Oligomer Differs from Typical Globular Protein Cold Denaturation, J. Phys. Chem. Lett. 10 (2019) 2453–2457. https://doi.org/10.1021/acs.jpclett.9b00709.
- [37] W. Humphrey, A. Dalke, K. Schulten, VMD: Visual molecular dynamics, J. Mol. Graph. 14 (1996) 33–38. https://doi.org/10.1016/0263-7855(96)00018-5.
- [38] A. Bondi, van der Waals Volumes and Radii, J. Phys. Chem. 68 (1964) 441–451. https://doi.org/10.1021/j100785a001.
- [39] F. Eisenhaber, P. Lijnzaad, P. Argos, C. Sander, et al., The double cubic lattice method: Efficient approaches to numerical integration of surface area and volume and to dot surface contouring of molecular assemblies, J. Comput. Chem. 16 (1995) 273–284. https://doi.org/10.1002/jcc.540160303.
- [40] A. Amadei, A.B.M. Linssen, H.J.C. Berendsen, Essential dynamics of proteins, Proteins Struct. Funct. Bioinforma. 17 (1993) 412–425. https://doi.org/10.1002/prot.340170408.
- [41] I.D.A. Amadei, Essential dynamics: foundation and applications, Wiley Interdiscip. Rev. Comput. Mol. Sci. 2 (2012) 762–770. https://doi.org/10.1002/wcms.1099.
- [42] Y.R. Espinosa, J.R. Grigera, E.R. Caffarena, Essential dynamics of the cold denaturation: pressure and temperature effects in yeast frataxin, Proteins Struct. Funct. Bioinforma. 85 (2017) 125–136. https://doi.org/10.1002/prot.25205.
- [43] B. Anumalla, N.P. Prabhu, Surface hydration and preferential interaction directs the charged amino acids-induced changes in protein stability, J. Mol. Graph. Model. 98 (2020) 107602. https://doi.org/10.1016/j.jmgm.2020.107602.

- [44] B.M. Baynes, B.L. Trout, Proteins in Mixed Solvents: A Molecular-Level Perspective, J. Phys. Chem. B. 107 (2003) 14058–14067. https://doi.org/10.1021/jp0363996.
- [45] G.S. Jas, E.C. Rentchler, A.M. Słowicka, J.R. Hermansen, et al., Reorientation Motion and Preferential Interactions of a Peptide in Denaturants and Osmolyte, J. Phys. Chem. B. 120 (2016) 3089–3099. https://doi.org/10.1021/acs.jpcb.6b00028.
- [46] D. Shukla, C. Shinde, B.L. Trout, Molecular Computations of Preferential Interaction Coefficients of Proteins, J. Phys. Chem. B. 113 (2009) 12546–12554. https://doi.org/10.1021/jp810949t.
- [47] B.L. Chen, J.A. Schellman, Low-temperature unfolding of a mutant of phage T4 lysozyme. 1. Equilibrium studies, Biochemistry. 28 (1989) 685–691. https://doi.org/10.1021/bi00428a041.
- [48] A. Pastore, S.R. Martin, A. Politou, K.C. Kondapalli, et al., Unbiased Cold Denaturation: Low- and High-Temperature Unfolding of Yeast Frataxin under Physiological Conditions, J. Am. Chem. Soc. 129 (2007) 5374–5375. https://doi.org/10.1021/ja0714538.
- [49] H.I. Rösner, M. Caldarini, A. Prestel, M.A. Vanoni, et al., Cold Denaturation of the HIV-1 Protease Monomer, Biochemistry. 56 (2017) 1029–1032. https://doi.org/10.1021/acs.biochem.6b01141.
- [50] J.M. Swails, A.E. Roitberg, Enhancing Conformation and Protonation State Sampling of Hen Egg White Lysozyme Using pH Replica Exchange Molecular Dynamics, J. Chem. Theory Comput. 8 (2012) 4393–4404. https://doi.org/10.1021/ct300512h.
- [51] Y. Mu, Y. Yang, W. Xu, Hybrid Hamiltonian replica exchange molecular dynamics simulation method employing the Poisson–Boltzmann model, J. Chem. Phys. 127 (2007) 84119. https://doi.org/10.1063/1.2772264.
- [52] H. Jalily Hasani, M. Ahmed, K. Barakat, A comprehensive structural model for the human KCNQ1/KCNE1 ion channel, J. Mol. Graph. Model. 78 (2017) 26–47. https://doi.org/10.1016/j.jmgm.2017.09.019.

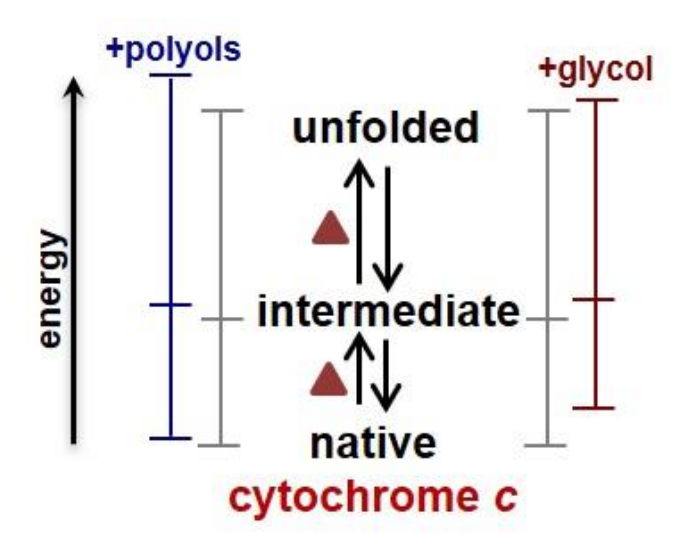
- [53] W. Kabsch, C. Sander, Dictionary of protein secondary structure: Pattern recognition of hydrogen-bonded and geometrical features, Biopolymers. 22 (1983) 2577–2637. https://doi.org/10.1002/bip.360221211.
- [54] R.A. Laskowski, PDBsum: summaries and analyses of PDB structures, Nucleic Acids Res. 29 (2001) 221–222. https://doi.org/10.1093/nar/29.1.221.
- [55] E.G. Hutchinson, J.M. Thornton, PROMOTIF--a program to identify and analyze structural motifs in proteins., Protein Sci. 5 (1996) 212–220. https://doi.org/10.1002/pro.5560050204.
- [56] B.A. Schulman, C. Redfield, Z. Peng, C.M. Dobson, et al., Different Subdomains are Most Protected From Hydrogen Exchange in the Molten Globule and Native States of Human α-Lactalbumin, J. Mol. Biol. 253 (1995) 651–657. https://doi.org/10.1006/jmbi.1995.0579.
- [57] E.S. Courtenay, M.W. Capp, C.F. Anderson, M.T. Record, Vapor Pressure Osmometry Studies of Osmolyte–Protein Interactions: Implications for the Action of Osmoprotectants in Vivo and for the Interpretation of "Osmotic Stress" Experiments in Vitro, Biochemistry. 39 (2000) 4455–4471. https://doi.org/10.1021/bi9928871.
- [58] D.R. Canchi, A.E. García, Cosolvent Effects on Protein Stability, Annu. Rev. Phys. Chem. 64 (2013) 273–293. https://doi.org/10.1146/annurev-physchem-040412-110156.
- [59] P.L. Privalov, Cold Denaturation of Protein, Crit. Rev. Biochem. Mol. Biol. 25 (1990)281–306. https://doi.org/10.3109/10409239009090613.
- [60] B.W.J. and S.J. A, Protein stability curves, Biopolymers. 26 (1987) 1859. http://dx.doi.org/10.1002/bip.360261104.
- [61] B. Shan, S. McClendon, C. Rospigliosi, D. Eliezer, et al., The Cold Denatured State of the C-terminal Domain of Protein L9 Is Compact and Contains Both Native and Nonnative Structure, J. Am. Chem. Soc. 132 (2010) 4669–4677. https://doi.org/10.1021/ja908104s.

- [62] P. Chatterjee, S. Bagchi, N. Sengupta, The non-uniform early structural response of globular proteins to cold denaturing conditions: A case study with Yfh1, J. Chem. Phys. 141 (2014) 205103. https://doi.org/10.1063/1.4901897.
- [63] C.L. Dias, T. Ala-Nissila, M. Karttunen, I. Vattulainen, et al., Microscopic Mechanism for Cold Denaturation, Phys. Rev. Lett. 100 (2008) 118101. https://doi.org/10.1103/PhysRevLett.100.118101.
- [64] A. Grimaldi, G. Graziano, Water and cold denaturation of small globular proteins, J. Mol. Liq. 264 (2018) 579–584. https://doi.org/10.1016/j.molliq.2018.05.094.
- [65] E. V Adrover M Martorell G, Pastore A and Temussi P A, Understanding cold denaturation: the case study of Yfh1, J. Am. Chem. Soc. 132 (2010) 16240. http://dx.doi.org/10.1021/ja1070174.
- [66] C. Alfano, D. Sanfelice, S.R. Martin, A. Pastore, et al., An optimized strategy to measure protein stability highlights differences between cold and hot unfolded states, Nat. Commun. 8 (2017) 15428. https://doi.org/10.1038/ncomms15428.
- [67] B. Luan, B. Shan, C. Baiz, A. Tokmakoff, et al., Cooperative Cold Denaturation: The Case of the C-Terminal Domain of Ribosomal Protein L9, Biochemistry. 52 (2013) 2402–2409. https://doi.org/10.1021/bi3016789.
- [68] R. Yan, P. DeLos Rios, A. Pastore, P.A. Temussi, The cold denaturation of IscU highlights structure—function dualism in marginally stable proteins, Commun. Chem. 1 (2018) 13. https://doi.org/10.1038/s42004-018-0015-1.
- [69] P.L. Privalov, Y.V. Griko, S.Y. Venyaminov, V.P. Kutyshenko, Cold denaturation of myoglobin, J. Mol. Biol. 190 (1986) 487–498. https://doi.org/10.1016/0022-2836(86)90017-3.
- [70] L. Hua, R. Zhou, D. Thirumalai, B.J. Berne, Urea denaturation by stronger dispersion interactions with proteins than water implies a 2-stage unfolding, Proc. Natl. Acad. Sci. 105 (2008) 16928 16933. https://doi.org/10.1073/pnas.0808427105.
- [71] S.N. Timasheff, G. Xie, Preferential interactions of urea with lysozyme and their linkage to protein denaturation, Biophys. Chem. 105 (2003) 421–448. https://doi.org/10.1016/S0301-4622(03)00106-6.

- [72] M. Hirai, S. Ajito, M. Sugiyama, H. Iwase, et al., Direct Evidence for the Effect of Glycerol on Protein Hydration and Thermal Structural Transition, Biophys. J. 115 (2018) 313–327. https://doi.org/10.1016/j.bpj.2018.06.005.
- [73] C. Olsson, S. Genheden, V. García Sakai, J. Swenson, Mechanism of Trehalose-Induced Protein Stabilization from Neutron Scattering and Modeling, J. Phys. Chem.
 B. 123 (2019) 3679–3687. https://doi.org/10.1021/acs.jpcb.9b01856.
- [74] L. Bekale, P. Chanphai, S. Sanyakamdhorn, D. Agudelo, et al., Microscopic and thermodynamic analysis of PEG–β-lactoglobulin interaction, RSC Adv. 4 (2014) 31084–31093. https://doi.org/10.1039/C4RA03303E.
- [75] L. Bekale, D. Agudelo, H.A. Tajmir-Riahi, Effect of polymer molecular weight on chitosan–protein interaction, Colloids Surfaces B Biointerfaces. 125 (2015) 309–317. https://doi.org/10.1016/j.colsurfb.2014.11.037.

CHAPTER 5

Effect of Polyols on Thermal Unfolding Intermediate of Cytochrome c



5.1. ABSTRACT

Studies on intermediate states of proteins provide essential information on folding pathway and energy landscape of proteins. Osmolytes, known to alter the stability of proteins, might also affect the structure and energy states of folding intermediates. This was examined using cytochrome c (Cyt) as a model protein which forms a spectroscopically detectable intermediate during thermal denaturation transition. Most of the secondary structure and the native hemeligation was intact in the intermediate state of the protein. Denaturants, urea and guanidinium hydrochloride, and ionic salt destabilizes the intermediate and drive the protein to follow twostate transition. The effect of polyol class of osmolytes, glycol, glycerol, erythritol, xylitol and sorbitol (with OH-groups two to six), on the intermediate was studied using Soret absorbance and far-UV circular dichroism. With the increasing concentration of any of the polyols, the transition-midpoint temperature (T_m) and the enthalpy change (ΔH_m) for native to intermediate transition was decreased. This indicated that the intermediate was destabilized by the polyols. However, the polyols increased the overall stability of the protein by increasing T_m and ΔH_m for intermediate to unfolded transition, except in the case of glycol which destabilized the protein. These results show that the polyols could alter the energy state of the intermediate, and the effect of lower and higher polyols might be different on the stability and folding pathway of the protein.

5.2. INTRODUCTION

Small globular proteins tend to exhibit 'all or none' two-state transition between their native to unfolded states upon chemical, thermal and mechanical perturbations [1–4]. The twostate behaviour could be attributed to weak non-covalent interactions stabilizing the native conformation against unfolded conformations [5]. These transitions could be modulated by change in the solvent conditions such as pH or by the addition of salts or small organic molecules [6–10]. At some instances, intermediate states could not be recognized due to the limitations of probes to distinguish the intermediate states from the native or unfolded conformations. However, using multiple spectroscopic probes, intermediates have been identified and characterized for small globular proteins that were earlier known to exhibit a two-state behaviour [11–13]. Identification of such intermediates is essential to understand the folding pathway and the energetics involved. One of the well-characterized intermediate state in many small globular proteins is a molten globule (MG) state [14]. MG state is an expanded state as compared to the native state, and it retains most of the native secondary structures, but lacks a tight packaging of the sidechains [14,15]. MG intermediate is identified under equilibrium conditions and it is also found transiently during the kinetics of refolding reactions [16,17].

Apart from the MG intermediates, there are other intermediate structures such as dry molten globules (DMG). DMG is an expanded form of the native state in which the hydrophobic core is not exposed to the solvent, but lacks the close packing found in the native structure [24]. For instance, ribonuclease A, dihydrofolate reductase, monellin and villin headpiece show DMG during their unfolding transitions [25–28]. Moreover, a close structural proximity has been established between the burst-phase kinetic intermediates and the equilibrium intermediates. For example, hydrogen exchange pulse labelling experiments on apomyoglobin shows that the kinetic intermediate formed within 5 ms has a structure similar to that of equilibrium MG [18]. Such reports are available for other proteins like α -lactalbumin, ribonuclease H and β -lactoglobulin as well [16,19,20]. Further, the kinetic intermediates may be an on-pathway (U to I transition leads the formation of N, U \leftrightarrow I \leftrightarrow N)

or an off-pathway (formation of I requires to attain again U state for proper refolding, I \leftrightarrow U \leftrightarrow N) [21–24]. On- pathway species are known to increases the rate of folding while the off-pathway intermediates slower down the folding rate [21].

Small organic molecules accumulated by living organisms to counter various environmental stresses are known as osmolytes [25]. Osmolytes are also widely used in biotechnology industries to supress protein aggregation, improve the refolding yield and to protect proteins during storage [26–31]. Polyols are a group of organic molecules and many of them serve as osmolytes in various living organisms [32]. They impart stability to proteins and stabilize certain intermediate structures as well [33]. For example, during the folding of L-amino acid oxidase, glycerol stabilizes the intermediate that allows the enzyme to fold correctly to the active conformation [34]. In case of cytochrome c and yeast hexokinase A, the acid unfolded structures (A-states) could be folded into MG states by the addition of polyols [8,35].

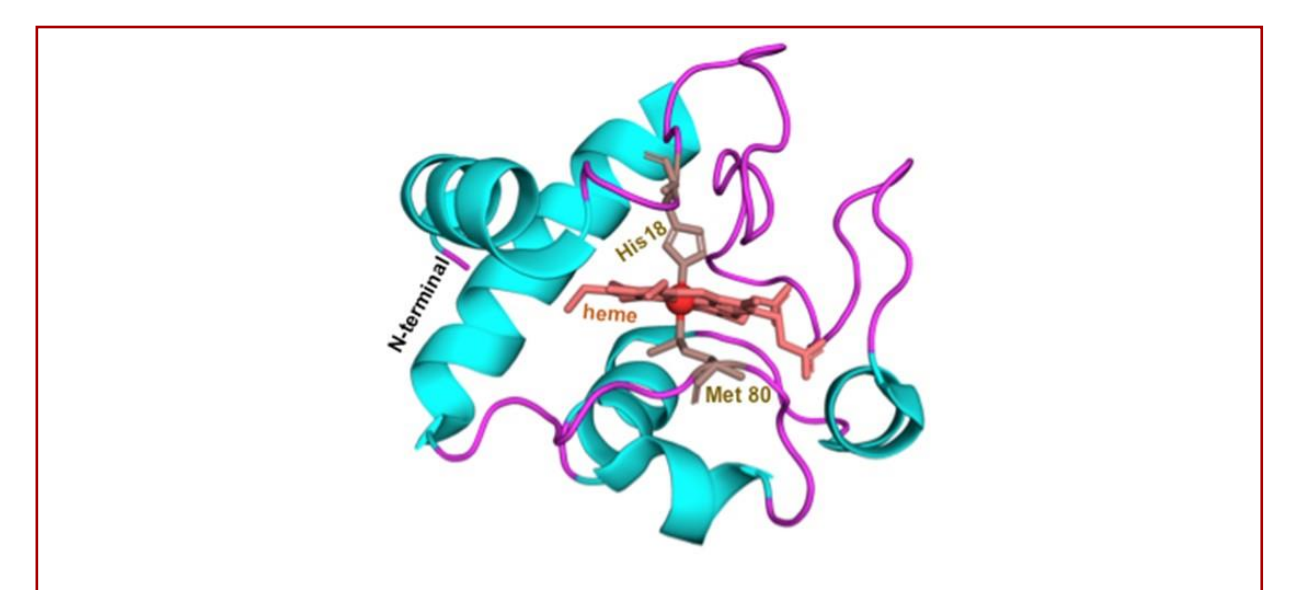


Fig. 5.1. Structure of cytochrome c (Cyt) obtained from protein data bank (Id: 1hrc). Helices and loops are represented in cyan and pink, respectively. The central heme and the coordinated amino acids, His18 and Met80, are represented as sticks. The central iron atom is shown as sphere.

Cytochrome *c* (Cyt, Fig. 5.1) is a small heme-protein (~12.4 kDa) which serves as a model to understand various aspects of protein folding [36–38]. Cyt contains a central heme, covalently linked by thioether linkages to Cys14 and Cys17, serves as a sensitive spectroscopic probe. The iron of the porphyrin is coordinated with His18 and Met80 of the protein main chain [39]. The stability and folding kinetics of Cyt varies depending on the oxidation state of the

central iron [40]. The reduced ferro-state (Fe²⁺) is relatively stable to pH variations [41] whereas the oxidized ferri-state (Fe³⁺) exhibits a large variation in the conformation depending on the pH [42]. The oxidized Cyt forms an unfolded state at acidic pH conditions (U_{acid}) which under low ionic strength is converted into a MG conformation (A-state). Similarly, at alkaline pH, Cyt forms MG-like states (B-state) which vary in conformation with pH and ionic strength of the solution [10,43,44]. Addition of ionic salts and polyols induces formation of intermediates similar to A-state or B-state [45,46] and a quasi-native state is also identified in the presence of glycerol [47]. Denaturants, guanidinium hydrochloride and urea also induces three-state conformational transitions with a detectable unfolding intermediate at pH 5 which resembles the alkaline-denatured state of Cyt [48]. Spectroscopically detectable intermediates have been identified for Cyt during temperature-induced denaturation as well. Though the thermal-intermediate state observed at neutral pH is similar to the alkaline-denatured state, at lower pHs, it is different in terms of heme ligation and secondary structure content [44,49].

In spite of the fact that polyol class of osmolytes are well-known for altering the stability of globular proteins [8,47,50–52] their effect on folding intermediates has not been fully understood. In the present study, we examine the effect of polyols, with OH-groups ranging from two to six, on the equilibrium intermediate identified during thermal denaturation of Cyt at pH 5 using absorption and circular dichroism spectroscopic methods. The effect of denaturants and an ionic salt on the stability of the intermediate is also studied to characterize the intermediate state. The results suggest that the intermediate state is destabilized by all the polyols. The overall stability of the protein is increased by the higher polyols (with OH-groups \geq 3) whereas the diol decreases the stability.

5.3. MATERIALS AND METHODS

5.3.1 Materials

Horse heart cytochrome c (Cyt) and polyols were purchased from Sigma- Aldrich and acetic acid from Merck. Sodium acetate, guanidine hydrochloride (Gdm), urea, and sodium chloride (NaCl) were purchased from SRL, India.

5.3.2. Spectroscopic measurements

All the experiments were carried out in 10 mM of acetate buffer at pH 5. The protein concentration was calculated from the absorbance value at 410 nm using the molar extinction coefficient value of 101.6 mM⁻¹ cm⁻¹. Absorbance spectra were recorded with the protein concentration of 10 μM in Cary 100 UV- Vis spectrophotometer equipped with a Peltier for temperature control. All the thermal denaturation transitions in presence of Gdm, urea, NaCl and polyols were measured at 395 nm with a scan rate of 1 °C/min. Ellipticity changes at farand near-UV regions were measured in Jasco J- 1500 spectropolarimeter equipped with a Peltier and supported with a circulating water bath. Far-UV CD measurements were performed using 2 mm path length cuvette with 15 μM of the protein while near UV- CD measurements were performed using 10 mm path length cuvette with 80 μM of the protein.

5.3.3. Data analysis

Thermal denaturation curves following a three-state transition (N \leftrightarrow I \leftrightarrow U) were analysed using the following equation, [9,53]

$$Y(T) = \frac{(y_f + m_f T) + (y_i + m_i T)e^{-\left[\frac{\Delta G_1}{RT}\right]} + (y_u + m_u T)e^{-\left[\frac{\Delta G_1 + \Delta G_2}{RT}\right]}}{1 + e^{-\left[\frac{\Delta G_1}{RT}\right]} + e^{-\left[\frac{\Delta G_1 + \Delta G_2}{RT}\right]}}$$
(5.3.1)

Where,

$$\Delta G_1 = \Delta H_{m1} \left\{ 1 - \left(\frac{T}{T_{m1}} \right) + \Delta C_{p1} \left(T - T_{m1} - \ln \left(\frac{T}{T_{m1}} \right) \right) \right\}$$

$$\Delta G_2 = \Delta H_{m2} \left\{ 1 - \left(\frac{T}{T_{m2}} \right) + \Delta C_{p2} \left(T - T_{m2} - \ln \left(\frac{T}{T_{m2}} \right) \right) \right\}$$

In the equation 5.3.1, Y is the normalized spectroscopic signal, y_f , y_i and y_u are the baselines corresponding to the native, intermediate and the unfolding transitions and m_f , m_i and m_u are the corresponding slopes. T_{m1} and T_{m2} are the transition midpoints, ΔH_{m1} and ΔH_{m2} are the enthalpy changes, and ΔC_{p1} and ΔC_{p2} are the change in the heat capacities associated with N \leftrightarrow I and I \leftrightarrow U transitions, respectively.

The thermal unfolding transitions that follow a two-state transitions (N \leftrightarrow U) were analysed using the following equation [54],

$$Y(T) = \frac{(y_f + m_f T) + (y_u + m_u T)e^{-\left[\frac{\Delta H_m (1 - \left(\frac{T}{T_m}\right) + \Delta C_p (T - T_m - \ln\left(\frac{T}{T_m}\right)}{RT}\right]}}{1 + e^{-\left[\frac{\Delta H_m (1 - \left(\frac{T}{T_m}\right) + \Delta C_p (T - T_m - \ln\left(\frac{T}{T_m}\right)}{RT}\right]}}$$
(5.3.2)

Where Y is the normalized spectroscopic signal, y_f and y_u are the intercepts of the native and unfolding transition, while m_f and m_u are the corresponding slopes. T_m , ΔH_m and ΔC_p are the transition midpoint temperature, change in enthalpy and change in heat capacity of the unfolding transition, respectively.

5.3.4. Global analysis

Global analysis was performed to obtain a single set of thermodynamic parameters for the three-state transition of native Cyt. For this process, the shared parameters employed were the baselines and the slopes $(y_f, y_i, y_u \text{ and } m_f, m_i \text{ and } m_u)$, while the global parameters were the thermodynamic parameters, T_m , ΔH_m , and ΔC_p .

5.4. RESULTS

5.4.1 Thermal unfolding of cytochrome *c*

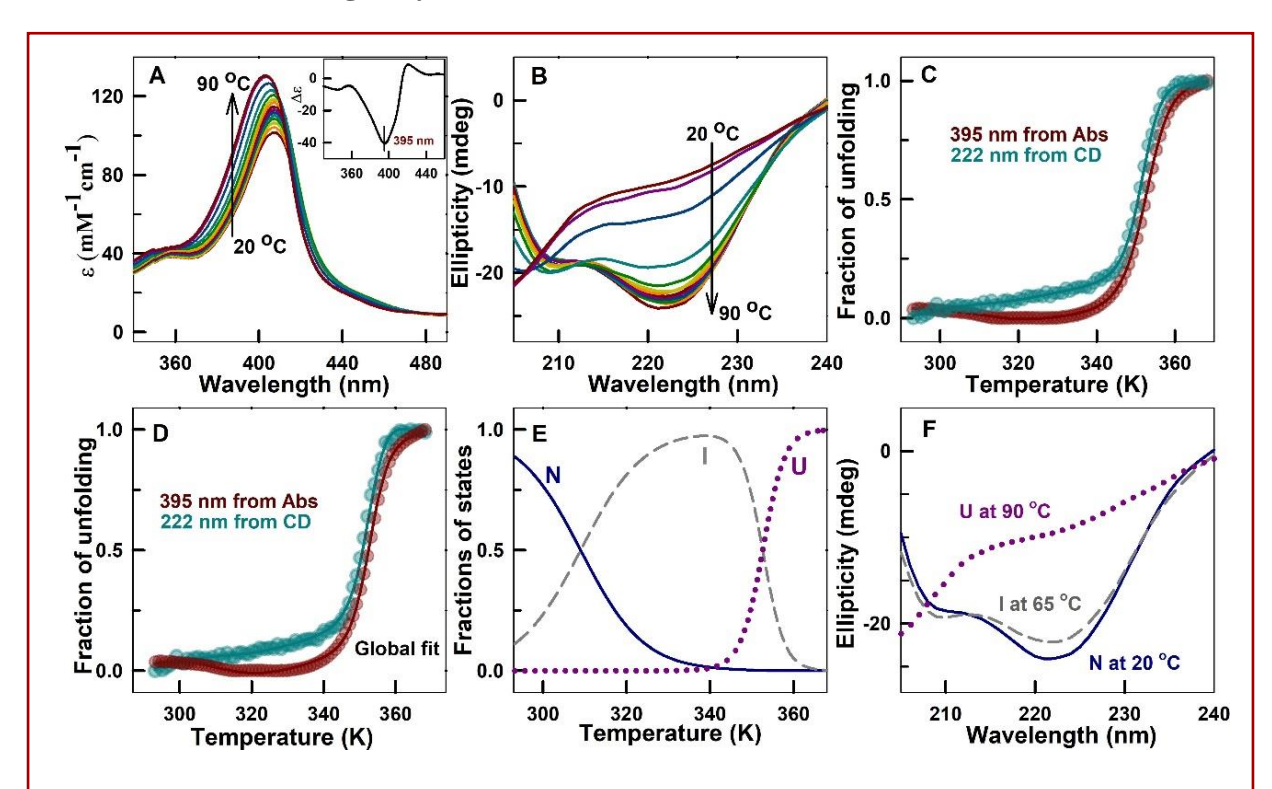


Fig. 5.2. Thermal unfolding of Cyt: (A) Soret absorption and (B) Far-UV circular dichroism spectra of Cyt at varying temperatures from 293 to 363 K. The inset shows the difference spectra between native and unfolded states correspond to 20 and 90 oC, respectively. (C and D) Fraction of unfolded states calculated from Soret absorption (at 395 nm, red) and CD (at 222 nm, cyan) spectra. The solid lines represent individual (panel C) or global (panel D) fit of the transitions with three-state assumption using equation 5.3.1. The parameters obtained from the curve-fit are presented in Table 5.1. (E) Fraction of the states calculated from global-fit of the unfolding transition and (F) representative far-UV CD spectra of native (blue), intermediate (gray) and unfolded (pink) states.

Conformational change in Cyt with increasing temperature was initially monitored by two different probes, Soret absorbance (350-450 nm) which is sensitive to the heme-environment [48] and far-UV CD corresponding to the secondary structural content of the protein [55]. Soret absorbance showed a hypsochromic shift along with an increase in absorbance (Fig. 5.2A) and the ellipticity values drastically decreased in far-UV region of CD (Fig. 5.2B) with increase in temperature suggested the unfolding of Cyt. The spectral changes, however, did not show any noticeable isosbestic or isochoric points. In the Soret region, a difference spectrum was calculated by subtracting the absorbance spectra at 293 K against 363

K which showed minima at 395 nm that was used to follow the unfolding transition of the protein. From far-UV CD, the ellipticity changes at 222 nm specific to the α -helix was used to monitor the thermal denaturation of the protein. The shape of the unfolding transition curves (Fig. 5.2C) showed a non-sigmoidal behaviour suggesting a deviation from a two-state (N \leftrightarrow U) process. Therefore, the data was fitted for a three-state model (N \leftrightarrow U) using equation 5.3.1. Comparison of the residual obtained from two-state and three-state models (Fig. 5.3) indicated that curve fit with the three-state assumption had less deviation from the experimental values, thus three-state model was considered. The thermodynamic parameters obtained from the data analysis are presented in Table 5.1 which is comparable to the earlier report [56].

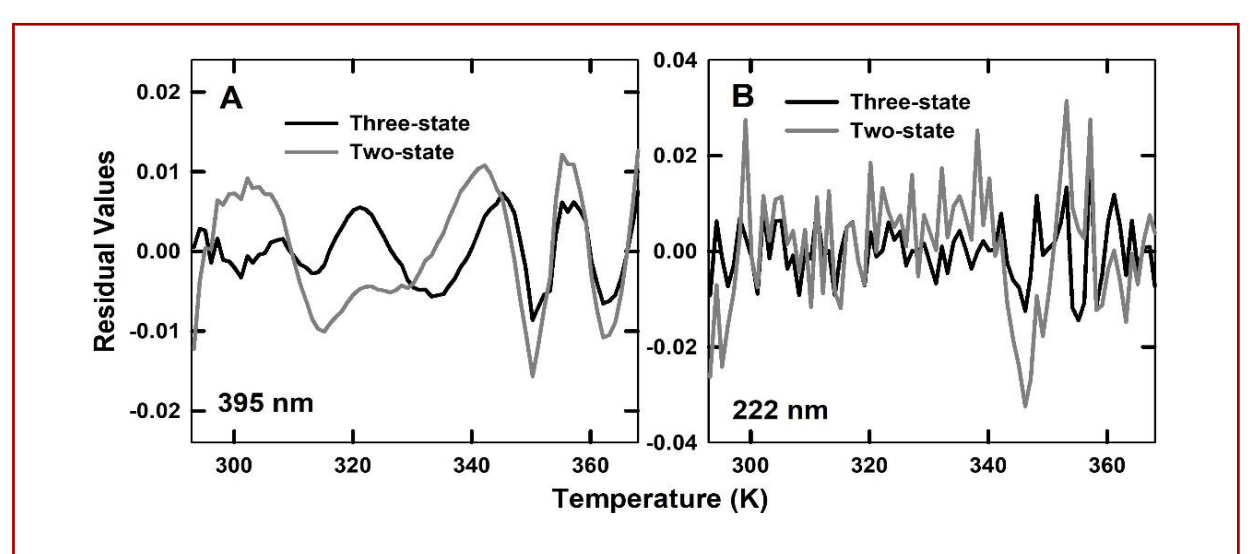


Fig. 5.3. The residual values obtained from the curve-fit of thermal unfolding transitions of Cyt from three-state (black) and two-state (grey) assumptions using equations 5.3.1 and 5.3.2, respectively. The unfolding transition was followed by (A) Soret absorbance at 395 nm and (B) ellipticity changes at 222 nm.

Further, to obtain a single set of thermodynamic parameters by combining the probes sensitive to different conformational changes, simultaneous fit (global analysis) of the data sets were performed (Fig. 5.2D). From the resultant parameters, the fractions of each states, native, intermediate and unfolded were calculated (Fig 5.2E). The intermediate population was found to be largest at 339 K. The far-UV CD spectrum of Cyt collected at 338 K (65 °C) showed that the ellipticity of intermediate state is slightly reduced at 222 nm compared to the native state (Fig. 5.2F). Further, the absorption and near-UV CD spectra of Cyt was also measured at 338 K (Fig. 5.4). Soret absorbance showed an increase in intensity without any significant hypsochromic shift generally observed for the unfolded states. The Q-band and charge transfer

band collected at 338 K were similar to that of native state of the protein. The near-UV CD spectrum of Cyt also did not show significant changes between native and intermediates species. These spectral changes suggested that the intermediate conformation retains the hemeligation state as in the native conformation and a slight loss of secondary structural content without significant change in tertiary packing of the protein.

Table 5.1. Thermodynamic parameters obtained from the thermal denaturation of Cyt.

Probe	T_{m1}	ΔH_{m1}	ΔC_{p1}	T_{m2}	ΔH_{m2}	ΔC_{p2}
	(K)	(kcal/mol)	(kcal/mol/K)	(K)	(kcal/mol)	(kcal/mol/K)
395 nm†	309 ± 1	26 ± 0.3	0.15 ± 0.05	352.6 ± 0.4	79.04 ± 3	1.4 ± 0.2
222 nm‡	308 ± 0.3	35 ± 2.3	0.1 ± 0.02	351.8 ± 0.45	89 ± 3	1.5 ± 0.15
Global	309 ± 0.52	25 ± 1.4	0.2 ± 0.04	352.6 ± 0.44	93.9 ± 2.3	1.5 ± 0.2

[†] from absorbance, ‡ from CD

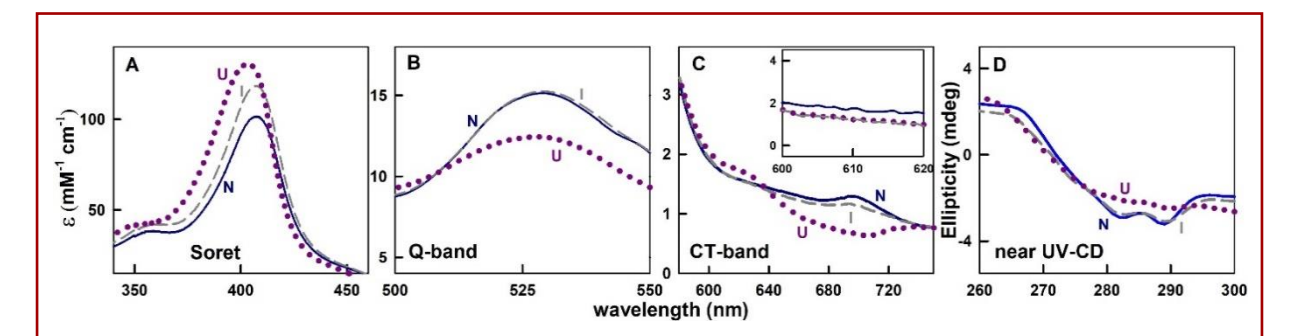


Fig. 5.4. Representative spectra of native (blue), intermediate (grey) and unfolded (pink) states measured at 293 K, 338 K and 363 K, respectively during thermal denaturation of Cyt using (A) Soret absorption, (B) Q-band absorption, (C) charge-transfer band and (D) near-UV CD.

5.4.2 Effect of denaturants and ionic salt on the intermediate

To investigate the interactions that might stabilize the equilibrium intermediate, thermal denaturation studies were carried out in presence of, urea (non-ionic denaturant), NaCl (ionic salt) and Gdm (ionic denaturant). The concentrations of the denaturants were chosen such that they were within the pre-transition baseline of the respective chemical denaturation curves [48].

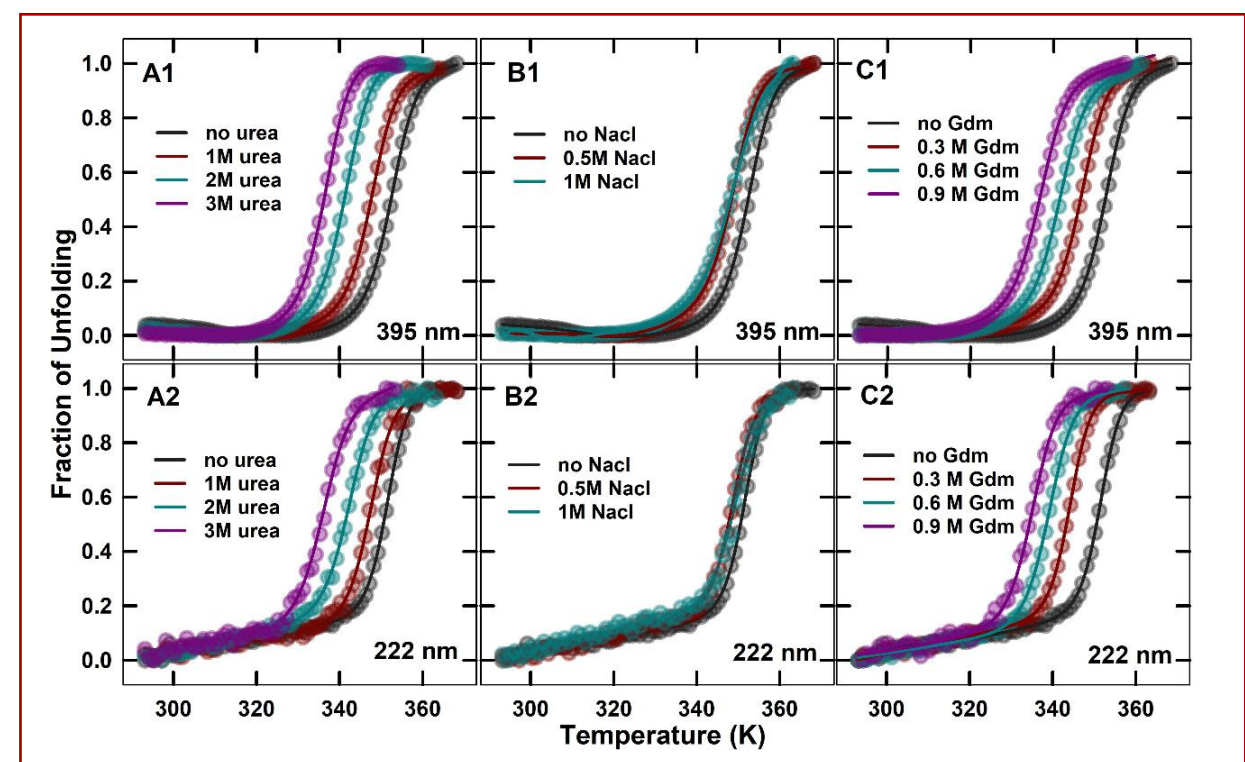


Fig. 5.5. Thermal denaturation transitions of Cyt followed by absorption changes at 395 nm (upper panels) and ellipticity changes at 222 nm (lower panels) in the presence of varying concentrations of urea (A1 and A2), NaCl (B1 and B2) and Gdm (C1 and C2). The solid lines represent the curve-fit using equation 5.3.1 for three-state transitions or equation 5.3.2 for two-state transitions. The parameters obtained from the curve-fit are presented in Table 5.2.

In the presence of low concentrations of urea (\leq 2 M urea) the intermediate was destabilized, and at 3M urea concentration the transition was found to be two-state (Fig. 5.5 A1-A2). Similarly, in presence of 0.5 M NaCl the intermediate was destabilized and upon increasing the concentration to 1 M, the transition was shifted into two-state (Fig. 5.5 B1-B2). When Gdm was added, the equilibrium-intermediate was completely destabilized and a two-state transition was observed even with a low concentration of Gdm, 0.6 M (Fig. 5.5 C1-C2). Thermodynamic parameters obtained from the respective data analysis are presented in Fig. 5.6. It was observed

that Gdm destabilizes the intermediate more effectively and the effect of urea and NaCl are similar.

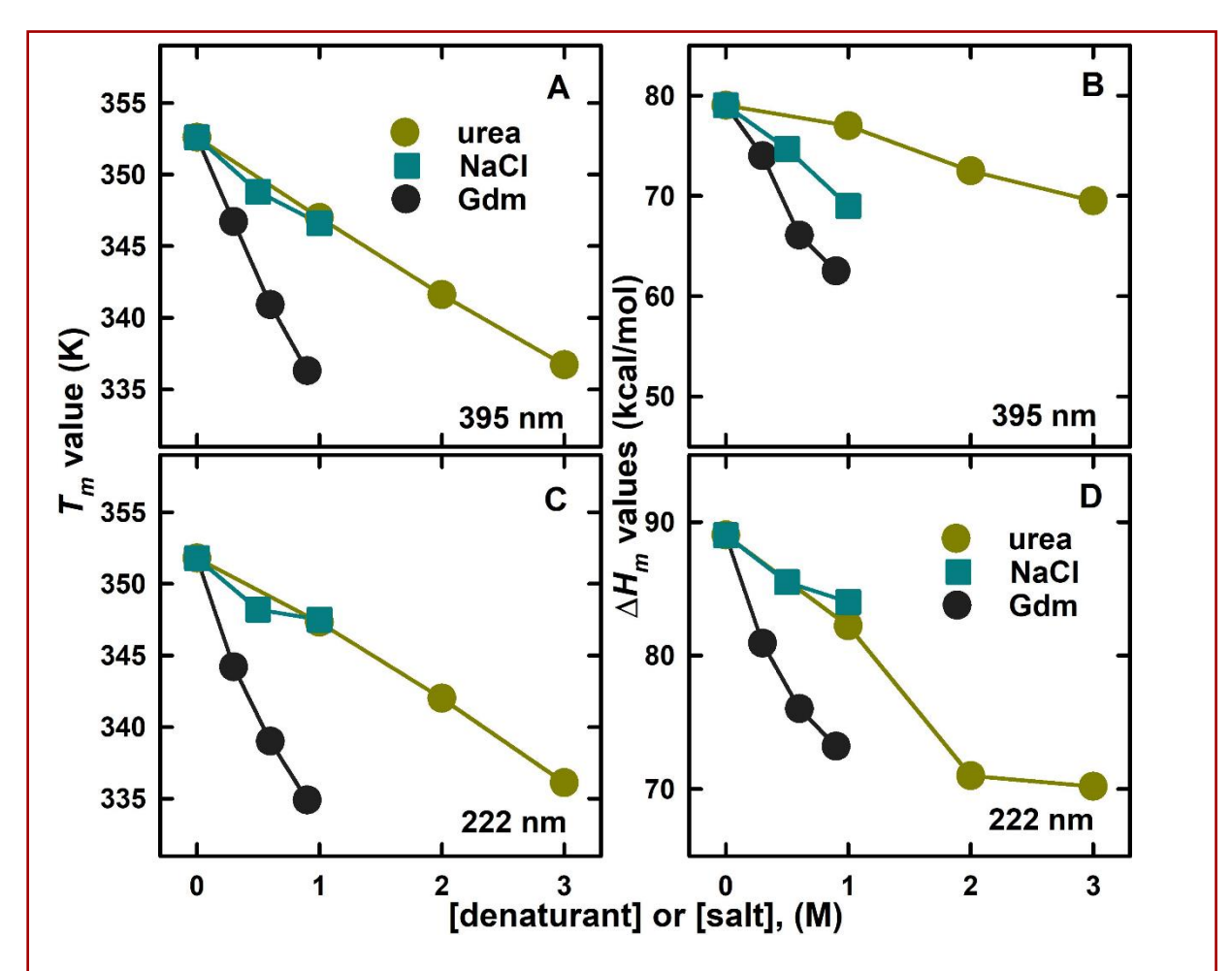


Fig. 5.6. Transition midpoint temperature (Tm) and enthalpy of unfolding (Δ Hm) of Cyt in different concentrations of urea (green), NaCl (cyan) and Gdm (black) calculated from the thermal transitions measured by absorbance (upper panels) and ellipticity changes (lower panels) that are shown in Fig. 5.5.

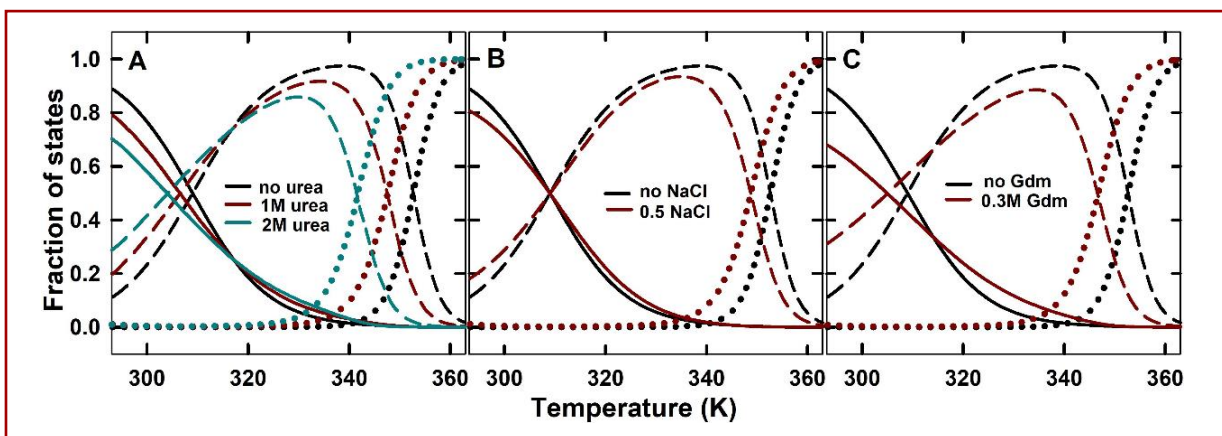


Fig. 5.7. Fraction of native (solid lines), intermediate (dashed lines) and unfolded (dotted lines) states of Cyt as a function of temperature in the presence of varying concentrations of (A) urea, (B) NaCl and (C) Gdm.

Further analysis on the fraction of intermediate against temperature (Fig. 5.7) shows that the fraction of intermediate was reduced and the temperature at maximum fraction of intermediate ($T_{max-inter}$) formed was shifted to lower temperature upon addition of the denaturants or NaCl. The far-UV CD spectra of Cyt at $T_{max-inter}$ were measured to analyse the structure of the intermediate. In the presence of both the denaturants and NaCl (Fig. 5.8), the intermediate showed only a slight structural loss similar to that observed in the absence of any cosolvent

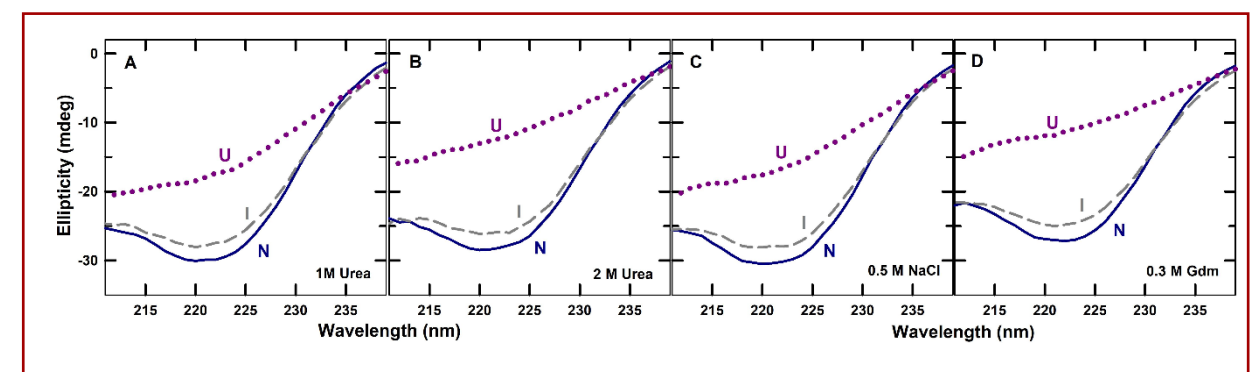


Fig. 5.8. Representative far-UV CD spectra of native (blue), intermediate (gray) and unfolded (pink) states of Cyt obtained from the thermal denaturation of the protein in the presence of (A) 1 M urea, (B) 2 M urea, (C) 0.5 M NaCl, and (D) 0.3 M Gdm.

5.4.3. Effect of polyols on the intermediate

The effect of polyols with varying number of -OH groups, ethylene glycol (EG, two -OH groups), glycerol (Gly, three -OH groups), erythritol (Ery, four -OH groups), xylitol (Xyl, five -OH groups) and sorbitol (Sor, six -OH groups), on the stability of the intermediate formed by Cyt was examined. Thermal denaturation studies of Cyt in presence of varying concentrations of these polyols were performed by following the change in Soret absorbance at 395 nm (Fig. 5.9A1-E1) and far-UV ellipticity at 222 nm (Fig. 5.9A2-E2). The addition of EG shifted the thermal denaturation curves of Cyt towards lower temperature for both Soret absorbance (Fig. 5.9A1) and far UV-CD (Fig. 5.9A2) suggesting destabilization of the protein upon addition of EG. Also, the early-transition region (temperature ranging from 295-340 K) showed significant changes in the presence of EG. The addition of Gly did not show significant shift in the transition curve, though there were slight changes in the early-transition phase (Fig. 5.9B1 and B2). The polyols, erythritol, xylitol and sorbitol shifted the transition curves toward higher

temperature suggesting increase in the overall stability of Cyt. They also significantly altered the early-transition region of the thermal unfolding curves (Fig. 5.9C1 - E2).

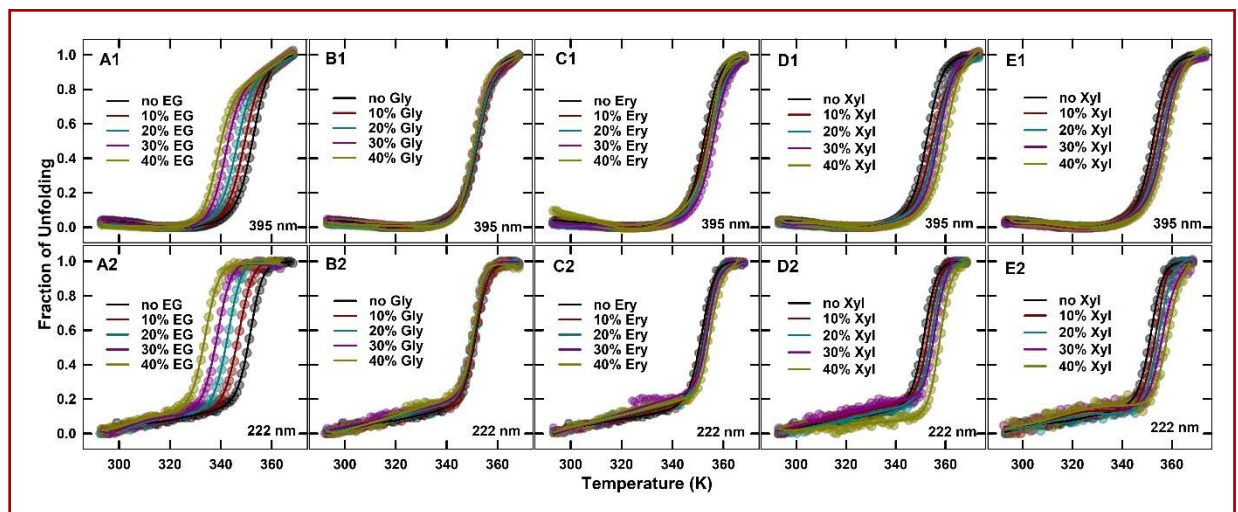


Fig. 5.9. Thermal denaturation transitions of Cyt followed by absorption changes at 395 nm (upper panels) and ellipticity changes at 222 nm (lower panels) in the presence of varying concentrations of (A1 and A2) EG, (B1 and B2) Gly, (C1 and C2) Ery, (D1 and D2) Xyl, and (E1 and E2) Sor. The solid lines represent the curve-fit using eq.5.3.1 for three-state transitions or eq.5.3.2 for two-state transitions. The parameters obtained from the curve-fit are presented in Fig. 5.10.

All the thermal transitions were analysed using eq.5.3.1 for three-state transition except for the far-UV CD data of 30% and 40% (v/v) EG. In these two conditions, data-fit with two-state assumption (eq. 5.3.2) had the residual values similar to three-state fit (Fig. 5.10), therefore,

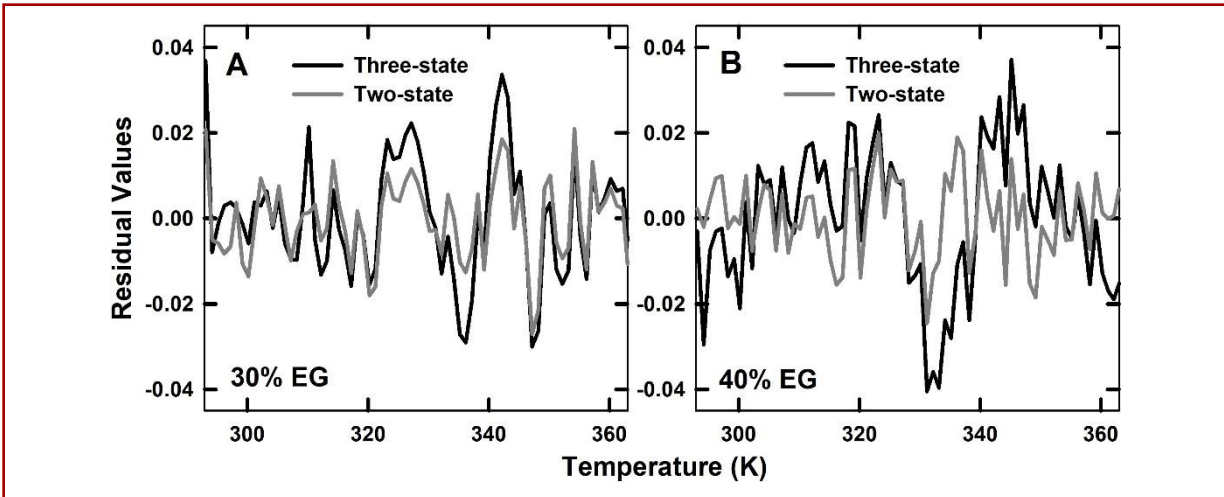


Fig. 5.10. The residual values obtained from the curve-fit of thermal unfolding transitions of Cyt in the presence of (A) 30 % EG and (B) 40 % EG using three-state (black) and two-state (gray) assumptions. The unfolding transitions were followed by ellipticity changes at 222 nm (Fig. 5.9-A2).

two-state transition model was considered for further analysis. The transition midpoints, T_{m1} and T_{m2} and enthalpies of unfolding, ΔH_{m1} and ΔH_{m2} obtained from the data-fit are presented in Fig. 5.11. The T_{m1} values correspond to the midpoint of $N \leftrightarrow I$ equilibrium decreases with the addition of any of the polyol (Fig. 5.11A1 and B1). This suggests that the transition is shifted to lower temperature and intermediate is destabilized by the addition of the polyols. This is complemented with the constant decrease in the value of ΔH_{m1} with the increasing concentration of any of the polyols (Fig. 5.11A3 and B3). Among the added polyols, EG showed the largest decrease in the T_{m1} value and in ΔH_{m1} as well. The effect of Xyl was found to be the least when probed with Soret absorption whereas Sor showed the least effect when probed with far-UV CD.

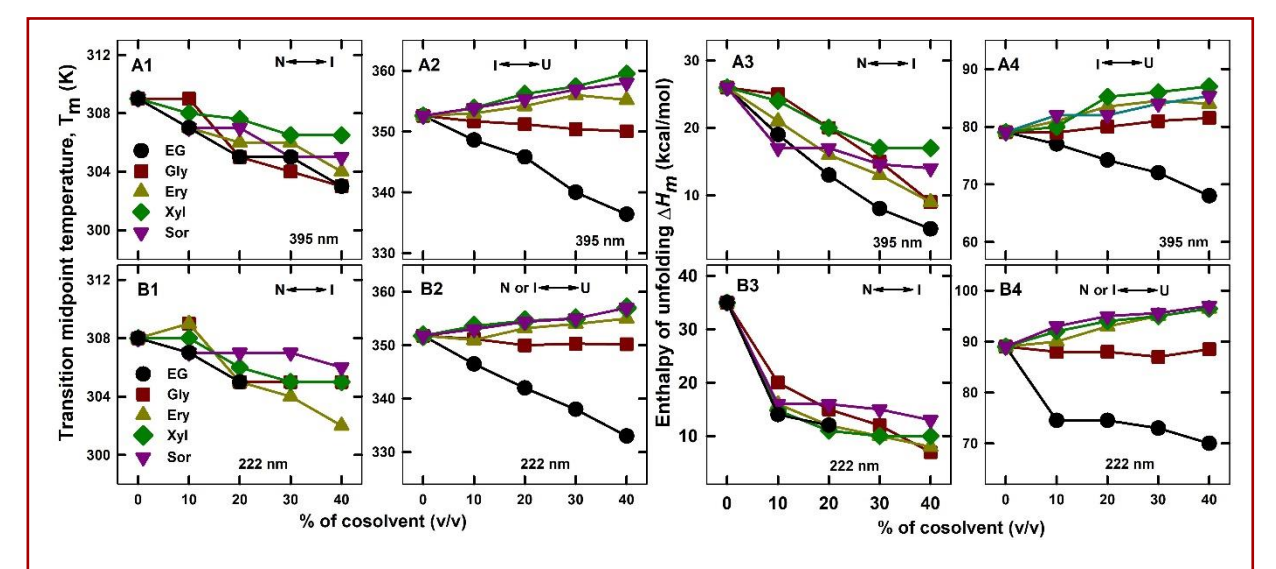


Fig. 5.11. (A1-B2) Transition midpoint temperature, Tm and (A3-B4) enthalpy of unfolding, Δ Hm for N \leftrightarrow I and I \leftrightarrow U transitions of Cyt in different concentrations of EG (black), Gly (red), Ery (green), Xyl (cyan) and Sor (ink) calculated from the thermal denaturation transitions measured by absorbance (upper panels) and ellipticity changes (lower panels) that are shown in Fig. 5.9.

The temperature midpoint, T_{m2} correspond to the transition I \leftrightarrow U suggested that EG significantly reduced the transition midpoint temperature (Fig. 5.11A2 and B2); however, Gly did not show significant changes in the T_{m2} values. Ery, Xyl and Sor increased the unfolding midpoint indicating stabilization of the protein against denaturation. Though Xyl displayed a slightly more increment in T_{m2} values compared to Ery and Sor when probed with Soret absorption, the increase in T_{m2} values were almost same when measured with far UV-CD. The

changes observed in ΔH_{m2} (Fig. 5.11A4 and B4) also indicated that EG destabilized the protein whereas Xyl, Ery and Sor stabilized the protein by increasing the enthalpy of unfolding.

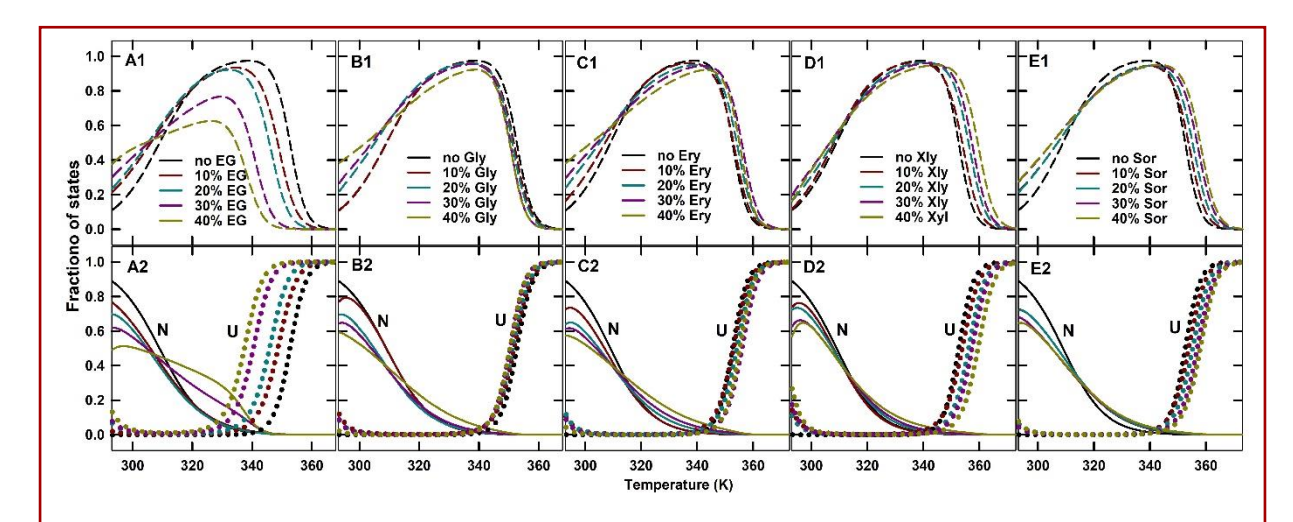


Fig. 5.12. Fraction of intermediate (upper panels), native and unfolded states (solid and dashed lines in lower panels, respectively) of Cyt as a function of temperature in the presence of varying concentrations of (A) EG, (B) Gly, (C) Ery, (D) Xyl, and (E) Sor.

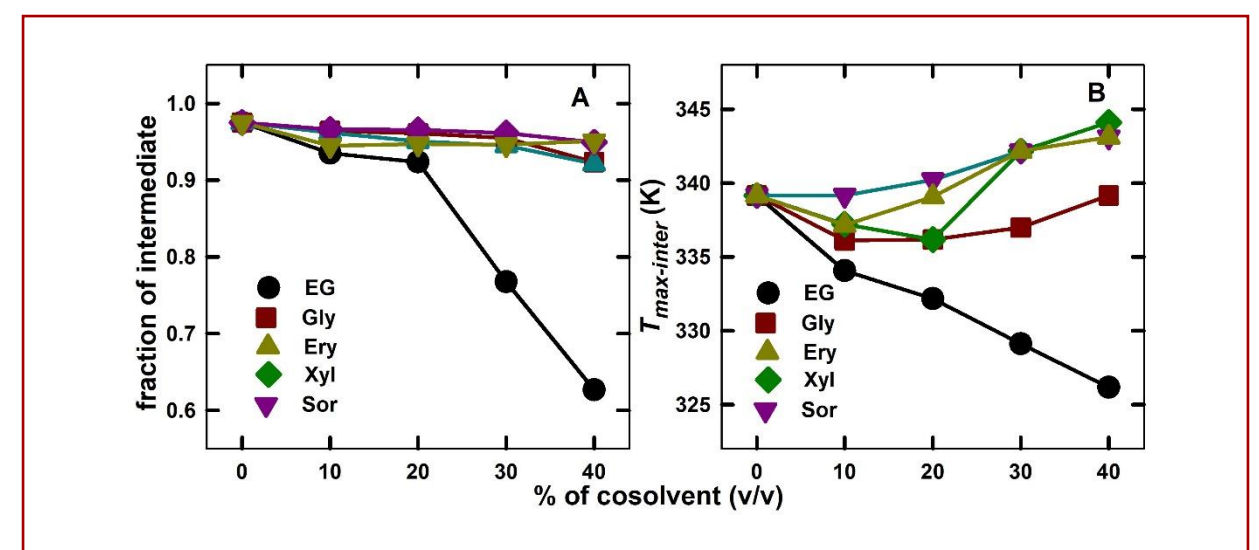


Fig. 5.13. (A) The maximum fraction of intermediate state and (B) the corresponding temperature observed for Cyt during thermal denaturation in varying concentrations of EG (black), Gly (red), Ery (green), Xyl (cyan) and Sor (pink). The values were evaluated from Fig. 5.11 (A1-E1).

For further analysis, the fraction of intermediate population was calculated in the presence of varying concentration of the polyols (Fig. 5.12A1-E1). The analysis indicated that increase in the concentration of EG decreased the fraction of intermediate population (Fig. 5.13A) and $T_{max-inter}$ values were gradually moved to lower temperature (Fig. 5.13B). The addition of Gly

slightly reduced the population of intermediate and the $T_{max-inter}$ was slightly moved to lower temperature at lower concertation of Gly (\leq 30%). In case of higher polyols, the population of intermediate was not significantly altered. $T_{max-inter}$ was slightly decreased in the presence of lower concentrations of the polyols whereas at above 20% of the polyols, $T_{max-inter}$ value shifted towards higher temperature. Structural content of the intermediate in the presence of the polyols was analyzed by measuring far-UV CD spectra of Cyt at the respective $T_{max-inter}$ values (Fig. 5.14). The spectra indicated that there was a minor structural loss compared to the native condition.

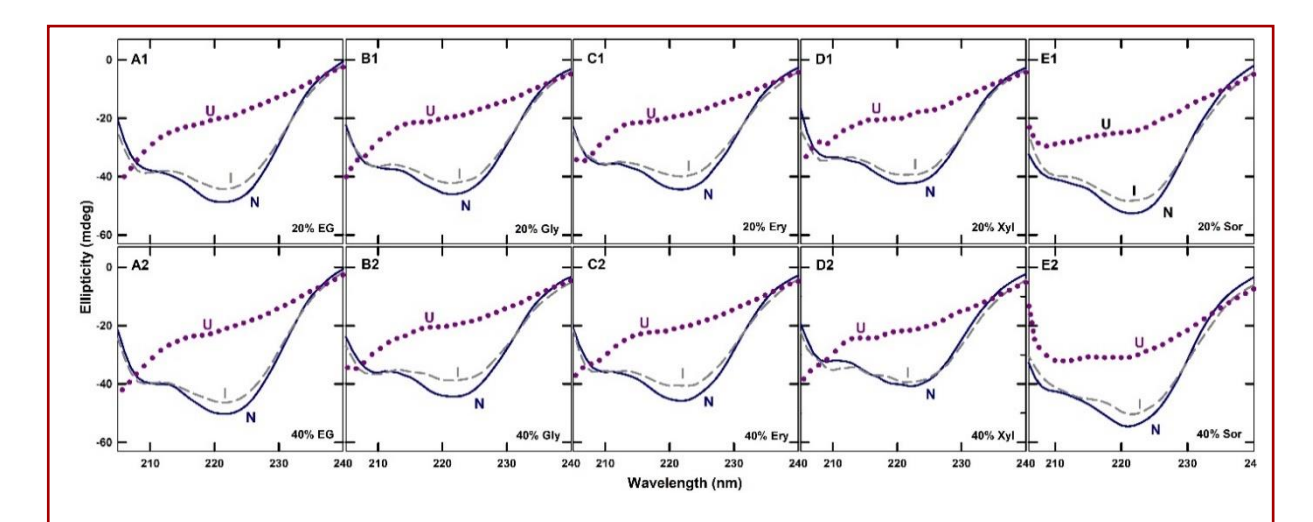


Fig. 5.14. Representative far-UV CD spectra of native (blue), intermediate (grey) and unfolded (pink) states of Cyt obtained from the thermal denaturation of the protein in the presence of 20% (upper panels) and 40% (lower panels) of (A) EG, (B) Gly, (C) Ery, (D) Xyl and (E) Sor.

5.5. DISCUSSION

Identifying and characterizing intermediate states of proteins is essential not alone to decipher the folding pathways, they also find relevance in explaining biological functions of the proteins. For instance, Cyt is proposed to adapt different conformational states during electron transport, peroxidase activity and apoptosis pathway [57–59]. Most of these conformational changes are related to the heme-ligation and conformational changes in Ω -loops of the protein [57]. These intermediates are similar to the states obtained *in vitro* conditions by altering pH, salt, and temperature [7,10,60]. Though the effect of osmolytes on

native state of Cyt has been well studied [51,61–63], their effect on structural intermediates are less understood. We here monitored the effect of polyol class of osmolytes on the intermediate state of Cyt identified during thermal unfolding of the protein and on the stability of the intermediate.

5.5.1 Characteristics of thermal denaturation intermediate of Cyt

Cyt undergoes a three-state unfolding transition at pH 5. This is evident from both absorbance and far-UV CD spectra recorded as a function of temperature that clearly lacking an isosbestic point and an isodichroic point, respectively. The intermediate population was maximum at 339 K and the spectral analysis of the protein at this temperature suggests that the low-spin state of the heme-iron with Fe³⁺-M80 ligation (Q- and CT-band, Fig. 5.4B-C) and the globular packing (near UV-CD, Fig 5.4-D) could be similar to the native conformation of the protein. However, there is a slight loss of secondary structure of the protein (far UV-CD, Fig 5.2F) and a hyperchromic shift in Soret absorption as well. This could be attributed to the conformational changes around the Ω -loops of the protein particularly the loop covering the residues 70-85. The weakening of Met80 ligation might increase the Soret absorption without significant shift in wavelength maximum. The disruption of this Ω -loop is reported to be the early stage of unfolding of Cyt [64,65]. Therefore, we could conclude that M80 is still intact though the conformational states around the loop is altered at 339 K. Similar intermediate conformation with weakened M80 ligation is observed at 345 K during thermal denaturation of Cyt at pH 7 [44]. This intermediate, labelled as III-h state also showed a loss of secondary structural content in the protein and well distinguished from the alkaline-transition state in which heme misligation is observed.

Increase in temperature above 339 K reduces the population of the intermediate (Fig. 5.2E) and the unfolded state's population starts increasing. Spectral analysis of the unfolded state at 363 K, where the unfolded population reaches its maximum, suggests that Cyt lost its secondary structural content (Fig. 5.2F) and tertiary packing (Fig. 5.4D) as well. Though the loss of 695 nm band indicates that heme-M80 ligation is disrupted, the absence of any band at 620 nm (Fig. 5.4D) suggests that the heme-iron still possesses a low-spin state. This could be probably due to the replacement of M80 by other strong field ligands such as H26 and H33 [64]. In earlier studies as well, a six-coordinated low-spin unfolded state of Cyt with bis-

histidine ligation has been observed in both thermal and denaturant-induced denaturation processes [56,66].

Table 5.2. Thermal denaturation of Cyt in presence of denaturants and salts

Cosolvent	Probe	T_{m1}	ΔH_{m1}	ΔC_{p1}	T_{m2}	ΔH_{m2}	ΔC_{p2}
		(K)	(kcal/mol)	(kcal/mol/K)	(K)	(kcal/mol)	(kcal/mol/K)
0.3 M Gdm	395 nm	305 ± 0.5	13 ± 1.2	0.24 ± 0.02	346.7 ± 0.3	74.0 ± 1.7	2.1 ± 0.6
	222 nm	308 ± 0.25	23.5 ± 0.25	0.2 ± 0.06	344.2 ± 0.3	80.9 ± 0.3	1.5 ± 0.4
0.6 M	395 nm				340.9 ± 0.1	66.1 ± 0.8	2.1 ± 0.1
\mathbf{Gdm}^{\dagger}	222 nm				339.0 ± 0.13	76.0 ± 2.4	2.0 ± 1.0
0.9 M	395 nm				336.3 ± 0.06	62.5 ± 0.6	2.1 ± 0.1
\mathbf{Gdm}^{\dagger}	222 nm				334.9 ± 0.26	73.2 ± 4.1	2.0 ± 0.8
1 M urea	395 nm	306.5 ± 1.2	19 ± 0.5	0.1 ± 0.02	347.5 ± 1.2	77.0 ± 3.0	2.3 ± 0.3
1 WI urea	222 nm	308 ± 0.1	20 ± 0.23	0.20 ± 0.07	347.3 ± 1.3	82.2 ± 6.0	1.7 ± 0.6
2 M urea	395 nm	304 ± 0.5	15 ± 0.1	0.1 ± 0.1	341.6 ± 0.9	72.5 ± 7.0	2.4 ± 1.1
2 Willied	222 nm	304 ± 0.4	14 ± 0.32	0.3 ± 0.06	342 ± 1.9	71.0 ± 1.5	2.3 ± 1
3 M urea [†]	395 nm				336.7 ± 0.06	69.5 ± 1.1	2.4 ± 0.1
5 W urea	222 nm				336.0 ± 0.3	70.2 ± 4.0	2.5 ± 0.1
0.5 M NaCl	395 nm	309 ± 0.3	20 ± 0.4	0.4 ± 0.06	348.8 ± 0.3	74.7 ± 3.5	2.2 ± 0.9
vio III IVACI	222 nm	309 ± 0.2	20 ± 0.6	0.4 ± 0.06	348.2 ± 0.6	85.5 ± 0.4	1.8 ± 0.5
1.0 M	395 nm				346.0 ± 0.14	69.0 ± 2.2	2.5 ± 0.1
NaCl [†]	222 nm				347.5 ± 0.6	84.0 ± 3.8	2.7 ± 0.3

[†] two-state transition

5.5.2 Interactions that stabilizing the intermediate state

The major factors that contribute to the stabilization of the intermediate could be analysed by studying the effect of ionic and non-ionic additives on the stability of the intermediate [9,67,68]. Addition of urea destabilizes the intermediate that is evident from the reduction of enthalpy of unfolding for N \leftrightarrow I transition, ΔH_m (Table 5.2). At higher concentrations, the intermediate is not detectable and the protein follows a two-state transition. The globular stability of the protein is also reduced by urea as expected for a denaturant (Fig. 5.6). Similarly, the addition of NaCl also reduces the stability of the intermediate and the protein adapts a two-state transition when the concentration of NaCl is above 0.5 M. Urea is known to destabilize native-folded structure by disrupting the intra-molecular and proteinwater hydrogen bonding interactions, and weakening the hydrophobic effect [69–72]. On the other hand, the destabilization effect of salts would arise from charge-charge interactions. The destabilization of intermediate by both urea and NaCl indicates that hydrogen bonding and Columbic interactions are the major factors stabilizing the structure.

The addition of Gdm, even at a low concentration (0.6 M), destabilized the formation of intermediate and the thermal unfolding transition showed a two-state process (Fig. 5.5C1-C2). Gdm disrupts both hydrogen bonding ionic interactions, thus, acting as a more effective denaturant than urea [71,72]. Gdm is found to be nearly two-times more effective on globular proteins and it can act as effectively as the equimolar mixture of urea and NaCl [73,74]. These observations support the fact that the globular structure of the protein is still intact in the intermediate state which could be destabilized by the addition of denaturants or NaCl.

5.5.3 Polyols alter the energy landscape of folding intermediates

Polyols having hydroxyl groups 3 or more are found to stabilize many globular proteins [8,47,50,51], whereas EG destabilizes proteins [52,75–77]. Polyols, EG, Gly, Ery, Xyl and Sor also show the similar trend on the globular stability of Cyt during thermal denaturation (Figs. 5.9 and 5.11). However, closer analysis on the individual transitions, N \leftrightarrow I and I \leftrightarrow U show that the intermediate is destabilized by all the polyols. This is evident from a decrease in T_m and ΔH_m (Fig. 5.11A3 and B3) for the transition N \leftrightarrow I. The enthalpy of unfolding for I \leftrightarrow U

is reduced by EG whereas it is increased in other polyols. It is interesting to note that the fraction of intermediate detectable and $T_{max-inter}$ is also reduced in the presence of EG. These changes suggest that EG destabilizes both the native and intermediate states and Gly has little effect on both the states. Higher order polyols destabilize the intermediate state, but the extent of destabilization is lesser that that of EG. On the other hand, they increase the overall stability of the protein by increasing the unfolding enthalpy of intermediate state.

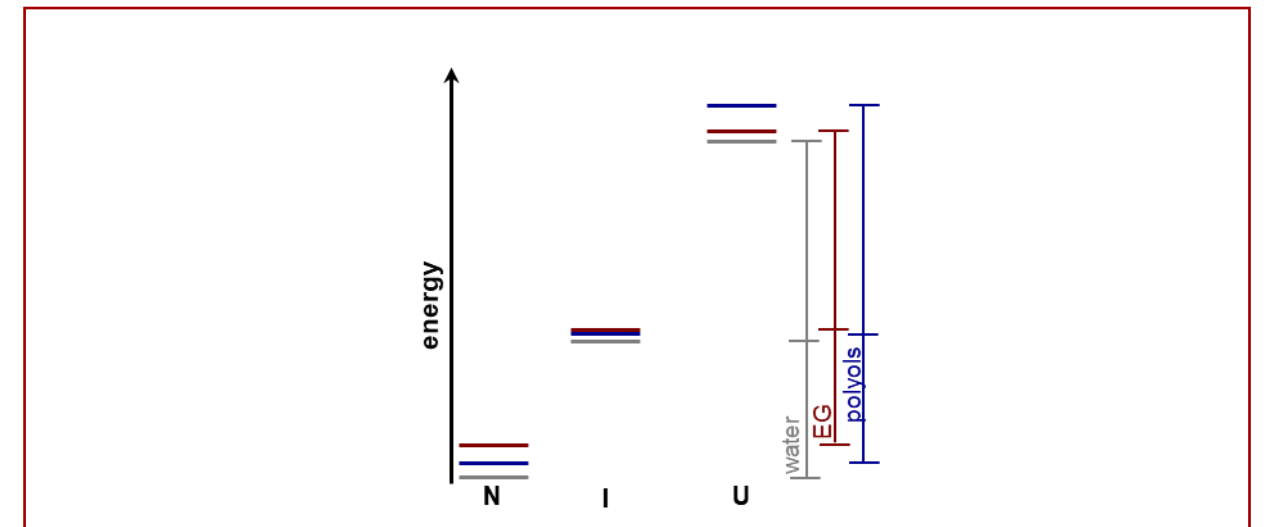


Fig. 5.15 Relative energy states of native, intermediate and unfolded conformations of Cyt in buffer (gray), in EG (red) and in other polyols (blue). The energy differences between native and unfolded states are shown as bar lines on the right. The values are only representative to visualize the differences, not depicting the absolute values.

Based on these observations, the probable energy states are depicted in Fig. 5.15. It shows that the addition of EG destabilizes the native state more than the unfolded state as generally suggested for denaturants [78,79]. The higher order polyols, however, destabilizes the unfolded state more than the native state. All the polyols might destabilize the intermediate state and the effect of EG could be slightly higher than the other polyols.

Structurally, the intermediate state retains most of the secondary structural contents (Fig. 5.14) and the heme-M80 ligation of the native state even in the presence of polyols. The conformational changes might occur around the Ω -loops covering the residues 70-85. Earlier studies have suggested that polyols can induce formation of MG state from the unfolded conformation of proteins, except in the presence of EG [8,35]. The proteins might attain a non-native state which is less stable than native conformation but more stable than unfolded

conformations [80]. In case of Gly, a quasi-native state has also been proposed which is suggested to follow an alternative folding pathway [47]. Also, the polyols increase the stability of proteins by increasing hydrophobic interactions of non-polar amino acids, since the free energy of transfer from water to polyols is positive for them [35,81,82]. Though such preferential exclusion of polyols from the surface of proteins has been suggested [76,83,84], existence of weak binding interactions are also reported between proteins and polyols [85–87]. EG, an exceptional case, shows preferential interaction with the proteins [52,75,88] and destabilizes. These observations indicate that preferential exclusion of polyols might provide a global stability to the protein; however, their weak interactions with the native-like structural intermediate (analogous to late-folding intermediates) might destabilize the formation of intermediate. Thus, polyols alter the energy states of different conformations of the protein.

5.6. CONCLUSION

Cyt forms an intermediate during thermal denaturation of the protein at pH 5. The intermediate retains most of the secondary structure; however, the heme-M80 ligand might be slightly weaken due to conformational changes in Ω -loop. It is stabilized by both hydrogen bonding and electrostatic interactions. Addition of polyols destabilizes the intermediate state and the destabilising effect is reduced with the increasing number of OH-groups. The population of intermediate and $T_{max-inter}$ is significantly reduced by EG whereas only slightly reduced in Gly. $T_{max-inter}$ values is increased by higher order polyols; however, they do not affect the population of intermediate. Moreover, EG reduces the overall stability of the protein and behaves like a mild-denaturant whereas other polyols increase the overall stability of the protein.

5.7. REFERENCES

- [1] Y. Zhou, C.K. Hall, M. Karplus, The calorimetric criterion for a two-state process revisited, Protein Sci. 8 (1999) 1064–1074. https://doi.org/10.1110/ps.8.5.1064.
- [2] A.C.M. Ferreon, D.W. Bolen, Thermodynamics of Denaturant-Induced Unfolding of a Protein That Exhibits Variable Two-State Denaturation, Biochemistry. 43 (2004) 13357–13369. https://doi.org/10.1021/bi048666j.
- [3] J. Ramprakash, V. Doseeva, A. Galkin, W. Krajewski, L. Muthukumar, S. Pullalarevu, E. Demirkan, O. Herzberg, J. Moult, F.P. Schwarz, Comparison of the chemical and thermal denaturation of proteins by a two-state transition model, Anal. Biochem. 374 (2008) 221–230. https://doi.org/10.1016/j.ab.2007.10.005.
- [4] J. Schönfelder, R. Perez-Jimenez, V. Muñoz, A simple two-state protein unfolds mechanically via multiple heterogeneous pathways at single-molecule resolution, Nat. Commun. 7 (2016) 11777. https://doi.org/10.1038/ncomms11777.
- [5] E. Freire, K.P. Murphy, Molecular basis of co-operativity in protein folding, J. Mol. Biol. 222 (1991) 687–698. https://doi.org/10.1016/0022-2836(91)90505-Z.
- [6] R. Khurana, A.T. Hate, U. Nath, J.B. Udgaonkar, pH dependence of the stability of barstar to chemical and thermal denaturation, Protein Sci. 4 (1995) 1133–1144. https://doi.org/10.1002/pro.5560040612.
- [7] D. Hamada, S. Kidokoro, H. Fukada, K. Takahashi, Y. Goto, Salt-induced formation of the molten globule state of cytochrome c studied by isothermal titration calorimetry, Proc. Natl. Acad. Sci. 91 (1994) 10325 10329. https://doi.org/10.1073/pnas.91.22.10325.
- [8] P.K. Devaraneni, N. Mishra, R. Bhat, Polyol osmolytes stabilize native-like cooperative intermediate state of yeast hexokinase A at low pH, Biochimie. 94 (2012) 947–952. https://doi.org/10.1016/j.biochi.2011.12.012.
- [9] B. Anumalla, N.P. Prabhu, Glutamate Induced Thermal Equilibrium Intermediate and Counteracting Effect on Chemical Denaturation of Proteins, J. Phys. Chem. B. 122 (2018) 1132–1144. https://doi.org/10.1021/acs.jpcb.7b10561.

- [10] R. Kumar, N.P. Prabhu, D.K. Rao, A.K. Bhuyan, The Alkali Molten Globule State of Horse Ferricytochrome c: Observation of Cold Denaturation, J. Mol. Biol. 364 (2006) 483–495. https://doi.org/10.1016/j.jmb.2006.09.025.
- [11] L. Mayne, S.W. Englander, Two-state vs. multistate protein unfolding studied by optical melting and hydrogen exchange, Protein Sci. 9 (2000) 1873–1877. https://doi.org/10.1110/ps.9.10.1873.
- [12] S.E. Radford, C.M. Dobson, P.A. Evans, The folding of hen lysozyme involves partially structured intermediates and multiple pathways, Nature. 358 (1992) 302–307. https://doi.org/10.1038/358302a0.
- [13] A.K. Bhuyan, J.B. Udgaonkar, Observation of Multistate Kinetics during the Slow Folding and Unfolding of Barstar, Biochemistry. 38 (1999) 9158–9168. https://doi.org/10.1021/bi990285w.
- [14] O.B. Ptitsyn, R.H. Pain, G. V Semisotnov, E. Zerovnik, O.I. Razgulyaev, Evidence for a molten globule state as a general intermediate in protein folding, FEBS Lett. 262 (1990) 20–24. https://doi.org/10.1016/0014-5793(90)80143-7.
- [15] A.K. Chamberlain, S.B.T.-A. in P.C. Marqusee, Comparison of equilibrium and kinetic approaches for determining protein folding mechanisms, in: Protein Fold. Mech., Academic Press, 2000: pp. 283–328. https://doi.org/10.1016/S0065-3233(00)53006-X.
- [16] K. Fujiwara, M. Arai, A. Shimizu, M. Ikeguchi, K. Kuwajima, S. Sugai, Folding–Unfolding Equilibrium and Kinetics of Equine β-Lactoglobulin: Equivalence between the Equilibrium Molten Globule State and a Burst-Phase Folding Intermediate, Biochemistry. 38 (1999) 4455–4463. https://doi.org/10.1021/bi982683p.
- [17] E. Judy, N. Kishore, A look back at the molten globule state of proteins: thermodynamic aspects, Biophys. Rev. 11 (2019) 365–375. https://doi.org/10.1007/s12551-019-00527-0.
- [18] P.A. Jennings, P.E. Wright, Formation of a molten globule intermediate early in the kinetic folding pathway of apomyoglobin, Science (80-.). 262 (1993) 892 896. https://doi.org/10.1126/science.8235610.

- [19] M. Ikeguchi, K. Kuwajima, M. Mitani, S. Sugai, Evidence for identity between the equilibrium unfolding intermediate and a transient folding intermediate: a comparative study of the folding reactions of .alpha.-lactalbumin and lysozyme, Biochemistry. 25 (1986) 6965–6972. https://doi.org/10.1021/bi00370a034.
- [20] T.M. Raschke, S. Marqusee, The kinetic folding intermediate of ribonuclease H resembles the acid molten globule and partially unfolded molecules detected under native conditions, Nat. Struct. Biol. 4 (1997) 298–304. https://doi.org/10.1038/nsb0497-298.
- [21] R.L. Baldwin, On-pathway versus off-pathway folding intermediates, Fold. Des. 1 (1996) R1–R8. https://doi.org/10.1016/S1359-0278(96)00003-X.
- [22] Y. Ivarsson, C. Travaglini-Allocatelli, P. Jemth, F. Malatesta, M. Brunori, S. Gianni, An On-pathway Intermediate in the Folding of a PDZ Domain, J. Biol. Chem. . 282 (2007) 8568–8572. https://doi.org/10.1074/jbc.M611026200.
- [23] A. Dasgupta, J.B. Udgaonkar, Four-State Folding of a SH3 Domain: Salt-Induced Modulation of the Stabilities of the Intermediates and Native State, Biochemistry. 51 (2012) 4723–4734. https://doi.org/10.1021/bi300223b.
- [24] S. Khorasanizadeh, I.D. Peters, H. Roder, Evidence for a three-state model of protein folding from kinetic analysis of ubiquitin variants with altered core residues, Nat. Struct. Biol. 3 (1996) 193–205. https://doi.org/10.1038/nsb0296-193.
- [25] P.H. Yancey, Organic osmolytes as compatible, metabolic and counteracting cytoprotectants in high osmolarity and other stresses, J. Exp. Biol. 208 (2005) 2819 2830. https://doi.org/10.1242/jeb.01730.
- [26] F. Franks, R.H.M. Hatley, Stability of proteins at subzero temperatures: thermodynamics and some ecological consequences, Pure Appl. Chem. 63 (1991) 1367–1380. https://doi.org/10.1351/pac199163101367.
- [27] W. Wang, Lyophilization and development of solid protein pharmaceuticals, Int. J. Pharm. 203 (2000) 1–60. https://doi.org/10.1016/S0378-5173(00)00423-3.

- [28] D. Samuel, T.K.S. Kumar, G. Ganesh, G. Jayaraman, P.-W. Yang, M.-M. Chang, V.D. Trivedi, S.-L. Wang, K.-C. Hwang, D.-K. Chang, C. Yu, Proline inhibits aggregation during protein refolding, Protein Sci. 9 (2000) 344–352. https://www.scopus.com/inward/record.uri?eid=2-s2.0-0034001362&partnerID=40&md5=e49441ab59b3f33603bcbd4c1a2bd1e2.
- [29] R.W. Ruddon, E. Bedows, Assisted protein folding, J. Biol. Chem. 272 (1997) 3125–3128. https://doi.org/10.1074/jbc.272.6.3125.
- [30] R. Rudolph, H. Lilie, In vitro folding of inclusion body proteins, FASEB J. 10 (1996) 49–56. https://doi.org/10.1096/fasebj.10.1.8566547.
- [31] T. Hasan, K. Kumari, S.C. Devi, J. Handa, T. Rehman, N.A. Ansari, L.R. Singh, Osmolytes in vaccine production, flocculation and storage: a critical review, Hum. Vaccin. Immunother. 15 (2019) 514–525. https://doi.org/10.1080/21645515.2018.1526585.
- [32] M.B. Burg, J.D. Ferraris, Intracellular Organic Osmolytes: Function and Regulation, J. Biol. Chem. . 283 (2008) 7309–7313. https://doi.org/10.1074/jbc.R700042200.
- [33] R. Mishra, R. Bhat, R. Seckler, Chemical chaperone-mediated protein folding: stabilization of P22 tailspike folding intermediates by glycerol, Biol. Chem. 388 (2007) 797–804. https://doi.org/10.1515/BC.2007.096.
- [34] A.A. Raibekas, V. Massey, Glycerol-induced development of catalytically active conformation of Crotalus adamanteus L-amino acid oxidase in vitro, Proc. Natl. Acad. Sci. 93 (1996) 7546 7551. https://doi.org/10.1073/pnas.93.15.7546.
- [35] T. Kamiyama, Y. Sadahide, Y. Nogusa, K. Gekko, Polyol-induced molten globule of cytochrome c: an evidence for stabilization by hydrophobic interaction, Biochim. Biophys. Acta Protein Struct. Mol. Enzymol. 1434 (1999) 44–57. https://doi.org/10.1016/S0167-4838(99)00159-4.
- [36] C.M. Jones, E.R. Henry, Y. Hu, C.K. Chan, S.D. Luck, A. Bhuyan, H. Roder, J. Hofrichter, W.A. Eaton, Fast events in protein folding initiated by nanosecond laser photolysis, Proc. Natl. Acad. Sci. 90 (1993) 11860 11864. https://doi.org/10.1073/pnas.90.24.11860.

- [37] T.R. Sosnick, L. Mayne, R. Hiller, S.W. Englander, The barriers in protein folding, Nat. Struct. Biol. 1 (1994) 149–156. https://doi.org/10.1038/nsb0394-149.
- [38] W. Hu, Z.-Y. Kan, L. Mayne, S.W. Englander, Cytochrome c folds through foldon-dependent native-like intermediates in an ordered pathway, Proc. Natl. Acad. Sci. 113 (2016) 3809 3814. https://doi.org/10.1073/pnas.1522674113.
- [39] G.W. Bushnell, G. V Louie, G.D. Brayer, High-resolution three-dimensional structure of horse heart cytochrome c, J. Mol. Biol. 214 (1990) 585–595. https://doi.org/10.1016/0022-2836(90)90200-6.
- [40] J. Trewhella, V.A.P. Carlson, E.H. Curtis, D.B. Heidorn, Differences in the solution structures of oxidized and reduced cytochrome c measured by small-angle x-ray scattering, Biochemistry. 27 (1988) 1121–1125. https://doi.org/10.1021/bi00404a007.
- [41] A.K. Bhuyan, J.B. Udgaonkar, Folding of horse cytochrome c in the reduced state, J. Mol. Biol. 312 (2001) 1135–1160. https://doi.org/10.1006/jmbi.2001.4993.
- [42] J.B. Soffer, R. Schweitzer-Stenner, Near-exact enthalpy-entropy compensation governs the thermal unfolding of protonation states of oxidized cytochrome c, JBIC J. Biol. Inorg. Chem. 19 (2014) 1181–1194. https://doi.org/10.1007/s00775-014-1174-x.
- [43] A.K. Bhuyan, The Off-Pathway Status of the Alkali Molten Globule Is Unrelated to Heme Misligation and Trans-pH Effects: Experiments with Ferrocytochrome c, Biochemistry. 49 (2010) 7774–7782. https://doi.org/10.1021/bi100881n.
- [44] A. Hagarman, L. Duitch, R. Schweitzer-Stenner, The Conformational Manifold of Ferricytochrome c Explored by Visible and Far-UV Electronic Circular Dichroism Spectroscopy, Biochemistry. 47 (2008) 9667–9677. https://doi.org/10.1021/bi800729w.
- [45] C. Bongiovanni, F. Sinibaldi, T. Ferri, R. Santucci, Glycerol-Induced Formation of the Molten Globule from Acid-Denatured Cytochrome c: Implication for Hierarchical Folding, J. Protein Chem. 21 (2002) 35–41. https://doi.org/10.1023/A:1014179031881.
- [46] Y.-S. Kim, L.S. Jones, A. Dong, B.S. Kendrick, B.S. Chang, M.C. Manning, T.W. Randolph, J.F. Carpenter, Effects of sucrose on conformational equilibria and fluctuations within the native-state ensemble of proteins, Protein Sci. 12 (2003) 1252–1261. https://doi.org/10.1110/ps.0242603.

- [47] K. Joshi, A.K. Bhuyan, Quasi-native transition and self-diffusion of proteins in water-glycerol mixture, Biophys. Chem. 257 (2020) 106274. https://doi.org/10.1016/j.bpc.2019.106274.
- [48] R.F. Latypov, H. Cheng, N.A. Roder, J. Zhang, H. Roder, Structural Characterization of an Equilibrium Unfolding Intermediate in Cytochrome c, J. Mol. Biol. 357 (2006) 1009–1025. https://doi.org/10.1016/j.jmb.2006.01.055.
- [49] R. Varhač, N. Tomášková, M. Fabián, E. Sedlák, Kinetics of cyanide binding as a probe of local stability/flexibility of cytochrome c, Biophys. Chem. 144 (2009) 21–26. https://doi.org/10.1016/j.bpc.2009.06.001.
- [50] A. Tiwari, R. Bhat, Stabilization of yeast hexokinase A by polyol osmolytes: Correlation with the physicochemical properties of aqueous solutions, Biophys. Chem. 124 (2006) 90–99. https://doi.org/10.1016/j.bpc.2006.06.003.
- [51] I. Haque, A. Islam, R. Singh, A.A. Moosavi-Movahedi, F. Ahmad, Stability of proteins in the presence of polyols estimated from their guanidinium chloride-induced transition curves at different pH values and 25 °C, Biophys. Chem. 119 (2006) 224–233. https://doi.org/10.1016/j.bpc.2005.09.016.
- [52] K.T. Naidu, D.K. Rao, N.P. Prabhu, Cryo vs Thermo: Duality of Ethylene Glycol on the Stability of Proteins, J. Phys. Chem. B. (2020). https://doi.org/10.1021/acs.jpcb.0c06247.
- [53] B. Beermann, J. Guddorf, K. Boehm, A. Albers, S. Kolkenbrock, S. Fetzner, H.-J. Hinz, Stability, Unfolding, and Structural Changes of Cofactor-Free 1H-3-Hydroxy-4-oxoquinaldine 2,4-Dioxygenase, Biochemistry. 46 (2007) 4241–4249. https://doi.org/10.1021/bi0622423.
- [54] V.R. Agashe, J.B. Udgaonkar, Thermodynamics of Denaturation of Barstar: Evidence for Cold Denaturation and Evaluation of the Interaction with Guanidine Hydrochloride, Biochemistry. 34 (1995) 3286–3299. https://doi.org/10.1021/bi00010a019.
- [55] A. Rodger, Far UV Protein Circular Dichroism BT Encyclopedia of Biophysics, in: G.C.K. Roberts (Ed.), Springer Berlin Heidelberg, Berlin, Heidelberg, 2013: pp. 726–730. https://doi.org/10.1007/978-3-642-16712-6_634.

- [56] R. Varhač, D. Sedláková, M. Stupák, E. Sedlák, Non-two-state thermal denaturation of ferricytochrome c at neutral and slightly acidic pH values, Biophys. Chem. 203–204 (2015) 41–50. https://doi.org/10.1016/j.bpc.2015.05.002.
- [57] L. Hannibal, F. Tomasina, D.A. Capdevila, V. Demicheli, V. Tórtora, D. Alvarez-Paggi, R. Jemmerson, D.H. Murgida, R. Radi, Alternative Conformations of Cytochrome c: Structure, Function, and Detection, Biochemistry. 55 (2016) 407–428. https://doi.org/10.1021/acs.biochem.5b01385.
- [58] Y.-L.P. Ow, D.R. Green, Z. Hao, T.W. Mak, Cytochrome c: functions beyond respiration, Nat. Rev. Mol. Cell Biol. 9 (2008) 532–542. https://doi.org/10.1038/nrm2434.
- [59] L.J. McClelland, T.-C. Mou, M.E. Jeakins-Cooley, S.R. Sprang, B.E. Bowler, Structure of a mitochondrial cytochrome c conformer competent for peroxidase activity, Proc. Natl. Acad. Sci. 111 (2014) 6648 – 6653. https://doi.org/10.1073/pnas.1323828111.
- [60] A. Naeem, R.H. Khan, Characterization of molten globule state of cytochrome c at alkaline, native and acidic pH induced by butanol and SDS, Int. J. Biochem. Cell Biol. 36 (2004) 2281–2292. https://doi.org/10.1016/j.biocel.2004.04.023.
- [61] J.K. Kaushik, R. Bhat, Thermal Stability of Proteins in Aqueous Polyol Solutions: Role of the Surface Tension of Water in the Stabilizing Effect of Polyols, J. Phys. Chem. B. 102 (1998) 7058–7066. https://doi.org/10.1021/jp9811191.
- [62] F. Anjum, V. Rishi, F. Ahmad, Compatibility of osmolytes with Gibbs energy of stabilization of proteins, Biochim. Biophys. Acta Protein Struct. Mol. Enzymol. 1476 (2000) 75–84. https://doi.org/10.1016/S0167-4838(99)00215-0.
- [63] S. Taneja, F. Ahmad, Increased thermal stability of proteins in the presence of amino acids, Biochem. J. 303 (1994) 147 153. https://doi.org/10.1042/bj3030147.
- [64] B.S. Russell, R. Melenkivitz, K.L. Bren, NMR investigation of ferricytochrome c unfolding: Detection of an equilibrium unfolding intermediate and residual structure in the denatured state, Proc. Natl. Acad. Sci. 97 (2000) 8312 – 8317. https://doi.org/10.1073/pnas.150239397.

- [65] Y. Xu, L. Mayne, S.W. Englander, Evidence for an unfolding and refolding pathway in cytochrome c, Nat. Struct. Biol. 5 (1998) 774–778. https://doi.org/10.1038/1810.
- [66] B.S. Russell, K.L. Bren, Denaturant dependence of equilibrium unfolding intermediates and denatured state structure of horse ferricytochrome c, JBIC J. Biol. Inorg. Chem. 7 (2002) 909–916. https://doi.org/10.1007/s00775-002-0381-z.
- [67] A.C. Apetri, W.K. Surewicz, Atypical Effect of Salts on the Thermodynamic Stability of Human Prion Protein, J. Biol. Chem. . 278 (2003) 22187–22192. https://doi.org/10.1074/jbc.M302130200.
- [68] X. Zhang, V.Q. Lam, Y. Mou, T. Kimura, J. Chung, S. Chandrasekar, J.R. Winkler, S.L. Mayo, S. Shan, Direct visualization reveals dynamics of a transient intermediate during protein assembly, Proc. Natl. Acad. Sci. 108 (2011) 6450 6455. https://doi.org/10.1073/pnas.1019051108.
- [69] A. Das, C. Mukhopadhyay, Urea-Mediated Protein Denaturation: A Consensus View,J. Phys. Chem. B. 113 (2009) 12816–12824. https://doi.org/10.1021/jp906350s.
- [70] C. Camilloni, A. Guerini Rocco, I. Eberini, E. Gianazza, R.A. Broglia, G. Tiana, Urea and Guanidinium Chloride Denature Protein L in Different Ways in Molecular Dynamics Simulations, Biophys. J. 94 (2008) 4654–4661. https://doi.org/10.1529/biophysj.107.125799.
- [71] D.R. Canchi, A.E. García, Cosolvent Effects on Protein Stability, Annu. Rev. Phys. Chem. 64 (2013) 273–293. https://doi.org/10.1146/annurev-physchem-040412-110156.
- [72] G.I. Makhatadze, P.L. Privalov, Protein interactions with urea and guanidinium chloride: A calorimetric study, J. Mol. Biol. 226 (1992) 491–505. https://doi.org/10.1016/0022-2836(92)90963-K.
- [73] C.E. Dempsey, T.J. Piggot, P.E. Mason, Dissecting Contributions to the Denaturant Sensitivities of Proteins, Biochemistry. 44 (2005) 775–781. https://doi.org/10.1021/bi048389g.
- [74] J.S. Smith, J.M. Scholtz, Guanidine Hydrochloride Unfolding of Peptide Helices: Separation of Denaturant and Salt Effects, Biochemistry. 35 (1996) 7292–7297. https://doi.org/10.1021/bi960341i.

- [75] K. Tejaswi Naidu, N. Prakash Prabhu, An able-cryoprotectant and a moderate denaturant: distinctive character of ethylene glycol on protein stability, J. Biomol. Struct. Dyn. (2020) 1–13. https://doi.org/10.1080/07391102.2020.1819422.
- [76] F.-F. Liu, L. Ji, L. Zhang, X.-Y. Dong, Y. Sun, Molecular basis for polyol-induced protein stability revealed by molecular dynamics simulations, J. Chem. Phys. 132 (2010) 225103. https://doi.org/10.1063/1.3453713.
- [77] Z.A. Parray, F. Ahmad, M.I. Hassan, I. Hasan, A. Islam, Effects of Ethylene Glycol on the Structure and Stability of Myoglobin Using Spectroscopic, Interaction, and In Silico Approaches: Monomer Is Different from Those of Its Polymers, ACS Omega. 5 (2020) 13840–13850. https://doi.org/10.1021/acsomega.0c01185.
- [78] S.N. Timasheff, The Control of Protein Stability and Association by Weak Interactions with Water: How Do Solvents Affect These Processes?, Annu. Rev. Biophys. Biomol. Struct. 22 (1993) 67–97. https://doi.org/10.1146/annurev.bb.22.060193.000435.
- [79] S.N. Timasheff, Protein-solvent preferential interactions, protein hydration, and the modulation of biochemical reactions by solvent components, Proc. Natl. Acad. Sci. 99 (2002) 9721 9726. https://doi.org/10.1073/pnas.122225399.
- [80] N. Cremades, J. Sancho, Molten Globule and Native State Ensemble of Helicobacter pylori Flavodoxin: Can Crowding, Osmolytes or Cofactors Stabilize the Native Conformation Relative to the Molten Globule?, Biophys. J. 95 (2008) 1913–1927. https://doi.org/10.1529/biophysj.108.130153.
- [81] K. GEKKO, Mecbanism of Polyol-Induced Protein Stabilization: Solubility of Amino Acids and Diglycine in Aqueous Polyol Solutions1, J. Biochem. 90 (1981) 1633–1641. https://doi.org/10.1093/oxfordjournals.jbchem.a133638.
- [82] D.W. Bolen, I. V Baskakov, The osmophobic effect: natural selection of a thermodynamic force in protein folding11Edited by D. Draper, J. Mol. Biol. 310 (2001) 955–963. https://doi.org/10.1006/jmbi.2001.4819.
- [83] R. Sinibaldi, M.G. Ortore, F. Spinozzi, F. Carsughi, H. Frielinghaus, S. Cinelli, G. Onori, P. Mariani, Preferential hydration of lysozyme in water/glycerol mixtures: A small-angle neutron scattering study, J. Chem. Phys. 126 (2007) 235101. https://doi.org/10.1063/1.2735620.

- [84] C.M. Sudrik, T. Cloutier, N. Mody, H.A. Sathish, B.L. Trout, Understanding the Role of Preferential Exclusion of Sugars and Polyols from Native State IgG1 Monoclonal Antibodies and its Effect on Aggregation and Reversible Self-Association, Pharm. Res. 36 (2019) 109. https://doi.org/10.1007/s11095-019-2642-3.
- [85] T. Arakawa, Protein—solvent interaction, Biophys. Rev. 10 (2018) 203–208. https://doi.org/10.1007/s12551-017-0339-6.
- [86] J.A. Schellman, Protein Stability in Mixed Solvents: A Balance of Contact Interaction and Excluded Volume, Biophys. J. 85 (2003) 108–125. https://doi.org/10.1016/S0006-3495(03)74459-2.
- [87] S.N. Timasheff, Control of Protein Stability and Reactions by Weakly Interacting Cosolvents: The Simplicity of the Complicated, in: E.B.T.-A. in P.C. Di Cera (Ed.), Link. Thermodyn. Macromol. Interact., Academic Press, 1998: pp. 355–432. https://doi.org/10.1016/S0065-3233(08)60656-7.
- [88] S.N. Timasheff, H. Inoue, Preferential binding of solvent components to proteins in mixed water-organic solvent systems, Biochemistry. 7 (1968) 2501–2513. https://doi.org/10.1021/bi00847a009.

List of Publications

- K. Tejaswi Naidu, N. Prakash Prabhu, An able-cryoprotectant and a moderate denaturant: distinctive character of ethylene glycol on protein stability, J. Biomol. Struct. Dyn. (2020) 1–13. https://doi.org/10.1080/07391102.2020.1819422.
- K.T. Naidu, D.K. Rao, N.P. Prabhu, Cryo vs Thermo: Duality of Ethylene Glycol on the Stability of Proteins, J. Phys. Chem. B. (2020), 10077-10088. https://doi.org/10.1021/acs.jpcb.0c06247.
- 3. K. Tejaswi Naidu, N. Prakash Prabhu, Effect of Polyols on Thermal Unfolding Intermediate of Cytochrome c (Manuscript in review)

Plagiarism Certificate

Effect of Ethylene glycol and Polyols on Thermal Stability of Globular Proteins

by Tejaswi K Naidu

Submission date: 04-Jan-2021 03:15PM (UTC+0530)

Submission ID: 1482879962

File name: Thesis_Plagiansm_Check_KTN_13LTPH03.pdf (8.02M)

Word count: 27112 Character count: 140477

Effect of Ethylene glycol and Polyols on Thermal Stability of Globular Proteins



Structure and Dynamics, 2020

Publication

- Zhou, R.. "Exploring the protein folding free <1% 6 energy landscape: coupling replica exchange method with P3ME/RESPA algorithm", Journal of Molecular Graphics and Modelling, 200405 Publication arxiv.org <1% Internet Source a100.gov.bc.ca 8 Internet Source konf2.ims.ac.jp <1% Internet Source www.churchofjesuschrist.org 10 Internet Source Tatiana Maximova, Ryan Moffatt, Buyong Ma, 11 Ruth Nussinov, Amarda Shehu. "Principles and Overview of Sampling Methods for Modeling Macromolecular Structure and Dynamics", PLOS Computational Biology, 2016 Publication
 - Andrea Arsiccio, James McCarty, Roberto Pisano, Joan-Emma Shea. "Heightened Cold-Denaturation of Proteins at the Ice–Water Interface", Journal of the American Chemical Society, 2020

		ca		

13	"Biomolecular Simulations", Springer Science and Business Media LLC, 2019 Publication	<1%
14	Submitted to Swinburne University of Technology Student Paper	<1%
15	Yuji Sugita. "Multidimensional replica-exchange method for free-energy calculations", The Journal of Chemical Physics, 2000 Publication	<1%
16	Richard Dods. "Concepts in Bioscience Engineering", Springer Science and Business Media LLC, 2019 Publication	<1%
17	Rabindra Kumar Behera, Hiroshi Nakajima, Jitumani Rajbongshi, Yoshihito Watanabe, Shyamalava Mazumdar. "Thermodynamic Effects of the Alteration of the Axial Ligand on the Unfolding of Thermostable Cytochrome ", Biochemistry, 2013	<1%
18	S. N. Timasheff. "Protein-solvent preferential interactions, protein hydration, and the modulation of biochemical reactions by solvent components", Proceedings of the National Academy of Sciences, 2002	<1%

Publication

19	Kamb, . "THE ALPHA HELIX AND THE STRUCTURE OF PROTEINS", World Scientific Series in 20th Century Chemistry, 2001. Publication	<1%
20	Hironori Kokubo, Yuko Okamoto. "Replica- exchange methods and predictions of helix configurations of membrane proteins", Molecular Simulation, 2006 Publication	<1%
21	opencpn.de Internet Source	<1%
22	Mrinmoy Mukherjee, Jagannath Mondal. "Bottom-Up View of the Mechanism of Action of Protein-Stabilizing Osmolytes", The Journal of Physical Chemistry B, 2020 Publication	<1%
23	ir.soken.ac.jp Internet Source	<1%
24	journal.hep.com.cn Internet Source	<1%
25	Fufeng Liu, Ying Wang, Jingcheng Sang, Wei Wei, Wenping Zhao, Beibei Chen, Fang Zhao, Longgang Jia, Fuping Lu. "Brazilin Inhibits α-Synuclein Fibrillogenesis, Disrupts Mature Fibrils, and Protects against Amyloid-Induced	<1%

Cytotoxicity", Journal of Agricultural and Food Chemistry, 2019

Publication

26	Ye Wu, Hanyu Liu, Haijun Huang, Yingwei Fei, Xiaolei Feng, Simon A. T. Redfern. "Pressure- induced structural modulations in coesite", Physical Review B, 2018	<1%
27	ufdc.ufl.edu Internet Source	<1%
28	Hueder Paulo Moisés de Oliveira, Marcelo Henrique Gehlen. "Characterization of Mixed Micelles of Sodium Dodecyl Sulfate and Tetraoxyethylene Dodecyl Ether in Aqueous Solution", Langmuir, 2002 Publication	<1%
29	"Chemoinformatics", Wiley, 2003	<1%
30	link.springer.com Internet Source	<1%
31	aip.scitation.org Internet Source	<1%
32	Advances in Experimental Medicine and Biology, 2014. Publication	<1%

hdl.handle.net

33	Internet Source	<1%
34	Nataša Tomášková, Rastislav Varhač, Veronika Lysáková, Andrej Musatov, Erik Sedlák. "Peroxidase activity of cytochrome c in its compact state depends on dynamics of the heme region", Biochimica et Biophysica Acta (BBA) - Proteins and Proteomics, 2018 Publication	<1%
35	Sanjoy Bandyopadhyay. "Coupling between hydration layer dynamics and unfolding kinetics of HP-36", The Journal of Chemical Physics, 2006 Publication	<1%
36	core.ac.uk Internet Source	<1%
37	"ABSTRACTS OF THE XXIV CONGRESS OF THE INTERNATIONAL SOCIETY ON THROMBOSIS AND HAEMOSTASIS", Journal of Thrombosis and Haemostasis, 2013. Publication	<1%
38	www.hybrid-analysis.com Internet Source	<1%
39	Holzammer, Tobias. "Homology modeling, molecular dynamics simulations and sitedirected mutagenesis of histamine H2	<1%

receptors", Publikationsserver der Universität Regensburg, 2013.

Publication

Genetische Grundlagen Physiologischer Vorgänge · Konstitution der Pflanzenzelle / Genetic Control of Physiological Processes · The Constitution of the Plant Cell, 1955.

<1%

Huan-Xiang Zhou, Xiaodong Pang.
"Electrostatic Interactions in Protein Structure,
Folding, Binding, and Condensation", Chemical
Reviews. 2018

<1%

Publication

Shu-Qun Liu, Xing-Lai Ji, Yan Tao, De-Yong Tan, Ke-Qin Zhang, Yun-Xin Fu. "Chapter 10 Protein Folding, Binding and Energy Landscape: A Synthesis", IntechOpen, 2012 <1%

Publication

W. Duo, J.P.K. Sevill, N.F. Kirkby, R. Clift.
"Formation of product layers in solid-gas reactions for removal of acid gases", Chemical Engineering Science, 1994

<1%

Publication

Yatani, A.. "Synthesis, structures and properties of the dinuclear copper(II) complexes triply bridged by two oximato and one pyrazolato or one phthalazine", Inorganica Chimica Acta,

<1%

20010507

Publication

Submitted to Mahidol University Student Paper

Jerson L. Silva, Andrea C. Oliveira, Tuane C. R. 46 G. Vieira, Guilherme A. P. de Oliveira, Marisa C. Suarez, Debora Foguel. "High-Pressure Chemical Biology and Biotechnology", Chemical Reviews, 2014

Publication

Exclude quotes

Exclude matches

< 14 words

Exclude bibliography

On On